

**Analysis and Mitigation of the Impacts of Integrating Fast-Charging Stations on the
Voltage Fluctuations**

by

Sami Mohammad Alshareef

A thesis submitted to the
School of Graduate and Postdoctoral Studies in partial
fulfillment of the requirements for the degree of

Doctor of Philosophy in Electrical Engineering

The Faculty of Engineering and Applied Science
University of Ontario Institute of Technology (Ontario Tech University)

Oshawa, Ontario, Canada

October 2020

© Sami Mohammad Alshareef, 2020

THESIS EXAMINATION INFORMATION

Submitted by: **Sami Mohammad Alshareef**

Doctor of Philosophy in Electrical Engineering

Thesis title: Analysis and Mitigation of the Impacts of Integrating Fast-Charging Stations on the Voltage Fluctuations

An oral defense of this thesis took place on September 9, 2019 in front of the following examining committee:

Examining Committee:

Chair of Examining Committee	Dr. Shahryar Rahnamayan
Research Supervisor	Dr. Walid Morsi
Examining Committee Member	Dr. Magdy Salama
Examining Committee Member	Dr. Lixuan Lu
Examining Committee Member	Dr. Moustafa El-Gindy
University Examiner	Dr. Ibrahim Dincer
External Examiner	Dr. Kankar Bhattacharya

The above committee determined that the thesis is acceptable in form and content and that a satisfactory knowledge of the field covered by the thesis was demonstrated by the candidate during an oral examination. A signed copy of the Certificate of Approval is available from the School of Graduate and Postdoctoral Studies.

ABSTRACT

As the number of electric vehicles increases, fast charging becomes a necessity in the electric service stations; not only to reduce the charging and waiting times for electric vehicles whether in service or in a queue, but also to increase their commercial benefits by increasing their utilization rates. Fast charging stations are characterized by their high-power consumption from the electric grids to fulfill these aforementioned aims. Times and periods of that consumption are indeterminate due to several uncertain parameters that are inherent in the electric vehicles charging process, such as their numbers, their battery capacities, their state-of-charge levels at time of arrivals, and their time of arrivals, which may all lead to a degradation in the quality of electric power delivered to the customers. The research presented in this thesis focuses on the impacts of fast charging stations on three power quality phenomena, namely voltage magnitude variations, voltage unbalance, and voltage fluctuation. The Markov Chain Monte Carlo is proposed to estimate the required energy from each fast charging station when it is utilized to charge the electric vehicles, considering their stochastic parameters. Two charging methods are implemented in this work: charging with an estimated output power and charging with an actual output power. The results reveal that the impact of fast charging stations on voltage fluctuation by either of these charging methods can lead to light flicker. When the estimated output power is utilized, the light flicker is higher compared to when the actual output power is utilized. When the operation of Fast Charging Stations causes a voltage fluctuation and light flicker, the FCSs may get disconnected which results in a financial losses represented by the FCS downtime. The FCS downtime can be avoided by mitigating the voltage fluctuation and light flicker. Several flicker mitigation devices are analyzed and compared based on different criteria. The comparison reveals that distribution static compensators considers the cheapest mitigation device, according to the cost per kVAr basis and the total annual equivalent cost. Besides, to mitigate the impact on the voltage and light flicker, a novel smart charging is proposed in this study in which customers can select one of three charging services available in the fast chargers: premium, regular, or economic charging power. The charging power is selected upon customer priority toward the time and cost which offers less control than those currently available in the literature. The proposed smart charging preserves the balance of customer's value of time and value of cost. The proposed smart charging achieves a tremendous reduction in the cost of mitigation the voltage fluctuation and light flicker. Annual cost of the proposed smart charging is less than the annual cost of distribution static compensators by a minimum of 90% to a maximum of 99 %. The proposed smart charging offers a compromise solution to satisfy several stakeholders with different interests. Thus, equipment of system's operator, investor of fast charging station, nearby customers, and owners of electric vehicles will not be impacted by integrating the fast charging station.

Keywords: Fast Charging Station; smart charging; voltage fluctuation; light flicker;

DSTATCOM

AUTHOR'S DECLARATION

I hereby declare that this thesis consists of original work of which I have authored. This is a true copy of the thesis, including any required final revisions, as accepted by my examiners.

I authorize the University of Ontario Institute of Technology (Ontario Tech University) to lend this thesis to other institutions or individuals for the purpose of scholarly research. I further authorize University of Ontario Institute of Technology (Ontario Tech University) to reproduce this thesis by photocopying or by other means, in total or in part, at the request of other institutions or individuals for the purpose of scholarly research. I understand that my thesis will be made electronically available to the public.

SAMI MOHAMMAD ALSHAREEF

STATEMENT OF CONTRIBUTIONS

I hereby certify that I am the sole author of this thesis. I have used standard referencing practices to acknowledge ideas, research techniques, or other materials that belong to others. Furthermore, I hereby certify that I am the sole source of the creative works and/or inventive knowledge described in this thesis.

Part of the work described in Chapter 6 has been published as:

Alshareef, Sami M., and Walid G. Morsi. "Probabilistic commercial load profiles at different climate zones." In 2017 IEEE Electrical Power and Energy Conference (EPEC), pp. 1-7. IEEE, 2017.

Alshareef, Sami M., and Walid G. Morsi. "Probabilistic Models for Residential and Commercial Loads with High Time Resolution." In 2019 IEEE Electrical Power and Energy Conference (EPEC), pp. 1-6. IEEE, 2019.

Part of the work described in Chapter 7 has been published as:

Alshareef, Sami M., and Walid G. Morsi. "Impact of fast charging stations on the voltage flicker in the electric power distribution systems." In 2017 IEEE Electrical Power and Energy Conference (EPEC), pp. 1-6. IEEE, 2017.

Alshareef, Sami M., and Walid G. Morsi. "Probabilistic Modeling of Plug-in Electric Vehicles Charging from Fast Charging Stations." In 2019 IEEE Electrical Power and Energy Conference (EPEC), pp. 1-6. IEEE, 2019.

ACKNOWLEDGEMENTS

First and foremost, eternal praise and glory are for the sempiternal Allah Almighty for His limitless and countless blessings upon his servant.

I would like to express my genuine gratitude to Professor Walid Morsi Ibrahim, my research supervisor. Also, I wish to thank my thesis committee Professor Kankar Bhattacharya, Professor Ibrahim Dincer, Professor Magdy Salama, Professor Lixuan Lu, and Professor Moustafa El-Gindy for their insightful comments and suggestions.

I am thankful to government of Saudi Arabia, as my research would not have been possible without the financial support of the Ministry of Education of Saudi Arabia, represented by AlJouf University.

I would like to express my sincere gratitude to my parents for their continued prayers and encouragement; to my wife and kids for their unlimited patience and emotional support; and, to my brothers and sisters for their care and love. You are all the pillars of my life.

DEDICATION

To my father Mohammad and my mother Nourah

To my wife Hayat, my son Battal, my daughters Shumokh, Nourah, and Judy

To my brothers and my sisters

To the soul of my uncle Yahya

TABLE OF CONTENTS

Table of Contents

ABSTRACT	ii
AUTHOR’S DECLARATION	iii
STATEMENT OF CONTRIBUTIONS	iv
ACKNOWLEDGEMENTS	v
DEDICATION	vi
TABLE OF CONTENTS	vii
LIST OF TABLES	xiii
LIST OF FIGURES	xv
LIST OF ABBREVIATIONS AND SYMBOLS	xviii
Chapter 1. Introduction	1
1.1 Motivation	1
1.2 Problem Statement	3
1.3 Research Objectives	4
1.4 Dissertation Outline.....	5
Chapter 2. Literature Review	7
2.1 Introduction	7
2.2 Fast Charging Station	7
2.3 Previous Works Discussing the Impact of FCS on Voltage Quality.....	9
2.3.1 The Impact of FCS on Voltage Magnitude Variations	10
2.3.2 Impact of FCS on Voltage Unbalance	10
2.3.3 Impact of FCS on Voltage Fluctuation and Light Flicker	11
2.4 Parameters Utilized to Shape the Charging Profile at FCS.....	12
2.4.1 Types of EVs Charged at FCS	12
2.4.2 Modelling EVs Arrival Time at the FCS	13
2.4.3 Modelling EVs Daily Distance Travelled and SOC	14
2.4.4 Time Scales of Quantifying the Impact of FCS.....	16
2.4.5 The Output Power of FCS.....	16
2.5 Mitigation Method of Power Quality Variations	17
2.5.1 Mitigation Using Energy Storage	17

2.5.2	Mitigation Using Distribution Static Compensators.....	20
2.5.3	Mitigation Using Smart Charging.....	21
2.6	Research Gaps	22
Chapter 3.	Response of Lighting Technology to Voltage Fluctuation.....	25
3.1	Introduction	25
3.2	Types of Lamps	26
3.2.1	Incandescent Lamps.....	26
3.2.2	Discharge Lamps	28
3.2.3	LED Lighting	30
3.3	Comparison of incandescent, FL, CFL, LED, and OLED lamps.....	30
3.3.1	Lamp Efficacy.....	30
3.3.2	Lamp Lifetime	31
3.3.3	Lamp Cost.....	32
3.3.4	Trends of Lighting Market.....	33
3.4	Voltage Fluctuation and its Impacts on the Modern Lighting System.....	35
3.4.1	Definition of Voltage Fluctuation.....	35
3.4.2	Adverse Impacts of Voltage Fluctuation	36
3.4.3	Effects of Flicker.....	36
3.4.4	Flicker Metrics	36
3.4.5	Modern Lighting Response to Voltage Fluctuation.....	44
3.4.6	Flicker in Incandescent Lamps	45
3.4.7	Flicker in Fluorescent Discharge Lighting	46
3.4.8	Flicker in High-Intensity Discharge Lamps.....	47
3.4.9	Flicker in Light-Emitting and Organic Light-Emitting Diodes Lamps	48
3.5	Other Effects of Voltage Fluctuation	51
Chapter 4.	The Mitigation of Voltage Fluctuation and Light Flicker.....	52
4.1	Introduction	52
4.2	General Utility Practice when Exceeding Flicker Limits.....	53
4.2.1	Customer Responsibilities	53
4.2.2	Responsibilities for Flicker Mitigation	53
4.3	Voltage Fluctuation Mitigation Technologies.....	54
4.4	Comparison of Voltage Fluctuation Mitigation Technologies.....	55

4.5	Control of Flicker Mitigation Technologies.....	62
4.5.1	Static Var Compensator	62
4.5.2	Distribution Static Compensator.....	63
4.5.3	Dynamic Voltage Restorer.....	64
4.5.4	Unified Power Quality Conditioner	65
4.5.5	Synchronous Condensers	66
4.5.6	Saturated-Core Reactor	66
4.5.7	Fixed Series Capacitors.....	67
4.6	Cost of Flicker Mitigation Technologies	70
4.7	Comparison of Costs of Flicker Mitigation Technologies	73
4.8	Comparison of Advantages and Disadvantages of Mitigation Technologies	75
4.9	Technology Selection.....	76
4.10	DSTATCOM Modelling	79
Chapter 5. Distribution System and Fast Charging Components: An Overview ..		84
5.1	Introduction	84
5.2	Electrical Power Distribution System Overview.....	85
5.2.1	Distribution Substations.....	85
5.2.2	Primary Distribution Systems	86
5.2.3	Secondary Distribution Systems	90
5.3	Energy Storage Systems Overview	91
5.4	Electric Vehicle Charging Stations Overview	92
5.4.1	Charging Sequence and Connector Interface.....	92
5.4.2	Connection to the Grid.....	94
5.5	Radial Distribution Feeder Analysis	94
Chapter 6. Probabilistic Load Modeling in Different Climate Zones		98
6.1	Introduction	98
6.2	Load Characteristics.....	98
6.3	Related Works	99
6.4	Load Modeling Approach	99
6.4.1	Background.....	99
6.4.2	Data Source and Description	101
6.4.3	Preliminary Data Processing.....	102

6.5	Generation of Load Profiles	102
6.5.1	Methodology	102
6.5.2	Cluster Assessment	104
6.6	Residential Load Profiles	107
6.7	Commercial Load Profiles	113
6.8	Load Profile Selection	119
Chapter 7.	Probabilistic Charging Demand Modeling.....	126
7.1	Introduction	126
7.2	Type Selection of Electric Vehicles	127
7.3	Battery Capacity and Driving Range	128
7.4	Distribution of Daily Mileage Travelled.....	129
7.4.1	The Canadian Plug-In Electric Vehicle Survey (CPEVS-2015).....	130
7.4.2	Fundamentals of Markov Chain Monte Carlo	135
7.5	Arrival Time Distribution and Rated Power of the FCSs	140
7.5.1	Typical Arrival Time and Rate at FCSs.....	141
7.6	Input Data Required for Vehicle Charging Model.....	143
7.6.1	Number of PBEVs	143
7.6.2	Type of PBEV and Charging Locations	144
7.6.3	Arriving Rate and Time at FCS	145
7.6.4	Chevy Bolt Driving Pattern and Level of their Charged Batteries at the FCS 145	
7.6.5	Charging Power	147
7.6.6	Length of Time with Chevy Bolt Drawing Power from FCS.....	149
7.7	Demand Profile of the FCS	152
Chapter 8.	Results of Flicker Mitigation Using DSTATCOM.....	154
8.1	Test System Description.....	154
8.2	Test System Modification	156
8.2.1	Primary Distribution System Expansion.....	156
8.2.2	Secondary Distribution System Representation.....	157
8.2.3	Fast Charging Stations' Inclusion.....	159
8.2.4	Battery Energy Storage Units' Integration	160
8.2.5	Distribution Static Compensators' Placement	161
8.3	Conducting the Load Flow Analysis	161

8.4	Scenarios and Results	162
8.4.1	Description of the Applied Scenarios	163
8.4.2	Voltage Quality Assessment Results and Discussion	165
Chapter 9. A Novel Smart Charging Method Applied on Fast Charging Stations to Mitigate Voltage Fluctuation and Light Flicker		182
9.1	Input Data Required for Vehicle Charging Model	182
9.1.1	Number of PBEVs	182
9.1.2	Types of PBEVs, their Shares and Charging Locations	183
9.1.3	PBEVs Arriving Rate at FCS	185
9.1.4	Level of Charged Batteries at the Starting of Charging from FCS	186
9.2	Length of Time with PBEVs Drawing Power from FCS	188
9.3	Length of Time with PBEVs Connected to FCS	190
9.4	Charging Power	191
9.4.1	Uncontrolled Charging	191
9.4.2	Smart (Controlled) Charging	191
9.5	Case Study and Assumptions	192
9.6	Smart Charging Constraints	193
9.7	Flicker Assessment and Relation to Output Power of Fast Charging Station..	200
9.7.1	Relative Voltage Change Assessment	200
9.7.2	Flicker Severity Caused by the FCS	202
9.8	Test System	205
9.9	Case Study	205
9.9.1	Results and Discussions	208
9.9.2	Effect of Full Charging of the Batteries on Flicker Severity	211
9.9.3	Effect of Envelope of Flickers	212
9.9.4	Effect of Smart Charging on Charging Duration	214
9.10	A comparative study	215
Chapter 10. A Novel Cost Model for Adopting the Smart Charging at the Fast Charging Station		219
10.1	Cost of Premium, Regular, and Economic Charging power	219
10.1.1	Determining the Per Unit Time of the Smart Charging	219
10.1.2	Determining the Per Unit Cost of the Smart Charging	220
10.1.3	The Per Unit Cost of The Premium Charging Power	221

10.1.4	The Per Unit Cost of The Regular Charging Power	222
10.1.5	The Per Unit Cost of The Economic Charging Power.....	222
10.2	Determining the Maximum Charging Cost.....	223
10.3	Determining the Maximum Charging Duration	225
10.4	FCS Data	225
10.5	Modelling of Per Event Energy Demand from the FCS	226
10.6	Modelling of Annual Energy Demand from the FCS	228
10.7	Computing the Cost of Smart Charging.....	231
10.7.1	Computing the Rebates	231
10.7.2	Computing the Revenue.....	234
10.8	Comparison of Rebate and Revenue	237
10.9	Results and Discussions	242
10.9.1	Per Unit Time and Per Unit Cost of the Smart Charging.....	242
10.9.2	Effect of Charging Power on Charging Duration and Charging Cost	243
10.9.3	Descriptive Statistics of Annual Data for Multiple FCSs.....	247
10.9.4	Average Annual Energy Required from FCS	248
10.9.5	Fast Charging Station Annual Revenue and Rebate	250
10.9.6	Cost Comparison of the Proposed Smart Charging and DSTATCOM	255
Chapter 11.	Conclusion and Future Work.....	259
11.1	Summary and Conclusions.....	259
11.2	Research Contributions of the Thesis.....	264
11.3	Future Work	265
Bibliography	267
Appendices		290
Appendix A.		290
A1.	IEEE 123-Bus Standard Test Distribution System Data	290
Appendix B.		300
B1.	Secondary Distribution System Data	300

LIST OF TABLES

TABLE 2-1 DIFFERENT CHARGING LEVELS AND THEIR CHARACTERISTICS [50]	9
TABLE 2-2 KEY POINTS OF DIFFERENCES IN THE SURVEYED WORKS	23
TABLE 2-3 KEY POINTS OF DIFFERENCES IN THE SURVEYED WORKS (CONTINUED).....	24
TABLE 3-1 PHASING-OUT OF INCANDESCENT LAMPS [99].....	27
TABLE 3-2 COMPARISON OF DIFFERENT TYPES OF LAMPS.....	31
TABLE 3-3 COST COMPARISON OF DIFFERENT TYPES OF LAMPS	33
TABLE 3-4 FLICKER PARAMETERS USING GE CURVE [113].....	42
TABLE 3-5 COMPATIBILITY LEVELS FOR PST AND PLT IN LV VOLTAGE POWER SYSTEM [116]	43
TABLE 3-6 LAMP FLICKER RESPONSE AND IMMUNITY LEVEL.....	45
TABLE 3-7 INCANDESCENT FILAMENT LAMPS FLICKER CHARACTERISTICS [119]	46
TABLE 3-8 DISCHARGE LAMPS FLICKER CHARACTERISTICS [108], [120]	46
TABLE 3-9 HIGH-INTENSITY DISCHARGE LAMPS FLICKER CHARACTERISTICS [119]	47
TABLE 3-10 FLICKER CHARACTERISTICS OF LED TECHNOLOGY [123], [124]	49
TABLE 3-11 STROBOSCOPIC/FLICKER CHARACTERISTICS OF LED/OLED TECHNOLOGY [123], [124]	50
TABLE 4-1 COMPARISON OF DIFFERENT VOLTAGE FLUCTUATION MITIGATION DEVICES [94], [148], [152]–[154]	69
TABLE 4-2 MAINTENANCE COST FOR FLICKER MITIGATION DEVICES.....	73
TABLE 4-3 COST OF VOLTAGE FLUCTUATION MITIGATING DEVICES.....	74
TABLE 4-4 ADVANTAGES AND DISADVANTAGES OF DIFFERENT TYPES OF COMPENSATING DEVICES	75
TABLE 4-5 COMPARISON OF DIFFERENT VOLTAGE MITIGATING DEVICES.....	77
TABLE 4-6 WEIGHTING OF THE COMPARATORS IN TABLE 4-5.....	78
TABLE 4-7 GRADING OF THE SELECTED MITIGATION DEVICES	78
TABLE 5-1 POWER SUBSYSTEMS AND THEIR VOLTAGE LEVELS	84
TABLE 6-1 CLASSIFICATION OF CLIMATE ZONES.....	101
TABLE 6-2 RESIDENTIAL WEEKLY PEAKS IN CLIMATE ZONE 4C	109
TABLE 6-3 RESIDENTIAL DAILY PEAKS IN CLIMATE ZONE 4C	110
TABLE 6-4 RESIDENTIAL HOURLY PEAK IN CLIMATE ZONE 4C.....	110
TABLE 6-5 COMPARISON BETWEEN WEEKDAY PROFILES IN CLIMATE ZONE 4C AND THE REST OF CLIMATE ZONES USING PMEI AND PTE.....	112
TABLE 6-6 COMPARISON BETWEEN WEEKEND PROFILES IN CLIMATE ZONE 4C AND THE REST OF CLIMATE ZONES USING PMEI AND PTE.....	113
TABLE 6-7 WEEKLY PEAK LOAD IN PERCENT OF ANNUAL PEAK FOR COMMERCIAL LOADS IN CLIMATE ZONE 4C	114
TABLE 6-8 WEEKLY PEAK LOAD IN PERCENT OF ANNUAL PEAK FOR COMMERCIAL LOADS IN CLIMATE ZONE 4C	114
TABLE 6-9 HOURLY PEAK LOAD FOR LARGE OFFICE IN PERCENT OF ANNUAL PEAK FOR COMMERCIAL LOADS IN CLIMATE ZONE 4C	115
TABLE 6-10 HOURLY PEAK LOAD FOR WAREHOUSE IN PERCENT OF ANNUAL PEAK FOR COMMERCIAL LOADS IN CLIMATE ZONE 4C	116
TABLE 6-11 COMPARISON BETWEEN WEEKDAY PROFILES FOR WAREHOUSE IN CLIMATE ZONE 4C AND THE REST OF CLIMATE ZONES USING PMEI AND PTE	116
TABLE 6-12 COMPARISON BETWEEN WEEKEND PROFILES FOR WAREHOUSE IN CLIMATE ZONE 4C AND THE REST OF CLIMATE ZONES USING PMEI AND PTE	118
TABLE 7-1 PBEV SPECIFICATION AND MARKET SHARES USED IN THIS STUDY	129
TABLE 7-2 FREQUENCY OF OCCURRENCE AND MEAN SSE VALUES FOR THE WINNING DISTRIBUTIONS.....	133
TABLE 7-3 CHARGE EVENTS AND MAXIMUM OUTPUT POWER OF FCSS UTILIZED IN THIS WORK.....	142
TABLE 8-1 LOCATIONS AND NUMBERS OF FCSS	160
TABLE 8-2 THE MAXIMUM VOLTAGE UNBALANCE ENCOUNTERED FOR EACH SCENARIO	175
TABLE 8-3 STATISTICS FOR VOLTAGE FLUCTUATION AND LIGHT FLICKER INDICES (FIRST AND SECOND SCENARIOS).....	177

TABLE 8-4 STATISTICS FOR VOLTAGE FLUCTUATION AND LIGHT FLICKER INDICES (THIRD AND FOURTH SCENARIOS).....	178
TABLE 9-1 NUMBER OF PBEVs CHARGING VIA FAST CHARGING STATION.....	208
TABLE 9-2 COMPARISON OF THE PREVIOUS WORK AND PROPOSED METHOD ACCORDING TO THEIR CHARGING TYPE AND EFFECT ON LIGHT FLICKER.....	216
TABLE 9-3 IMPACT OF CHARGING METHOD AND TYPE [251]	216
TABLE 9-4 COMPARISON OF THE PREVIOUS WORK AND PROPOSED METHOD ACCORDING TO FLICKER LEVEL.....	218
TABLE 10-1 MAX., MIN., AND QUANTILE ANNUAL ENERGY REQUIRED BY DIFFERENT PENETRATION LEVELS OF THE PROPOSED SMART CHARGING	250
TABLE A-1 THREE-PHASE SWITCH POSITIONS	290
TABLE A-2 OVERHEAD LINE CONFIGURATION DATA.....	290
TABLE A-3 UNDERGROUND LINE CONFIGURATION DATA	290
TABLE A-4 PRIMARY TRANSFORMER DATA.....	291
TABLE A-5 SHUNT CAPACITORS DATA	291
TABLE A-6 REGULATOR DATA.....	291
TABLE A-7 SPORT LOAD DATA	291
TABLE A-8 SPORT LOAD DATA	292
TABLE A-9 SPORT LOAD DATA	293
TABLE A-10 LINE SEGMENT DATA	294
TABLE A-11 LINE SEGMENT DATA	295
TABLE A-12 LINE SEGMENT DATA	296
TABLE B-1 SECONDARY DISTRIBUTION TRANSFORMER DATA	300
TABLE B-2 SECONDARY TYPE AND CONDUCTOR DATA	300

LIST OF FIGURES

FIGURE 1.1 CARBON EMISSION FROM FOSSIL FUEL COMBUSTION IN THE TRANSPORTATION WORLDWIDE AND IN THE U.S.....	2
FIGURE 1.2 PRICES OF A GALLON OF GASOLINE AND BARREL OF CRUDE OIL	3
FIGURE 2.1 SHOWS DIFFERENT ASPECTS UTILIZED TO STRUCTURE THE CURRENT CHAPTER.....	8
FIGURE 3.1 CLASSIFICATION OF LIGHT SOURCES [94].....	25
FIGURE 3.2 EVOLUTION OF LIGHTING EFFICACY [95]	26
FIGURE 3.3 MARKET SHARE OF MAGNETIC AND ELECTRONIC BALLASTS [103]	29
FIGURE 3.4 RATED LIFETIME OF DIFFERENT TYPES OF LAMPS	32
FIGURE 3.5 AVERAGE PRICE, WATTS, AND EFFICACY OF TRADITIONAL AND LED LAMPS.....	33
FIGURE 3.6 FORECAST OF COMMERCIAL LAMPS STOCKED BY TECHNOLOGY	34
FIGURE 3.7 LED FORECAST IN U.S	35
FIGURE 3.8 FORECAST OF ENERGY SAVINGS IN LED TECHNOLOGY IN IN U.S. MARKET	35
FIGURE 3.9 FLICKER INDEX CALCULATION USING THE LIGHT OUTPUT	37
FIGURE 3.10 FLICKER PERCENT CALCULATION USING THE LIGHT OUTPUT	38
FIGURE 3.11 GE FLICKER CURVE [113]	41
FIGURE 3.12 PICTURES OF VARIOUS LEDs UTILIZED IN TABLE 3-10 [122]	48
FIGURE 4.1 LAYOUT OF THIS CHAPTER.....	52
FIGURE 4.2 CLASSIFICATION OF VOLTAGE FLUCTUATION MITIGATION DEVICES [129]	55
FIGURE 4.3 SCHEMATIC DIAGRAM OF TSC COMPENSATOR [129]	57
FIGURE 4.4 SCHEMATIC DIAGRAM OF FC/TCR COMPENSATOR [94]	58
FIGURE 4.5 A BLOCK SCHEME OF AN SVC CONTROLLER [143]	63
FIGURE 4.6 A DSTATCOM DIAGRAM [142].....	64
FIGURE 4.7 A BLOCK SCHEME OF A DVR CONTROLLER [145].....	65
FIGURE 4.8 A BLOCK DIAGRAM OF UPQC [146]	66
FIGURE 4.9 A SATURATED REACTOR [148]	67
FIGURE 4.10 CIRCUIT WITHOUT (A) AND WITH (B)SERIES CAPACITOR [132].....	68
FIGURE 4.11 DSTATCOM INSTALLED AT BUS $n+1$	80
FIGURE 5.1 A SINGLE-LINE DIAGRAM OF A DISTRIBUTION SUBSTATION SHOWN BASIC COMPONENTS [168].....	86
FIGURE 5.2 FRONT VIEW FOR THE CHAdeMO CHARGER	94
FIGURE 5.3 GENERIC SERIES MODEL OF DISTRIBUTION FEEDER COMPONENT	95
FIGURE 5.4 BASIC FLOWCHART SHOWS THE FORWARD/BACKWARD SWEEP PROCEDURE	97
FIGURE 6.1 AVERAGE WEEKDAY LOAD PROFILE IN MAY	100
FIGURE 6.2 NUMBER OF CITIES IN EACH CLIMATE ZONE.....	104
FIGURE 6.3 TOTAL VARIANCE EXPLAINED BY THE FIRST TWO PRINCIPAL COMPONENTS.....	105
FIGURE 6.4 VARIATIONS OF PEAK VALUES AND TIMES FOR RESIDENTIAL LOADS IN DIFFERENT CLIMATE ZONES	111
FIGURE 6.5 VARIATIONS OF PEAK VALUES AND TIME FOR LARGE OFFICE LOADS IN DIFFERENT CLIMATE ZONES.....	117
FIGURE 6.6 VARIATIONS OF PEAK VALUES AND TIME FOR WAREHOUSE LOADS IN DIFFERENT CLIMATE ZONES	118
FIGURE 6.7 VARIANCE OF FIRST PRINCIPLE COMPONENT FOR COMMERCIAL PROFILE	120
FIGURE 6.8 CLUSTER ASSESSMENT FOR RESIDENTIAL LOAD PROFILE IN CLIMATE ZONE 4C	120
FIGURE 6.9 CLUSTER ASSESSMENT FOR SUPERMARKET LOAD PROFILE IN CLIMATE ZONE 4C.....	121
FIGURE 6.10 FREQUENCY OF OCCURRENCE OF LOAD PROFILE LOCATED IN CLIMATE ZONE 4C	122
FIGURE 6.11 MAX., MIN., AND QUANTILE VALUES OF THE RESIDENTIAL CLUSTERS IN CLIMATE ZONE 4C	123
FIGURE 6.12 MAX., MIN., AND QUANTILE VALUES OF THE COMMERCIAL (SUPERMARKET) CLUSTERS IN CLIMATE ZONE 4C.....	124
FIGURE 6.13 MAX., MIN., AND QUANTILE VALUES FOR THE RESIDENTIAL LOAD	124
FIGURE 6.14 MAX., MIN., AND QUANTILE VALUES FOR THE COMMERCIAL LOAD	125
FIGURE 7.1 PBEVS SALES AND THEIR SHARE IN THE CANADIAN MARKET [208]	128
FIGURE 7.2 PBEVS BATTERY CAPACITIES AND THEIR DRIVING RANGES [210].....	129

FIGURE 7.3 DAILY DISTANCE TRAVELLED DISTRIBUTION BASED ON 568 DRIVING DAYS	132
FIGURE 7.4 DAILY DISTANCE TRAVELLED UTILIZED TO VERIFY THE PROPOSED APPROACH [210].....	134
FIGURE 7.5 DISTRIBUTION OF VEHICLE ARRIVAL TIME AT FCS PRIOR TO CHARGE [221]	145
FIGURE 7.6 BATTERY STATE OF CHARGE AT END OF CHARGING FROM HOME CHARGER PRIOR TO DRIVING [222]	146
FIGURE 7.7 DAILY DISTANCE TRAVELLED DISTRIBUTION [211].....	146
FIGURE 7.8 A TYPICAL OUTPUT OF FCS WHEN IT CHARGES A DEPLETED CHEVY BOLT [223].....	149
FIGURE 7.9 DISTRIBUTION OF LENGTH OF TIME WITH A VEHICLE DRAWING POWER FROM FCS PER CHARGING EVENT [222]	
.....	150
FIGURE 8.1 IEEE 123-NODE TEST FEEDER [224]	155
FIGURE 8.2 LAYOUT OF SECONDARY DISTRIBUTION CIRCUITS USED TO SUPPLY RESIDENTIAL HOMES.....	158
FIGURE 8.3 SAMPLE OF THREE-PHASE SECONDARY LOADS CONNECTED TO THE PRIMARY FEEDER	159
FIGURE 8.4 MINIMUM AND MAXIMUM VOLTAGE EXPERIENCED BY EACH PRIMARY NODE WHEN ONLY FCSs ARE CONNECTED (FIRST SCENARIO)	167
FIGURE 8.5 VOLTAGE WAVEFORM MEASURED AT PCC AT NODE 65 WHEN ONLY FCSs ARE CONNECTED (FIRST SCENARIO)	168
FIGURE 8.6 VOLTAGE WAVEFORM MEASURED AT PCC AT NODE 65 WHEN FCSs ARE EQUIPPED BESUS IN DISCHARGING MODE ONLY (SECOND SCENARIO).....	170
FIGURE 8.7 VOLTAGE WAVEFORM MEASURED AT PCC AT NODE 65 WHEN FCSs ARE EQUIPPED WITH BESUS IN DISCHARGING AND CHARGING MODES (THIRD SCENARIO)	172
FIGURE 8.8 VOLTAGE WAVEFORM MEASURED AT PCC AT NODE 65 WHEN FCSs ARE CONNECTED AND D-STATCOMs ARE PLACED IN THE PRIMARY SYSTEM (FOURTH SCENARIO)	173
FIGURE 8.9 MINIMUM AND MAXIMUM VOLTAGE EXPERIENCED BY EACH PRIMARY NODE WHEN FCSs ARE CONNECTED AND D- STATCOMs ARE PLACED IN THE PRIMARY SYSTEM (FOURTH SCENARIO)	174
FIGURE 8.10 PERCENTILE LONG TERM (PLT) FLICKER SEVERITY INDEX CORRESPONDING TO THE FIRST SCENARIO.....	179
FIGURE 8.11 PERCENTILE SHORT TERM (PST) FLICKER SEVERITY INDEX CORRESPONDING TO THE FIRST SCENARIO	179
FIGURE 8.12 PERCENTILE LONG TERM (PLT) FLICKER SEVERITY INDEX CORRESPONDING TO THE FOURTH SCENARIO.....	180
FIGURE 8.13 PERCENTILE SHORT TERM (PST) FLICKER SEVERITY INDEX CORRESPONDING TO THE FOURTH SCENARIO	180
FIGURE 9.1 CHARGING EVENTS BY LOCATIONS [211].....	185
FIGURE 9.2 PERCENT OF PBEVs ARRIVING PER HOUR AT THE FAST CHARGING STATION (ARRIVAL RATE) [221]	186
FIGURE 9.3 NISSAN BATTERY STATE OF CHARGE AT THE STARTING OF CHARGING EVENTS [233]	187
FIGURE 9.4 CHEVROLET BATTERY STATE OF CHARGE AT THE STARTING OF CHARGING EVENTS [233].....	187
FIGURE 9.5 AVERAGE BATTERY STATE OF CHARGE AT THE STARTING OF CHARGING EVENTS AT FCS.....	188
FIGURE 9.6 DISTRIBUTION OF LENGTH OF TIME WITH A VEHICLE DRAWING POWER FROM FCS PER CHARGING EVENT [222]	
.....	189
FIGURE 9.7 BATTERY STATE OF CHARGE AT END OF CHARGING FROM FCS PRIOR TO DRIVING.....	190
FIGURE 9.8 DISTRIBUTION OF LENGTH OF TIME WITH A VEHICLE CONNECTED TO FCS PER CHARGING EVENT [222]	191
FIGURE 9.9 FLICKER CURVES FOR INCANDESCENT LIGHT [130]	203
FIGURE 9.10 DAILY DEMAND PER EACH CHARGING POWER IN FCS	210
FIGURE 9.11 COMPARISON OF FLICKER LEVEL FOR THE UNCONTROLLED AND PROPOSED SMART CHARGING.....	211
FIGURE 9.12 FLICKER LEVEL WHEN THE PENETRATION ON THE PROPOSED SMART CHARGING INCREASES	213
FIGURE 9.13 CHARGING DURATION TO INCREASE BATTERY SOC FROM 20% TO 80% USING THE SMART AND UNCONTROLLED CHARGING.....	215
FIGURE 9.14 COMPARISON OF SMART CHARGING AND SERVICES PROVIDED TO THE GRID [252].....	218
FIGURE 10.1 REQUIRED TIME AND COST TO CHARGE 1KWH BY THE SMART CHARGING	244
FIGURE 10.2 REQUIRED TIME AND COST TO CHARGE 25KWH BY THE SMART CHARGING	245
FIGURE 10.3 REQUIRED TIME AND COST TO ADD 70% SOC INTO BOLT EV BATTERY.....	246
FIGURE 10.4 REQUIRED TIME AND COST TO ADD 70% SOC INTO LEAF EV BATTERY.....	246
FIGURE 10.5 REQUIRED TIME AND COST TO ADD 70% SOC INTO TESLA MODEL S BATTERY	247
FIGURE 10.6 A BOXPLOT OF THE ENERGY DEMAND ON FCS PER CHARGING EVENT IN A YEAR.....	248
FIGURE 10.7 NUMBER OF ANNUAL CHARGING EVENTS FOR DIFFERENT FCSs	248

FIGURE 10.8 THE ENERGY REQUIRED PER CHARGING EVENT AND THE AVERAGE NUMBERS OF EVENTS.....	249
FIGURE 10.9 REVENUE AND REBATE OF THE MINIMUM ANNUAL CHARGING ENERGY.....	253
FIGURE 10.10 REVENUE AND REBATE OF THE 25 TH PERCENTILE ANNUAL CHARGING ENERGY.....	254
FIGURE 10.11 REVENUE AND REBATE OF THE MEDIAN ANNUAL CHARGING ENERGY.....	254
FIGURE 10.12 REVENUE AND REBATE OF THE 75 TH PERCENTILE ANNUAL CHARGING ENERGY.....	255
FIGURE 10.13 REVENUE AND REBATE OF THE MAXIMUM ANNUAL CHARGING ENERGY.....	255
FIGURE 10.14 EFFECT OF VOLTAGE FLUCTUATIONS ON DIFFERENT STAKEHOLDERS.....	256
FIGURE 10.15 ANNUAL COST OF THE PROPOSED SMART CHARGING.....	257
FIGURE 10.16 COMPARISON OF COSTS OF THE PROPOSED SMART CHARGING AND DSTATCOM.....	258

LIST OF ABBREVIATIONS AND SYMBOLS

Acronyms

FCSs	Fast charging stations
EVs	Electric vehicles
PHEVs	Plug-in hybrid electric vehicles
HEVs	Hybrid electric vehicles
PBEVs	Plug-in battery electric vehicles
SVCs	Static var compensators
TSCs	Thyristor switched capacitors
FC/TCRs	Fixed capacitors/thyristor-controlled reactors
DSTATCOMs	Distribution static compensators
DVRs	Dynamic voltage restorers
UPQCs	Unified power quality conditioners
BESUs	Battery energy storage units
SCs	Synchronous condensers
VRs	Voltage regulators
ILs	Incandescent lamps
HLs	Halogen lamps
DLs	Discharge lamps
FLs	Fluorescent lamps
CFLs	Compact fluorescent lamps
LEDs	Light-emitting diodes
OLEDs	Organic light-emitting diodes
APTm	Average power time mismatch
ASC	Average silhouette coefficient
AWG	American wire gage
PCA	Principle component analysis
MCMC	Markov chain Monte Carlo
MCS	Monte Carlo simulation
SDF	Standard distribution function
ANSI	The American national standard
SOC	State-of-charge
SSE	Sum of squares error

Indices

i^{th}	Index of hours
d^{th}	Index for a day number

g_t	Index for clusters
b^{th}	Index for climate zones
C^{th}	Index for cities
i	Index for FCS, $i = 1, 2, \dots, f$
f	Total number of considered fess

Parameters

Λ^y	The total annual equivalent cost, $\$/year$
\mathbb{C}^y	The annual equivalent cost of capital invested, $\$/year$
\mathcal{M}^y	The annual equivalent cost of maintenance, $\$/year$
ζ	The first cost of installed flicker mitigation device, $\$$
\mathcal{S}	The estimated salvage value at the end of the device useful life, $\$$
μ'	The capital recovery factor
ℓ'	The single-payment discount factor
λ	The fixed charge rate, %
η	The useful life in years (flicker mitigation device lifetime), years
Γ	The cost per unit of installed flicker mitigation device, $\$/kVAr$
Ω	The salvage value per kvar at the end of η , $\$/kVAr$
φ	The operating range of the flicker mitigation device, $MVAr$
Γ_{UPQC}	The per unit cost of the Unified Power Quality Conditioner, $(\$/kVAr)$
$\Gamma_{DSTATCOM}$	The per unit cost of the Distribution Static Compensator, $(\$/kVAr)$
Γ_{TSC}	The per unit cost of the Thyristor Switched Capacitor, $(\$/kVAr)$
Γ_{FCTCR}	The per unit cost of the Fixed Capacitors/Thyristor Controlled Reactors, $(\$/kVAr)$
Γ_{DVR}	The per unit cost of the Dynamic Voltage Restorer, $(\$/kVAr)$
Γ_{FSC}	The per unit cost of the Fixed Series Capacitor, $(\$/kVAr)$
φ_{UPQC}	The operating range of the Unified Power Quality Conditioner, $MVAr$
$\varphi_{DSTATCOM}$	The operating range of the Distribution Static Compensator, $MVAr$
φ_{TSC}	The operating range of the Thyristor Switched Capacitor, $MVAr$
φ_{FCTCR}	The operating range of the Fixed Capacitors/Thyristor Controlled Reactors, $MVAr$
φ_{DVR}	The operating range of the Dynamic Voltage Restorer, $MVAr$
φ_{FSC}	The operating range of the Fixed Series Capacitor, $MVAr$
γ	The maintenance cost in percent of the first cost, (%)
\mathcal{N}^{BPEV}	Number of electric vehicles in the system
x^{pen}	Share of electric vehicles with respect to the total number of vehicles in the system, 10% - 50%
n^{house}	Number of residential houses in the system, 750 houses
n^{car}	Number of vehicles per house, 2 vehicles/house
kWh^{FCS}	Energy required for vehicle v from FCS, kwh

L^{FCS}	Length of time with vehicle v connected to the fast charger, minute
μ^v	Battery capacity of vehicle v , kwh
η^{FCS}	Efficiency of the fast charger, %
ϑ	Factor to convert hour into minutes
β_t^p	Premium charging power, kw
β_t^r	Regular charging power, kw
β_t^e	Economic charging power, kw
\mathcal{N}_t^p	Number of PEV that charging using premium charging power at time t
\mathcal{N}_t^r	Number of PEV that charging using regular charging power at time t
\mathcal{N}_t^e	Number of PEV that charging using economic charging power at time t
β	Maximum charging power per port, kw
\bar{p}	Factor to set the upper limits of premium charging power, %
\underline{p}	Factor to set the lower limits of premium charging power, %
\bar{r}	Factor to set the upper limits of regular charging power, %
\underline{r}	Factor to set the lower limits of regular charging power, %
\bar{e}	Factor to set the upper limits of economic charging power, %
\underline{e}	Factor to set the lower limits of economic charging power, %
\mathcal{N}^{PBEV}	Number of PBEV in the system
Λ^{FCS}	Share of PBEV that uses FCS, $p. u.$
η^s	Share of PBEV with small battery capacity s charges at the FCS at time t , $p. u.$
η^m	Share of PBEV with medium battery capacity m charges at the FCS at time t , $p. u.$
η^l	Share of PBEV with large battery capacity l charges at the FCS at time t , $p. u.$
$\alpha_{t,bc,p}^{de}$	Share of PBEV that have battery capacity bc charged using premium charging power at FCS at time t and required departure time of de , $p. u.$
$\alpha_{t,bc,r}^{de}$	Share of PBEV that have battery capacity bc charged using regular charging power at time t and required departure time of de , $p. u.$
$\alpha_{t,bc,e}^{de}$	Share of PBEV that have battery capacity bc charged using economic charging power at time t and required departure time of de , $p. u.$
\mathcal{V}_{FCS}^s	Number of PEV with small battery capacity uses the FCS
\mathcal{V}_{FCS}^m	Number of PEV with medium battery capacity uses the FCS
\mathcal{V}_{FCS}^l	Number of PEV with large battery capacity uses the FCS
\mathcal{L}^{ports}	Number of ports in the fast charging station
$\mathcal{V}_{FCS,p}^v$	A set of PEVs uses the premium charging power
$\mathcal{V}_{FCS,r}^v$	A set of PEVs uses the regular charging power
$\mathcal{V}_{FCS,e}^v$	A set of PEVs uses the economic charging power
soc_t^v	State-of-charge of vehicle v at time t , %
soc_{t-1}^v	State-of-charge of vehicle v at time $t - 1$, %
μ^v	Battery capacity of vehicle v , kwh

ϑ	Factor to convert hour into minutes
μ^s	Capacity of small battery, <i>kwh</i>
μ^m	Capacity of medium battery, <i>kwh</i>
μ^l	Capacity of large battery, <i>kwh</i>
$soC_{des,p}^v$	Desired state-of-charge at the departure time t_v^{de} Of vehicle v charging by premium power, %
$soC_{des,r}^v$	Desired state-of-charge at the departure time t_v^{de} Of vehicle v charging by regular power, %
$soC_{des,e}^v$	Desired state-of-charge at the departure time t_v^{de} Of vehicle v charging by economic power, %
$soC_{t,p}^v$	State-of-charge of vehicle v charging by premium power at time t , %
$soC_{t,r}^v$	State-of-charge of vehicle v charging by regular power at time t , %
$soC_{t,e}^v$	State-of-charge of vehicle v charging by economic power at time t , %
t_v^{de}	The departure time of vehicle v
Γ	Relative voltage changes caused by FCS at point-of-common, %
$\Delta \mathcal{U}$	Voltage variation at point-of-common coupling, <i>kV</i>
\mathcal{U}_{pcc}	Nominal voltage at point-of-common, <i>kV</i>
ΔS	Apparent power variation at point-of-common coupling, <i>kVA</i>
$\Delta \mathfrak{P}$	Active power load change at point-of-common coupling, <i>kw</i>
$\Delta \mathfrak{Q}$	Reactive power load change at point-of-common coupling, <i>kVAr</i>
ΔI	Current load change at point-of-common coupling, <i>Amp</i>
θ	Network impedance angle, degree
χ_{pcc}	Network reactance at point-of-common, ohms
r_{pcc}	Network resistance at point-of-common, ohms
\mathcal{F}	Flicker time represents the flicker impression of a single voltage change, second
φ	Factor represents the waveform shape of voltage fluctuation, rectangular change
ℓ	Factor to comply with the flicker curve (Figure 9.8)
γ	Coefficient to describe the source of disturbance
ξ	Summation of all flicker times, minute
Ω	Number of voltage dips per minute
ζ	Total time interval of all flicker times, second
\mathcal{T}^p	The time it takes to charge 1kwh by premium power, (<i>min./kwh</i>)
\mathcal{T}^r	The time it takes to charge 1kwh by regular power, (<i>min./kwh</i>)
\mathcal{T}^e	The time it takes to charge 1kwh by economic power, (<i>min./kwh</i>)
Γ^p	The per unit cost of the premium charging, (<i>\$/kwh</i>)
Γ^r	The per unit cost of the regular charging, (<i>\$/kwh</i>)
Γ^e	The per unit cost of the economic charging, (<i>\$/kwh</i>)
\mathfrak{h}	The per hour PBEV Fast charging cost, (<i>\$/h</i>)
\mathcal{C}	The per minutes PBEV Fast charging cost, (<i>\$/min.</i>)

C^{max}	The maximum cost of charging a PBEV from FCS, \$
Γ^{FCS}	The per unit cost of fast charging, \$/kwh
SoC^{max}	The maximum allowable SOC for any PBEV, <i>p. u.</i>
SoC^{min}	The minimum allowable SOC for any PBEV, <i>p. u.</i>
$\bar{\ell}$	A percent to determine the maximum SOC, <i>p. u.</i>
$\underline{\ell}$	A percent to determine the minimum SOC, <i>p. u.</i>
μ^v	Capacity of a PBEV battery, <i>kwh</i>
μ^s	Capacity of a small battery, <i>kwh</i>
μ^m	Capacity of a medium battery, <i>kwh</i>
μ^l	Capacity of a large battery, <i>kwh</i>
\mathcal{V}_s^{FCS}	A set of PEVs with small battery capacity uses the FCS
\mathcal{V}_m^{FCS}	A set of PEVs with medium battery capacity uses the FCS
\mathcal{V}_l^{FCS}	A set of PEVs with large battery capacity uses the FCS
\mathbb{T}^{max}	The maximum time it takes a PBEV to be charged, from its minimum to its maximum state-of-charge, using FCS, (<i>min.</i>)
\mathcal{J}^{FCS}	The per unit time it takes to charge a PBEV, from its minimum to its maximum state-of-charge, using FCS, (<i>min./kwh</i>)
\underline{q}_i	The 25th percentile of charging energy per charging event of FCS <i>i</i> in a year, (<i>kwh</i>)
q_i	The 50th percentile of charging energy per charging event of FCS <i>i</i> in a year, (<i>kwh</i>)
\bar{q}_i	The 75th percentile of charging energy per charging event of FCS <i>i</i> in a year, (<i>kwh</i>)
ul_i^{max}	The maximum of charging energy per charging event of FCS <i>i</i> in a year, (<i>kwh</i>)
ul_i^{min}	The minimum of charging energy per charging event of FCS <i>i</i> in a year, (<i>kwh</i>)
\underline{Q}	The average value of the first quartile of charging energy per charging event in a year, for <i>f</i> number of fcss, (<i>kwh/event</i>)
Q	The average value of the second quartile of charging energy per charging event in a year, for <i>f</i> number of fcss, (<i>kwh/event</i>)
\bar{Q}	The average value of the third quartile of charging energy per charging event in a year, for <i>f</i> number of fcss, (<i>kwh/event</i>)
UL^{max}	The average value of the maximum of charging energy per charging event in a year, for <i>f</i> number of fcss, (<i>kwh/event</i>)
LL^{min}	The average value of the minimum of charging energy per charging event in a year, for <i>f</i> number of fcss, (<i>kwh/event</i>)
$\bar{\varepsilon}$	The average number of annual charging events in <i>f</i> number of fcss, (<i>event/year</i>)
ε_i	The number of annual charging events in FCS <i>i</i>
\underline{U}	The estimated 25th percentile value of annual charging energy for a FCS, (<i>kwh/year</i>)
U	The estimated 50th percentile value of annual charging energy for a FCS, (<i>kwh/year</i>)
\bar{U}	The estimated 75th percentile value of annual charging energy for a FCS, (<i>kwh/year</i>)
U_{max}	The estimated maximum value of annual charging energy for a FCS, (<i>kwh/year</i>)

U_{min}	The estimated minimum value of annual charging energy for a FCS, ($kwh/year$)
\underline{C}^{Reb}	The 25 th percentile annual rebate paid to customers for using smart charging power, ($\$/year$)
\bar{C}^{Reb}	The median annual rebate paid to customers for using smart charging power, ($\$/year$)
\underline{C}^{Reb}	The 75 th percentile annual rebate paid to customers for using smart charging power, ($\$/year$)
C_{max}^{Reb}	The maximum annual rebate paid to customers for using smart charging power, ($\$/year$)
C_{min}^{Reb}	The minimum annual rebate paid to customers for using smart charging power, ($\$/year$)
r	A uniform random number
η^{sm}	Share of PBEV that utilize smart charging power at FCS, $p. u.$
$\underline{\mathcal{R}}^{Rev}$	The 25 th percentile annual revenue from customers for using smart charging power, ($\$/year$)
$\bar{\mathcal{R}}^{Rev}$	The median annual revenue from customers for using smart charging power, ($\$/year$)
$\underline{\mathcal{R}}^{Rev}$	The 75 th percentile annual revenue from customers for using smart charging power, ($\$/year$)
\mathcal{R}_{max}^{Rev}	The maximum annual revenue from customers for using smart charging power, ($\$/year$)
\mathcal{R}_{min}^{Rev}	The minimum annual revenue from customers for using smart charging power, ($\$/year$)
$\mathcal{R}^{Rev,r}$	Revenue from a customer when the regular charging power is utilized, $\$$
$C^{Reb,r}$	Rebate paid to a customer when the regular charging power is utilized, $\$$
p^{op}	Optimal factor to set the limit of premium charging power, $p. u.$
r^{op}	Optimal factor to set the limit of regular charging power, $p. u.$
$\mathcal{R}^{Rev,e}$	Revenue from a customer when the economic charging power is utilized, $\$$
$C^{Reb,e}$	Rebate paid to a customer when the economic charging power is utilized, $\$$
SSE	Sum of squares error,
$APTM$	Average power time mismatch,
ASC	The average silhouette coefficient
$PMEI$	The Peak Magnitude Error Index, %
PTE	The Peak Time Error, hour
$MAPE$	The Mean Absolute Percentage Error, %

Variables

$l^n + j\zeta^n$	Line impedance between buses n and $n+1$, ohm
$i^n \angle \alpha$	Line current flows out of bus n after DSTATCOM installed, ampere
$i^{DSTATCOM}$	Current injected by DSTATCOM, ampere
$\angle \left(\vartheta^{n+1} + \frac{\pi}{2} \right)$	Phase angle of current injected by DSTATCOM, degree
$Q^{DSTATCOM}$	Reactive power injected by the DSTATCOM, kvar
$\bar{U}^{n+1} \angle \bar{\vartheta}^{n+1}$	Voltage at bus $n+1$ before DSTATCOM installed, volt

$U^{n+1} \angle \theta^{n+1}$	Voltage at bus $n+1$ after DSTATCOM installed, volt
$U^n \angle \theta^n$	Voltage at bus n after DSTATCOM installed, volt
$P^n + jQ^n$	Constant load connected at bus n , kw+ kvar
$P^{n+1} + jQ^{n+1}$	Constant load connected at bus $n+1$, kw+ kvar
V_n^{itr}	The line-to-neutral voltage of node n in the current iteration, volt
V_n^{itr-1}	The line-to-neutral voltage of node n in the previous iteration, volt
$V_n^{nominal}$	The nominal phase voltage of node n , volt

Chapter 1. Introduction

1.1 Motivation

The number of electric vehicles is growing. According to [1], more than 700 million passenger vehicles existed in the world in 2010 and this number is forecasted to increase to 1.1 billion by 2030 and to 1.5 billion by 2050. In order to meet the energy demand required to use these vehicles, either petroleum production must increase to 200% or automobiles will need to be operated by different means [1]. The first option is not preferable as a long-term solution; this is not only because it will lead to an exhaustion of the world's fossil fuel resources, but it will also increase the pollution caused by Internal Combustions Engines which are used in conventional vehicles. In 2016, nearly 70% of the total petroleum consumed in the United States (US) (13.89 million barrels/per day) [2] were used for transportation with highway vehicles sharing nearly 60%. Figure 1.1 shows the carbon dioxide emissions for the world along with the US in one side and the transportation emissions for the US on the other side. The figure indicates that more than 28% of the transportation emission was produced by the passenger vehicles and trucks on US highways in 2016. Also, the uncertainty of oil prices, as depicted in Figure 1.2, is another motivation in finding alternative means to operate vehicles worldwide. Among the varying technologies (e.g. biofuels, compressed natural gas, hydrogen) that might be utilized to substitute fuel in vehicles, electricity will be a front-runner in powering the fleet of automobiles worldwide. According to [3], by 2040, it is predicted that electric vehicles (EVs) will share 33% of the global fleet and 55% of all new car sales. In

fact, according to statistics, EVs are currently on the road and sales have grown each year. Several factors are attributed to this increase including: an increase in battery capacity, a reduction in battery price, incentives to EVs buyers, and developing infrastructure whether in private (e.g. home charger) or public (commercial charger) places.

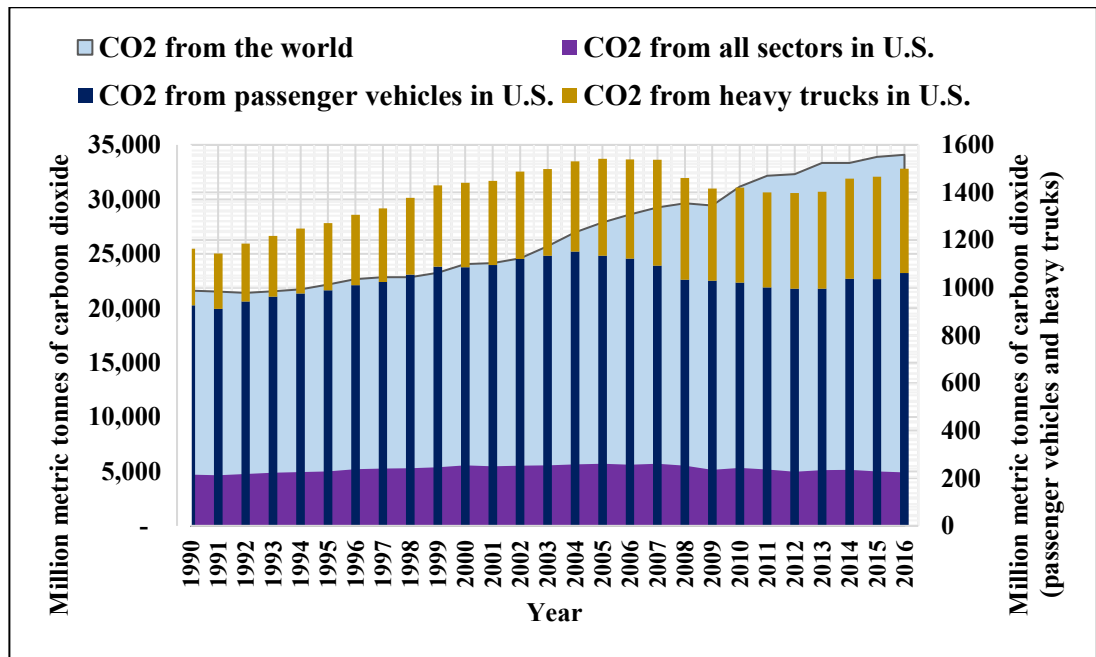


Figure 1.1 Carbon Emission from Fossil Fuel Combustion in the Transportation Worldwide and in the U.S.

Among these factors, public charging stations (e.g. Fast Charging Stations (FCSs)) represent the key in not only increasing the reliability of this new technology, but also in supporting the use of EVs for long-distance travel. FCSs must be supplied with high power relying mainly on the electric power system not only to minimize the charging time required to recharge EVs with large battery capacity, but to also fulfil the needs of other highway EVs. However, FCSs may increase the burden on the electric grids and affecting their voltage quality. In order to address the impact of

FCSs on the electric power distribution system, the following questions related to the stochastic nature of the EV charging process must be taken into consideration: what is the battery capacity of EVs? What is the battery State-Of-Charge (SOC) at its time of arrival? What is the EV time of arrival at the FCS? What is the rated power of the FCS? Admittedly, there is no certain answer for any of the first three questions. As a result, the effect of FCSs on the electric distribution system is quantified probabilistically.

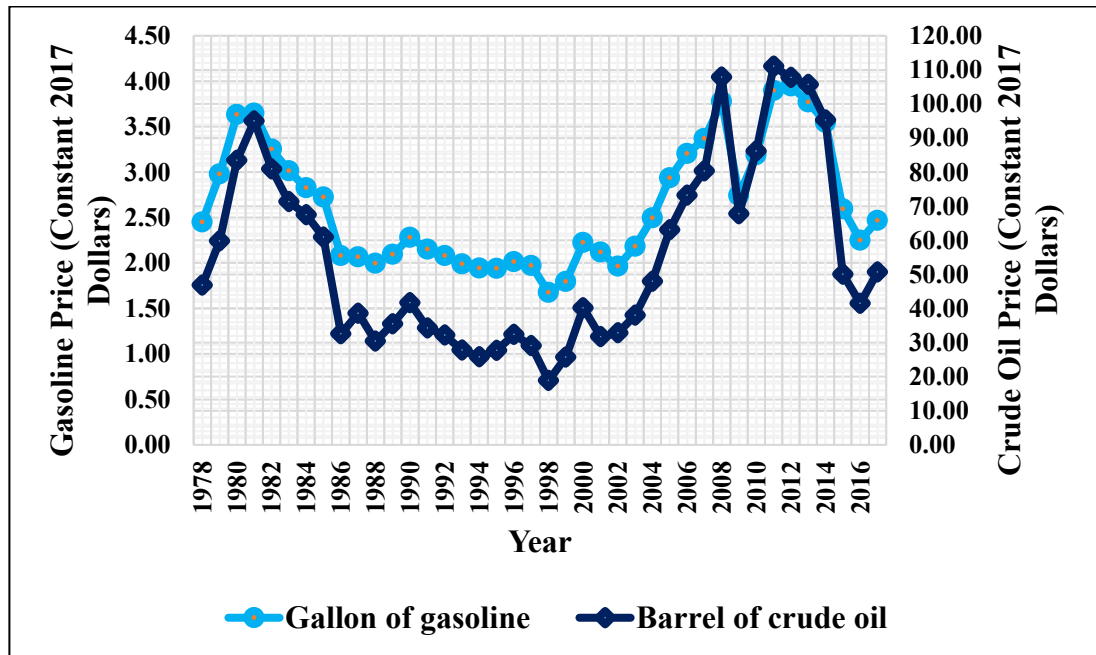


Figure 1.2 Prices of a Gallon of Gasoline and Barrel of Crude Oil

1.2 Problem Statement

From the perspective of stakeholders, FCSs are intended to meet various objectives such as reducing the charging and waiting time of EVs and supporting long-distance trips; with these needs met, the public will be able to rely on and adopt such technology [4]. From the perspective of the distribution power system, EVs are a major challenge due to the uncertainty in their consumption patterns or time of

demand, considering the distribution grid is mainly designed to serve specific patterns of electric power consumption. Although EVs are considered as mobile electric load, their impact on the electric power distribution system varies based on: the period of charging, the instant of charging, and the power drawn from the grid [5]. An FCS requires high power to charge EVs in a short period of time which may inflict stress on the aging electric power distribution system infrastructure currently in place. Most FCSs are connected to the primary distribution system to fulfill the EVs expectation; however, this may lead to potential problems on distribution networks leading to violation to the existing standard. The aim is to investigate the quality of the service voltage in the presence of FCSs in the distribution grids.

1.3 Research Objectives

This main objectives of the research in this these can be outlined as follows:

- Quantify the impact of the FCSs on the voltage fluctuation and light flicker and reduce that impact by mitigation technology selected based on defined criteria.
- Propose a smart charging approach that has three characteristics: able to mitigate the impact of the FCS on the light flicker, able to preserve the balance of customer's value of time and value of cost, and not costly.
- Highlight impact of the FCS on the system when the output power of FCSs are estimated, and when the output power of FCSs are actual.

- Developing probabilistic residential and commercial load profiles at different climate zones whereas these profiles are utilized to represent the base load in the system.

1.4 **Dissertation Outline**

Chapter 2 surveys the previous work related to the impacts of FCSs and outlines the existing techniques used to mitigate such impacts.

Chapter 3 discusses the impacts of voltage fluctuation on the lighting technology.

Chapter 4 introduces and compares different mitigation technologies utilized to reduce the voltage fluctuation and light flicker.

Chapter 5 introduces an overview of the electric power distribution system, starting from the upstream components at the substation down to the customer service line, and the energy storage systems.

Chapter 6 proposes new probabilistic models for two types of loads: commercial and residential loads in different climate zones. These loads are utilized in the electric distribution system under study.

Chapter 7 proposes probabilistic models for two methods of charging: when the power profile of FCS is estimated and when the power profile of FCS is real.

Chapter 8 develops and modifies the test system to encompass fast charging stations, commercial loads, and residential houses. Different scenarios were applied to quantify and mitigate the impact of the FCSs.

Chapter 9 presents the novel smart charging approach to mitigate the voltage fluctuation and light flicker. Also, uncontrolled charging method is modelled and compared with the smart charging.

Chapter 10 proposes a generic cost of the smart charging under different penetrations.

Chapter 11 highlights the key findings, research contributions, and outlines potential future works.

Chapter 2. Literature Review

The aim of this chapter is to survey previous works related to the impact of fast charging station on electric power quality in the electric power distribution systems.

2.1 Introduction

The previous works shed light on EVs and their charging methods. Most of these works focused on the impact of home EV charging stations on the electric power distribution systems and their components [6]–[21]. Some studies looked at the impact of FCSs on electric power distribution systems and their components [20]–[46]. Although home chargers and FCS are connected to the distribution system, their output power varies considerably in favor of FCS. Moreover, FCSs are intended for commercial use and most FCSs are located close to the highways in order to be available to many customers contrary to the home chargers which are private and only used in the homes [22]. Electric vehicles battery packs can be charged with either an on-board or off-board charger. The former method uses low charging power, while the latter method uses high charging power [23]. The aim of this chapter is to survey previous works related to FCSs and their impact on the electric power quality. Several charging methods, their corresponding configurations, and their maximum output power are shown in Table 2-1.

2.2 Fast Charging Station

According to the literature, a FCS can be supplied by an AC power bus [24], DC power bus [25], or hybrid AC-DC power buses [26]. The impact of fast charging stations is generally studied on the electric power distribution system, on the MV

power distribution network as in Europe and most of the world,[27]–[32] and on the LV power distribution network as in North America [33]–[35]. Installing the FCS in LV is preferable because it will reduce energy loss by reducing the required line/cable (length) in LV and hence minimize the operating and installation costs [36]. Both the benchmark distribution test system [37] and the real system [38] are utilized to address the impact of fast charging stations. Different time resolutions were considered in quantifying the impact of FCS ranges from an hourly basis [39] to a per minute scale [40]. The objective of previous works related to fast charging stations can be categorized into three aspects: 1) optimum planning [41]–[44], 2) robust design for power components [45], and power quality issues [46]–[49]. The previous works related to the impact of FCSs on power quality is reported below.

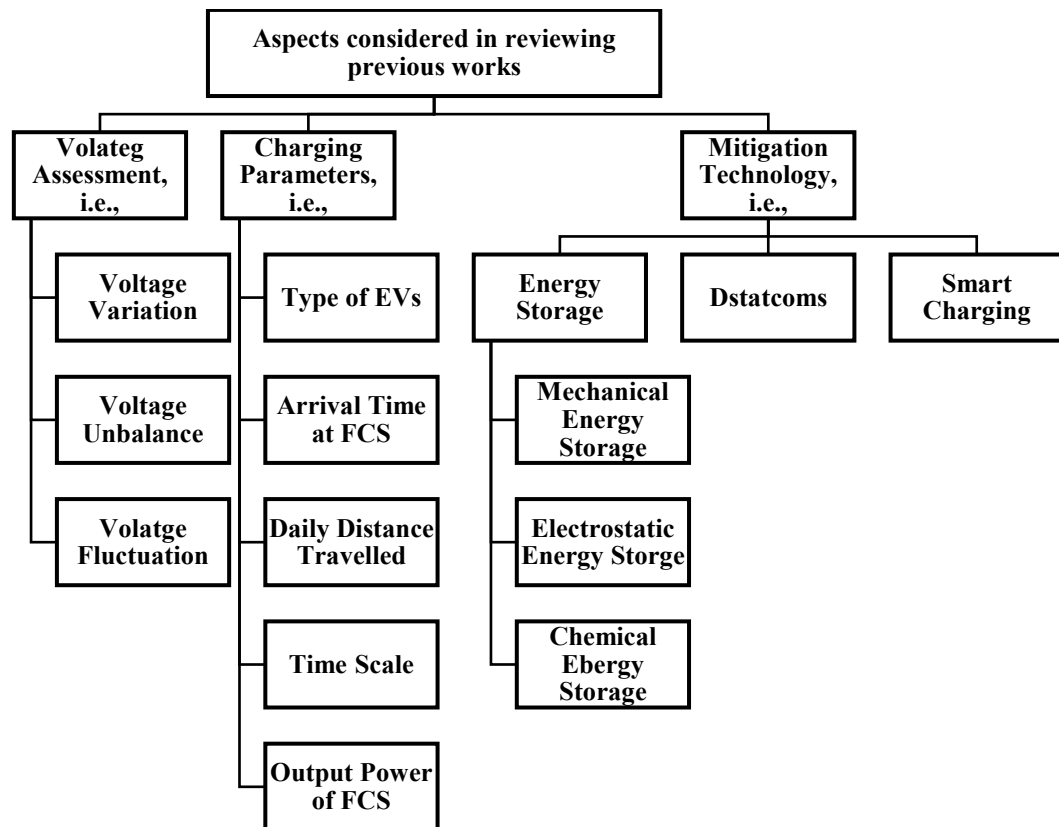


Figure 2.1 shows different aspects utilized to structure the current chapter.

Table 2-1 Different Charging Levels and their Characteristics [50]

Charger Level	Port Terminal Voltage	Maximum Power kW	Required Charging Time	System-Level Connection
AC Level 1	120 V, 1-ph	2	10-13 H	Residential/Commercial
AC Level 2	240 V, 1-ph	20	1-4 H	Secondary Customer
AC Level 3	240 V, 3-ph	43.5	~1 H	120 and 240 V
DC Level 1	200-450 V	36	0.5 – 1.44 H	Commercial Primary Customer 480 V
DC Level 2	200-450 V	96	0.2 – 0.58 H	
DC Level 3	200-600 V	200	~10 M	

2.3 Previous Works Discussing the Impact of FCS on Voltage Quality

From the FCS point of view, transportation systems and electric power systems are influenced by both driving behavior and charging behavior of electric vehicles [20]. Different parameters may be utilized to model these two patterns leading to shape the FCS demand profile which, in turn, may adversely affect several power quality phenomena such as voltage magnitude variation, voltage unbalance, and voltage fluctuation. These parameters include the arrival time at the FCS, the battery capacities of EVs, their daily distance travelled, and the output power of the FCS. In this work, the aforementioned power quality phenomena, charging, and driving parameters are utilized to differentiate and compare between the previous works in relation to FCSs. Moreover, time resolutions are another aspect that may influence the quantification method and its findings, which distinguishes it from the previous works. Finally, there are two approaches to quantifying the impact of FCS on the electric power quality: the deterministic approach and the probabilistic approach. The FCS demand profile is a function of different parameters, as explained previously; these parameters are stochastic (random) in nature and thus, the probabilistic approach is proposed in this work to quantify the impact of FCSs on the electric voltage quality in the electric power distribution systems.

2.3.1 The Impact of FCS on Voltage Magnitude Variations

The work in [35] uses FCSs rated at 50 kW to highlight their impact on the distribution system when different penetration levels of EVs are utilized. The findings show that voltage deviations will increase as the penetration level of EVs is increased. However, the results of the voltage deviations were not compared to the standard. The work in [49] investigated the effect of EV charging stations on power quality. The findings point out that the voltage deviation is within the limit of the European standard EN 50160 [51]. Similarly, the work in [52] compares only the voltage deviation to the EN 50160 [51]. Likewise, the work in [31] explores the effect of increasing the penetration level of EVs on the voltage drop. The findings show that the voltage drop on the further bus in the system is within the allowable limit, compared to the standard. However, studies [31], [49], [52] do not consider the voltage unbalance or voltage fluctuation and light flicker. The impact of using ultra FCSs on voltage deviation is discussed in [47]. The results are compared to these standards [53], [54]. The authors conclude that the deviation is 3% and satisfies both standards. However, the voltage fluctuation and light flicker were not considered.

2.3.2 Impact of FCS on Voltage Unbalance

The work in [48] aims to analyze the power quality issues of FCS. The study relies on data extracted from a monitor placed at a FCS. Voltage deviation and voltage unbalance are investigated and compared to the national standards. Results reveal that voltage deviation is slightly affected by EVs, whereas voltage unbalance is

mostly affected by the on-board charging mode, which requires single-phase chargers. However, voltage fluctuation was not considered in this study.

2.3.3 Impact of FCS on Voltage Fluctuation and Light Flicker

The work in [32] aims to quantify the influence of FCSs on the voltage profile of the electric power distribution system by studying the effect of adding a FCS. The findings indicate the presence of voltage fluctuation when a FCS is installed. The study in [32] proposed the installation of capacitors to remove the voltage fluctuation, which improved the feeder voltage, but voltage fluctuation remained. However, the findings were not compared to the standards. In [24], the authors state that the demand on FCSs may lead to voltage flickering in the distribution system. Therefore, a stochastic FCS profile for EVs is generated, aiming to quantify their impacts on a real distribution network. In the test-bed distribution grid, three FCSs are deployed in the system where each one consists of four chargers, assuming that their charging power level is a 250 kW/ charger. The resultant charging profiles from these fast chargers are a function of the arrival time of EVs to the stations, their battery size, and their state-of-charge. The arrival time for 500 cars at a petrol gas station in a day is used to generate the probability distribution of the time of arrival to these three FCSs. According to [24], the results of voltage flickers are compared with [55] and show that voltage flickers are produced by the FCS where the extreme value is almost 2%. Based on their findings, the authors propose that the adverse impacts of FCSs on the grid bus voltages can be eliminated by integrating an energy storage system.

However, the proposed solution was not investigated. Furthermore, in this study, the results of voltage flickering were not compared to the standard.

2.4 Parameters Utilized to Shape the Charging Profile at FCS

2.4.1 Types of EVs Charged at FCS

The work in [56] relies on MCS to model different parameters, such as the EVs' state of charge. The authors only consider EVs with small battery capacities. The impact of FFC rated as 50 kW is experimentally analyzed in [26]. The results indicate that the period to charge an EV from a FCS with a low SOC level is less than the period if the SOC level is high (e.g. 80%-100%). The work considers only EVs with small battery capacities. Similarly, the work in [38] and [57] utilize one type of EV with a small battery capacity of 24 kWh to address the impact of FCSs on the voltage profile. In contrast, the work in [58] selects different types of EVs such as vans, SUVs, and light trucks which all have small battery capacities ranging from 3.47 – 11.2 kWh. In [35], two parameters are utilized: battery capacity and energy consumption, to investigate the impact of DC Fast Charging Station on coordinated and uncoordinated grid-to-vehicle and vehicle-to-grid modes. Different vehicle types with different operating modes are simulated to represent the first parameter, while the second parameter is represented by modelling a user behavior whereby the user behavior is extracted from the national household travel survey [59]. Only vehicles with small battery capacities are explored in this study. In [52], the impact of EV charging stations is addressed on a real medium voltage distribution system. Private charging, fast charging stations are considered in the study. Different penetration

levels of electric vehicles are examined. However, the paper assumes that all vehicles have the same battery capacity corresponding to 24 kWh. The findings of the paper confirm that the impact of the charging stations on the distribution power system is a function of the EVs' penetration level and that these impacts can be minimized by regulating the process of the charging.

2.4.2 Modelling EVs Arrival Time at the FCS

The work in [60] relied on the Markov Chain with discrete state-space to model the charging stations, whereby the arrival times to the charging station are derived from a Poisson process. The authors in [32] and [38] project the arrival time at gas stations to generate the arrival times at FCSs. In [61], the charging curves of the EVs are based on unjustified random arrival times at the FCS. Furthermore, the work in [57] assumes that there are two types of EV owners, workers and non-workers, and they charge their EVs at different times relying on normal distribution. The work in [39] randomly represents the default arrival and departure times at FCSs by random values selected from a closed interval. Multiple different scenarios are considered, and in each scenario the arrival and departure times at FCS can vary by ± 15 minutes from the default arrival/departure times. The work in [62] applies the fuzzy logic inference system to determine the probability of each EV to arrival at/departure from the FCS. MC is utilized to determine the arrival time at the FCS. The integration of the FCS is discussed in [25] based on two methods: direct connection to the grid and indirect connection to the grid through an energy storage. The study investigates supplying fast charging stations from medium-voltage and low-voltage grids. Four

possible scenarios are reported to propose the charging process for electric vehicles at these stations. The first scenario assumes that there is one fast charging station fed by a low-voltage point. The electric vehicle is charged at the station every 30 minutes in the daytime and eight charging processes are assumed in the nighttime. In the second scenario, the charging station is connected at the same point, as in the first scenario, but beside an energy storage unit to relieve the loading on the grid. Here, the charging station has a continuous demand in the daytime. Four charging stations are considered in the third scenario where these stations are integrated to a medium-voltage point. Their loading profiles are assumed, as in the first case. The last case is similar to the second one; however, EVs here are assumed to be charged every 40 minutes from two charging stations with two installed energy storages. In this study, the proposed charging profiles are stationary in their nature and do not emulate the stochastic nature for the arrival time of these electric vehicles to the stations.

2.4.3 Modelling EVs Daily Distance Travelled and SOC

The research in [38] generates the EVs' daily travelling distance using the data published in [63]. The work in [32] does not take into consideration the daily travelling distance by EVs. Instead, the authors generate the EVs' SOC based on unjustified probability density function. Also, the work in [57] generates the SOC of the battery based on a random number generator. The work in [64] models the EVs daily distance travelled using normal distribution. The work in [39] defines the battery SOC based on upper and lower limits and then randomly selects a SOC. Multiple different scenarios are considered and in each scenario the battery SOC can

vary by $\pm 28\%$. Two methods are utilized to generate the SOC of two groups of EVs, private commuters and ride service as in [65]. The first method, for private commuters, describes the daily distance based on a normal distribution bounded by a period. Additionally, the first method utilizes traditional working times to represent the actual time of arrival at work and generate the commute distance based on normal distribution. Finally, the obtained SOC can be calculated based on the difference between the EV range and the commute distance. Instead of using the average trip distance, the second method is based on an average driving speed as per [66]. The study in [34], assumes a fixed SOC of all EVs equal to 25% of their capacity. The work in [67], distributes DC fast chargers in the network and proposes to charge several fully-depleted electric vehicle batteries at the same time during the peak load. The voltage profiles at the substations and low voltage distribution networks are utilized to address the effect of these quick chargers on the system. The results show that the network voltage impacts are varied based on the location of the charging station. The grid voltage drop goes below the standard when the DC fast charging station is assumed to be at the furthest point of the receiving end. However, the grid voltage drop does not violate the safe operating limits when the DC fast chargers are located close to the sending end. The study does not consider the variation of the load base profile in the grid. The substations are modeled to have the same constant power load with the same power factor at any feeder in the system. It assumes that feeders are feeding the DC fast chargers with the same power simultaneously. However, the generated charging profile does not consider the stochastic nature of EVs and the variations in their state-of-charge.

2.4.4 Time Scales of Quantifying the Impact of FCS

The study in [68] utilizes a FCS with 50 kW rated power to charge different types of EVs. Parameters such as battery SOC, daily distance travelled, average speed, and parking time are generated using probability distributions (e.g. uniform and normal distributions). Monte Carlo Simulation is utilized in [68] to sample these distributions in order to generate the daily profile. This profile represents EV charging pattern at the FCS. The authors stated that although the calculation was made in minute resolution, the results were shown in an hourly scale. The study in [46] investigates the impact of the FCS on power quality in the MV system. The FCS demand profile was derived from [69] whereas the output of the FCS was extracted from [70]. The analysis is done at the substation level by increasing the penetration level of EVs. The findings state that there is no impact of EVS and FCS on the upstream voltage. However, the study is conducted on an hourly basis whereas the FCS may deliver the required energy in a range of minutes.

2.4.5 The Output Power of FCS

Previous works address the output power of the FCS using two approaches. The first approach assumes that the output power is stationary, does not change over time, and always equals the rated power of the FCS. This method is utilized by [35], [68], [39], and [71] where the used rated powers are 50 kW, 50 kW, 120 kW, and 350 kW respectively. This method is proposed when it is difficult to obtain a real FCS profile, whether a general profile or for a specific EV. However, this approach presumes that the EV SOC is increased by a fixed rate depending on the rated power of the FCS;

this leads to a reduction in waiting time at the FCS to charge many EVs and then to an increased burden on the grid. The second approach involves real output power profiles of the FCS that changes over time, depending on the change of EV SOC. The profile is usually extracted from a fast charger fact sheet as in [46], or obtained experimentally as in [26].

2.5 Mitigation Method of Power Quality Variations

Energy storage may be utilized to feed the charging stations beside the power bus [14]. The energy storage is utilized to relieve the loading caused by the charging station on the power distribution network. The study in [72] concluded that charging many EVs at the FCS can adversely affect the electric power system. However, integrating an Energy Storage System (ESS) with the FCS is a key factor in mitigating these effects. Authors in [31] conclude that the energy storage inside the FCS may be used to support the FCS and relieve the demand on the grid, as the storage can be used to accumulate the energy. Three main types of energy storages are utilized in previous works to mitigate the impact of the electric vehicle charging stations on the distribution systems. These three types are mechanical energy storages (e.g. flywheel storage), electrostatic energy storages (e.g. ultra-capacitor), and chemical energy storages (e.g. battery storage) [73].

2.5.1 Mitigation Using Energy Storage

2.5.1.1 Mitigation Using Mechanical Energy Storage

The studies in [74] and [75] proposed a strategy to control the FCS adjacent to the Flywheel energy storage system. Flywheels store the energy in mechanical form,

where the amount of energy stored is proportional to its moment of inertia and the square of the flywheels rotational speed. Although flywheel devices have long lifespans, they need more time to respond to load variations in the distribution grid, especially in the era of the FCS [74].

2.5.1.2 Mitigation Using Electrostatic Energy Storage

Ultra-capacitors represent electrostatic energy storages. Electrostatic devices charge and discharge in a short time in comparison to other energy storage devices. They also have a longer lifespan and increased efficiency; however, electrostatic devices have low energy density. Ultra-capacitors were used in previous works to improve the voltage drop and power quality caused by the FCS. The study in [32] investigates the effect of the fast charging station in medium voltage distribution system. It analyzes the voltage drop and voltage fluctuation. The study indicates that the voltage drop occurs by the base loads and it is a function of the load location of the substation. Moreover, it points out that the fast charging station causes voltage fluctuations in the distribution system. To reduce the drop and fluctuation in the voltage, a capacitor is installed. However, the study concludes that although the capacitor reduces the voltage drop, it cannot remove the voltage flickers in the distribution system. Instead of using the common ultra-capacitors, due to their energy values, a storage system is included in the power conditioner, specifically lithium-ion ultra-capacitors as in [76]. A power conditioning system is utilized to improve the quality of the power supply by relieving the resultant stress from the fast charging station on the grid. The ultra-capacitors are preferable due to their shorter time response, and their longer life in terms of cycles. Furthermore, it does not depend on the temperature. According to

[76], the lithium-ion ultra-capacitors can operate in temperature ranges from -30C to +70C and their performance is not influenced.

2.5.1.3 Mitigation Using Chemical Energy Storage

Batteries are chemical energy storages characterized by their high energy density. The performance of chemical energy storages degrades after a specific numbers of charging and discharging events, which represents the main drawback of the chemical energy storage, as shown in [74] and [75]. In [77], the charging station is assumed to draw a constant rate of power from the grid. Energy storage is equipped in the charging station to support the charging demand and thus the drawn power from the grid remains constant. In the study, each charging station includes two types of chargers, fast and slow chargers. It is assumed that the power rating for these chargers are assigned based on customers' demand and their vehicles' capability to be charged from one of these chargers. Thus, the charging profiles are generated using a survey. From the grid perspective, electric vehicles can be seen as sizable electric loads due to their stochastic state of charge. When the power network is assumed to supply these charging stations by constant power, the impact of the fast charging station on the grid is eliminated even if the time of arrival for electric vehicles to these stations is varied. In [23], a DC bus is utilized to feed DC ultra-FCS charging stations to increase the operating efficiency and to reduce the conversion ratio between the DC bus and the ultra-FCS. Additionally, energy storage is used as a buffer to relieve the stress on the low voltage grid. The study considers the control mechanism of these fast charging stations, but it does not focus on the impact of the DC fast charging stations on power quality and the voltage profile of the grid. The

work in [78] studies the impact of the fast charging station on the distribution system where an energy storage is integrated. The power flow and short circuit analysis are investigated. Authors in [78] raise concerns to protect the distribution system in the presence of the fast charging station. The study in [79] reports the design requirements and the control mechanism for the configuration of the DC micro-grid for the fast charging station. The FCS was supplied with Energy Storage System (ESS) and Photovoltaic (PV) in [80]. The work introduces a leader-followers game, whereas the FCS acts as leader of the game and the EV acts as a follower. To increase its revenues, the FCS managed the renewable resources and regulated the prices for both energy and reserves. The results showed that the proposed method decreased the burden on the electric grid. The work in [81] suggests to equip the FCS with a stationary battery (SB) to support the grid and reduce the its connection cost. The findings conclude that a SB with 250 kWh would reduce the cost by about 30%, based on cost benefit analysis in [82], and [83]. According to [73], lithium-ion batteries outperform other types of batteries due to their small and light size; they are also more powerful.

2.5.2 Mitigation Using Distribution Static Compensators

The study in [84] investigates coupling Distribution Static Compensators (D-STATCOMs) with energy storage aiming to improve the active power exchange between the energy storage and the system. The work in [85] focuses on modeling and controlling D-STATCOMs with ultra-capacitor energy storage where the objective is to enhance the power quality in the system. Moreover, D-STATCOMs

are utilized to mitigate the voltage sag according to [86]. The work in [87] introduces a strategy to improve the microgrids' power quality relying on D-STATCOMs. According to [88], integrating D-STATCOMs with Ultra-capacitors, in the microgrids, is effective in mitigating the impact of increasing wind power penetration. The study in [89] discusses the optimal location for placing D-STATCOMS in mesh distribution networks to enhance voltage stability and improve the reactive loading capability. Table 2-2 and Table 2-3 summarize the surveyed studies related to the FCSs and their impacts on the distribution system voltage quality. A close visual inspection of these two tables indicate that none of the surveyed work considered all three power quality phenomena mentioned earlier, and/or compared them with the relevant standards. Also, none of the related work investigated the integration of the D-STATCOMs to mitigate the impact of FCSs on the electric power quality in the electric power distribution systems. Moreover, the climate zone was not considered whether in the EVs driving or charging pattern which, in turn, may adversely affect the required energy from the FCSs.

2.5.3 Mitigation Using Smart Charging

Smart charging has been considered by several previous works in the literature [90]–[93]; however, to the best of the author knowledge none of the previous work consider mitigating the impact of fast charging station on the voltage quality and light flicker using the smart charging.

2.6 Research Gaps

The aim of the work in this thesis is to fulfill the research gaps in the published works, which can be summarized as follows:

- To the best of the author knowledge, none of the reported works have quantified the impact of FCS on the voltage fluctuation and light flicker and mitigated that impact by a smart charging.
- Most of the relevant works assume the output power of the FCS is constant without justification and do not consider the power variation over time when the EV SOC is increased.
- Most of the previous works have quantified the impact of the FCS on an hourly basis. Vehicles with small battery capacities, that take a couple of minutes to recharge, may not be considered, which indicates that the impact may not be quantified properly.
- The climate zone may affect the EVs driving or charging pattern. To the best of the author's knowledge, none of the previous works take the climate zone into consideration when studying the impact of the FCS on electric power quality.

Table 2-2 Key Points of Differences in the Surveyed Works

		Relevant Works										
		[35]	[31]	[47]	[49]	[52]	[48]	[32]	[24]	[56]	[26]	
Characteristics												
Quantification Method Utilized	Voltage Deviation	✓	✓	✓	✓	✓	✓	✓	✓	✓	✗	✗
	CWS	✗	✓	✓	✓	✓	✓	✗	✗	✗	✗	✗
	Voltage Unbalance	✗	✗	✗	✗	✗	✓	✗	✗	✗	✗	✗
	CWS	✗	✗	✗	✗	✗	✓	✗	✗	✗	✗	✗
	Voltage Fluctuation	✗	✗	✗	✗	✗	✗	✓	✓	✗	✗	✗
	CWS	✗	✗	✗	✗	✗	✗	✗	✗	✗	✗	✗
	Time Scales	M	H	M	S	H	M	M	M	M	H	M
EVs Parameters	Large Battery Capacity	✓	✗	✓	✗	✗	✓	✗	✓	✗	✗	✗
	Different Types	✓	✗	✗	✗	✗	✓	✗	✓	✓	✓	✓
	Market Share	✗	✗	✗	✗	✗	✗	✗	✗	✗	✗	✗
	Daily Distance	✓	✓	✗	✗	✗	✗	✓	✓	✓	✓	✗
	Varied SOC Level	✗	✗	✓	✓	✗	✓	✓	✓	✓	✓	✓
FCS Features	Output Power	C	C	V	V	C	V	C	C	C	C	V
	Arrival Times	✓	✓	✗	✗	✗	✗	✓	✓	✓	✓	✗
	Energy Storage Incl.	✗	✓	✗	✗	✗	✗	✓	✗	✗	✗	✗
	DSTATCOM Incl.	✗	✗	✗	✗	✗	✗	✗	✗	✗	✗	✗
Climate Zone	Base Load Profiles	✗	✗	✗	✗	✗	✗	✗	✗	✗	✗	✗
	EVs Parameters	✗	✗	✗	✗	✗	✗	✗	✗	✗	✗	✗
	FCS Profiles	✗	✗	✗	✗	✗	✗	✗	✗	✗	✗	✗

CWS: Compared with Standard; Incl.: Included; H: Hour; M: Minute; S: Second

Table 2-3 Key Points of Differences in the Surveyed Works (Continued)

		Relevant Works										
		[38]	[57]	[58]	[39]	[62]	[25]	[64]	[34]	[67]	[68]	
Characteristics												
Quantification Method Utilized	Voltage Deviation	✓	✗	✗	✗	✗	✗	✗	✓	✗	✓	✗
	CWS	✗	✗	✗	✗	✗	✗	✗	✗	✗	✗	✗
	Voltage Unbalance	✗	✗	✗	✗	✗	✗	✗	✗	✗	✗	✗
	CWS	✗	✗	✗	✗	✗	✗	✗	✗	✗	✗	✗
	Voltage Fluctuation	✗	✗	✗	✗	✗	✗	✗	✗	✗	✗	✗
	CWS	✗	✗	✗	✗	✗	✗	✗	✗	✗	✗	✗
	Time Scales	M	H	M	M	H	H	H	H	M	M	M
EVs Parameters	Large Battery Capacity	✗	✗	✗	✓	✗	✗	✗	✓	✓	✓	
	Different Types	✗	✗	✓	✓	✓	✗	✗	✓	✓	✓	
	Market Share	✗	✗	✗	✗	✗	✗	✗	✗	✗	✗	
	Daily Distance	✓	✓	✓	✗	✓	✗	✓	✗	✗	✓	
	Varied SOC Level	✓	✓	✓	✓	✓	✓	✓	✓	✓	✗	✓
FCS Features	Output Power	C	C	C	C	C	C	C	C	C	V	C
	Arrival Times	✓	✓	✓	✓	✓	✗	✗	✗	✗	✗	✓
	Energy Storage Incl.	✗	✗	✓	✓	✗	✓	✗	✓	✗	✗	✗
	DSTATCOM Incl.	✗	✗	✗	✗	✗	✗	✗	✗	✗	✗	✗
Climate Zone	Base Load Profiles	✗	✗	✗	✗	✗	✗	✗	✗	✗	✗	✗
	EVs Parameters	✗	✗	✗	✗	✗	✗	✗	✗	✗	✗	✗
	FCS Profiles	✗	✗	✗	✗	✗	✗	✗	✗	✗	✗	✗

CWS: Compared with Standard; Incl.: Included; H: Hour; M: Minute; S: Second

Chapter 3. Response of Lighting Technology to Voltage Fluctuation

3.1 Introduction

Lamps can be classified into four main categories: Incandescent, Gas Discharge, Induction, and Solid State [94]. Figure 3.1 below illustrates the different types of lamps. In this section, a description of each type of lamp is provided. Figure 3.2 shows a historical development of the lighting industry. From Figure 3.2 it can be seen that remarkable developments have occurred throughout the last decade, and this is especially the case in LED lighting.

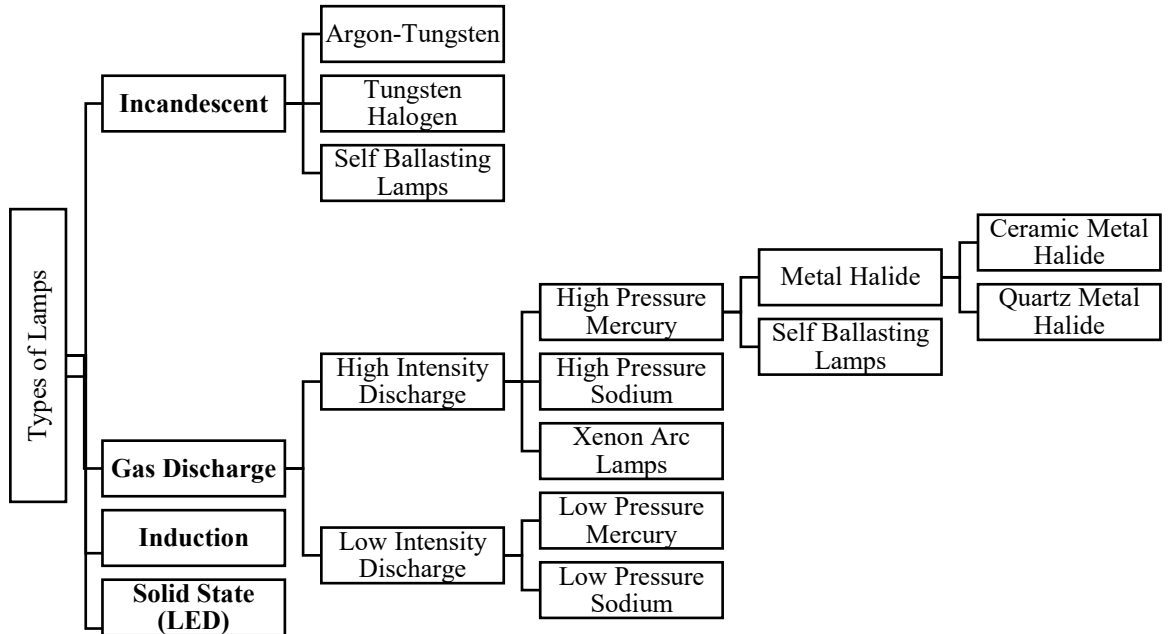


Figure 3.1 Classification of light sources [94]

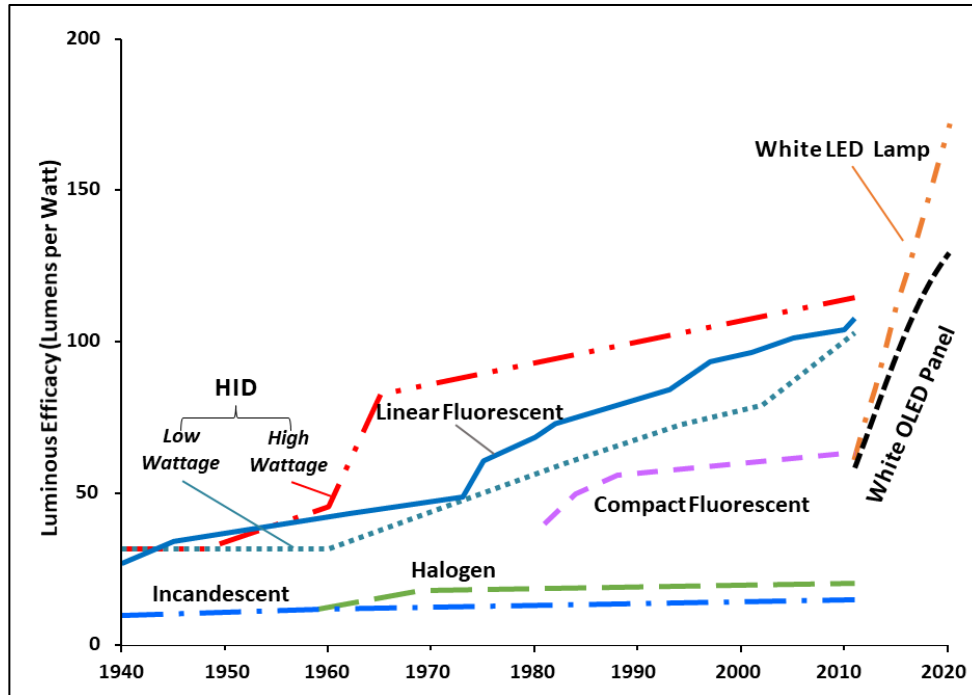


Figure 3.2 Evolution of lighting efficacy [95]

3.2 Types of Lamps

3.2.1 Incandescent Lamps

Heating of the tungsten filament produces the light in incandescent lamps (IL). Both the voltage of the lamp and its current have a sinusoidal waveform [96]. A sinusoidal waveform also characterizes the incandescent lamp's illuminance. As the lamp voltage changes, the lamp current increases or decreases linearly. This demonstrates the incandescent lamps' resistive load characteristic. 90% of the input energy of ILs is lost as heat output. This is why ILs' are viewed as a very inefficient source of light [97]. For increasing the rated lifetime of IL's, halogen gas is used. This is added within the IL glass. It is the evaporated tungsten element that the halogen gas reacts with, then the evaporated tungsten is deposited back onto the filament. A lamp like

this is called a halogen lamps (HL). A HL works much the same way as an incandescent lamp [98].

Advantages and Disadvantages of ILs: People are familiar with ILs and thus they prefer them. ILs are also relatively cheap, switch on immediately, quiet, and dimmable. However, numerous governments have developed regulations replace ILs, because they are inefficient, with alternative lamps that are more efficient, as shown in Table 3-1.

Table 3-1 Phasing-out of incandescent lamps [99]

	2008	2009	2010	2011	2012	2013	2014	2015	2016	2017
SA	100W					HAL available				
	75W						HAL available			
	40W & 60W							HAL available		
EU	100W	HAL available								
	75W & 60W					HAL available				
China	100W				HAL available					
	60W						HAL available			
	15W							HAL available		
Japan	All Incandescent						HAL available			
Malaysia	≥1000W					banned all filament lamps				
Russia	100W					HAL available				
	75W						HAL available			
	25W									
Brazil	100W					HAL available				
	60W						HAL available			
	40W							HAL available		
Canada	100W & 75W						HAL available			
	60W & 40W						HAL available			
Cuba	Since 2005, banned all IL filament lamps including HAL									
	Phase out of IL									
	Allowing for higher efficacy filament lamp									
	No filament lamps allowed									

3.2.2 Discharge Lamps

In discharge lamps (DL) an electric discharge creates the light. This occurs inside a gas or a vapor. These lamps are much more efficient than ILs. They also have a longer life. Fluorescent lamps (FLs) and compact fluorescent lamps (CFLs) are two common types of discharge lamps [100]. The major difference between FLs and CFLs is that CFLs use a point source of light, while the light source for FLs is linear. The luminous flux changes inversely proportional to the square of the distance between the light source and an illuminated object in CFLs, while the luminous flux change is inversely proportional to the distance of the light source and illuminated object in FLs [100].

3.2.2.1 Fluorescent Lighting (FL)

The most common gas discharge lighting used in commercial and industrial settings since their commercialization in 1937 is fluorescent lighting [94]. FL is cheaper, more effective, and longer lasting than ILs. For starting and current control, FL uses an electromagnetic or electronic ballast. Electromagnetic ballasts are heavier, larger, less efficient, and more sensitive to voltage changes [101]. However electronic ballasts allow lamps to be operated at significantly higher frequencies through the use of electronic reactors. Electronic ballasts are smaller, lighter, and have a longer life comparing to the Electromagnetic ballasts. Electronic ballasts are also quieter, flicker less, and even without the use of a power factor correction capacitor they have a power factor of one [94]. Figure 3.3 shows the magnetic and electronic ballast historical market share.

3.2.2.2 Compact Fluorescent Lighting (CFL)

CFL is considered to have various advantages over FL. CFL can use the same power socket previously used by IL. It uses significantly less power but provides a lot more lumens than what is provided by an equivalent IL [100]. CFL performance is hindered by the magnitude of the supply voltage as well as voltage sags and a rapid change in voltage. CFLs use complex electronic ballasts which minimize variations in light output from the supply voltage. However, increased lamp brightness is created by higher voltages, while decreased brightness results from lower voltage levels [102]. Also, other electronic components in the ballast as well as the DC bus capacitors, are sensitive to the magnitude of supply voltage. A reduced lifespan results from higher supply voltage levels especially with frequent switching of the lamp on and off [102].

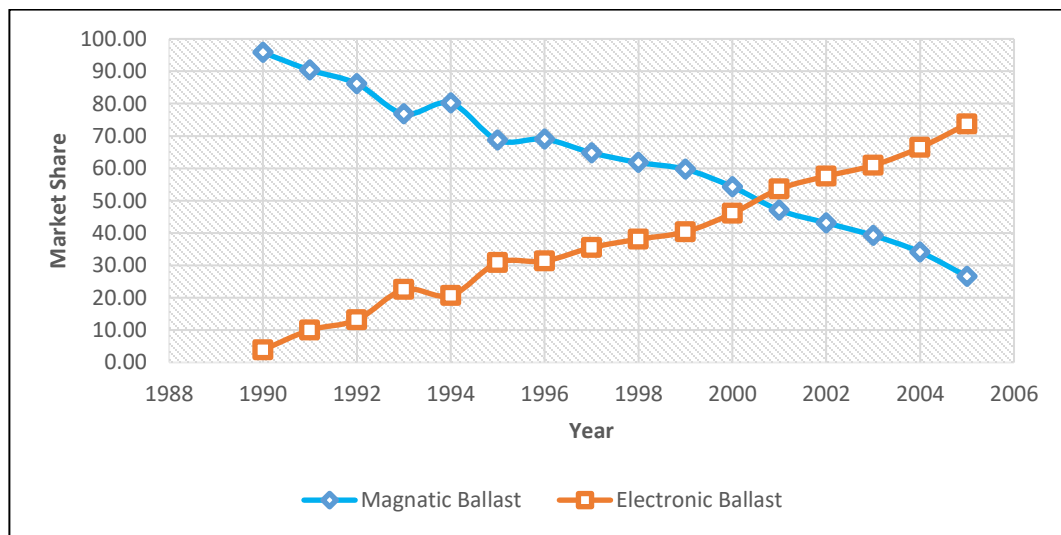


Figure 3.3 Market share of magnetic and electronic ballasts [103]

Advantages and Disadvantages of CFLs: CFLs are quiet, smaller, lighter, start immediately, have reduced lamp flicker, and overall they are more efficacious [94].

However, in comparison to standard ILs, CFLs are not as quick in ramping-up to full luminous output, and most CFLs are typically not dimmable. However, the perception of some consumers is that CFLs provide inferior light quality in comparison to traditional lighting sources. Also, there are health and environmental concerns in relation to how mercury containing CFL lamps are disposed of [98].

3.2.3 LED Lighting

LED lighting is a form of solid-state lighting (SSL). SSL is a lighting technology where both light-emitting and organic light-emitting diodes (LEDs and OLEDs) are used. These are semiconductor devices that produce light as a current passes through them [3]. The use of LED lighting technology has become much more common over time as its cost has decreased. Now, LED lighting is considered to be the mass produced lighting technology that is most energy efficient [102]. In regard to simplicity, lifespan, color and starting capability, LED lighting is advantageous when compared to CFL lighting. Led lighting uses one or more LEDs to condition the input voltage as required using a lighting system containing an electronic driver circuit [102]. On the other hand, OLEDs are much less costly than LEDs but less advanced in in performance improvements [94].

3.3 Comparison of incandescent, FL, CFL, LED, and OLED lamps

3.3.1 Lamp Efficacy

Efficacy is a ratio of lumens per watt. Lumens measures the light or total number of lines of lighting flux from a particular light source [104]. Color rendering index (CRI) is a light source's ability to render colors naturally under a full spectrum

radiator, and without distortion of the hues. The range covered by a CRI is from 0 (poor quality) to 100 (close to natural daylight) [100]. ILs have more CRI but much less efficacy in comparison to other lamps, whereas with FL and OLED lamps the average efficacy is much the same. Amongst all lamps, however, LED lamps have the highest efficacy [94].

Table 3-2 Comparison of different types of lamps

	Lamp Type	Efficacy (lm/W)	Color rendering	Relight time
IL	Light globes	8-17	100	Immediate
	Halogen	20-30	100	Immediate
DL	Fluorescent	60-100	50-98	Immediate
	Compact Fluorescent	50-65	50-80	Immediate-3sec
SSL	LED	200	>80	Immediate
	OLED	100	<95	Immediate

3.3.2 Lamp Lifetime

The average life of ILs is usually around 10,000 h. This is significantly lower than any other lighting lamps [100]. HLs have a lifetime of up to 20,000 h. On the other hand, discharge lamps have a much longer life lifetime than ILs. Figure 3.4 summarizes rated lifetimes of different light sources [105]. Various factors are involved in determining the lifespan of lamps. One of these factors which affects lamp life is the frequency switching a lamp on and off. However, the frequency of switching operations does not affect halogen based ILs [100]. This varies from FLs where each occurrence of switching a lamp on or off causes the electrodes to lose a tiny amount of their coating. As time passes, the lamp no longer starts after the destruction of the electrode coating reaches a certain level. Thus, where usage of a lamp requires frequent on/off switching, it is recommended that discharge lamps

such as FLs not be used. CFL and LED lamps are the other lamps that are also highly affected by switching operations. For these lamps the cause lies in electronic components failing prematurely [100].

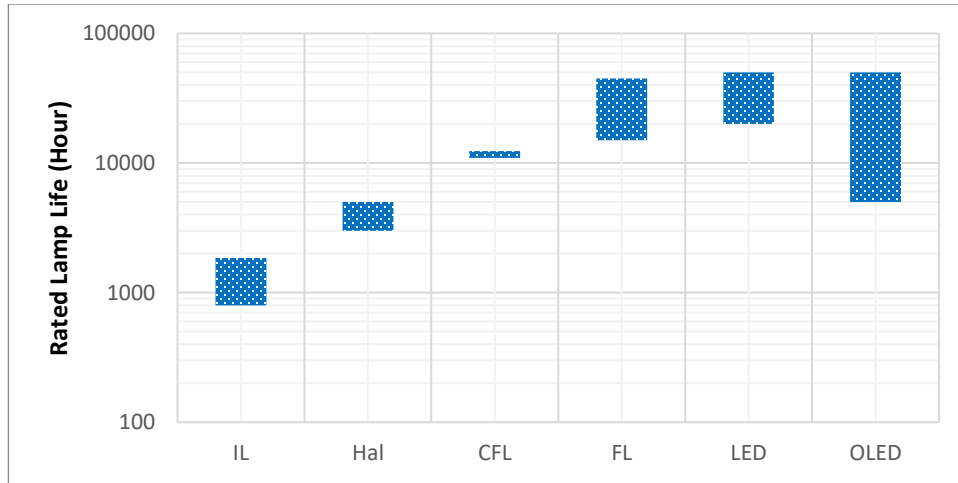


Figure 3.4 Rated lifetime of different types of lamps

3.3.3 Lamp Cost

ILs cost significantly less than all other lighting lamps. ILs have lower efficacy because most of their input energy is lost as heat output. However, CFL and LED lamps have the characteristics of being 75% more energy efficient, and lasting longer, than ILs. This is why the cost of CFL and LED lamps is significantly higher than the cost of ILs. In [100], the cost comparisons are compared on a per kilo lumen basis in relation to light sources. The results are indicated in Table 3-3. From This table it is to be noted that the initial costs of FLs is twice that of CFLs and HLs for the same amount of light flux (lumens). Although LED lamps have a longer lifetime than any other lamp, they also have the highest initial cost. Figure 3.5 shows the trend in purchase cost of traditional and led lamps. From Figure 3.5, it can be

observed that the cost trend of LED lamps is decreasing and will likely decrease further in the near future [100].

Table 3-3 Cost comparison of different types of lamps

Lamp type	Cost (\$/kilo-lumens)	Rated Life (h)	Cost (\$/kilo-lumens-h)
Halogen lamp (A19 43W, 750 lm)	2.5	5,000	0.00050
CFL (13W, 800 lm)	2	12,000	0.00017
CFL (13W, 800 lm dim.)	10	12,000	0.00083
Fluorescent lamp and ballast	4	25,000	0.00016
Led lamp (A19 60W, 800 lm)	30	25,000	0.00120
Led lamp (A19 60W, 800 lm dim.)	30	50,000	0.00060

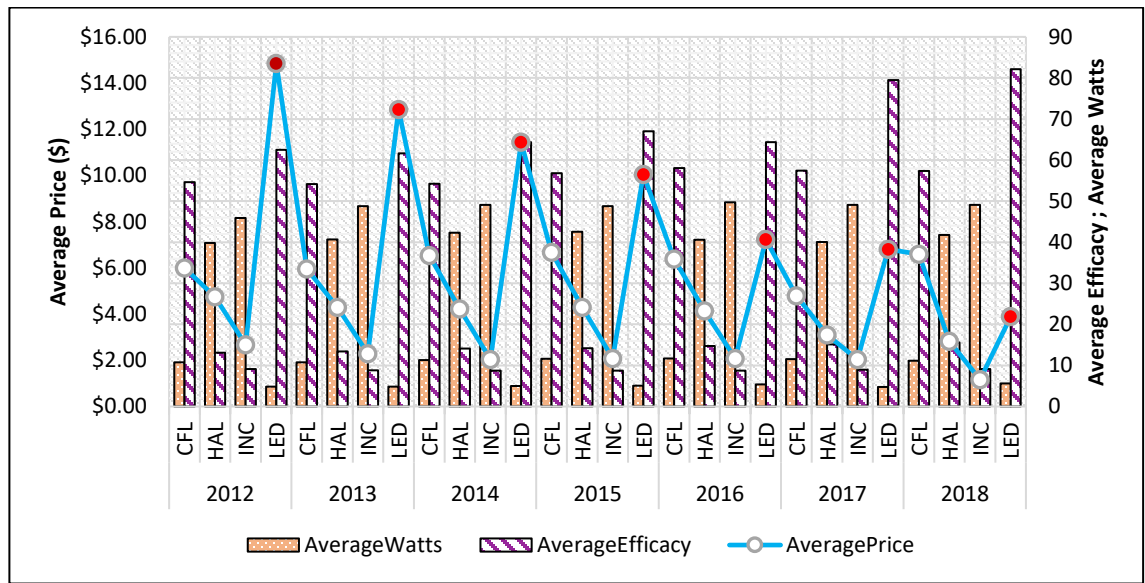


Figure 3.5 Average price, Watts, and efficacy of traditional and LED lamps

3.3.4 Trends of Lighting Market

Figure 3.6 illustrates how of lighting stock for installation is projected to change over time from 2017 in the US in the residential sector. Figure 3.7 shows that there is a nearly linear steady, decline expected in conventional technologies between 2017 and 2035 [106]. Use of both connected and non-connected LED lighting is expected

to increase to consist of up 54% of the residential sector stock by 2035 [106]. Figure 3.8 presents the growth in LED lighting stock will occur across all sectors. It is expected that the residential sector will be dominated LED lamps and their installation. It is anticipated that as more LED lighting is used, total energy use will continue to decrease. As shown in Figure3.8, in 2017 LED lighting will already have been providing 1.1 quadrillion, or nearly 322×10^9 KWh of energy savings. If the lighting market continues as it is, by 2035 there will be a total annual energy savings of 4.8 quadrillion by the time 2035 is reached [106].

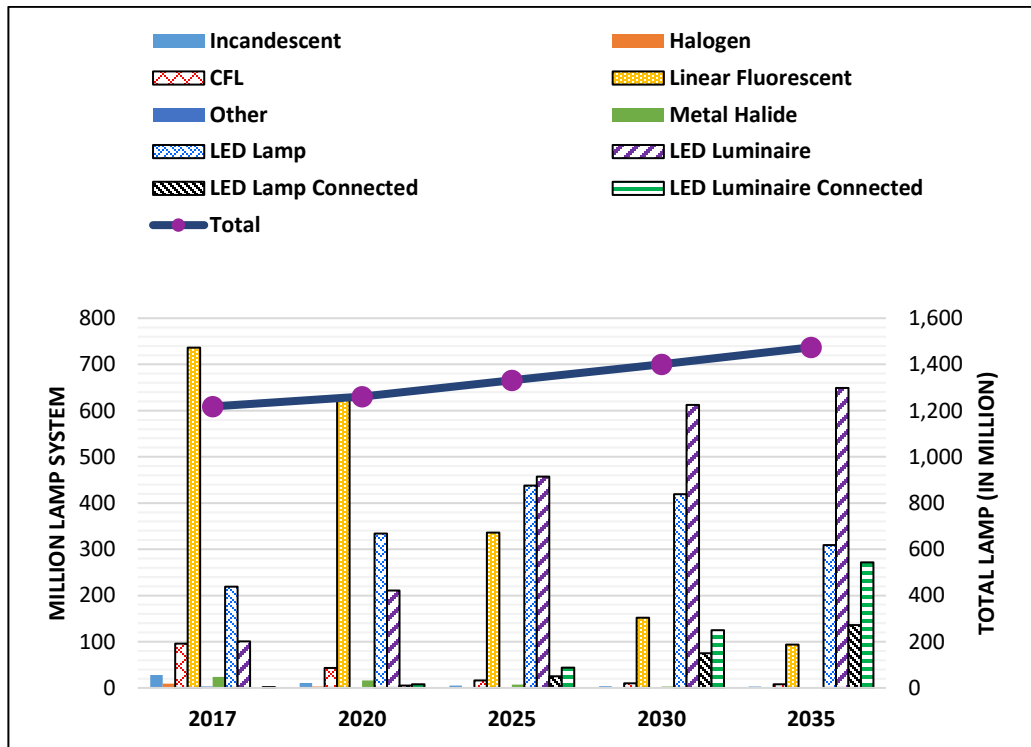


Figure 3.6 Forecast of commercial lamps stocked by technology

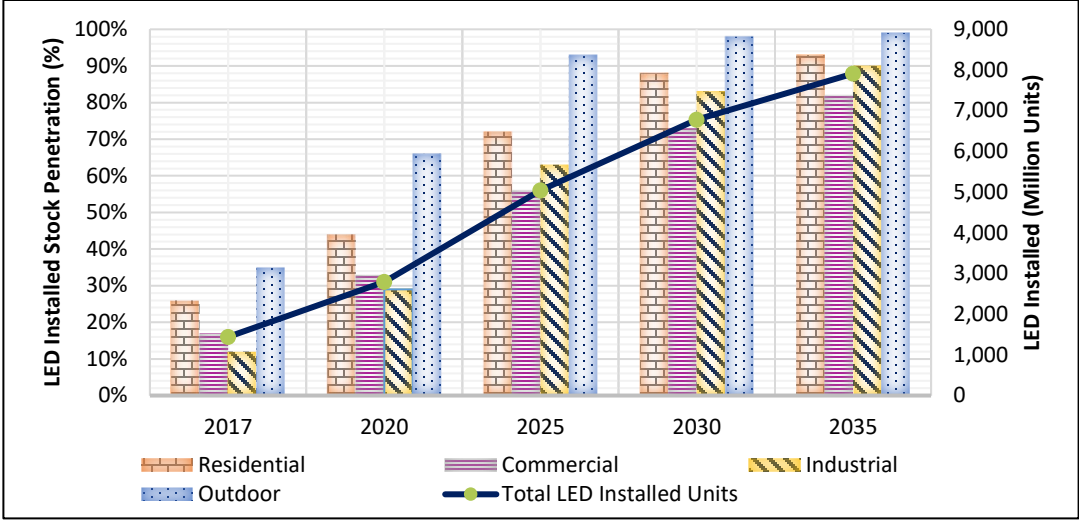


Figure 3.7 LED Forecast in U.S

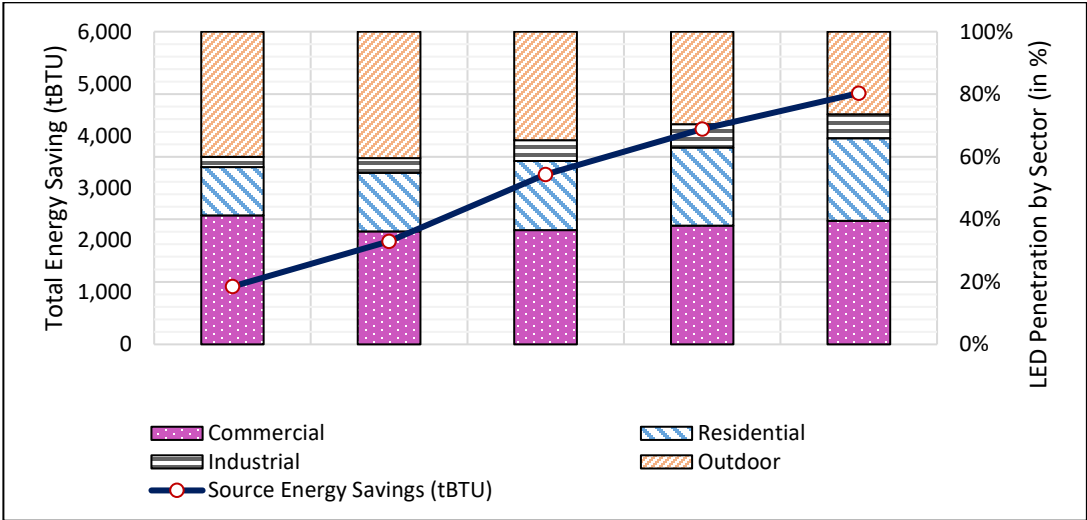


Figure 3.8 Forecast of energy savings in LED technology in U.S. market

3.4 Voltage Fluctuation and its Impacts on the Modern Lighting System

3.4.1 Definition of Voltage Fluctuation

Voltage Fluctuation can be defined as a cyclical variation of the waveform of voltage envelope. The profile of the voltage is determined by the current drawn by the load. Voltage fluctuations happen when sudden changes occur in the real and reactive power that is drawn by a load. Voltage fluctuation characteristics are dependent on

various factors, such as load type, load size, and the capacity of the power system. The changes in voltage may be sinusoidal, rectangular, or irregular in shape.

3.4.2 Adverse Impacts of Voltage Fluctuation

Lamp flicker, which is the most significant effect of voltage fluctuations, results from the magnitude of the supply voltage initiating variations in lamp light intensity. The human eye can feel aggravated (annoyed) by this changing intensity. Irritation of the eye can occur, but the extent of this will vary between individuals [107].

3.4.3 Effects of Flicker

The particular effects of flicker are influenced by various factors [108]. These include: the tasks undertaken by the user and their sensitivity to the light, the characteristics of the source, and the ambient light conditions. Also, the consequences of the light flicker can be significant on the light user in the space. It can range from headaches, fatigue, blurred vision, and eyestrain; to seizures for those with photosensitive epilepsy, and for others a lessened ability to perform visual tasks [108].

3.4.4 Flicker Metrics

Various measures have been suggested for quantify flicker visibility. These measures include: Flicker Index, Flicker Percent, Visibility Measures, General Electric Flicker Curve, and Percentile Short Term and Long-Term flicker severity indices.

3.4.4.1 Flicker Index

A Flicker Index (I_F) has been created by the Illuminating Engineering Society of North America (IESNA). It is defined as the area between the curve representing a waveform, and the average light level, divided by the total area below the curve for a single cycle of a fluctuation [109]. If we refer to $A1$ as the area between the curve representing the waveform and the average light level, and $A2$ as the area below the average light level and the curve, then the Flicker Index, can be computed (see Figure 3.9) as:

$$I_F = \frac{A1}{A1 + A2} \quad 3.1$$

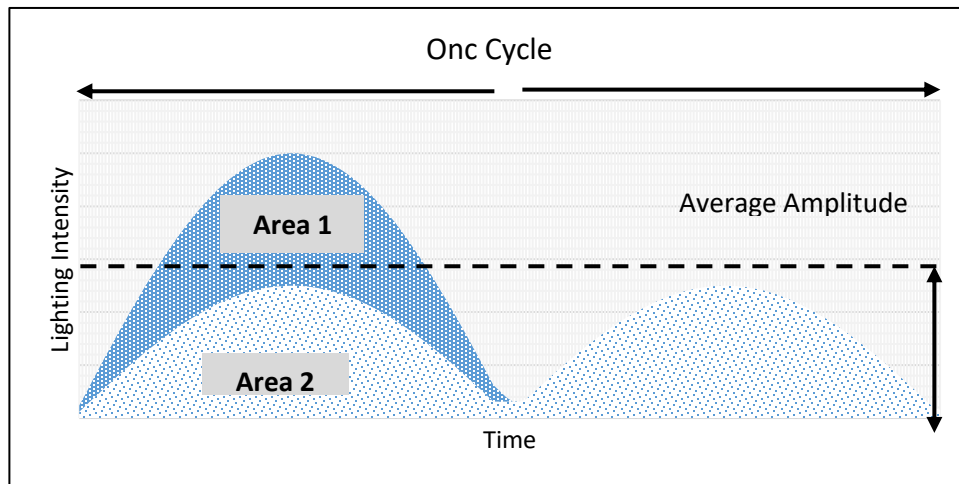


Figure 3.9 Flicker index calculation using the light output

I_F has a range of 0 to 1 where '0' denotes a steady output of light. An increased chance of noticeable flicker and stroboscopic effects occur with higher values. According to IESNA recommendations, I_F must remain below 0.1 for good lighting quality [109]. The flicker index is measured over one cycle of periodic waveform.

3.4.4.2 Percent Flicker

The Percent Flicker or Percent Modulation is defined by IESNA as “the maximum decrease in the luminance from its peak value, normalized to the average luminance in terms of percentage”. Referring to Figure 3.10, the Percent Flicker (P_F) is calculated as [109]:

$$P_F = \frac{L_{max} - L_{min}}{L_{max} + L_{min}} * 100\% \quad 3.2$$

The PF has a range of 0 to 100%. Lower values mean better light quality. A higher value points to an increased chance of noticeable flicker. As with I_F , P_F does not consider the effect of frequency nor the shape of the waveform [109].

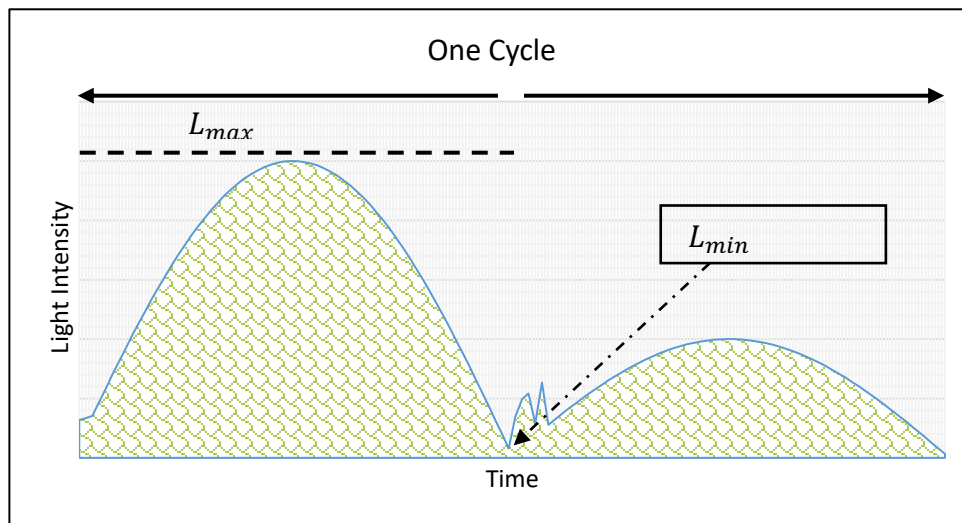


Figure 3.10 Flicker percent calculation using the light output

3.4.4.3 Visibility Measure

The Visibility Measure (V_F) is used for the purpose of evaluating the Temporal Light Artefacts (TLA) of LED light sources [110]. Neither the Flicker Index nor the Percent Flicker can evaluate TLA which is defined to as ‘an undesired change in

visual perception'. This includes changes created by a "light stimulus whose luminance or spectral distribution fluctuates with time" through the eyes of an observer in particular environments [111]. There are three kinds of TLA: flickers, stroboscopic effects, and phantom array effects. It is assumed that flicker phenomena are seen in frequencies ranging from zero to less than 80 Hz, and in situations where the observer and their environment are static [112]. Stroboscopic effects (SVMs) and phantom array effects (PVMs) are different in that can happen in a non-static environment, and in a frequency range that is higher than the optimum range for flicker phenomena in a range of between 80Hz-2kHz [112]. The primary difference between SVMs and PVMs is that Stroboscopic effects take place when the observer's eyes are immobile, while phantom array effects happen when the eyes of the observer are moving (non-static). The VM is calculated using the following equation [109]:

$$V_F = \left(\sum_{m=1}^{\infty} \left(\frac{C_m}{T_m} \right)^n \right)^{1/n} \quad 3.3$$

where C_m is the amplitude of the m -th Fourier component and T_m is the visibility threshold for the effect for a sine wave at the frequency of the m -th Fourier component. The summation is used over all the signal elements with corresponding frequencies having a defined visibility threshold, T_m , for the sensitivity curve that is used. The Sensitivity curves ($T_V(f)$) of the SVM and the PVM are respectively calculated as follows [109]:

$$T_V(f) = \frac{1}{1 + e^{-a(f-b)}} + 20 \times e^{\frac{-f}{10\text{Hz}}} \quad 3.4$$

$$T_V(f) = \frac{4 \times (1 - 0.1)}{2500Hz - 120Hz} \times (f - 120Hz) + 0.1 \times \frac{4}{\pi} \quad 3.5$$

The parameter n is the Minkowski norm parameter. The Minkowski exponent ranged between 2 and 4 [110].

$$V_F = \begin{cases} < 1 & \text{not visible} \\ = 1 & \text{just visible} \\ > 1 & \text{visible} \end{cases} \quad 3.6$$

If the visibility measure has a value that is equal to one, then a temporal artefact that is only just visible is produced: this is the visibility threshold. The artefact is detectable by the typical observer with a probability of 50 %. If the visibility measure value is greater than unity, there more than a 50% probability of detection. If it is less than unity, there is less than a 50% probability of detection. These figures relate to an average human observer [109].

3.4.4.4 General Electric Flicker Curve

The General Electric (GE) Flicker Curve, also known as IEEE 141, stems from testing GE undertook on several utilities. The GE Flicker Curve has been used frequently and over many years [113]. It is two curves that are shown in the GE Flicker Curve: these are the threshold of perception and the threshold of irritation. Square-wave changes to voltages form the basis of the GE Flicker curve, at the frequencies indicated on the graph. When the load is slower than in a voltage step like a square wave, the flicker is much less difficult to see. Rapid changes in light intensity demand a more sensitive human eye-brain response than slow changes light intensity [113]. The number of dips per second, minute, or hour is what forms the

basis of the GE Flicker Curve, with the change of apparent light intensity varying in accordance with the type of light that is used [113]. The GE flicker curve is outlined in Figure 3.11 and mapped in Table 3-4. The table shows three parameters: the period of the flicker, the voltage dip tolerance, which represents borderline of irritation, and the acceptable number of dips at that tolerance. The voltage dip tolerance is derived from Figure 3.11. Exceeding the tolerance presupposes exceeding the borderline of irritations, which causes a noticeable light flicker. For example, the tolerance for one-minute period can be calculated using Table 3-4 as follows:

$$\left(\frac{10 \text{ dips}}{60 \text{ sec}}\right) \times \left(\frac{60 \text{ sec}}{1 \text{ min}}\right) = \left(\frac{10 \text{ dips}}{1 \text{ min}}\right) \quad 3.7$$

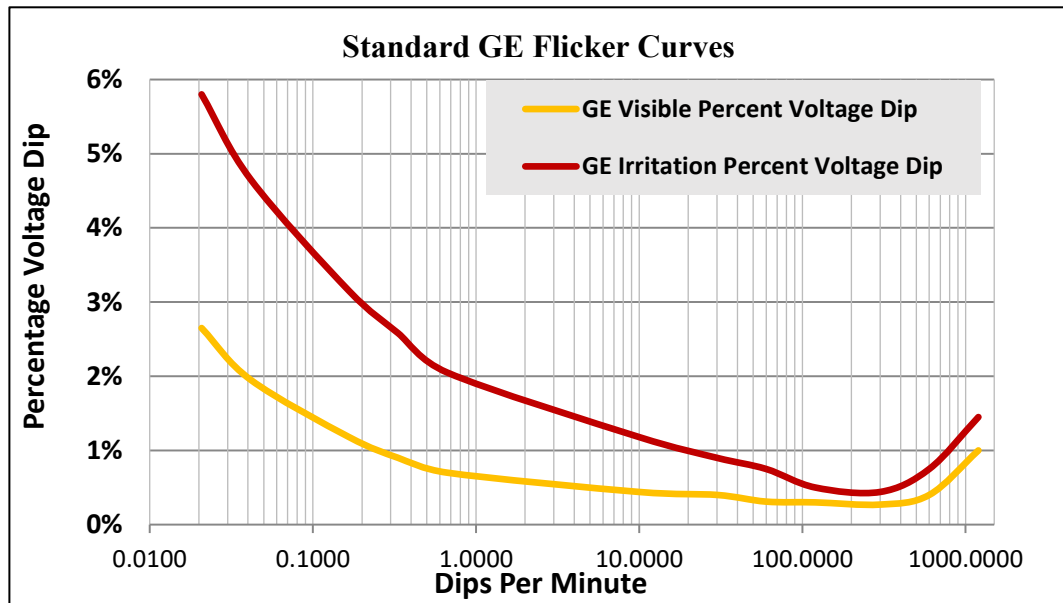


Figure 3.11 GE flicker curve [113]

From Equation (3.8), the corresponding tolerance of irritation is 1.18% approximated in Table 3-4.1 to 1.2%. It means that if the voltage dips 10 times in a period of one-minute and the ratio of the voltage deviation to the nominal voltage is 1.2% or more, then that will lead to noticeable rapid variations in the light brightness.

Table 3-4 Flicker parameters using GE curve [113]

Period	Tolerance (1-7%)	Limit (1-255)
10 Seconds	0.9	5
1 Minute	1.2	10
15 Minute	2.1	10
30 Minute	2.6	10
1 Hour	3.1	10
4 Hour	4.7	10
8 Hour	5.7	10
12 Hour	6	10
24 Hour	7	10

3.4.4.5 Percentile Short-Term and Long-Term Flicker Indices

The IEEE standard 1453 adopts the IEC 61000-4-15 Standard flicker meter. The IEC flicker meter aims to model the human visual system and quantifying its response to the light flicker. The model operates on a ‘block’ system where its main feature is that each block provides an output which becomes an input for the next block [114]. The IEEE 1453 Flicker Meter uses block number one to bring the input voltage signal to a reference per unit level. Block number two is used for the extraction of the fluctuation from the carrier signal, which is done using a squaring demodulator. The third block uses filters to eliminate unwanted frequencies. It also copies the ‘lamp-eye-brain’ behaviors by measuring the weight of the voltage fluctuation. Block number four uses a sliding mean filter to personify how the human brain reacts to the light flicker, while block number five carries out statistical analysis. This final block determines the percentile short term flicker severity index P_{ST} [115]. This P_{ST} severity index is calculated in ten-minute intervals using supporting values, as seen in (3.9).

$$P_{ST} = \sqrt{(0.0314 \times P_{99.9}) + (0.0525 \times P_{99}) + (0.0657 \times P_{97}) + (0.28 \times P_{90}) + (0.08 \times P_{50})} \quad 3.8$$

where $P_{99.9}$, P_{99} , P_{97} , P_{90} , and P_{50} symbolizes the flicker levels not exceeded by 99.9%, 99%, 97%, 90%, and 50% during the observation period. The following smoothed assessment calculates this:

$$P_{99} = \frac{(P_{99.3} + P_{99} + P_{98.5})}{3} \quad 3.9$$

$$P_{97} = \frac{(P_{97.8} + P_{97} + P_{96})}{3} \quad 3.10$$

$$P_{90} = \frac{(P_{94} + P_{92} + P_{90} + P_{87} + P_{83})}{3} \quad 3.11$$

$$P_{50} = \frac{(P_{70} + P_{50} + P_{20})}{3} \quad 3.12$$

Disturbances from loads with long duty-cycles or by the random operation of combined sources can be calculated by adopting the percentile long term flicker severity index P_{LT} . This P_{LT} is calculated by measuring 12 consecutive values of P_{ST} (over two-hours). This is done using the following formula [116]:

$$P_{LT} = \sqrt[3]{\frac{1}{12} \left(\sum_{a=1}^{12} P_{ST}(a)^3 \right)} \quad 3.13$$

Table 3-5 shows the compatibility levels for P_{ST} and P_{LT} in the LV power system [116]. The compatibility levels are utilized to assess the impact of voltage fluctuation on the power system. The compatibility levels represent the limits, if these limits are exceeded, the customers will observe the light flicker.

Table 3-5 Compatibility levels for PST and PLT in LV voltage power system [116]

Compatibility Levels	
	LV
P_{ST}	1.0
P_{LT}	0.8

3.4.5 Modern Lighting Response to Voltage Fluctuation

Different flicker metrics have been discussed in Chapter 3, Section 3.4.4. The general electric flicker curve was proposed based on incandescent lights; the percentile short flicker severity index based on the interaction of incandescent bulbs and the human-eye-brain. Both metrics are specific for one type of lamp that is incandescent bulbs. A recent study claims that percentile short flicker severity index is not suitable for quantifying the effect of voltage fluctuation on light flicker [117]. Instead, the Flicker Index (I_F) is utilized, as per IEEE Std 1789-2015 [118], to determine the flicker response of the different types of lamps considered in the chapter,

The range of I_F is 0 to 1 where 1 means a light is flickering. A proposed immunity index (Λ) is utilized to evaluate the lamp immunity level and scale to the flicker using the flicker index (I_F). The lamp immunity level is proposed as in (3.14):

$$\Lambda = |\log(I_F)|, \quad \forall I_F \in \mathbb{R}_{>0} \quad 3.14$$

where I_F is the flicker index. When the value of the flicker index is small (close to zero), the resultant value of immunity level is high and thus the immunity scale is assumed to be high as well. When the I_F is high (close to one), the resultant immunity level as per (3.14) is expected to be low. Table 3-6 illustrates the proposed immunity levels, scales, and color codes. Note that the flicker values are reported below as found in the relevant works, but the immunity/susceptibility level is proposed in this work based on the proximity to the extreme values (0 and 1).

Table 3-6 Lamp flicker response and immunity level

Immunity Level based on the Proposed Index	Performance Color Codes	Lamp Response to Flicker	Immunity Scale Out of 8
$\Lambda \leq 0.25$		Susceptible	0
$0.25 < \Lambda \leq 0.50$		Susceptible	1
$0.50 < \Lambda \leq 0.75$		Susceptible	2
$0.75 < \Lambda \leq 1.0$		Susceptible	3
$1.0 < \Lambda \leq 1.25$		Immune	4
$1.25 < \Lambda \leq 1.5$		Immune	5
$1.5 < \Lambda \leq 1.75$		Immune	6
$1.75 < \Lambda \leq 2.0$		Immune	7
$\Lambda > 2.0$		Immune	8

3.4.6 Flicker in Incandescent Lamps

Flicker related standards have been developed in relation to the characteristics of incandescent lighting technology [102]. The lamp filament in incandescent lighting has a very short thermal time constant, and this allows modulation of the voltage waveform to be conveniently observed. For example, a 230V, 60W light bulb will have a time constant shorter than that of a 110V, 60W light bulb as it has a thinner filament [102]. A noticeable flicker and even a stroboscopic effect can be produced by ILs when operating below 25 Hz [119]. If the filament is larger and operated at a higher wattage supply frequency, then the flicker from incandescent lighting will be less. When operating at 60 Hz, modern incandescent light sources do not produce a noticeable flicker or stroboscopic effect. The flicker index of several ILs operated at 25 Hz and 60 Hz is shown in Table 3-7.

Table 3-7 Incandescent filament lamps flicker characteristics [119]

Incandescent Filament Lamps	Watts	Flicker Index		Lamp Performance at 60 Hz		Lamp Performance at 25 Hz	
		60 Hz	25 Hz	Response	Scale	Response	Scale
Vacuum	6	0.092	0.220	Immune	4	Susceptible	2
	10	0.054	0.127	Immune	5	Susceptible	3
	25	0.032	0.089	Immune	5	Immune	4
Gas-filled	60	0.025	0.060	Immune	6	Immune	4
	100	0.016	0.045	Immune	8	Immune	5
Coiled-coil filament	40	0.041	0.092	Immune	5	Immune	4
	200	0.013	0.035	Immune	7	Immune	5
	300	0.010	0.025	Immune	7	Immune	6
	500	0.006	0.019	Immune	8	Immune	6
	1000	0.003	0.013	Immune	8	Immune	7

3.4.7 Flicker in Fluorescent Discharge Lighting

Instantaneous power input varies light output from both FLs and CFLs. Fluctuating light output is too quick for most people to see in typical fluorescent discharge lighting, such as using a magnetic ballast with a 60-Hz power input frequency [119]. However, the inability to notice fluctuating light assumes a power input free of electrical noise. Electrical noise can cause frequencies that create a noticeable flicker. In noise-free operating conditions, according to [119], the flicker index for common FLs ranges from 0.01 to approximately 0.1 for lamps operating with electromagnetic ballasts. It is significantly lower when using high frequency electronic ballasts [119]. The flicker index of several FLs is shown in Table 3-8.

Table 3-8 Discharge lamps flicker characteristics [108], [120]

Lamp type	Watts and Description	Ballast	Flicker Index	Lamp Flicker Response	Immunity Scale
FL	T8 Dimmable	Electronic	0.007	Immune	8
	T12	Magnetic	0.011	Immune	7
CFL	Quad Tube	Magnetic	0.110	Susceptible	3
	A19	Magnetic	0.010	Immune	7
	Quad Tube	Electronic	0.000	Immune	8

3.4.8 Flicker in High-Intensity Discharge Lamps

There is some degree of variation in the light output of all High-Intensity Discharge (HID) lamps. This is due to cyclic changes of the line voltage. The flicker that may result is determined by the ballast circuit and lamp type [119]. Table 3-9 illustrates the variation in flicker index for mercury, metal halide, and high-pressure sodium lamps for several ballast types operated at 60 Hz. In 50-Hz power systems the flicker index is considerably higher. However, the flicker effect can be eliminated through the use of electronic ballasts with high-frequency or rectangular wave characteristics.

Table 3-9 High-intensity discharge lamps flicker characteristics [119]

Lamp type	Watts and Description	Flicker Index	Lamp Flicker Response	Immunity Scale
Mercury	250 Warm Deluxe	0.127	Susceptible	3
	250 Cool Deluxe	0.137	Susceptible	3
	250 Deluxe White	0.131	Susceptible	3
	250 Deluxe White	0.172	Susceptible	3
	100 Deluxe White	0.142	Susceptible	3
	100 Deluxe White	0.183	Susceptible	2
	400 Deluxe White	0.121	Susceptible	3
	400 Deluxe White	0.144	Susceptible	3
High Pressure Sodium		0.131	Susceptible	3
		0.200	Susceptible	2
Metal Halide	250 High Color Quality	0.080	Immune	4
	250 High Color Quality	0.102	Susceptible	3
	175 Coated	0.083	Immune	4
	175 Clear-Vertical	0.078	Immune	4
	175 Clear-Horizontal	0.092	Immune	4
	250 Coated (A)	0.070	Immune	4
	250 Clear-Vertical	0.102	Susceptible	3
	250 Clear-Horizontal	0.121	Susceptible	3
	250 Coated (B)	0.092	Immune	4
	250 Clear-Vertical	0.088	Immune	4
	400 Clear-Horizontal	0.097	Immune	4
	400 Clear-Vertical	0.086	Immune	4
	400 Clear-Horizontal	0.095	Immune	4
	1000 Clear- Vertical	0.067	Immune	4
175 (3200K)	0.090	Immune	4	

3.4.9 Flicker in Light-Emitting and Organic Light-Emitting Diodes Lamps

Led lighting functions by converting AC voltage to DC voltage, and operates on an electronic driver circuit [102]. Some LED lighting systems are highly sensitive, and easily affected by changes in the supply voltage magnitude, and thus they may flicker [102]. This can happen in various circumstances, such as with some waveform distortion, particularly in relation to certain combinations of dimmer and driver circuits [102]. The flicker from both LEDs/OLEDs (Organic Light Emitting Diodes) is also highly dependent on the driver [121]. It can vary with the same type of LEDs/OLEDs according to the driver design. Table 3-10 and 3-11 detail the results of temporal light artifacts characteristics of OLED/LED lighting systems.



Figure 3.12 Pictures of various LEDs utilized in Table 3-10 [122]

Table 3-10 Flicker characteristics of LED technology [123], [124]

LED ID	Flicker Index		Switch-Based		Dim-Based	
	Switch	Dim	Response to Flicker	Immunity Scale	Response to Flicker	Immunity Scale
12-62	0.0028	0.0028	Immune	8	Immune	8
12-64	0.0148	0.0156	Immune	7	Immune	7
12-65	0.1367	0.1561	Susceptible	3	Susceptible	3
12-66	0.0372	0.037	Immune	5	Immune	5
12-67	0.0026	0.0027	Immune	8	Immune	8
12-72	0.0083	0.0052	Immune	8	Immune	8
12-73	0.104	N/A	Susceptible	3	N/A	N/A
12-74	0.0793	0.0932	Immune	4	Immune	4
12-75	0.035	N/A	Immune	4	N/A	N/A
12-76	0.051	N/A	Immune	4	N/A	N/A
12-77	0.0044	0.005	Immune	8	Immune	8
12-78	0.0148	0.0146	Immune	7	Immune	7
12-79	0.0052	0.0059	Immune	8	Immune	8
12-80	0.0021	0.0025	Immune	8	Immune	8
12-81	0.0012	0.0016	Immune	8	Immune	8
12-82	0.1071	0.1264	Susceptible	3	Susceptible	3
12-85	0.0048	0.0046	Immune	8	Immune	8
12-86	0.0059	0.0062	Immune	8	Immune	8
12-87	0.0496	0.0514	Immune	5	Immune	5
12-88	0.0668	0.0815	Immune	4	Immune	4
12-89	0.003	N/A	Immune	8	N/A	N/A
12-90	0.0146	N/A	Immune	7	N/A	N/A
12-91	0.0029	0.0032	Immune	8	Immune	8
12-92	0.156	0.1803	Susceptible	3	Susceptible	3
12-93	0.067	0.0849	Immune	4	Immune	4
12-94	0.017	N/A	Immune	7	N/A	N/A
12-95	0.0016	0.0014	Immune	8	Immune	8
12-96	0.0949	0.1174	Immune	4	Susceptible	3
12-97	0.004	N/A	Immune	8	N/A	N/A
12-98	0.4255	0.5693	Susceptible	1	Susceptible	0
12-99	0.0035	0.0033	Immune	8	Immune	8
12-100	0.0135	0.0133	Immune	7	Immune	7
12-102	0.035	N/A	Immune	5	N/A	N/A
12-103	0.1034	N/A	Susceptible	3	N/A	N/A

Table 3-11 Stroboscopic/flicker characteristics of LED/OLED technology [123], [124]

Lamp type	Space	Photo	Dim Level	I_F	V_F	Immunity Level to Stroboscopic/ Flicker
Organic Light-Emitting Diodes Lamps (OLED)	Break room		Full	0	0.034	
			Minimum	0.077	0.231	
	Entry corridor		Full	0	0.002	
			Minimum	N/A	N/A	N/A
	Conference room		Full	0.004	0.017	
			Minimum	0.032	0.067	
	Conference room		Full	0.001	0.006	
			Minimum	0.007	0.026	
	Reception area		Full	0.123	0.369	
			Minimum	N/A	N/A	N/A
	Copy room		Full	0.0001	0.004	
			Minimum	0.034	0.109	
Training room		Full	0.003	0.009		
		Minimum	0.123	0.026		
Training room		Full	0.001	0.004		
		Minimum	0.067	0.191		
Light-Emitting Diodes Lamps (LED)	Enclosed interior office		Full	0.006	0.23	
			Minimum	0.204	0.558	
	Open office		Full	0.006	0.23	
			Minimum	N/A	N/A	N/A
	Breakroom		Full	0.012	0.056	
			Minimum	0.126	0.249	
Corridor		Full	0.147	1.674		

3.5 **Other Effects of Voltage Fluctuation**

Other effects of voltage fluctuation are mentioned in [107]. Voltage fluctuations may lead to false tripping of relays, tripping out of electronic equipment, as well as the interference with communication equipment. The more severe fluctuations may prevent other loads from starting. Induction motors may stall during large voltage fluctuations, but usually only when operating at maximum torque [107].

Chapter 4. The Mitigation of Voltage Fluctuation and Light Flicker

4.1 Introduction

The main objective of this chapter is to address the following (Figure 4.1):

- the standard utility practice when a customer’s equipment violates the flicker limit and the corresponding impact on the operation of the Fast Charging Station (FCS),
- the responsibility to mitigate the voltage fluctuation and light flicker,
- how the flicker can be mitigated,
- the pros, cons, and costs of flicker mitigation techniques, and
- the selection of the best flicker mitigation device, according to the defined criteria in this study.

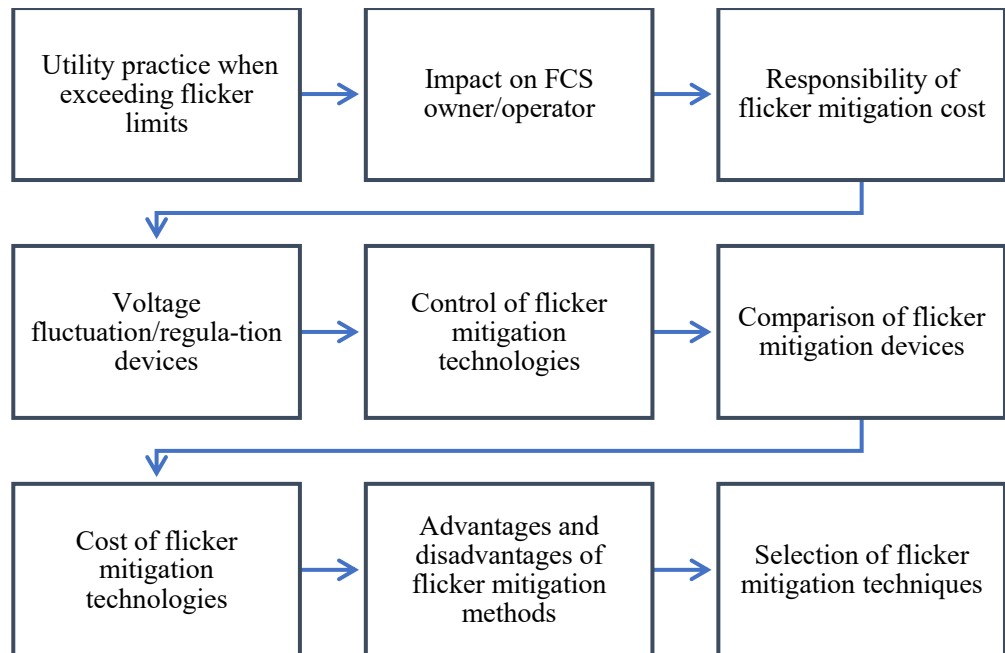


Figure 4.1 Layout of this Chapter

4.2 General Utility Practice when Exceeding Flicker Limits

4.2.1 Customer Responsibilities

It is not permitted for any customer to cause a voltage fluctuation in the system leading to a light flicker in nearby customers [125]. It is the responsibility of the facility owner/operator to limit voltage fluctuation caused by the operation of their equipment [126]. If corrective action was not taken by the operator of the facility, after a notice by the energy provider, the service may get disconnected until the issue with the flicker is rectified. In [127], if the flicker emission levels are violated by the operation of customer equipment, the network operator may:

- a) require mitigative action taken by the customer,
- b) require a disconnection of the customer's equipment until mitigative action can be taken.
- c) consider a service disconnection of the fluctuating facility.

4.2.2 Responsibilities for Flicker Mitigation

There are several loads that may cause voltage fluctuation, such as a motor and [Fast Charging Stations]. When the operation of such equipment causes voltage fluctuation and exceeds the flicker limits, the customer may be required to install mitigation devices or limit the operation of the disturbing equipment, at their own cost. Further connection to the grid will not be permitted without corrective devices [128].

4.3 Voltage Fluctuation Mitigation Technologies

Voltage fluctuation is a function of its amplitudes and its rate of occurrences. Regulating these two factors leads to regulating the fluctuation. In general, the voltage fluctuation can be reduced by two approaches [107]:

1. Increasing the level of the short-circuit power,
2. Decreasing the fluctuation of the load reactive power.

The first approach is applied, to which the offending load is connected, by [107]:

- Installing the fluctuation load at a higher voltage level,
- Installing series capacitors,
- Feeding the offending load from a dedicated line,
- Using a three-winding transformer to isolate the varying loads from the steady loads,
- Increasing the power rating of the transformer, by which the offending load is supplied.

In the second approach, the voltage fluctuation is regulated by connecting a flicker mitigation device. Figure 4.2 depicts different devices for mitigating voltage fluctuation.

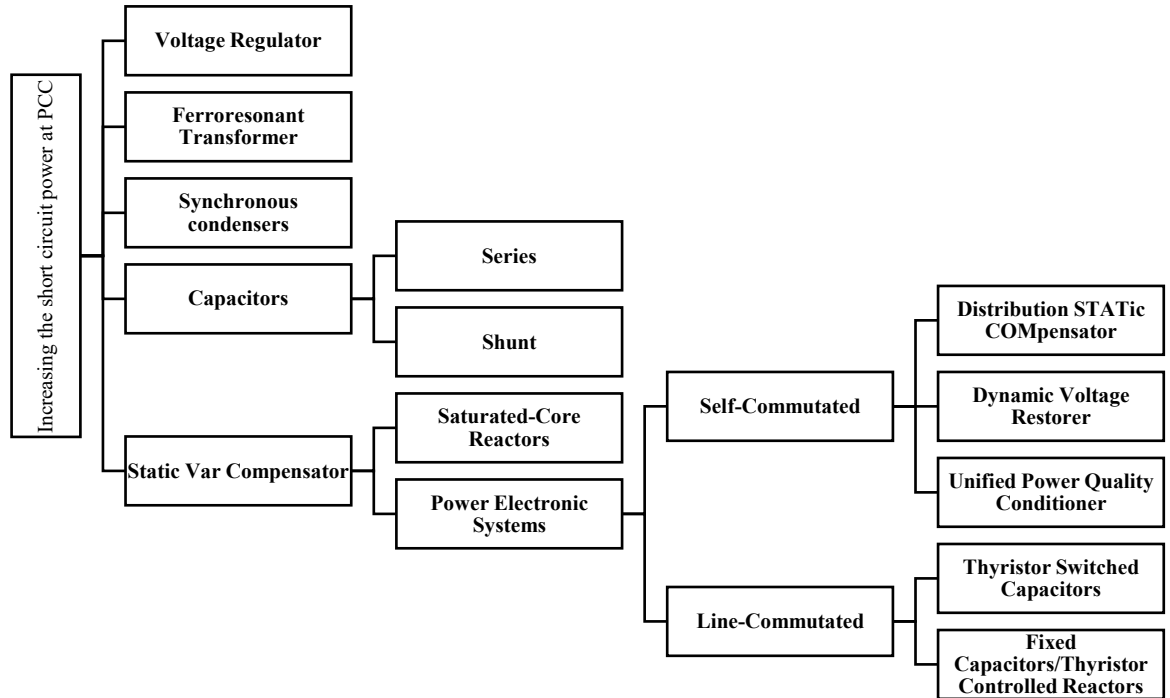


Figure 4.2 Classification of voltage fluctuation mitigation devices [129]

4.4 Comparison of Voltage Fluctuation Mitigation Technologies

Static Var Compensators [130]: An SVC is classified based on the electronic circuits into line- and self-commutated converters (Figure 4.2). A static var compensator generally consists of reactors and/or capacitors controlled using thyristors. One application of an SVC in the distribution system is used to mitigate the system voltage fluctuation by compensating the reactive power. When the system voltage at the load terminal is low, the SVC reacts and increases the system voltage by injecting reactive power. In contrast, the SVC regulates the system voltage by absorbing reactive power when the voltage is high [130]. There are several types of SVCs explained below.

Saturable-core Reactors [129]: A reactor has a defined threshold and a wide current operating range. When the voltage across the reactor exceeds the defined threshold, the reactor current is changed and taken out of the saturation region. When the voltage across the reactor is at the minimum value, the reactor flows a magnetizing current to stabilize the system voltage [129]. At nominal system voltage, the reactor is saturated, which may generate harmonics and adversely increase the losses. The SR has a fast response time of less than one cycle [131].

Thyristor Switched Capacitors (TSC) [132]: A TSC includes numerous shunt capacitors (Figure 4.3). Each capacitor is controlled by a thyristor to determine the amount of the injected vars to the system by switching it ON or OFF. A fixed inductor may be connected in parallel with the switched capacitor to control the injection and absorption of the reactive power. The control circuit of the TSC relies on the voltage, current, and/or reactive power flow of the line. The TSC can be utilized to compensate a three-phase or single-phase load. The latter offers more regulation when an unbalanced load causes a flicker. The TSC has a fast-dynamic response of 0.5-1 cycle [132]. The response time may be delayed and adversely affected by the control settings. The TSC does not produce harmonics, but due to the combination of the inductor and the capacitor, a series resonance may occur [129].

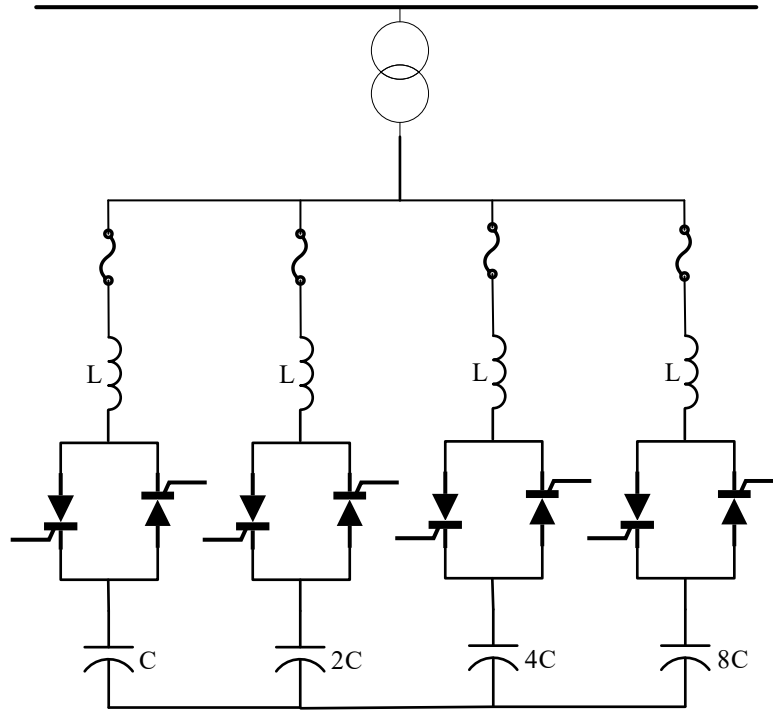


Figure 4.3 Schematic Diagram of TSC Compensator [129]

Fixed Capacitors/Thyristor Controlled Reactors (FC/TCR) [129]: An FC/TCR consists of a fixed capacitor bank and inductance controlled by thyristor (Figure 4.4). The fixed capacitor injects leading reactive power, whereas the thyristor-controlled reactor is switched ON and OFF to control the amount of injected reactive power. Higher odd-order harmonics may be generated because of gating the thyristor ON and OFF. Also, even-order harmonics are produced when retardation angles are not equal for the thyristors [129]. In practice, a filter network is utilized, instead of the fixed capacitor, to generate low impedance at specific frequencies, to shunt components of the dominant harmonics generated by the thyristors.

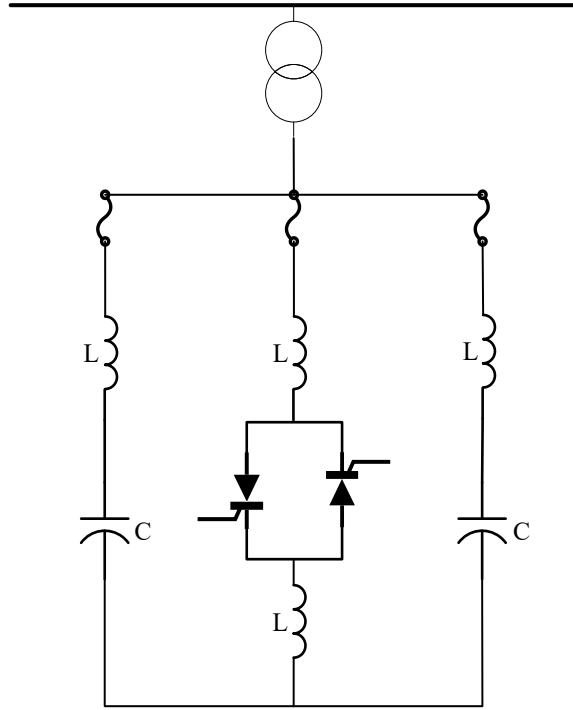


Figure 4.4 Schematic Diagram of FC/TCR Compensator [94]

Distribution Static Compensator [133]: A DSTATCOM is utilized in the distribution system to improve power quality. A DSTATCOM can be connected to load terminals or to the distribution bus, to perform load compensation or to perform voltage regulation, respectively. In the first mode of connection, a DSTATCOM can improve and correct the power factor and balance the load, whereas the bus voltage remains constant against disturbances in the second mode of connection. A DSTATCOM consists of several Voltage Source Converters (VSCs) and a dc storage capacitor utilized as a common point to connect the VSCs. A transformer in delta or star connections is utilized to isolate the inverter legs and prevents the dc capacitor from shorting. A DSTATCOM is costly and may not be a feasible solution for small power customers [133].

Dynamic Voltage Restorer [134]: A DVR is a custom power device installed between the supply and critical load. A DVR contains inverters and energy storage connected to the network through a series transformer. The inverter is utilized to restore voltage quality at the critical load by injecting a series voltage. A DVR is characterized by its fast response to the variation and thus the control system of a DVR is complex, because it needs to detect and determine the reference signal of the series injected voltage [134]. Determining the reference signal is affected by several factors, such as the type of energy storage system, its capability to generate active power, and its load sensitivity to the disturbance. One of the main limitations of a DVR is the complexity of protecting the device and preventing interference with the existing equipment during a short circuit [134].

Unified Power Quality Conditioner [135]: A UPQC contains series and shunt active power filters integrated in the dc side via a common dc capacitor. The series component regulates the fluctuation in the supply side by injecting voltages to improve the load voltage quality at a certain level. The shunt component improves the current quality and mitigates disturbances caused by the power consumers by providing currents to the network to make the source currents and voltages balanced and in phase [135].

Synchronous Condensers [131]: A synchronous condenser is a synchronous machine that works by providing only reactive power. SCs are utilized in the distribution network to stabilize system voltage under different load conditions. SCs are integrated to the grid as shunt devices to reduce network reactance. An SC is

rarely utilized today for the following drawbacks: it requires auxiliary devices for starting and protections, it is noisy, it has more losses compared to static compensators, and it adversely contributes to the short-circuit current [131].

Voltage Regulators [130]: The aim of using voltage regulators in a distribution system is to maintain the output voltage with a defined limit, regardless of the variation in the input voltage. VRs are standard transformers and include taps on the winding to adjust the output voltage. There are two main types of VRs: the step-type and the induction-type (rarely used) [130].

Traditional Voltage Regulator [136]–[139]: Step-type VRs are either station-type, utilized for bus voltage regulation or feeder voltage regulation, or distribution-type, utilized to regulate a single-phase overhead primary feeder. Step-type VRs have two main components: autotransformer and a tap-changer. It detects the input voltage and accordingly changes to a tap in order to compensate for the systems under or over voltage. Step-type voltage regulation is designed to regulate the $\pm 10\%$ of the line voltage in 32 steps with 20/32% voltage changes per step. Connection of the internal coils of a regulator determines the regulation range. If two coils are connected in series, the regulation range is $\pm 10\%$, whereas if they are connected in parallel the regulator can be utilized for $\pm 5\%$, but the regulator's current rating will increase to 160% [136]–[139]. Because of their relatively slow response time, step-types, whether electromechanical or electronic tap switching, are not functional in mitigating fast and frequent voltage variations. They are utilized to regulate long-term voltage variations but are not effective in mitigating a flicker [136]–[139].

Capacitor: Capacitors are utilized in parallel or in series configurations to regulate the system voltage.

Shunt Capacitor [140]: Shunt capacitors are utilized in parallel with the power line to counteract the lagging component by absorbing a leading current. When it overcompensates, shunt capacitors increase reactive power to the network, which causes overvoltage problems. To regulate the voltage at a high load and avoid overcompensation at a low load, the automatic switching is used. However, switching capacitors ON and OFF would make the voltage inside the consumer facilities have more variations. Also, shunt capacitors can produce harmonics. One of the main applications of a shunt capacitor is to improve the power factor and to support the voltage, long-term. The starting voltage may be decreased by a shunt capacitor but the relative voltage change ($\Delta V/V$) is not decreased and, thus, voltage flickers are not compensated by shunt capacitors and may make it worse [140].

Series Capacitors [141]: Unlike shunt capacitors, series capacitors can be used to mitigate voltage fluctuation and flicker. Series capacitors are connected in series with the load, which make them respond instantaneously to load variations. One of the main limitations of series capacitors is that they can only compensate their downstream side, but upstream voltages are not supported. Also, series capacitors reduce system impedances which may require one to modify the short-circuit protection scheme. Series capacitors are custom devices and nonstandard, thus their cost is high [141].

Load Changes [132]: One cost-effective option is to solve the flicker at the source of the problem is by controlling the operation limits of the offending load. The source of the problem, in this study, is the FCS. Changing the operation limits can be applied by reducing the rated output power of the fluctuated loads. This option does not require any physical modification [132].

4.5 **Control of Flicker Mitigation Technologies**

4.5.1 Static Var Compensator

An automatic voltage controller is utilized to control the static var compensator (Figure 4.5). The controller first compares a reference voltage to the measured value and accordingly determines the required amount of reactive power by issuing command signals. These command signals are either converted into digital or into analogue signals, in order to switch thyristors ON and OFF or to control their firing angles. The compensator control may be interrupted when the system voltage exceeds, for a long period of time, a predetermined value defined by the network operator [142]. In contrast, during transients, such as switch capacitor bank, the static compensator control operates without interruptions, although the bus voltage may be affected for a short period of time. In this case, the SVC generates a command signal to either firing a delay angle α that mitigates the transient effect (if the capacitor current is not zero) or to blocking the thyristors (if the capacitor current is zero).

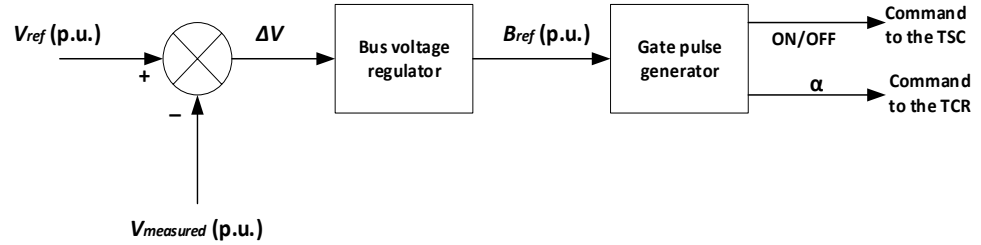


Figure 4.5 A Block Scheme of an SVC Controller [143]

4.5.2 Distribution Static Compensator

A DSTATCOM is shown in Figure 4.6. A DSTATCOM is utilized to inject or absorb a leading/lagging current into the distribution grid via the shunt transformer (Figure 4.6), relying on a pulse-width modulation. The control system of a DSTATCOM has three levels, listed below [144]:

1. Fast voltage regulator
2. Fast current limiter with overload management control
3. Slow reset control

The first level of control relies on a closed-loop function to maintain the voltage within a predetermined range for a short period of cycles. The function of the second level of control is to enhance the equipment's performance and prevent it from interruption, in case of overload. The last level of control is utilized to prevent the device from remaining near or in limits for a long period of time. This is to avoid any delay for subsequent disturbances [144].

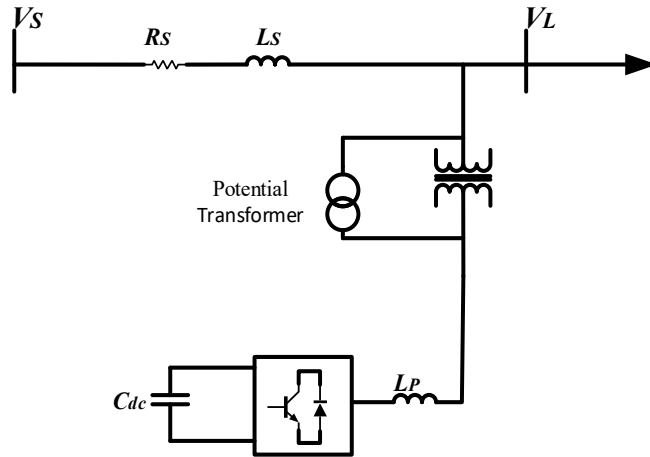


Figure 4.6 A DSTATCOM Diagram [142]

4.5.3 Dynamic Voltage Restorer

A DVR operates in two modes, standby and boost operating modes. Under normal load conditions, the system voltage is at its nominal value and thus a DVR does not supply voltage to the system because it operates in standby mode. When the system voltage deviates above/under certain limits, a DVR provides, for a short period of time, a three-phase voltage to the network synchronized with the grid voltage. In this mode, a DVR supplies the load with the required active and reactive power. The active power is drawn from the equipped energy source. Figure 4.7 shows an open-loop control circuit of a DVR. The controller measures the three-phase system voltage and transform them into α - β components via a stationary frame. A phase locked loop is utilized to transform α - β components via a rotating reference frame into d-q components [145]. These components are subtracted from reference voltage values to determine the injected voltage to the load.

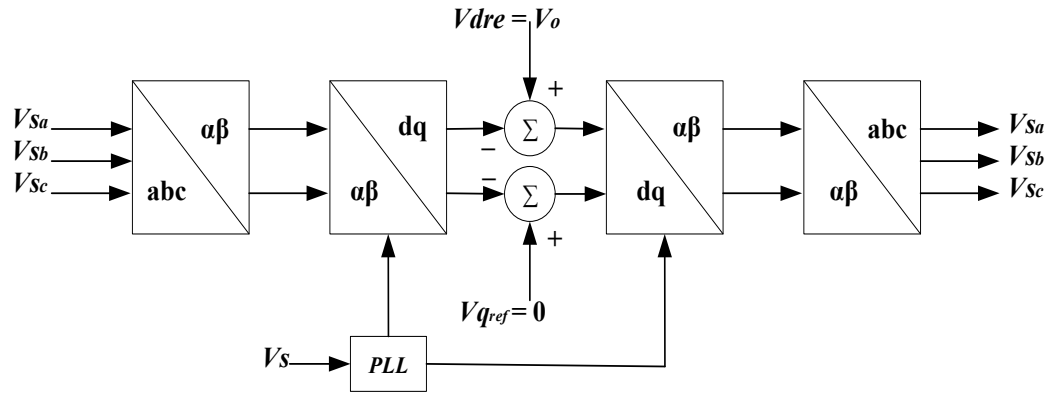


Figure 4.7 A Block Scheme of a DVR Controller [145]

4.5.4 Unified Power Quality Conditioner

A UPQC is shown in Figure 4.8, it has two control circuits connected in series and parallel. The series control circuit functions as a filter to extract a sinusoidal reference voltage and match it with the supply voltage. The amount of compensation is determined by taking the difference between the system and the reference voltages. The difference is provided to the network through the inverter and the series transformer to mitigate power quality disturbances in the source side. The parallel control circuit also works as a filter, but to extract a sinusoidal reference current and compare it with the load current. In the parallel control circuit, the amount of compensation is determined by taking the difference between the system and the reference currents. The difference is injected to the network through the inverter and the parallel transformer is used to mitigate the power quality disturbances in the load side [144].

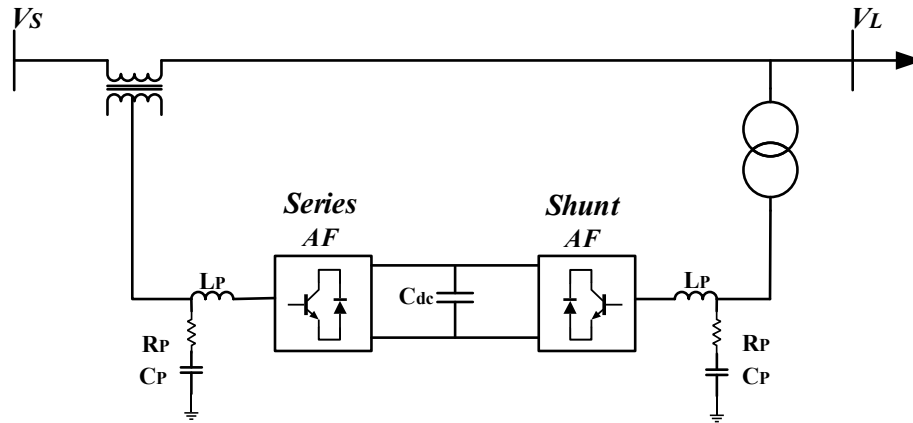


Figure 4.8 A Block Diagram of UPQC [146]

4.5.5 Synchronous Condensers

The controller in the synchronous condenser can be set to manage the regulation in different operation modes. The controller has a digital voltage regulator in order to control the terminal voltage by adjusting the DC field current of the condenser. Regulating the DC field current determines the amount of reactive power that is injected or absorbed to/from the power network, which stabilizes the power system against short-term disturbances. In the case of voltage sags, the synchronous condenser draws a leading current, which in turn increases the excitation of the generator and supports the quick voltage regulation [147].

4.5.6 Saturated-Core Reactor

The SCR consists of a transformer, a damping filter, a slope correction capacitor, a series capacitor with damping filter, and a shunt capacitor with an inductor in series (Figure 4.9). The SCR is connected to the grid via a coupling transformer. The reactance of the saturated reactor ranges from 8 to 15% of its own rating [148]. The slope-correcting capacitor is connected in series with the reactor to decrease the

ranges to 3 to 5% for voltage regulation; however, it adversely reduces the response time [148]. The damping filter is installed in parallel with the slope correcting capacitor to avoid the subharmonics that may occur when the slope correcting capacitor interacts with the grid reactance. The series capacitor with the damping filter is utilized to enhance the voltage regulation capability by offsetting the transformer reactance. The parallel capacitor is utilized to extend the control range of reactive power control, whereas the series inductor is utilized as a tuning filter. The SR is able to regulate the system overload of 3 to 4 p.u. and its response time is about 1.5 to 2 cycles [148].

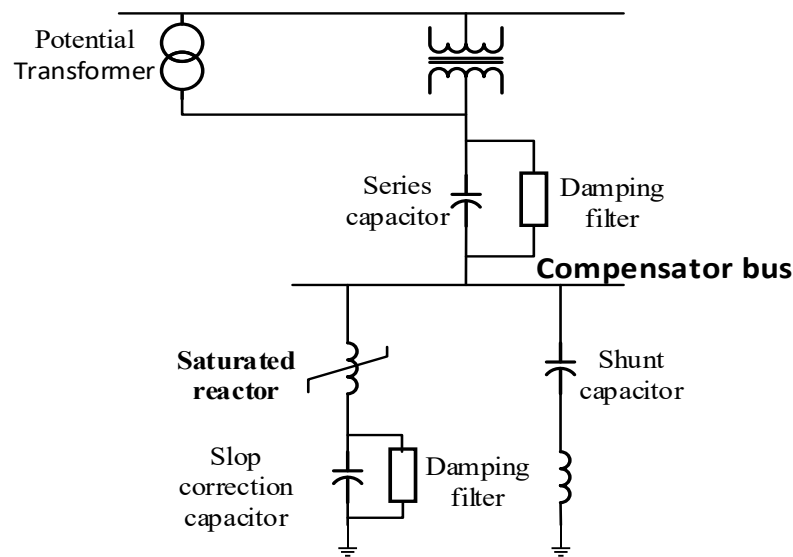


Figure 4.9 A Saturated Reactor [148]

4.5.7 Fixed Series Capacitors

Series capacitors are utilized in the circuit to raise the voltage drop created by the circuit's inductive reactive loads (Figure 4.10). Inserting a series capacitor makes downstream voltage directly varied with the load current, unlike installing a shunt capacitor which results in a fixed voltage support, regardless of the load current

[149], [150]. Therefore, as the downstream load increases, the series capacitor results in a voltage increase proportional to the increase of the load. At no load, the voltage rise is zero. The feeder voltage drop is expressed as [138]:

$$VD = iR \cos \theta + iX_L \sin \theta \quad 4.1$$

where R and X_L are the resistance and the inductive reactance of the feeder circuit, whereas $\cos \theta$, and $\sin \theta$ are the receiving-end power factor and power factor angle, respectively. When a series capacitor is inserted, it injects a capacitive reactance X_C that decreases the X_L in the circuit. This results in decreasing the load current i , which decreases the drop in the voltage as in (4.2) [138]:

$$VD = iR \cos \theta + i(X_L - X_C) \sin \theta \quad 4.2$$

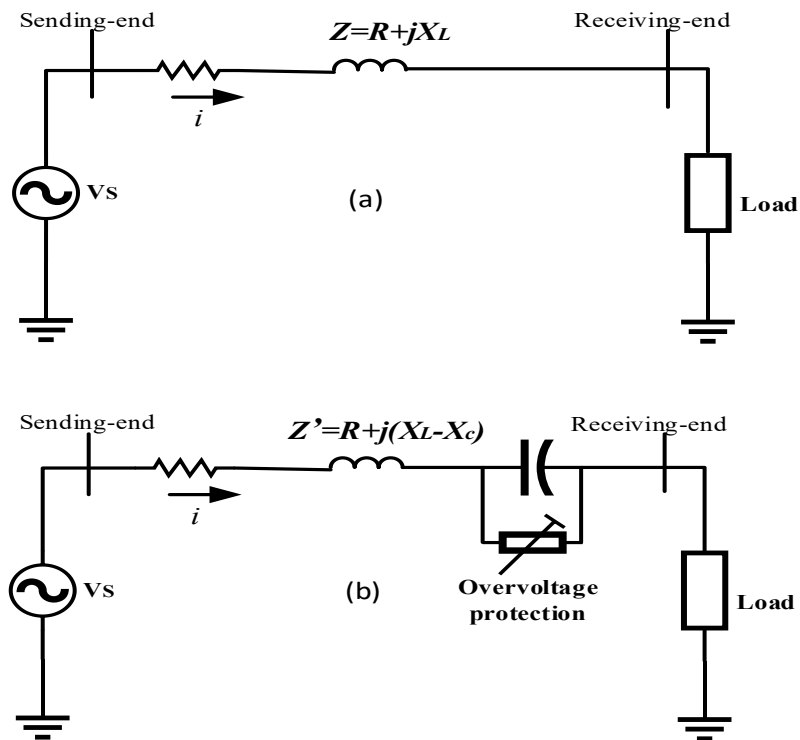


Figure 4.10 Circuit without (a) and with (b) Series Capacitor [132]

A comparative summary of different types of compensation technologies is given in

Table 4-1.

Table 4-1 Comparison of Different Voltage Fluctuation Mitigation Devices [94], [148], [152]–[154]

	I	II	III	IV	V	VI	VII	VIII
	Synchronous condensers	Series Capacitors	Saturated Reactors	FC/TCR	TSC	DSTATCOMs	DVR	UPQC
Steady state Characteristic	Automatic voltage regulator, easily adjustable	Self-regulation	Restricted adjustment possible on site	Controller easily adjustable	Controller easily adjustable	Controller easily adjustable	Controller easily adjustable	Controller easily adjustable
Control range	generation and absorption.	Capacitive	W/capacitor generation & absorption	generation and absorption	Capacitive	Both generation and absorption	Both generation and absorption	Both generation and absorption.
Harmonic content	Negligible	Negligible	Internally, compensated in balanced 3-ph system	Requires filters	Negligible	Small low order. Large: high order	Small; depends on the hardware	Small low order; eliminated by a shunt filter
Losses	High at full output. Low at zero var output	Negligible	Low at full generation. High at full absorption	Low at full generation. High at full absorption	High at full output. Low at zero var output	High at full output. Low at zero var output	Low	Low
Overload capability	Up to two times	Limited to capacitor rating	Limited to the slop-correcting capacitor	Limited to capacitor rating	Limited to capacitor rating	Limited to rating of shunt compensator	Up to 150% for 30 s	Up to 150%
Response time in the system	0.2 s	0-0.05 s	0-0.05 s	0.02-0.06 s	0.02-0.06s	0.01-0.02 s	0.01-0.02 s	0.01-0.02 s
Maintenance requirements	As for any rotating plant	Moderate	Small as for an outdoor equipment	Moderate as for electronic indoor equipment	Moderate	Moderate	Moderate	Moderate
Response to rapidly fluctuating load	Relatively slow	Inherently fast	Inherently fast	Less rapid than III	Slower than IV	Faster than V	Faster than V	Faster than V
Voltage control under line outage	Good, but relatively less rapid	Requires metal varistor for protection	May require switched capacitors to support voltage	Require switched capacitors to support voltage	Require switched capacitors to support voltage	Require switched capacitors to support voltage	Require energy storage to provide power	Require a DC capacitor to support voltage
Behavior following system fault	Swinging and loss of synchronism	Can't tolerate fault current; automatic switch req.	Inherent response as a constant voltage device	Auxiliary controls used to damp load swings	Auxiliary controls used to damp load swings	Auxiliary controls used to damp load swings	Auxiliary controls used against overcurrent	Series converter utilized to improve system stability

4.6 Cost of Flicker Mitigation Technologies

This section attempts to quantify and compare the costs of the various mitigation devices discussed above. These devices are UPQC, DSTATCOM, TSC, FCTCR, DVR, and FSC. For these technologies, there will be two costs involved. The first is the initial purchase price of the equipment, while the second is the maintenance costs associated with the selected equipment. The cost of power quality mitigation devices is determined based on their power rating such as \$/kVar [142]. This cost represents a rough estimate of the equipment; however, the total system cost may contain additional elements [142].

The total annual equivalent cost of installing a voltage flicker mitigation device can be found as:

$$A^y = \mathbb{C}^y + \mathcal{M}^y \quad 4.3$$

Where

A^y the total annual equivalent cost, \$/year

\mathbb{C}^y the annual equivalent cost of capital invested, \$/year

\mathcal{M}^y the annual equivalent cost of maintenance, \$/year

The annual equivalent capital cost is called capital recovery cost, \mathbb{C}^y

$$\mathbb{C}^y = \zeta \cdot \mu' - \mathcal{S} \cdot \ell' \quad 4.4$$

Where

- ζ the first cost of installed flicker mitigation device, \$
- \mathcal{S} the estimated salvage value at the end of the device useful life, \$
- μ' the capital recovery factor
- ℓ' the single-payment discount factor

$$\mu' = \left(\frac{\lambda \cdot (\lambda + 1)^\eta}{(\lambda + 1)^\eta - 1} \right) \quad 4.5$$

$$\ell' = \left(\frac{\lambda}{(\lambda + 1)^\eta - 1} \right) \quad 4.6$$

Where

- λ the fixed charge rate, %
- η the useful life in years (flicker mitigation device lifetime), years

The total annual equivalent cost (ζ) and salvage value (\mathcal{S}) are estimated as:

$$\zeta = \Gamma \cdot \varphi \quad 4.7$$

$$\mathcal{S} = \Omega \cdot \varphi \quad 4.8$$

Where

- Γ the cost per unit of installed flicker mitigation device, \$/kVAr
- Ω the salvage value per kVAr at the end of η , \$/kVAr
- φ the operating range of the flicker mitigation device, MVar

The cost of installation (Γ) of different flicker mitigation equipment are given in [148], [155]–[158] as follows:

$$\Gamma_{UPQC} = 0.0003. \varphi_{UPQC}^2 - 0.2691. \varphi_{UPQC} + 188.2 \quad 4.9$$

$$\Gamma_{DSTATCOM} = 0.0002478. \varphi_{DSTATCOM}^2 - 0.2261. \varphi_{DSTATCOM} + 60 \quad 4.10$$

$$\Gamma_{TSC} = 0.0003. \varphi_{TSC}^2 - 0.305. \varphi_{TSC} + 127.4 \quad 4.11$$

$$\Gamma_{FCTCR} = 0.0003. \varphi_{FCTCR}^2 - 0.305. \varphi_{FCTCR} + 127.4 \quad 4.12$$

$$\Gamma_{DVR} = 0.0015. \varphi_{DVR}^2 - 0.713. \varphi_{DVR} + 153.8 \quad 4.13$$

$$\Gamma_{FSC} = 0.000541. \varphi_{FSC}^2 - 0.3902. \varphi_{FSC} + 90.8 \quad 4.14$$

Where

Γ_{UPQC}	the per unit cost of the Unified Power Quality Conditioner, ($\$/kVAr$)
$\Gamma_{DSTATCOM}$	the per unit cost of the Distribution Static Compensator, ($\$/kVAr$)
Γ_{TSC}	the per unit cost of the Thyristor Switched Capacitor, ($\$/kVAr$)
Γ_{FCTCR}	the per unit cost of the Fixed Capacitors/Thyristor Controlled Reactors, ($\$/kVAr$)
Γ_{DVR}	the per unit cost of the Dynamic Voltage Restorer, ($\$/kVAr$)
Γ_{FSC}	the per unit cost of the Fixed Series Capacitor, ($\$/kVAr$)
φ_{UPQC}	the operating range of the Unified Power Quality Conditioner, $MVAr$
$\varphi_{DSTATCOM}$	the operating range of the Distribution Static Compensator, $MVAr$
φ_{TSC}	the operating range of the Thyristor Switched Capacitor, $MVAr$
φ_{FCTCR}	the operating range of the Fixed Capacitors/Thyristor Controlled Reactors, $MVAr$
φ_{DVR}	the operating range of the Dynamic Voltage Restorer, $MVAr$
φ_{FSC}	the operating range of the Fixed Series Capacitor, $MVAr$

The annual equivalent cost to maintain the flicker mitigation device (\mathcal{M}^y) is calculated per kVAr per year as in (4.15):

$$\mathcal{M}^y = \gamma \cdot \Gamma \cdot \varphi \cdot \mu' \tag{4.15}$$

Where

γ The maintenance cost in percent of the first cost, (%)

λ is the fixed interest rate at 6% and n is the lifetime of the project of 10 years. If the salvage value is assumed to be negligible, the different mitigation methods are calculated as in Table 4-2.

Table 4-2 Maintenance Cost for Flicker Mitigation Devices

Mitigation device	% of the first cost	The source
\mathcal{M}_{UPQC}^y	10	[159]
$\mathcal{M}_{DSTATCOM}^y$	5	[160]
\mathcal{M}_{TSC}^y	10	[161]
\mathcal{M}_{FCTCR}^y	10	[161]
\mathcal{M}_{DVR}^y	5	[162]
\mathcal{M}_{FSC}^y	1	[163]

4.7 Comparison of Costs of Flicker Mitigation Technologies

As per the general utility practice, the annual fixed charge rate is estimated based on the summation of the following costs: costs of capital, depreciation, taxes, insurance, and operation and maintenance expenses. However, only the capital and maintenance costs are considered in calculating the Λ^y in Table 4-3. Also, the salvage value is assumed to be zero at the end of the project lifetime.

Table 4-3 Cost of Voltage Fluctuation Mitigating Devices

Parameters	Mitigation Techniques					
	UPQC	DSTATCOM	TSC	FC-TCR	DVR	FSC
Lifetime η , (years)	20	20	20	20	20	20
Charge rate λ , (%)	6	6	6	6	6	6
Maintenance cost in % of first cost γ , (%)	10	5	10	10	5	1
Reactive power range φ , (MVar)	2	2	2	2	2	2
The per kVAr cost Γ , (\$/kVAr)	187.66	79.55	126.8	126.8	153.3	89.97
Salvage value per kVAr Ω , (\$/kVAr)	0	0	0	0	0	0
Cost of installation, ζ (\$)	375,320	159,100	253,600	253,600	306,600	179,940
Salvage at end of device lifetime, \mathcal{S} (\$)	0	0	0	0	0	0
capital recovery factor, μ'	0.0872	0.0872	0.0872	0.0872	0.0872	0.0872
Single-payment discount factor, ℓ'	0.0272	0.0272	0.0272	0.0272	0.0272	0.0272
Capital recovery cost, \mathcal{C}^y , (\$/year)	32,728	13,874	22,114	22,114	26,735	15,691
Annual maintenance cost, \mathcal{M}^y , (\$/year)	3,272	694	2,211	2,211	1,337	157
Total annual equivalent cost, \mathcal{A}^y (\$/year)	36,000	14,568	24,325	24,325	28,072	15,848

Table 4-3 shows a range of costs for a number of the mitigation technologies discussed above. According to the comparison, the DSTATCOM is the cheapest mitigation technology on a cost per kVAr basis and is based on the total annual equivalent cost (14,568 \$/year). In contrast, the UPQC has the highest annual cost and per kVAr cost.

4.8 Comparison of Advantages and Disadvantages of Mitigation Technologies

Table 4-4 illustrates the advantages and the disadvantages of each flicker mitigation technique explained in this chapter.

Table 4-4 Advantages and Disadvantages of Different Types of Compensating Devices

Mitigation Techniques	Advantages	Disadvantages
TSC	<ul style="list-style-type: none"> ▪ Fast response time, less than 20 ms. ▪ Effective in reducing the impacts of fast load fluctuations and flicker. ▪ Free harmonic generation. ▪ No switching transients. ▪ Effective control to prevent overcurrents and overvoltages. 	<ul style="list-style-type: none"> ▪ Susceptible to series resonance, appropriate connection is required to prevent it. ▪ A delay in the response time may occur due to complicated control system. ▪ Higher losses than that in pure capacitor losses.
FC/TCR	<ul style="list-style-type: none"> ▪ Operate in inductive and capacitive modes. ▪ Flexible control during light and heavy loading periods. 	<ul style="list-style-type: none"> ▪ High steady-state losses ▪ Limitation in the injections or the absorption of reactive power. ▪ Can't disconnect the capacitor in exigencies.
Saturable reactors	<ul style="list-style-type: none"> ▪ Instantaneous intervention in fluctuations of the load current. ▪ Suppressed flicker to large extend. ▪ Lower short-circuit current via forced magnetized. ▪ Stabilized levels of PCC voltage and load current. 	<ul style="list-style-type: none"> ▪ Distorts of the consumed load current. ▪ Generates high order current harmonics. ▪ Slow time response in a single-phase operation.
Dynamic Voltage Restorer	<ul style="list-style-type: none"> ▪ Fast dynamic response to the disturbance. ▪ Different modes of operations. ▪ Compensate for the inductive drop in the line. ▪ Limiting fault current by providing a leading voltage. 	<ul style="list-style-type: none"> ▪ Requires active power during the compensation. ▪ Causes phase jump at load voltage. ▪ Partially provides power to the load during extreme variations.
DSTATCOMs	<ul style="list-style-type: none"> ▪ Ability to perform different functions at the same time. ▪ Ability to follow rapid load variations. ▪ Smaller than that of corresponding SVC systems. 	<ul style="list-style-type: none"> ▪ Compensates only for reactive power at the fundamental frequency. ▪ Limited overload capability.
Synchronous condensers	<ul style="list-style-type: none"> ▪ Reducing the voltage flicker. ▪ Stabilize the voltage at PCC. ▪ High temporary overload capability. 	<ul style="list-style-type: none"> ▪ High losses, 1.25-5.5% of the nominal power. ▪ Unit cost increases with the decrease in the power of the device.
Shunt capacitors	<ul style="list-style-type: none"> ▪ Mounted sequentially which decrease initial investment. ▪ Voltage support and power factor correction. ▪ Low power losses, 0.25-0.30% of the nominal power. 	<ul style="list-style-type: none"> ▪ Relatively long response time. ▪ Do not minimize flicker. ▪ Leads to rise/dips the voltage by switching on and off. ▪ Do not allow continuous control of the voltage. ▪ Do not absorb the capacitive power of the lines.
Series capacitors	<ul style="list-style-type: none"> ▪ Minimizing light flicker on radial feeders. ▪ Improving voltage regulation on radial feeders. ▪ Increasing power transfer ability. ▪ Controlling load sharing between parallel feeders. 	<ul style="list-style-type: none"> ▪ Compensation available only downstream the capacitor. ▪ May cause resonance phenomena. ▪ Affecting distance estimation for distance relay. ▪ Self-excitation of synchronous machines.

Ferroresonant transformers	<ul style="list-style-type: none"> ▪ Superior Voltage Regulation. ▪ Effective during momentary voltage interruptions. ▪ Ride-through capability. ▪ Ability to inject a constant current output rather than constant voltage. 	<ul style="list-style-type: none"> ▪ Low efficiencies decrease more when the loading reduces. ▪ Oversized by 2 to 3 times the rated load current ▪ Large size and noisy. ▪ Relatively high cost.
Voltage regulator	<ul style="list-style-type: none"> ▪ Cost-efficient. ▪ Can control the active and reactive power. ▪ Perform shunt and series compensation. 	<ul style="list-style-type: none"> ▪ Do not minimize flicker. ▪ Slow time response.
UPQC	<ul style="list-style-type: none"> ▪ Flexible overall control. ▪ Efficient runs near nominal operating point. ▪ Small physical size and light weight. 	<ul style="list-style-type: none"> ▪ Low efficiency when load power is low. ▪ Limited lifetime of the electrolyte capacitor.

4.9 Technology Selection

In this comparison, several parameters are utilized to select the best flicker mitigation device. These parameters are as follows:

1. Overload capability
2. Losses
3. Response Time
4. Reactive power range
5. Investment costs
6. Control interaction
7. Special requirements (i.e., protection devices; special connection; customization).
8. Efficiency during low/high loading
9. Single-Phase control
10. Energization

In choosing the best option for reducing voltage flicker caused by the FCS, it is important to consider the cost and benefit of each method that is available. In this study, two stages are utilized to select the best flicker mitigation technique. In the first stage, a linguistic comparative is utilized to compare between each mitigation method, as shown in Table 4-5. The first column in Table 4-5 represents parameters utilized to differentiate between each mitigation technique listed in the first row.

Then, each linguistic comparator, utilized in Table 4-5, is given a score based on a user defined criterion. Four types of scores are utilized to distinguish between each mitigation method, that are: -, --, +, and ++. This method of comparison has been utilized in the literature as per [164]. The value (score) of each group of linguistic comparators is shown in Table 4-6. In the second stages, the linguistic comparators are mapped based on their given score as shown in Table 4-7. Each mitigation technique is given a weight based on the difference of its total positive scores and its total negative scores. The mitigation technique which possesses the maximum positive weight is considered the best flicker mitigation option, as per the parameters defined in this study.

Table 4-5 Comparison of Different Voltage Mitigating Devices

	Mitigating Techniques					
	FSC	FC/TCR	TSC	DSTATCOMs	DVR	UPQC
Overload capability	Limited	Limited	Limited	Limited	Good	Good
Losses	small	Moderate	Small	Small	Small	Small
Response Time	Very fast	fast	fast	fast	Very fast	Very fast
Reactive power range	Capacitive	Capacitive inductive	Capacitive	Capacitive inductive	Capacitive inductive	Capacitive inductive
Capital costs	Good	High	High	Good	Very high	Very high
Maintenance costs	Very good	Good	Good	Good	Very high	Very high
Control interaction	Limited	Good	Good	Good	Good	Good
Special requirements	Overvoltage resonance	Harmonic	Resonance	Short-circuit	Short-circuit	Short-circuit
Efficiency during low/high loading	Good	Good	Good	Good	Good	Limited
Single-Phase control	Yes	Yes	Yes	Yes	Yes	Yes
Energization	Fast & direct	Fast w/control	Fast w/control	Fast w/control	Fast w/control	Fast w/control

Table 4-6 Weighting of the comparators in Table 4-5

Given Weight			
+	-	++	--
Cheap	High	Very fast	Very high
Fast	Slow	Fast & direct	Very slow
Fast w/control	Short-circuit	Very good	Cost \$/kVA > 150
Capacitive	Moderate	Cost \$/kVA ≤ 50	7.5 < γ ≤ 10%
Yes	Limited	γ ≤ 2.5%	
Good	Resonance		
Small	Harmonic		
Inductive	100 < Cost \$/kVA ≤ 150		
50 < Cost \$/kVA ≤ 100	Overtoltage		
2.5% < γ ≤ 5%	No		
	5% < γ ≤ 7.5 %		

Table 4-7 Grading of the Selected mitigation Devices

	Mitigation Techniques					
	FSC	FC/TCR	TSC	DSTATCOMs	DVR	UPQC
Overload capability	-	-	-	-	+	+
Losses	+	-	+	+	+	+
Response Time	++	+	+	+	++	++
Reactive power range	+	++	+	++	++	++
Cost per kVAr	+	-	-	+	--	--
Maintenance Cost	++	--	--	+	+	--
Control interaction	-	+	+	+	+	+
Single-Phase control	+	+	+	+	+	+
Special requirements	--	-	-	-	-	-
low/high loading Eff.	+	+	+	+	+	-
Energization	++	+	+	+	+	+
Sum (-)	-4	-6	-5	-2	-3	-6
Sum (+)	11	7	7	10	11	9
Sum (total)	7	1	2	8	8	3

In Table 4-7, the results show that DSTATCOM and DVR have equivalent positive weights. This means that both represent the best mitigation solutions based on the defined criteria. However, their capital costs are varied distinctly. If the highest priority is to minimize cost, the DSTATCOM has lower cost per kVAr than the DVR and thus it represents the preferred solution. In contrast, if the priority is efficiency and fast action, the DVR represents the best solution.

4.10 DSTATCOM Modelling

The DSTATCOM is modeled, as proposed in [165]. Figure 4.11 shows a simple three-phase balanced distribution system in which the power is transferred radially. In this system, a DSTATCOM is installed to inject reactive power and improve the voltage profile. The mathematical representation of a DSTATCOM is described below to calculate the current injected from the DSTATCOM.

$l^n + j\zeta^n$	Line impedance between buses n and $n+1$
$i^n \angle \alpha$	Line current flows out of bus n after DSTATCOM installed
$i^{DSTATCOM}$	Current injected by DSTATCOM
$\angle \left(\vartheta^{n+1} + \frac{\pi}{2} \right)$	Phase angle of current injected by DSTATCOM
$Q^{DSTATCOM}$	Reactive power injected by the DSTATCOM
$\bar{U}^{n+1} \angle \bar{\vartheta}^{n+1}$	Voltage at bus $n+1$ before DSTATCOM installed
$U^{n+1} \angle \vartheta^{n+1}$	Voltage at bus $n+1$ after DSTATCOM installed
$U^n \angle \vartheta^n$	Voltage at bus n after DSTATCOM installed
$P^n + jQ^n$	Constant load connected at bus n

$P^{n+1} + jQ^{n+1}$ Constant load connected at bus $n+1$

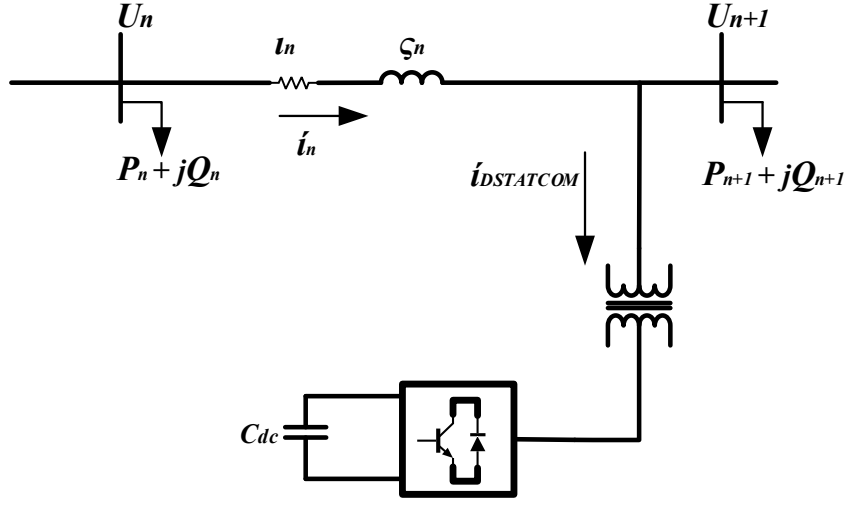


Figure 4.11 DSTATCOM Installed at Bus $n+1$

The new voltage after installing DSTATCOM is expressed as in (4.16)

$$U^{n+1} \angle \vartheta^{n+1} = U^n \angle \vartheta^n - (l^n + j\zeta^n) \cdot i^n \angle \alpha - (l^n + j\zeta^n) \cdot i^{DSTATCOM} \angle \left(\vartheta^{n+1} + \frac{\pi}{2} \right) \quad 4.16$$

Equations (4.17) and (4.18) are obtained by splitting (4.16) into real and imaginary parts.

$$\begin{aligned} U^{n+1} \cdot \cos(\vartheta^{n+1}) &= \Re(U^n \angle \vartheta^n) - \Re(l^n \cdot i^n \angle \alpha) + \zeta^n \cdot i^{DSTATCOM} \cdot \sin\left(\vartheta^{n+1} + \frac{\pi}{2}\right) \\ &\quad - l^n \cdot i^{DSTATCOM} \cdot \cos\left(\vartheta^{n+1} + \frac{\pi}{2}\right) \end{aligned} \quad 4.17$$

$$\begin{aligned} U^{n+1} \cdot \sin(\vartheta^{n+1}) &= \Im(U^n \angle \vartheta^n) - \Im(\zeta^n \cdot i^n \angle \alpha) - \zeta^n \cdot i^{DSTATCOM} \cdot \cos\left(\vartheta^{n+1} + \frac{\pi}{2}\right) \\ &\quad - l^n \cdot i^{DSTATCOM} \cdot \sin\left(\vartheta^{n+1} + \frac{\pi}{2}\right) \end{aligned} \quad 4.18$$

Solving (4.17) and (4.18) yields (4.19) and (4.20).

$$i^{DSTATCOM} = \frac{U^{n+1} \cdot \cos(\vartheta^{n+1}) - \Re(U^n \angle \vartheta^n) + \Re(i^n \cdot i^n \angle \alpha)}{i^n \cdot \sin(\vartheta^{n+1}) + \zeta^n \cdot \cos(\vartheta^{n+1})} \quad 4.19$$

$$i^{DSTATCOM} = \frac{U^{n+1} \cdot \sin(\vartheta^{n+1}) - \Im(U^n \angle \vartheta^n) + \Im(\zeta^n \cdot i^n \angle \alpha)}{\zeta^n \cdot \sin(\vartheta^{n+1}) - i^n \cdot \cos(\vartheta^{n+1})} \quad 4.20$$

Equation (4.21) is found by equating (4.19) and (4.20).

$$\begin{aligned} & \frac{U^{n+1} \cdot \cos(\vartheta^{n+1}) - \Re(U^n \angle \vartheta^n) + \Re(i^n \cdot i^n \angle \alpha)}{i^n \cdot \sin(\vartheta^{n+1}) + \zeta^n \cdot \cos(\vartheta^{n+1})} \\ &= \frac{U^{n+1} \cdot \sin(\vartheta^{n+1}) - \Im(U^n \angle \vartheta^n) + \Im(\zeta^n \cdot i^n \angle \alpha)}{\zeta^n \cdot \sin(\vartheta^{n+1}) - i^n \cdot \cos(\vartheta^{n+1})} \end{aligned} \quad 4.21$$

Equation (4.21) can be arranged in standard quadratic equation form, as in (4.22)

Where,

$$\begin{aligned} \phi &= (\Re(U^n \angle \vartheta^n) - \Re(i^n \cdot i^n \angle \alpha)) \cdot \zeta^n - (\Im(U^n \angle \vartheta^n) - \Im(\zeta^n \cdot i^n \angle \alpha)) \cdot i^n \\ &= (\Re(U^n \angle \vartheta^n) - \Re(i^n \cdot i^n \angle \alpha)) \cdot i^n - (\Im(U^n \angle \vartheta^n) - \Im(\zeta^n \cdot i^n \angle \alpha)) \cdot \zeta^n \end{aligned} \quad 4.22$$

$$(\phi^2 + \psi^2) \cdot \sin(\vartheta^{n+1})^2 = (2 \cdot \phi \cdot U^{n+1} \cdot i^n) \cdot \sin(\vartheta^{n+1}) - ((U^{n+1})^2 \cdot (i^n)^2 - \psi^2) \quad 4.23$$

Solution of (4.24) can be obtained as:

$$\sin(\vartheta^{n+1}) = \frac{-\xi \pm \sqrt{(\xi)^2 - 4 \cdot \beta \cdot \eta}}{2 \cdot \beta} \quad 4.24$$

Where,

$$\begin{aligned} \xi &= -2 \cdot \left((\Re(U^n \angle \vartheta^n) - \Re(i^n \cdot i^n \angle \alpha)) \cdot \zeta^n \right. \\ &\quad \left. - (\Im(U^n \angle \vartheta^n) - \Im(\zeta^n \cdot i^n \angle \alpha)) \cdot i^n \right) \cdot U^{n+1} \cdot i^n \end{aligned} \quad 4.25$$

$$\begin{aligned} \beta = & \left((\Re(U^n \angle \vartheta^n) - \Re(i^n \cdot i^n \angle \alpha)) \cdot \zeta^n - (\Im(U^n \angle \vartheta^n) - \Im(\zeta^n \cdot i^n \angle \alpha)) \cdot i^n \right)^2 \\ & + \left((\Re(U^n \angle \vartheta^n) - \Re(i^n \cdot i^n \angle \alpha)) \cdot i^n \right. \\ & \left. - (\Im(U^n \angle \vartheta^n) - \Im(\zeta^n \cdot i^n \angle \alpha)) \cdot \zeta^n \right)^2 \end{aligned} \quad 4.26$$

$$\begin{aligned} \eta = & \left((U^{n+1})^2 \cdot (i^n)^2 \right. \\ & \left. - \left((\Re(U^n \angle \vartheta^n) - \Re(i^n \cdot i^n \angle \alpha)) \cdot i^n \right. \right. \\ & \left. \left. - (\Im(U^n \angle \vartheta^n) - \Im(\zeta^n \cdot i^n \angle \alpha)) \cdot \zeta^n \right)^2 \right) \end{aligned} \quad 4.27$$

Solving equation (4.25) yields two solutions and the correct one is determined based on the boundary conditions as in (4.29):

$$U^{n+1} = \bar{U}^{n+1} \Rightarrow \begin{cases} i^{DSTATCOM} = 0 \\ \vartheta^{n+1} = \bar{\vartheta}^{n+1} \end{cases} \quad 4.28$$

Accordingly, equation (4.29) satisfies the boundary conditions.

$$\sin(\vartheta^{n+1}) = \frac{-\xi + \sqrt{(\xi)^2 - 4 \cdot \beta \cdot \eta}}{2 \cdot \beta} \quad 4.29$$

Therefore, $\angle i^{DSTATCOM}$ and $i^{DSTATCOM}$ can be found as in equation (4.31) and (4.32):

$$\angle i^{DSTATCOM} = \vartheta^{n+1} + \frac{\pi}{2} = \sin^{-1} \left(\frac{-\xi + \sqrt{(\xi)^2 - 4 \cdot \beta \cdot \eta}}{2 \cdot \beta} \right) + \frac{\pi}{2} \quad 4.30$$

$$\begin{aligned} i^{DSTATCOM} &= |i^{DSTATCOM}| \angle \vartheta^{n+1} + \frac{\pi}{2} \\ &= |i^{DSTATCOM}| \angle \sin^{-1} \left(\frac{-\xi + \sqrt{(\xi)^2 - 4 \cdot \beta \cdot \eta}}{2 \cdot \beta} \right) + \frac{\pi}{2} \end{aligned} \quad 4.31$$

Magnitude of the injected current by DSTATCOM as well as the reactive power to the bus can be expressed as in (4.33), (4.34), and (4.35).

$$|i^{DSTATCOM}| = \frac{U^{n+1} \cdot \cos(\vartheta^{n+1}) - \Re(U^n \angle \vartheta^n) + \Re(i^n \cdot i^n \angle \alpha)}{i^n \cdot \sin(\vartheta^{n+1}) + \zeta^n \cdot \cos(\vartheta^{n+1})} \quad 4.32$$

$$jQ^{DSTATCOM} = (U^{n+1} \angle \vartheta^{n+1}) \cdot i^{DSTATCOM} \quad 4.33$$

$$jQ^{DSTATCOM} = (U^{n+1} \angle \vartheta^{n+1}) \cdot \left(|i^{DSTATCOM}| \angle \left(\sin^{-1} \left(\frac{2 \cdot \xi + \sqrt{(\xi)^2 - 4 \cdot \beta \cdot \eta}}{2 \cdot \beta} \right) + \frac{\pi}{2} \right) \right)^* \quad 4.34$$

Chapter 5. Distribution System and Fast Charging Components: An Overview

The aim of this chapter is to introduce the main components of distribution power systems as well as their characteristics. Also, the procedure of power flow analysis in distribution networks is outlined in this chapter.

5.1 Introduction

The power system mainly consists of four subsystems; these are the generation, transmission, sub-transmission, and distribution subsystems. Each subsystem is characterized by its own voltage level as shown in Table 5-1. The sub-transmission is utilized to interconnect Ultra-High Voltage (UHV), Extra-High Voltage (EHV), and High Voltage (HV) transmission systems to distribution systems.

Table 5-1 Power Subsystems and their Voltage Levels

System	Voltage Levels (kV)
Generation	1-30
UHV transmission	>765
EHV transmission	345-765
HV transmission	115-230
Sub-transmission	35-115
Distribution	0.120-35

This research is focused on the distribution system as it distributes electricity to local customers and while also supplying FCSs. Therefore, we need to model the distribution system in order to conduct our study and analyze the impact of FCSs on the system power quality as well as on customers. The configuration of distribution

systems is determined based on three factors: the type of electric power system whether AC (single/polyphase), or DC, the type of arrangement such as radial, loop, or network types, and the type of construction whether overhead wires or underground cables [166].

5.2 **Electrical Power Distribution System Overview**

The distribution system can be broadly divided into three subsystems: Distribution Substations, Primary Distribution Systems, and Secondary Distribution Systems where each part of them has its own functions and components. The sub-transmission system may be considered as part of the distribution system as in [138].

5.2.1 Distribution Substations

Each distribution system starts with distribution substation and interconnects the transmission and sub-transmission lines to primary networks via one or more three-phase primary feeders radially emanated, in most cases. The main functions of the distribution substations are switching, voltage transformation, voltage regulation, protection, and metering [167]. Switching at the distribution substations is performed using switching devices and protection devices. The switching devices are switches and usually located at the high-side of the substation transformer to connect/disconnect different parts of the electric network. The protection devices are circuit breakers, reclosers, and fuses, usually located at the low-side of the substation transformers. Another function of the substation is to transform the sub-transmission voltage level to the primary distribution voltage level using three single-phase transformers called transformer banks. These transformers are commonly connected

in a delta-grounded wye configuration in case of a four-wire wye feeder, and in a delta-delta connection in case of a three-wire delta feeder [167]. The third function of the substation mentioned above is to regulate the voltage at the substation using low-voltage load tap changing (LTC), in order to maintain the voltage limits within the standards for those customers who are close to the substation under light loading conditions, and to maintain voltage limits for those that are in the far-end of the feeders under peak loading. The metering at the substation is utilized to monitor the output of each substation transformer or the output of each feeder to record the average, minimum, and maximum values for different parameters such as voltage, current, and power over a fixed period of time using analogue or digital meters.

Figure 5.1 shows the layout of the distribution substation.

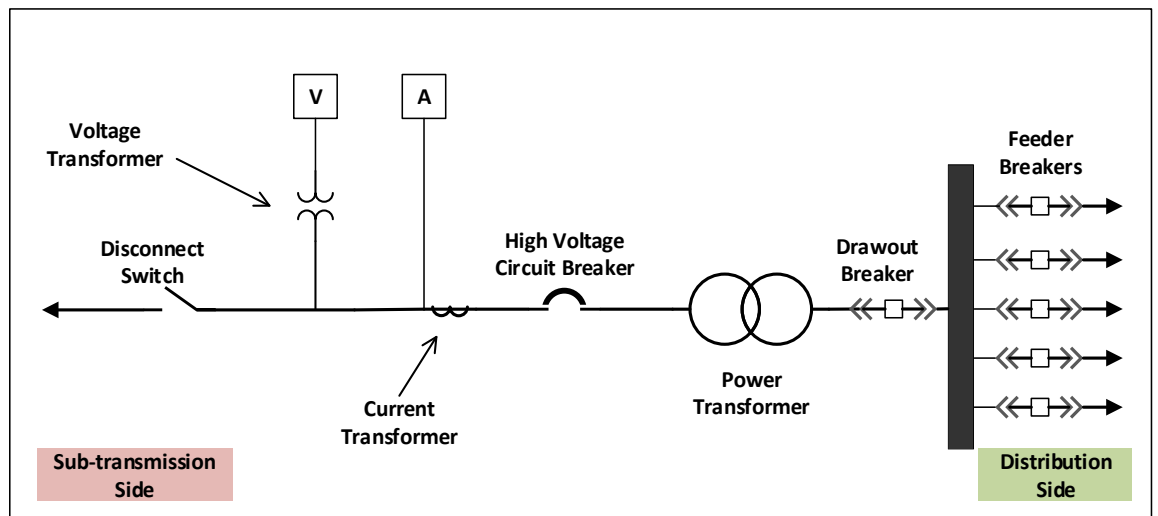


Figure 5.1 A Single-Line Diagram of a Distribution Substation Shown Basic Components [168]

5.2.2 Primary Distribution Systems

The primary system mainly consists of a main feeder called a mainline and laterals branch out from the main feeder. The mainlines mostly overhead three-phase wires

while the laterals can be overhead or underground single, two, and/or three-phase laterals. These feeders and laterals are utilized to flow the power from the source (distribution substation), which steps down voltages to distribution levels using power transformers, into the distribution transformers, which step down voltages to the utilization levels. Several standard voltage levels are commonly utilized in primary distribution systems such as 4.16 kV, 7.2 kV, 12.47 kV, 13.2 kV, 14.4 kV, 23.9 kV, and 34.5 kV [167]. Yet the equipment in distribution systems are specified as per four main voltage classes that are 5 kV, 15 kV, 25 kV, and 35 kV where 15 kV voltage class is the most prevalently used, according to [169].

5.2.2.1 Feeder Components

Feeder components can be classified as overhead feeder components and underground feeder components. The overhead equipment is characterized by many features such as ease of installation, ease of maintenance, and decreased installation cost when compared to wires buried underground. Disadvantages of overhead equipment are that they are more susceptible to damage, either due to weather conditions or by birds and trees. Also, landscape view is adversely affected with overhead wires. Underground lines are more reliable and more aesthetically pleasing, but in contrast, are much more expensive to install when compared to overhead lines and carry less ampacity compared to an equivalent amount of overhead lines [170]. Finally, another important feature in underground cables that is not available with overhead lines, is the use of insulation. Some of those overhead and underground components are utilized to model the electric distribution system in this work and thus are briefly explained below.

5.2.2.1.1 Overhead Feeder Components

Poles are utilized to support the overhead equipment in distribution systems and are mostly made of treated wood. Poles are classified based on their height and strength into different types. The height is described in feet while the strength is categorized into different classes that are 7, 6, 5, 4, 3, 2, 1, H1, H2, and H3, reported as per [171]. The most common classes utilized in distribution systems are classes 5, 4, and 3 whereas the most common height is 30 to 40 [feet] [168].

Overhead lines are utilized to carry the electric current and described by their material, size, impedance, and ampacity [168]. Lines are classified into bare and insulated conductors. The conductor consists of one or more wires and is usually made of either copper or aluminum. Aluminum conductor is lightweight and less expensive in comparison to copper conductor. Common types of aluminum conductor in overhead lines are All Aluminum Conductor, All Aluminum Alloy Conductor, Aluminum Conductor Steel Reinforced, Aluminum Conductor Alloy Reinforced (ACAR), and Aluminum Conductor Steel Supported, where the ACSR is mostly used due to its high conductivity and strength. The size of the conductor is measured by using American Wire Gage (AWG) and using circular mils (cmil). The conductor diameter is increased as the AWG is decreased. The largest AWG size is AWG 0000 written as 4/0 and pronounced as four-ought'. Conductor size larger than 4/0 is specified in thousands of circular mils (kcmil). One circular mil is the area of a circle with a diameter of one mil which is one thousandth of an inch [172]. Overhead lines are influenced by impedance and ampacity of the conductor. The impedance is represented by a resistance and a reactance that impedes the current

flow and determines the power losses and voltage drop along the line. Resistance is affected by the line material while reactance is affected by the distance between the conductors. Ampacity represents the maximum flowing current on the line and is influenced by ambient temperature and wind speed [168], [172].

Pole-mounted transformers are utilized to step down the overhead lateral voltage levels (2.4-34.5 kV) to the utilization levels (1200 – 600 V). Pole-mounted transformers are used as either a single-phase transformer feeding a single-phase service, or as three single-phase units in different configurations supplying a three-phase service. They are specified by voltage and kVA ratings and are characterized as conventional transformers and completely self-protecting (CSP) transformers [138]. Standard three-phase distribution transformers range from 30 kVA to 5000 kVA and standard single-phase distribution transformers range from 5 kVA to 500 kVA where the 25 kVA is the commonly used. Typical impedance for units under 50 kVA is less than 2.2%. Lower transformer impedance is better to regulate the voltage and to reduce the impact of load fluctuations, but it increases the fault currents on the primary side of the transformers [172].

5.2.2.1.2 Underground Feeder Components

Riser poles are utilized to interface overhead lines with underground cables. Cables, unlike the overhead lines, consist of one or more insulated wires. The most prevalent insulating materials used in underground cables are paper-insulated lead-covered (PILC), ethylene propylene rubber (EPR), and cross-linked polyethylene (XLPE) [168]. Most underground residential distribution (URD) cable is a single-phase conductor made of EPR or XLPE, with a concentric neutral ‘full neutral’ and ‘one-

third neutral' to carry the currents of unbalanced load and, buried to feed pad-mounted distribution transformers. Pad-mounted distribution transformers range from 10 kVA to 500 kVA and 75 kVA to 5000 kVA for single-phase and three-phase units, respectively [138].

5.2.2.2 Primary Distribution Configurations

There are three general types of configurations for primary distribution systems: radial, loop, and primary network [166]. The radial system includes independent feeders where each customer is supplied by a single feeder. It is the most prevalent system due to its simple operation and low cost, however, any upstream fault occurrence leads to power outage for all downstream customers [138]. The loop system consists of tie switches normally open utilized to interconnect two feeders, emanating from the same distribution substation; they are placed together so that when one has a fault, the second will supply the downstream customers. The size of the feeder conductor in loop system is selected to feed both feeders in the loop and thus, unlike the radial system, the conductor size will not be reduced as the downstream current flow is reduced. The primary network consists of interlinked feeders emanating from several distribution substations [138].

5.2.3 Secondary Distribution Systems

The secondary system connects the primary system to the customer's property via four main components namely distribution transformers, secondary mains, service drops, and meters. The secondary distribution systems step down the primary voltage levels to distribute energy at the customer utilization voltages. The service drops are

utilized to supply energy to the customers either by connecting directly to transformer secondary connections for close customers or by tapping off the secondary mains fed by either pole-mounted or pad-mounted distribution transformers. A typical 25 kVA pole-mounted distribution transformer distributes service drops to 4-7 dwellings [168]. The commonly used conductor size for secondary mains range from 4/0 [AWG] to 500 [kcmil] [173]. Typical secondary distribution voltages are single-phase three-wires 120/240 V for residential areas, three-phase four-wires 208Y/120 V for commercial and high-density residential areas, and three-phase four-wires 480Y/277 V for industrial, high-density commercial areas, and high-rise buildings [174]. Also, three-phase four-wires 600Y/346 V voltage is used for some applications in the secondary distribution system such as an FCS. Secondary systems can be categorized into four common types: common secondary main (radial system), individual distribution transformer per customer, secondary network, and spot network [174]. The last three types are utilized in some areas where the priority is placed on reliability not on cost [138]. In most cases, the secondary system is radial whereby one distribution transformer is utilized to feed a group of customers via secondary mains called service lines.

5.3 Energy Storage Systems Overview

Energy Storage System (ESSs) can be deployed in the power system as a grid connected or a grid influencing energy storages. In the grid connected deployment, the stored energy is injected to the grid directly using an inverter. In the influencing connected deployment, the stored energy cannot be utilized by the grid directly [175].

Energy storage technologies are utilized in electric power systems for different purposes; however, the main objective for using them in the distribution systems is to mitigate transmission congestion during the day. ESSs can be classified into two general types: physical energy storages and chemical energy storages. Physical energy storages rely on fluid (e.g. pumped hydro and compressed air), momentum (e.g. flywheels), thermal (e.g. ice and molten salts), and electromagnetic fields (e.g. super conductors and capacitors). Batteries are a typical example of chemical energy storages. There are two types of batteries: nonchargeable called primary batteries and rechargeable called secondary batteries. The latter can be subdivided into ambient or high based on their operating temperatures. When charging at ambient operating temperature, batteries consist of either aqueous or nonaqueous electrolytes and when charging at high operating temperatures, batteries consist of either solid or molten electrolytes [138]. Battery Energy Storage Units (BESUs) can be utilized in distribution systems close to load centers for different applications such as storing energy from variable resources (e.g. solar and wind power), shaving the peak load, operating in islanding mode, power quality control, and local voltage control.

5.4 Electric Vehicle Charging Stations Overview

5.4.1 Charging Sequence and Connector Interface

Figure 5.2 shows the connector pin layout for a CHAdeMO fast charger, which is utilized to demonstrate the charging sequence between the CHAdeMO and a compatible electric car. The connector layout consists of 10 pins that are classified based on their functions into power lines, analog control lines, and Control Area

Network (CAN) bus [176]. Pins numbers 5 and 6 represent the negative and positive power lines respectively. Pins number 1, 2, 4, 7, and 10 are analogue control lines. Pins number 8 and 9 are the CAN bus and utilized for a bidirectional communication between EV and the charger. Parameters like voltage limit, maximum current, and EV battery capacity are transmitted via pins 8 and 9 from the EV to the charger. Upon receiving this information, the charger responds by transmitting its maximum output current and output voltage to EV through the CAN bus. If the EV is compatible with the information sent by the charger, it sends a permission via pin 4 to start the charging process. After that, the connector is interlocked with the inlet of the EV to apply an insulation test. The test is conducted to avert any short-circuit happening in the connector wires whether due to misuse or aging deterioration. Upon accomplishing the insulation test, the charger via analog pin number 4 informs the EV that the preparation of charging is completed. Analog pins number 2 and 10 are used for starting or stopping the charging process. In order to end the charging process, the CAN bus receives a zero-current signal from the EV which makes the charger pause its output and the EV open its contactor. Analog pin number 7 is utilized as proximity detection to detect whether the connector is inserted in the vehicle's inlet or not. Analog Pin number 3 is not assigned. Pin number 1 is a ground wire [176].

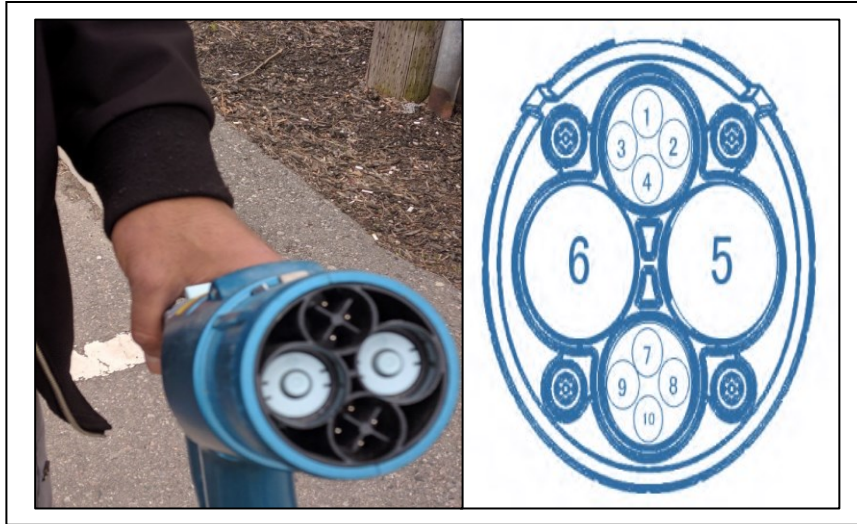


Figure 5.2 Front View for the CHAdeMO Charger

5.4.2 Connection to the Grid

In order to install a FCS in the distribution system, it is considered as a continuous load and thus electrical size wires and relevant elements are determined accordingly [177]. Each FCS is installed via a separate branch circuit, protected by a two-pole breaker, and no other loads except ventilation equipment is connected to that branch circuit. FCSs are connected as a three-phase equipment to a 208 V, 480 V, or 600 V supply via distribution transformers. The loading caused by the FCS must be equivalently distributed among the three phases [177].

5.5 Radial Distribution Feeder Analysis

Radial distribution feeders can be analyzed by studying the power flow from their substation into the loads. They are characterized by unbalanced loading and non-transposed conductors. This makes the power flow solution procedure in the radial distribution feeders different than those utilized in the transmission lines. Therefore, power flow is solved by using an iterative approach called the forward/ backward

sweep [167]. The method starts by specifying the voltage magnitude at the substation and the complex power of the loads. The aim of each backward sweep is to estimate the currents flowing through the feeder's components; the aim of each forward sweep is to compute the voltage at each node, to which two or more feeder's components are connected, using the estimated currents calculated as per the forward sweep. Components of the distribution feeder, whether in the primary or secondary circuits, may be classified based on their connections to series or shunt. All these components may be generalized, as shown in Figure 5.3. The backward sweep is given in matrix representation in (5.1) and (5.2) and utilized to relate the input voltage/current (node voltage and component current) at node n to the output (load current and node voltage) at node m . Similarly, the equation of forward sweep is shown in (5.3), utilized to relate the output voltage at node m to the input at node n .

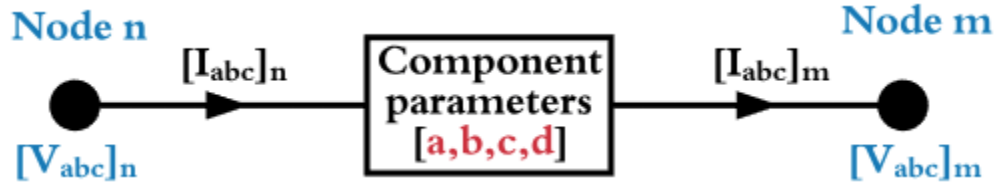


Figure 5.3 Generic Series Model of Distribution Feeder Component

$$[I_{abc}]_n = [c] \cdot [VLN_{abc}]_m + [d] \cdot [I_{abc}]_m \quad 5.1$$

$$[VLN_{abc}]_n = [a] \cdot [VLN_{abc}]_m + [b] \cdot [I_{abc}]_n \quad 5.2$$

$$[VLN_{abc}]_m = [a]^{-1} \cdot [VLN_{abc}]_n - [a]^{-1} \cdot [b] \cdot [I_{abc}]_n \quad 5.3$$

At the first iteration, the forward sweep is utilized under no load conditions and thus the voltage $[VLN_{abc}]_m$ at the far-end node (e.g. node m) is equal to the substation voltage. Given the load complex power (at node m), the flowing current $[I_{abc}]_m$ can

be determined. Then, the backward sweep is applied from downstream toward upstream, relying on Kirchhoff's Current Law (KCL) to find the emanated current from each upstream node, as illustrated in (5.2), and Kirchhoff's Voltage Law (KVL) is used to compute the voltage at each upstream node, as outlined in (5.3). After this, the second forward sweep is applied, starting from the substation, to find the downstream voltages as presented in (5.4), using the estimated current calculated as per the last backward sweep. As the procedure is repeated back and forth, the voltages and currents are updated until the tolerance is attained. The tolerance is a specified value (e.g. $ST=0.00001$) as proposed in [167], and calculated as in demonstrated equation (5.1).

$$\frac{\left| |V_n^{itr}| - |V_n^{itr-1}| \right|}{V_n^{nominal}} \leq ST \quad 5.4$$

Where V_n^{itr} and V_n^{itr-1} are the line-to-neutral voltage of node n in the current and the previous iterations (itr); $V_n^{nominal}$ is the nominal phase voltage of node n . In the case of single- or two- phase components, the unconnected phase will not be considered in Figure 5.3 or (equal zero) in the parameters of (5.2), (5.3), and (5.4). The generalized matrices a , b , c , and d are different for each component connected in a series (e.g. lines, transformers, and voltage regulators) or in shunt (e.g. spot loads, distributed loads, induction machines, and capacitors). The quantities of these matrices for several feeder components are developed in [167]. The forward/backward sweep method is outlined in Figure 5.4.

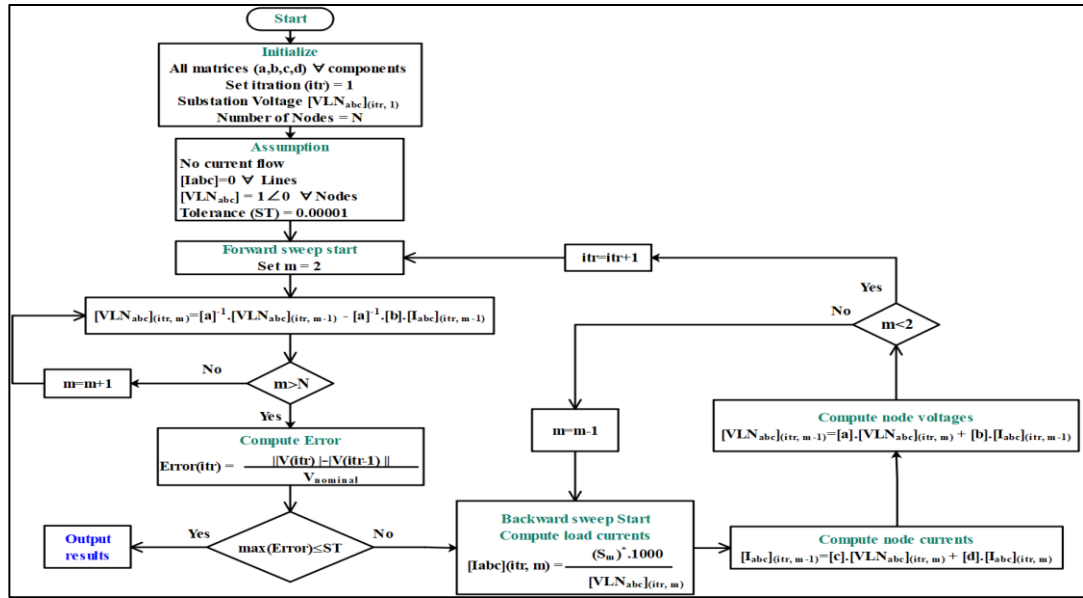


Figure 5.4 Basic Flowchart Shows the forward/Backward Sweep Procedure

Chapter 6. Probabilistic Load Modeling in Different Climate Zones

The objective of this chapter is to obtain probabilistic load profiles and report the profiles numerically for both commercial and residential loads, located in different climate zones.

6.1 Introduction

A load is the required electric power of a customer needs in kW or kVA. To know how and when that required power has been utilized, a load profile is needed [178]. A load profile indicates the amount of electricity utilized over a period of time. It is considered an important factor in shaping a time series of load patterns, which can be analyzed either in time-domain as in [179]–[182] or in spectral-domain as in [183], [184]. Energy consumption data are time series in their nature and thus the time-domain is utilized commonly in the literature to study the load information [185].

6.2 Load Characteristics

A power requirement for a customer varies from time to time, day to day, and season to season. However, load can be classified into a few categories as their demands are similar. Loads are broadly classified into 1) residential loads, 2) commercial loads, 3) industrial loads, 4) agricultural loads, and 5) other loads such as street lights [186]. The test bed system, utilized in this thesis, includes residential and commercial loads and therefore we focus only on these two types of loads.

6.3 Related Works

The time series load modeling is utilized widely in the literature for both the planning and operation of electric power distribution systems [187]–[191]. It is also used to enhance accuracy in both the long-term and short-term load forecasting studies [192]–[194]. In addition, load modeling contributes to improve the energy demand management as reported in these studies [195]–[197]. The electric load profiles can be generated using two methods of load modelling: deterministic and stochastic. The deterministic approach does not consider the random behavior of the electric loads and is only able to deal with predetermined cases. Alternatively, the stochastic approach takes into account the stochastic behavior of the electric loads [198]. Previous works are more extensive with regards to residential load profiles but few researchers focuses on commercial load modeling [199]–[201]. Nevertheless, both of them utilize the graph representation to describe the demand for a specific load or at a specific location.

6.4 Load Modeling Approach

The stochastic approach is adopted in this thesis to generate numerical commercial load profiles and residential load profiles.

6.4.1 Background

Commercial buildings and their facilities can be utilized to support some of the smart grid applications by decentralizing electric power. For instance, electric vehicle charging stations can be installed in their parking lots. Also, energy storage systems can be integrated there as well. Obtaining load profiles for these buildings will

contribute positively to examining the impact of such applications and lead to appropriate actions aimed to control the electric power systems. The annual load profiles of 16 different commercial buildings are obtained in this chapter. The commercial buildings are as follows: 1) primary school, 2) secondary school, 3) small hotel, 4) large hotel, 5) small office, 6) medium office, 7) large office, 8) quick service restaurant, 9) full-service restaurant, 10) midrise apartment, 11) standalone retail, 12) outpatient health care, 13) warehouse, 14) strip mall, 15) supermarket, 16) hospital. The daily load profiles for the aforementioned large hotel, large office, supermarket, and warehouse are averaged in Figure 6.1. The profiles in Figure 6.1 are normalized to obtain the daily profile per each hour as a percent of the annual peak. The idea is to depict the daily profile for different commercial facilities on a common scale.

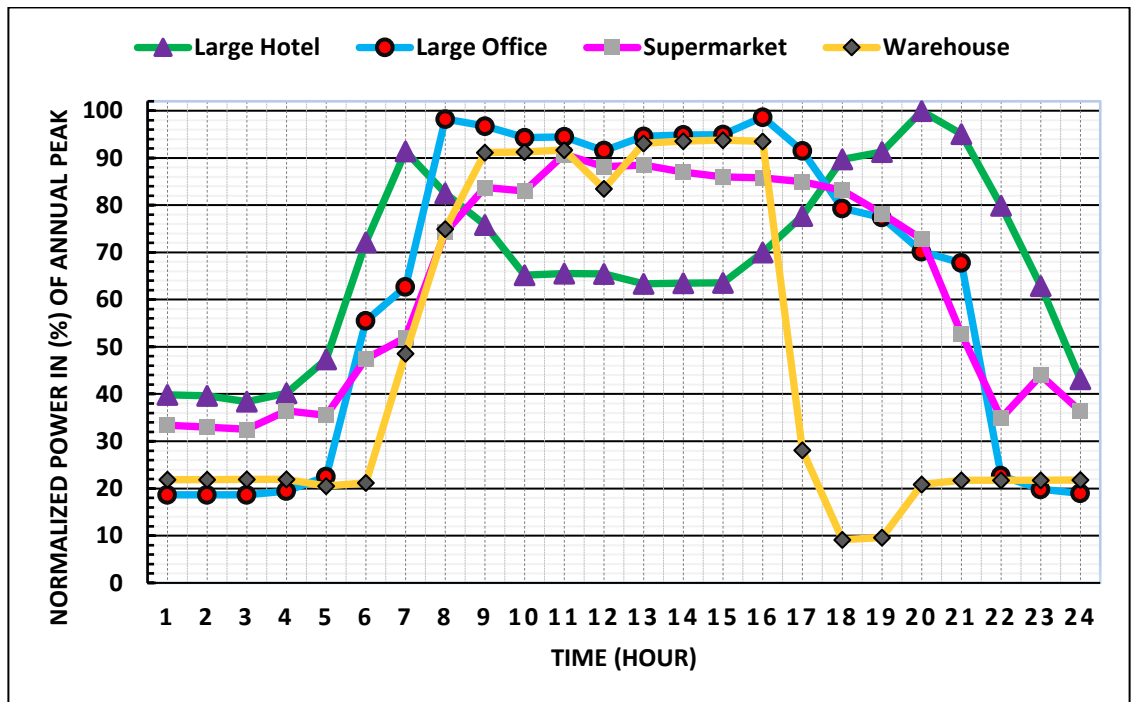


Figure 6.1 Average Weekday Load Profile in May

6.4.2 Data Source and Description

Benchmark models for the residential loads and 16 different commercial buildings, mentioned above, were published by the United State Department of Energy (DOE) [202]. Each residential load or commercial building is utilized as prototype to represent the same residential load or the same commercial buildings in 936 cities located in 50 states in the United States. The 50 states can be projected into 16 different climate zones whereas their cities can be characterized based on their geographic coordinates to one or more climate zones. The residential and commercial load profiles are generated for a year (8760 hour) at climate zones, as shown in Table 6-1.

Table 6-1 Classification of Climate Zones

Number	Climate Zone	Climate
1	1A	Very Hot, Humid
2	2A	Hot, Humid
3	2B	Hot, Humid, Dry
4	3A	Warm, Humid
5	3B-Coast	Warm, Humid, Dry
6	3B	Warm, Humid, Dry
7	3C	Warm, Marine
8	4A	Mixed, Humid
9	4B	Mixed, Humid, Dry
10	4C	Mixed, Marine
11	5A	Cool, Humid
12	5B	Cool, Humid, Dry
13	6A	Cold, Humid
14	6B	Cold, Humid, Dry
15	7	Very Cold
16	8	Subarctic

6.4.3 Preliminary Data Processing

Anomaly detection and normalization are utilized in this step to collect a complete yearly load profiles and to minimize variation in the load patterns, respectively. An uncompleted load profile for any city will not be considered in this study. The complete profiles will be scaled independently based on their annual peak value for that load at that climate zone. Let $(C = 1,2,3, \dots, 935)$ and $(b = 1,2,3, \dots, 16)$ vectors represent the cities and the climate zones, respectively. Then, P_b^C is a vector of 8760 hour represented in the load profile (residential or commercial) of the b^{th} climate zone at the C^{th} city. The normalized load profile can be found as follows [203]:

$$P_b^C = \frac{P_b^C}{\max \{P_b^C\}} \quad 6.1$$

6.5 Generation of Load Profiles

6.5.1 Methodology

After the complete data were normalized, 16 load matrices, corresponding to the 16 commercial buildings, are utilized to generate the commercial load profiles. Each load matrix consists of 8,760 rows and 935 columns. The number of rows represents the annual load profile (8,760 hour) and the number of columns represents profiles for the same prototype but located in a different city (935 cities). After that, each load matrix is projected into 16 different climate zones. Cities located in different states may be categorized in the same group based on their climate zone. Cities located in the same states may not be gathered in the same group. The geographic coordinates

(latitude and longitude) are extracted from [204], and used to assemble the cities as demonstrated in Figure 6.2. For example, climate zone 1A is utilized to gather cities from Florida state (9 cities) and Hawaii state (10 cities) and therefore their corresponding load profile are assembled in the same group. Similarly, different cities in Florida state (33 cities) belong to climate zone 2A as shown in Figure 6.2. The acronyms indicate to the state name [205].

The following summarizes the procedure to construct 16 load matrices where each matrix includes the aggregate load profiles for each climate zone [203].

1. For each matrix, the corresponding load profiles are grouped based on their climate zone and therefore each matrix is divided into 16 groups equal to the number of climate zones.
2. Each load profile in each group representing a specific climate zone, is portioned into four subgroups (winter, spring, summer, and fall) using the meteorological seasons in the northern hemisphere.
3. Each subgroup is divided into weekday and weekend profiles whereby the number of rows is equal to the number of cities multiplied by the number weekdays/weekends in that season, and the number of columns are equal to the number of hours in that day (24 hours).
4. The aggregated data in step 3 are reduced based on the principle component analysis (PCA) and thus the number of columns are reduced and equal to the number of components. In this study, the variance is assumed to be 90% or

more and thence two components are utilized to describe most of the cases, as shown in Figure 6.3.

- For each season, the reduced data in step 4 are clustered based on k-means where the clusters' number is equal to weekdays'/weekends' number in that season.

6.5.2 Cluster Assessment

The aim of using k-means is to divide the data into k groups and minimize the within-group distance. To explore the data set and to reduce the effect of the initial point on the cluster, k-means is repeated many times (100 times) with different initial points (50 points) for each time.

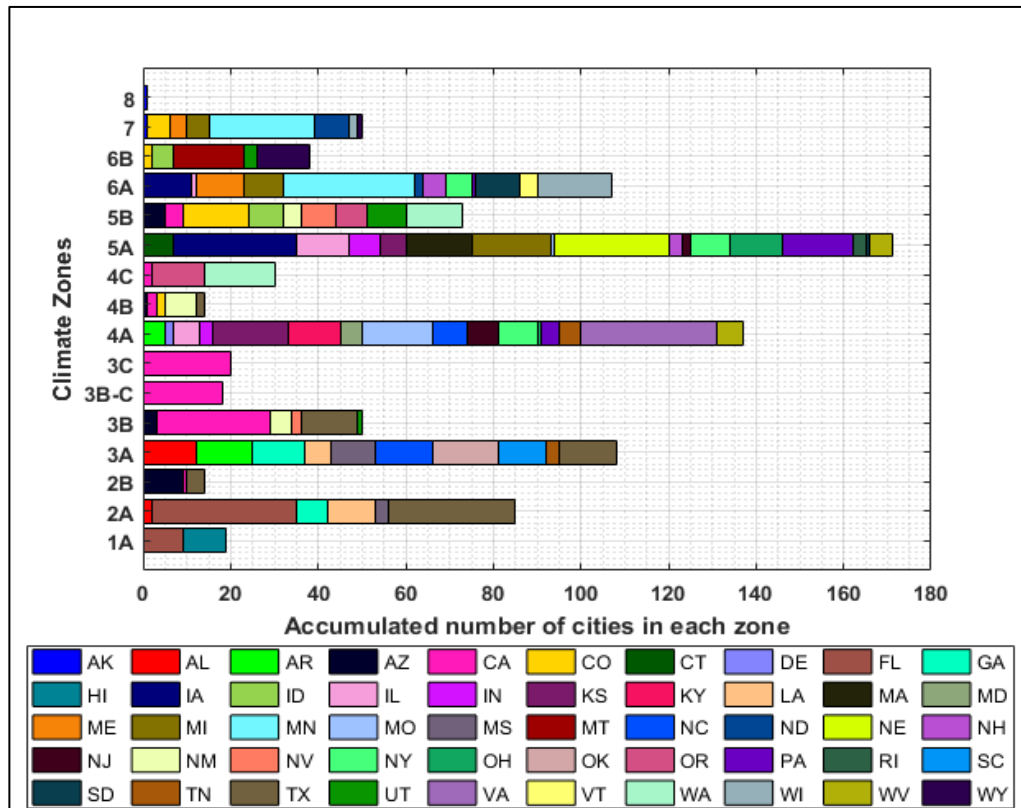


Figure 6.2 Number of Cities in each Climate Zone

The cluster can be assessed using external validity indices and/or internal validity indices that depend on the supervised learning and unsupervised learning, respectively [198]. Average Silhouette Coefficient (ASC) and Sum of Squares Error (SSE) are illustrated in (6.2) and (6.3), depend on unsupervised learning. Equation (6.4) demonstrates Average Power Time Mismatch (APTMM), which belongs to class of external validity indices. The aforementioned indices can be weighted as shown in (6.5) to measure the proximity and accordingly to choose the best number of clusters [206].

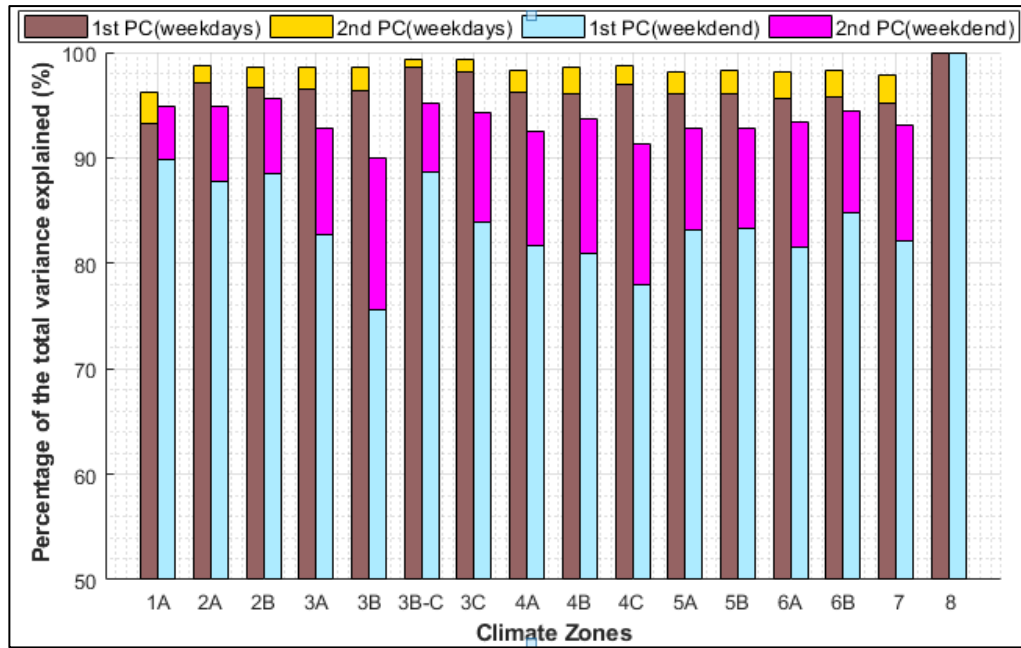


Figure 6.3 Total Variance Explained by the First Two Principal Components

$$S_i = \frac{-(R_i - T_i)}{\max\{R_i, T_i\}} \quad 6.6$$

$$SSE = \sum_{t=1}^k \sum_{z \in g_t} dist^2(n_t, z) \quad 6.7$$

$$APT M = \frac{1}{24 \times L} \left(\sum_{i=1}^{24} \sum_{d=1}^L \left| 1 - \frac{F(i, d)}{O(i, d)} \right| \right) \quad 6.8$$

$$WEQ = \left(\frac{1 - \lambda}{2} \right) .ASC + \left(\frac{1 - \lambda}{2} \right) .SSE + \lambda .APT M \quad 6.9$$

Where S_i represents the silhouette coefficient for the i^{th} point, R_i and T_i represent the average distance of the i^{th} point to all points of the same cluster and to all points of the other clusters, respectively. k is user defined and represents the number of clusters, the function $dist$ indicates the within-group Euclidean distance between the point z in the t^{th} cluster g_t and its centroid n_t , L is equal to cities' number having the same climate zone multiplied by weekdays'/weekends' number in each season, $F(i, d)$ represents to a fictitious load profile whereas $O(i, d)$ indicates the original load profile of the i^{th} hour and d^{th} day, and λ is a scaling factor increased by 0.1 from 0 to 1 [203]. Equation (6.10) above, was proposed by [206] to evaluate the clusters. The same equation is utilized in this study with some modification. For instance, the load profile of 365 days was represented by a specific number of clusters. The cluster may include days from different seasons and may comprise weekdays and weekends. The centroid of each cluster is utilized to represent that cluster. If the centroid of the cluster is an actual hour, then their corresponding daily profile is utilized to represent that cluster. If the centroid of the cluster is not an actual in the original data, then the nearest actual hour is used to represent that cluster and therefore its corresponding daily profile is utilized to represent the cluster. In contrast, the proposed method in this chapter is different than the work in [206] for two reasons. This is because this work is based on two steps: dividing the annual load

profiles into four seasons (winter, spring, summer, and fall) and dividing each season's profile into weekdays and weekends. The variations of different seasons or between weekdays and weekends profiles were not considered in [206]. It is also because the aim of this chapter is to obtain an annual load profile at different climate zones, which was not investigated in previous literature. A third difference is the number of clusters. In this work, the number of clusters for each season's profile, corresponds to the number of weekdays and/or number of weekends. For example, there are 19 cities (10 from Hawaii and 9 from Florida) in climate zone 1A, according to Figure 6.2. Depending on the northern hemisphere, the winter season starts in December and ends in February, which consists of 90 days. These days are divided into weekdays (63 days) and weekends (27 days). Their corresponding profiles are generated in two matrices where the number of rows equal to $(63 \times 19) / (27 \times 19)$ and the number of columns equal to (24 hours), respectively. To obtain the winter profile for each climate zone, the number of clusters are equal to the number of weekdays (63 clusters) /weekends (27 clusters) in the winter season and the same procedure can be applied for the other seasons. Seasons' days are arranged based on their frequency of occurrence in each cluster [203].

6.6 Residential Load Profiles

The published data for the residential profiles is in three types and representing three different load models: these include the high load model, the low load model, and the base load model. The base load model is proposed in this study and the annual residential load profile at one climate zone is presented numerically in this section.

Climate zone 4C is characterized as mixed-marine, as reported in Table 6-1. In this work, it is assumed that the year begins from January and ends on December where Sunday is the first and the last day of the year. Then, the year is divided based on their weeks to 52 weeks. At each climate zone, the weekly peak load (for both weekdays and weekends) for each week in the year is reported as a percent of the annual peak, as reported in Table 6-2. After that, these weekly peak loads are utilized to scale and specify their daily peak loads, which in turn are utilized to specify in which hour and in which season the daily peaks occurred, as listed in Table 6-3, and 6-4, respectively. For instance, the maximum loading values for climate zone 4C occurs in the winter in week numbers 3, 5, 6, and 49, and in the spring in week number 17. The peak days exist on Tuesdays and Wednesdays. The peak hours occur at 7 a.m., 7 p.m., and 8 p.m. in the winter season whereas the peak hour occurs at 5 a.m. in the spring seasons. This means that the peak values occur in 26 different times in the year $[4(\text{winter weekly peaks}) \times 3(\text{peak hours}) + 1(\text{spring weekly peak}) \times 1(\text{peak hour})] \times 2$ (Tuesday and Wednesday). In contrast, the summer season includes the minimum loading values for climate zone 4C. For example, the minimum loading hour occurs on weekends at 2 a.m. and Saturdays represent the minimum loading values. Tables 6-2, 6-3, and 6-4 below can be used to generate annual load profile consisting of 8,760 hours for climate zone 4C. For illustration, any hour can be generated as (specified hour \times specified day \times specified week \times AP). For example, the fifth hour (5 a.m.) of the last day of the year (Sunday) is extracted as $(0.543 \times 0.96 \times 0.878 \times \text{AP})$ whereas the fifth hour (5 a.m.) of the last (Monday) of the year is extracted as $(0.808 \times 0.953 \times 0.878 \times \text{AP})$. AP represents the actual annual peak

value for that residential load located in a city classified as a 4C climate zone. The week value (0.878) for the previous two examples was not changed for both Sunday and Monday because both are in week number 52. The rest of the hours can be generated using the same approach whether at this climate zone or at different climate zones. Figure 6.4 depicts variations of the residential loads in two aspects their peak values and the corresponding peak times in different climate zones.

Table 6-2 Residential Weekly Peaks in Climate Zone 4C

Climate Zone 4C (Mixed, Marine)			
Week	Peak Load	Week	Peak Load
1	97.9	27	79.7
2	93.5	28	79.2
3	100	29	67.4
4	95.3	30	86.2
5	100	31	95.8
6	100	32	79.6
7	92.9	33	94.3
8	80.0	34	91.1
9	81.7	35	90
10	81.2	36	88.6
11	81.2	37	89.4
12	79.6	38	86.2
13	73.5	39	84.7
14	78.8	40	89.2
15	75.5	41	92.4
16	75.1	42	89.7
17	100	43	87.5
18	75.4	44	90.2
19	86.3	45	91.1
20	81.2	46	78.3
21	89.4	47	90.2
22	93.3	48	92.6
23	91.3	49	100
24	73.5	50	97.4
25	79.3	51	84.8
26	74.6	52	87.8

The figure can be used to illustrate the variations between the peak values and/or peak times for weekdays/weekends in the same climate zone but in different seasons and for weekdays/weekends in the same season but in different climate zones.

Table 6-3 Residential Daily Peaks in Climate Zone 4C

Climate Zone 4C (Mixed, Marine)	
Day	Peak Load
Monday	95.3
Tuesday	100
Wednesday	100
Thursday	97.4
Friday	97.1
Saturday	94.2
Sunday	96

Table 6-4 Residential Hourly Peak in Climate Zone 4C

Hour	Winter Weeks		Spring Weeks		Summer Weeks		Fall Weeks	
	1 - 9 & 49 - 52		10 - 22		23 - 35		36 - 48	
	Wkdy	Wknd	Wkdy	Wknd	Wkdy	Wknd	Wkdy	Wknd
24-1	85.7	32.5	76.8	36.5	45.2	45.3	39.7	37
1-2	94.2	28.5	95	32.9	40.9	41.7	35.4	32.8
2-3	84.9	38.5	99.7	31.2	38.5	39.6	33.9	30.9
3-4	83.3	47.1	99.6	31	37.3	39	33.8	30.8
4-5	80.8	54.3	100	34.8	40.9	42.4	34.2	31.4
5-6	81	65.7	70.5	47.2	57	55	40.7	38.2
6-7	100	87.8	55.8	56.5	64.7	61	54.5	52.4
7-8	84.8	83.5	52.6	54.2	61.1	58.5	56	55
8-9	74.2	76.5	52.8	53.6	59.7	56.9	54.5	53.1
9-10	74.1	60.7	60.8	59.1	67.3	64.4	49.4	48
10-11	68.8	63.6	59.2	58.9	66.9	63.7	51.2	48.8
11-12	65.8	58.4	59.6	59.8	67.8	63.9	49.8	47.2
12-13	64.2	59.2	61.6	60.2	70.5	65.3	47.5	45
13-14	66.2	61.3	64.7	62.8	75.7	68.4	45.3	43.2
14-15	70.1	65.3	69.4	67.9	79.9	74.8	45.2	42.3
15-16	71.4	65.2	77.5	75.2	84.9	81.2	48.7	48.8
16-17	77.5	71.5	89.4	85	94.3	95.8	61.2	62.6
17-18	95.2	84.1	89.6	86.3	93.8	93.3	82.7	80.2
18-19	100	94.3	87.2	83.3	89.7	87.9	92.6	90.2
19-20	100	96	88.4	85.7	90.2	91.3	87.1	85.4
20-21	93.9	90.8	87.9	84	90.4	89.2	83.3	81.8
21-22	84.6	82	76.2	75.2	77.6	75.3	76.8	75.5
22-23	69.5	67.1	63.5	61	64.1	61.7	63.5	62.4
23-24	54.6	52	48	46.7	50.8	48	51	49.9

The variations of peak values at different climate zones and their corresponding peak times, as shown in Figure 6.4, can be evaluated using several indices such as the Peak Magnitude Error Index (PMEI), the Peak Time Error (PTE), and the Mean Absolute Percentage Error (MAPE).

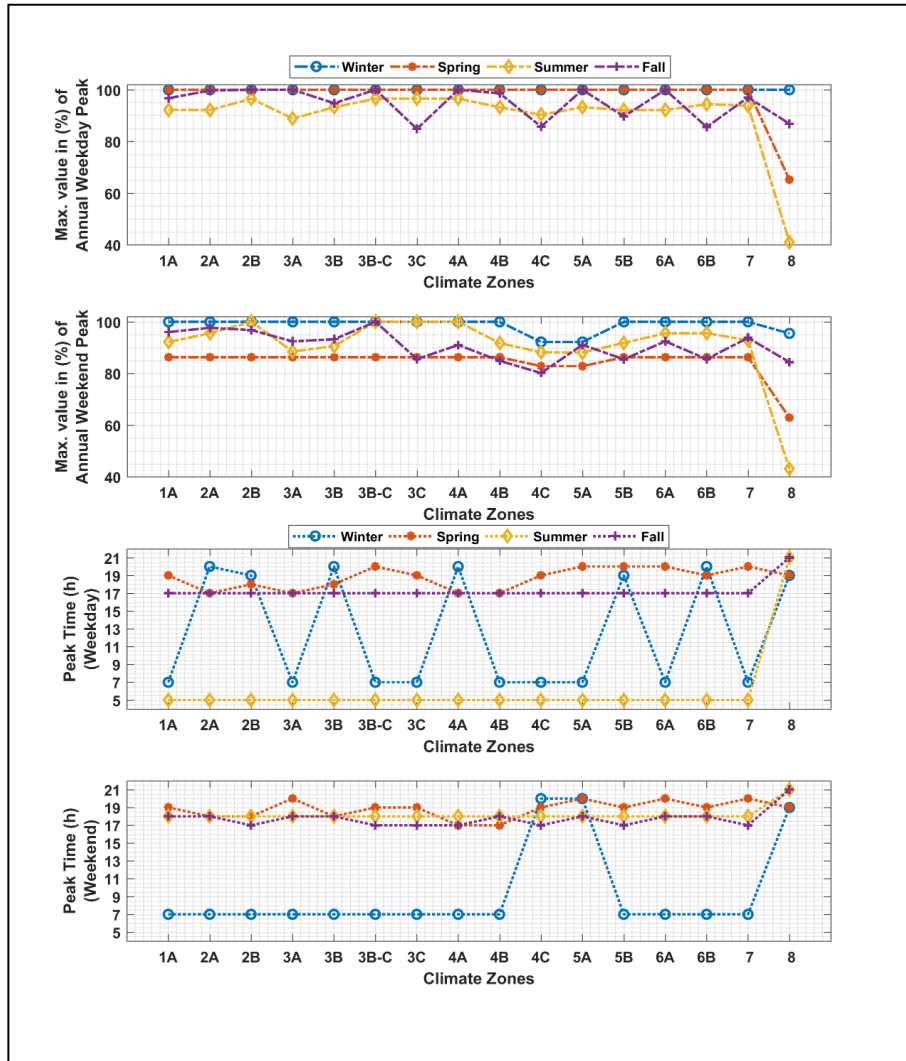


Figure 6.4 Variations of Peak Values and Times for Residential Loads in Different Climate Zones

These indices were utilized in previous works for similarity assessment [184], [192], [207] and illustrated in (6.6), (6.7), and (6.8).

$$PMEI = \left| \frac{\max(v) - \max(v_j)}{\max(v)} \right| \cdot 100\% \quad 6.11$$

$$PTE = t_{\max(v)} - t_{\max(v_j)} \quad 6.12$$

$$MAPE = \frac{1}{15} \left(\sum_{j=1}^{15} \left| \frac{\max(v) - \max(v_j)}{\max(v)} \right| \right) \cdot 100\% \quad 6.13$$

Where v symbolizes to the load profile of weekdays/weekends in different season. For example, climate zone 4C whereas $t_{\max(v)}$ is the peak time; v_j is the profile in the rest of climate zones while $t_{\max(v_j)}$ represents the corresponding peak times. The variations of peak values in any climate zone and the rest of the climate zones are considered satisfactory if the PMEI and MAPE are less than 5% while PTE is less than or equal to 2 hours, as recommended in [207]. The results of the comparison using PMEI and PTE are shown in Table 6-5 and 6-6 for weekdays and weekends, respectively.

Table 6-5 Comparison Between Weekday Profiles in Climate Zone 4C and the Rest of Climate Zones Using PMEI and PTE

Zones	Winter Season		Spring Season		Summer Season		Fall Season	
	PMEI (%)	PET (Hour)	PMEI (%)	PET (Hour)	PMEI (%)	PET (Hour)	PMEI (%)	PET (Hour)
1A	0	0	0	0	2.1	0	12.8	0
2A	0	13	0	2	2	0	16.3	0
2B	0	12	0	1	6.9	0	16.6	0
3A	0	0	0	2	1.6	0	16.6	0
3B-Coast	0	13	0	1	3.2	0	10.6	0
3B	0	0	0	1	6.9	0	16.6	0
3C	0	0	0	0	6.9	0	1	0
4A	0	13	0	2	6.9	0	16.6	0
4B	0	0	0	2	3.2	0	15	0
5A	0	0	0	1	3.2	0	16.6	0
5B	0	12	0	1	2	0	4.6	0
6A	0	0	0	1	2	0	16.6	0
6B	0	13	0	0	4.5	0	0.2	0
7	0	0	0	1	3.6	0	13.2	0
8	0	12	34.8	0	54.5	16	1.3	4

The results show that the variations of peak values and/or peak times are not satisfactory and beyond the tolerance in many cases.

Table 6-6 Comparison Between Weekend Profiles in Climate Zone 4C and the Rest of Climate Zones Using PMEI and PTE

Zones	Winter Season		Spring Season		Summer Season		Fall Season	
	PMEI (%)	PET (Hour)	PMEI (%)	PET (Hour)	PMEI (%)	PET (Hour)	PMEI (%)	PET (Hour)
1A	8.5	13	4.2	0	4.6	0	19.8	1
2A	8.5	13	4.2	1	8.4	0	21.8	1
2B	8.5	13	4.2	1	13.4	0	20.7	0
3A	8.5	13	4.2	1	0.3	0	15.3	1
3B-Coast	8.5	13	4.2	1	2.8	0	16.3	1
3B	8.5	13	4.2	0	13.4	0	24.7	0
3C	8.5	13	4.2	0	13.4	0	6.7	0
4A	8.5	13	4.2	2	13.4	0	13.5	0
4B	8.5	13	4.2	2	4.1	0	5.9	1
5A	0	0	0	1	0.1	0	13.6	1
5B	8.5	13	4.2	0	4.1	0	6.6	0
6A	8.5	13	4.2	1	8.4	0	15.3	1
6B	8.5	13	4.2	0	8.4	0	6.7	1
7	8.5	13	4.2	1	5.3	0	17	0
8	3.6	1	24.1	0	51.1	3	5.3	4

6.7 Commercial Load Profiles

The load profiles for commercial buildings in climate zone 4C can be extracted using the same probabilistic approach as presented in Sections 6.5 and 6.6. The numerical profiles for the large office and warehouse are demonstrated below whereas the numerical profile of the supermarket is illustrated in [203]. The weekly and the daily peak loads, for these commercial profiles, are shown in Table 6-7 and 6-8. The hourly peak loads are presented in Table 6-9 and 6-10, whereas the variations of peak values and peak times are depicted in Figure 6.7 and 6.8. For consistency, similarity assessment is applied on a commercial property using (6.6), (6.7), and (6.8). The supermarket profile is chosen to compare between weekdays/weekends profiles in climate zone 4C and in the other zones, as illustrated in Table 6-11 and 6-12. Figure

6.9 describes the variations of the supermarket, located in different climate zones, using the MAPE index.

Table 6-7 Weekly Peak Load in Percent of Annual Peak for Commercial Loads in Climate Zone 4C

Large Office				Warehouse			
Week	Peak Load	Week	Peak Load	Week	Peak Load	Week	Peak Load
1	94.2	27	93.2	1	97.9	27	87.4
2	90.4	28	96.9	2	82.9	28	87.9
3	85.9	29	94.6	3	97.8	29	90.2
4	84.9	30	100	4	93.4	30	99.5
5	94.1	31	97.0	5	81.1	31	96.0
6	77.2	32	97.4	6	97.9	32	99.6
7	90.5	33	96.5	7	97.2	33	95.4
8	90.2	34	97.2	8	100	34	97.3
9	77.2	35	98.9	9	95.7	35	100
10	88.7	36	97.3	10	95.7	36	97.9
11	88.9	37	91.2	11	76.1	37	89.6
12	82.8	38	94.7	12	93.4	38	94.1
13	94.7	39	95.8	13	93.4	39	97.8
14	94.2	40	90.2	14	87.6	40	88.0
15	94.1	41	95.4	15	88.8	41	96.5
16	96.8	42	78.6	16	88.8	42	95.1
17	91.8	43	97.1	17	89.4	43	89.4
18	96.6	44	96.7	18	83.8	44	97.9
19	97.7	45	98.0	19	86.1	45	92.4
20	96.4	46	95.7	20	85.5	46	93.5
21	93.3	47	93.7	21	88.5	47	83.7
22	98.0	48	94.4	22	95.7	48	96.2
23	97.3	49	92.4	23	92.5	49	96.2
24	99.2	50	83.7	24	98.8	50	91.5
25	82.4	51	91.9	25	97.4	51	92.8
26	96.5	52	73.7	26	94.5	52	98.1

Table 6-8 Weekly Peak Load in Percent of Annual Peak for Commercial Loads in Climate Zone 4C

Large Office		Warehouse	
Day	Peak Load	Day	Peak Load
Monday	97.4	Monday	100
Tuesday	97.3	Tuesday	97.9
Wednesday	99.2	Wednesday	96.5
Thursday	98.0	Thursday	97.9
Friday	100	Friday	100
Saturday	77.5	Saturday	87.4
Sunday	77.5	Sunday	92.8

Table 6-9 Hourly Peak Load for Large office in Percent of Annual Peak for Commercial Loads in Climate Zone 4C

Hour	Winter Weeks		Spring Weeks		Summer Weeks		Fall Weeks	
	1 - 9 & 49 - 52		10 - 22		23 - 35		36 - 48	
	Wkdy	Wknd	Wkdy	Wknd	Wkdy	Wknd	Wkdy	Wknd
24-1	20.2	16.7	20.1	16.6	23.7	16.6	20.1	16.4
1-2	20.2	16.7	20.1	16.6	20.1	16.6	20.1	16.4
2-3	20.2	16.7	20.1	16.6	20.1	16.6	20.1	16.4
3-4	20.2	16.7	21.0	17.5	21.0	17.5	21.0	17.2
4-5	21.1	17.5	24.5	18.9	24.5	19.2	24.5	19.0
5-6	24.6	19.2	48.2	50.5	54.7	50.0	55.1	57.6
6-7	39.0	41.2	55.7	51.9	61.4	51.9	59.4	56.2
7-8	43.9	41.4	94.2	68.6	100	70.1	97.1	71.3
8-9	86.7	61.2	93.2	66.5	98.2	70.2	96.9	69.3
9-10	90.0	63.6	92.3	63.5	95.6	67.4	93.4	67.4
10-11	89.1	61.7	94.1	63.9	95.6	68.3	94.4	67.3
11-12	89.7	62.3	91.7	65.0	92.2	68.3	91.7	67.1
12-13	87.0	63.2	94.0	66.5	95.3	68.3	94.9	66.8
13-14	90.1	63.6	94.0	59.0	95.7	51.8	95.5	50.1
14-15	91.9	45.7	94.3	51.3	95.4	52.1	94.8	50.1
15-16	92.0	44.9	97.7	55.2	98.9	55.2	98.0	53.3
16-17	94.2	45.5	96.6	53.1	90.2	52.7	94.7	50.9
17-18	86.4	42.0	88.3	46.1	76.9	49.8	88.4	46.1
18-19	70.6	24.4	76.4	44.1	76.4	48.2	79.7	32.2
19-20	69.2	22.6	68.4	41.1	69.3	49.7	73.5	22.3
20-21	59.2	22.6	64.5	22.0	67.8	38.7	67.2	21.4
21-22	57.9	20.9	47.4	20.3	29.4	23.4	61.5	19.8
22-23	24.5	19.2	24.4	18.6	24.2	21.6	24.5	18.1
23-24	21.0	17.5	21.0	17.0	24.4	16.6	21.0	16.5

Table 6-10 Hourly Peak Load for Warehouse in Percent of Annual Peak for Commercial Loads in Climate Zone 4C

Hour	Winter Weeks		Spring Weeks		Summer Weeks		Fall Weeks	
	1 - 9 & 49 - 52		10 - 22		23 - 35		36 - 48	
	Wkdy	Wknd	Wkdy	Wknd	Wkdy	Wknd	Wkdy	Wknd
24-1	26.0	26.7	25.9	25.8	22.9	22.2	23.9	25.1
1-2	25.7	27.2	26.4	25.8	22.9	22.2	24.0	26.2
2-3	26.2	26.6	26.5	26.2	22.9	22.2	24.2	25.5
3-4	25.9	26.9	26.5	26.1	23.0	22.2	24.1	26.7
4-5	26.4	26.4	27.1	26.3	22.9	22.2	24.3	25.8
5-6	26.1	26.8	33.8	24.9	27.3	11.8	33.8	26.8
6-7	33.8	26.4	52.6	21.5	50.4	21.4	59.0	25.8
7-8	59.4	32.9	78.5	22.7	78.5	22.7	78.5	23.1
8-9	78.5	22.7	95.7	36.3	95.7	36.3	95.7	36.3
9-10	95.7	36.3	95.7	36.3	95.7	36.3	95.7	36.3
10-11	95.7	36.3	95.7	36.3	95.7	36.3	95.7	36.3
11-12	95.7	36.3	95.7	36.3	86.4	21.4	95.7	36.3
12-13	86.4	21.4	95.7	21.4	95.7	22.1	95.7	20.9
13-14	95.7	21.4	95.7	21.4	98.1	28.1	95.7	20.9
14-15	95.7	21.4	95.7	21.4	100.0	31.9	95.7	20.9
15-16	95.7	21.4	95.7	20.9	99.6	30.4	95.7	20.9
16-17	100	19.9	95.7	10.4	44.3	25.1	97.9	20.7
17-18	44.6	24.1	33.2	12.1	23.7	26.4	44.1	23.0
18-19	25.9	25.0	23.6	23.7	25.2	20.4	23.6	24.1
19-20	25.4	25.7	24.7	24.2	22.9	24.5	23.6	24.2
20-21	26.4	25.9	24.7	24.0	22.9	22.2	23.6	25.4
21-22	25.7	26.6	24.9	24.4	22.9	22.2	23.5	24.9
22-23	26.6	26.5	25.3	24.5	22.9	22.2	23.5	26.0
23-24	26.2	27.4	26.0	24.8	22.9	22.2	23.5	25.1

Table 6-11 Comparison Between Weekday Profiles for Warehouse in Climate Zone 4C and the Rest of Climate Zones Using PMEI and PTE

Zones	Winter Season		Spring Season		Summer Season		Fall Season	
	PMEI (%)	PET (Hour)	PMEI (%)	PET (Hour)	PMEI (%)	PET (Hour)	PMEI (%)	PET (Hour)
	1A	33.6	3	7.9	4	0	1	4.4
2A	48.2	0	8	5	0	1	4.4	2
2B	56.8	7	2.8	7	0	0	2	1
3A	37.1	0	14.5	7	0.2	0	4.4	2
3B-Coast	35.6	0	3.2	7	0	0	4.4	2
3B	6.7	0	2.5	6	0	1	4.4	3
3C	4.5	0	0.6	0	0	2	4.4	2
4A	30.7	7	8.1	6	0	1	0.8	1
4B	25.2	0	1.8	7	0	0	4.4	3
5A	17.2	0	10.9	7	0	0	3	1
5B	23.5	0	11.7	7	0	1	8.6	2
6A	8.4	0	11.8	0	0	2	4.4	8
6B	18.1	0	10	0	0	1	11.9	0
7	0	7	2.3	0	0	1	2.8	2
8	0	7	12.9	0	2.6	1	4.4	7

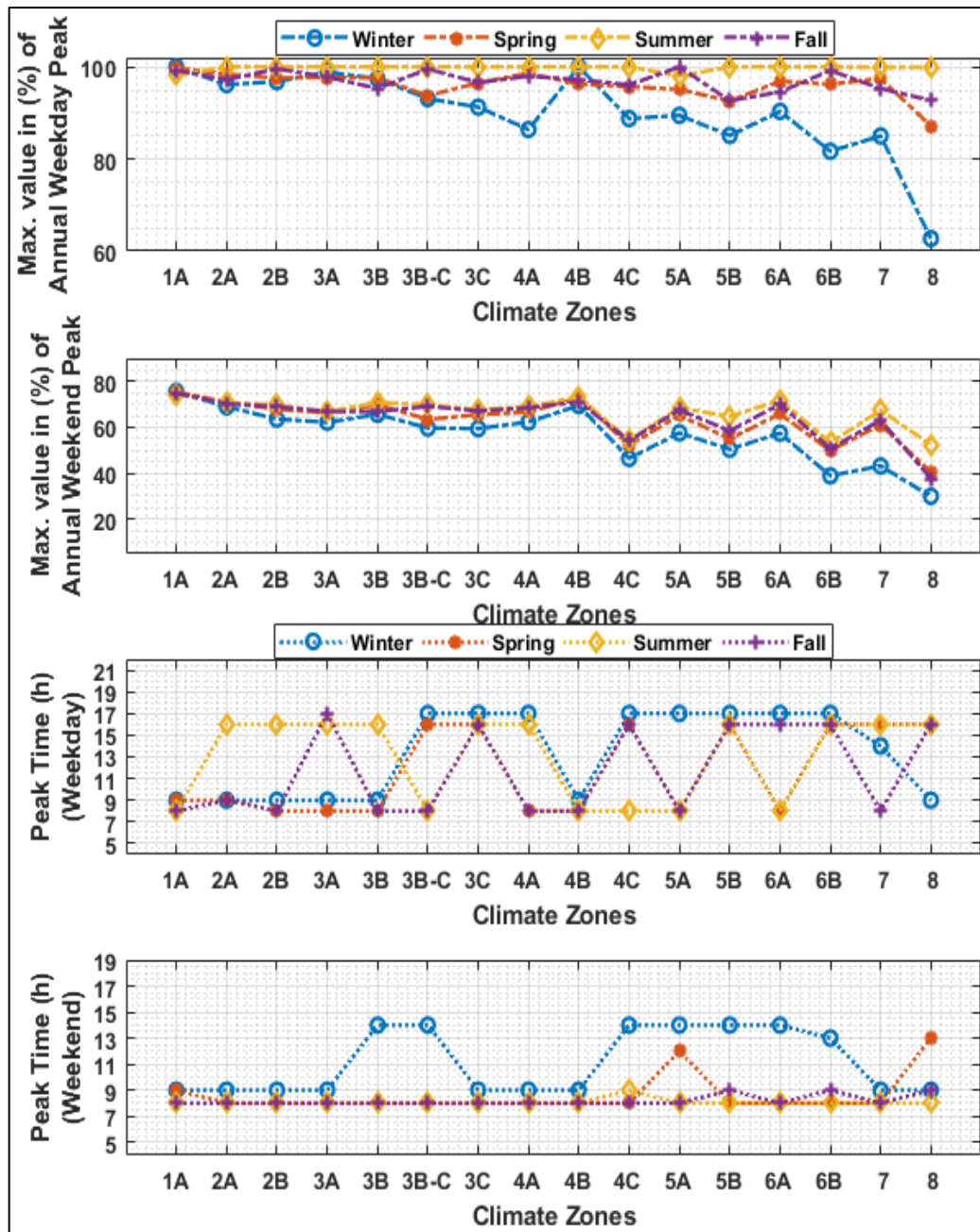


Figure 6.5 Variations of Peak Values and Time for Large Office Loads in Different Climate Zones

Table 6-12 Comparison Between Weekend Profiles for Warehouse in Climate Zone 4C and the Rest of Climate Zones Using PMEI and PTE

Zones	Winter Season		Spring Season		Summer Season		Fall Season	
	PMEI (%)	PET (Hour)	PMEI (%)	PET (Hour)	PMEI (%)	PET (Hour)	PMEI (%)	PET (Hour)
1A	7.1	2	47.5	2	124	2	77	3
2A	60.9	0	28.6	2	2.6	2	3	6
2B	65.8	0	26.9	6	0.6	6	11.1	2
3A	51.5	0	35.9	2	0.3	2	2.3	6
3B-Coast	49.5	0	36	0	3.4	2	0.2	2
3B	22.4	0	18.7	0	9.3	2	18	2
3C	16.4	0	17.2	0	14.4	2	14.3	2
4A	32.8	1	19	0	9.8	2	94	1
4B	37.3	0	28.6	0	6.5	6	1	6
5A	26.7	0	24.2	0	11	2	0.7	6
5B	27.9	0	20.2	0	2	6	24.9	0
6A	0.7	0	1.8	0	36.2	2	4.8	1
6B	11	0	0.2	0	5.1	2	4.7	1
7	32.4	0	17.6	1	17.6	0	19.1	0
8	23.8	0	43.9	0	40.2	2	22.3	1

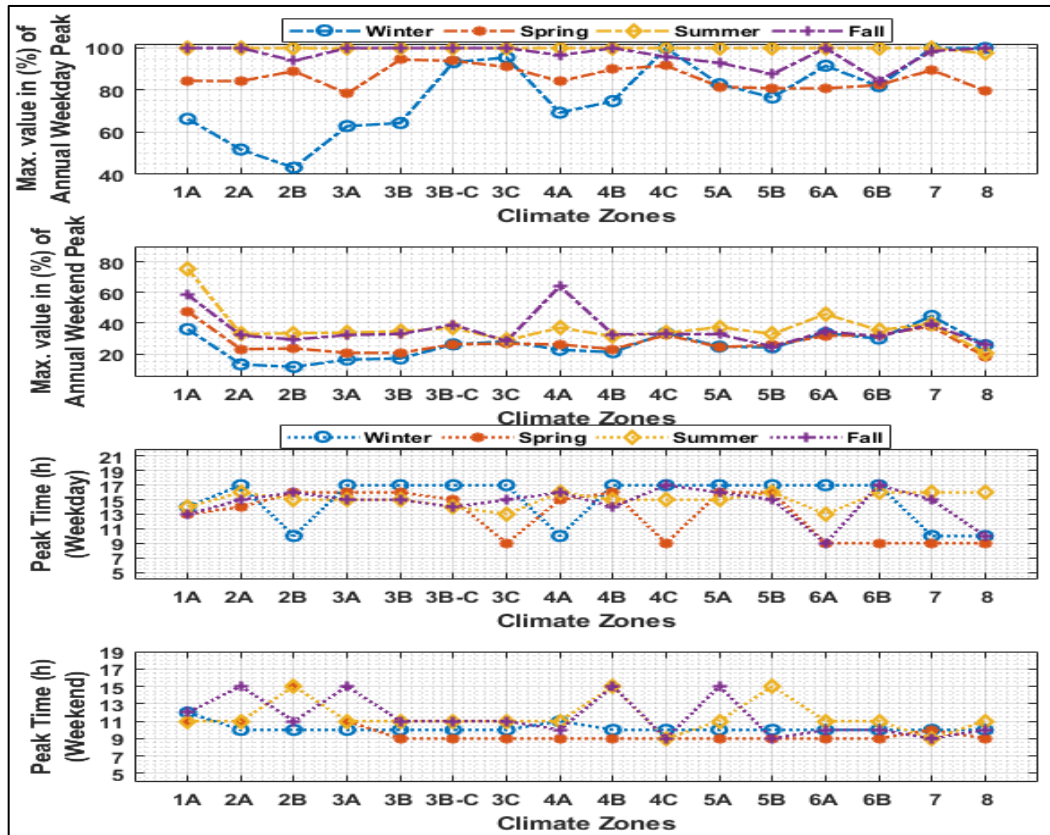


Figure 6.6 Variations of Peak Values and Time for Warehouse Loads in Different Climate Zones

6.8 Load Profile Selection

In the preceding sections 6.6 and 6.7, the load profiles are gathered based on their climate zones and then clustered to form an annual load profile in each climate zone. Those profiles ($365 \text{ days} \times 24 \text{ hour/ day}$) are utilized in this section and reduced to obtain representative days of each load. Each profile is divided into four seasons and then the PCA is adopted to get rid of the curse of dimensionality. The results in Figure 6.10 show that the minimum percentage variance explained by the first principal component is more than 90% for all seasons for a commercial load in climate zone 4C. This means that instead of representing the 365 days by 24 hours, we can represent them by the first principal component for each season and we can retrieve more than 90% of the variability of each profile. Therefore, each day of each profile is represented by one hour instead of 24 hours. After that, k-means is utilized to group the similar days of each season. For each season, k-means is repeated 250 times with different initial points (50 points) to minimize the effect of the initial point on the groups. Clusters are evaluated using both supervised and unsupervised measures, as represented in (6.2), (6.3), and (6.4) in section 6.5.2. Figure 6.11 and 6.12 show cluster evaluation for residential and commercial (supermarket) load profiles located in climate zone 4C.

For each season, the best number of clusters is chosen based on (6.5), as proposed in [206]. After (250×11) times the simulation will start from 50 different initial points in each time for each season, the results indicate that the best number of clusters are 8 clusters (8 days) and is thus proposed in this study. For example, in climate zone

4C, there are 30 cities, which means their load profiles of 10,950 days ($30 \text{ city} \times 365 \text{ day/city}$) is represented by 8 days for each season. Those 8 days represent the centroid of the 8 clusters. The frequency of occurrence of these 8 days in each season is influenced by the number of days grouped in the same cluster.

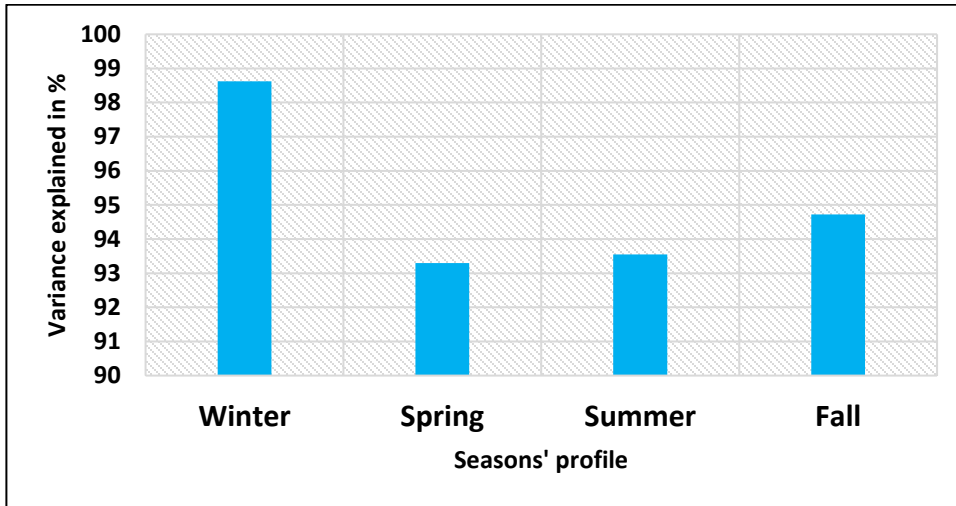


Figure 6.7 Variance of First Principle Component for Commercial Profile

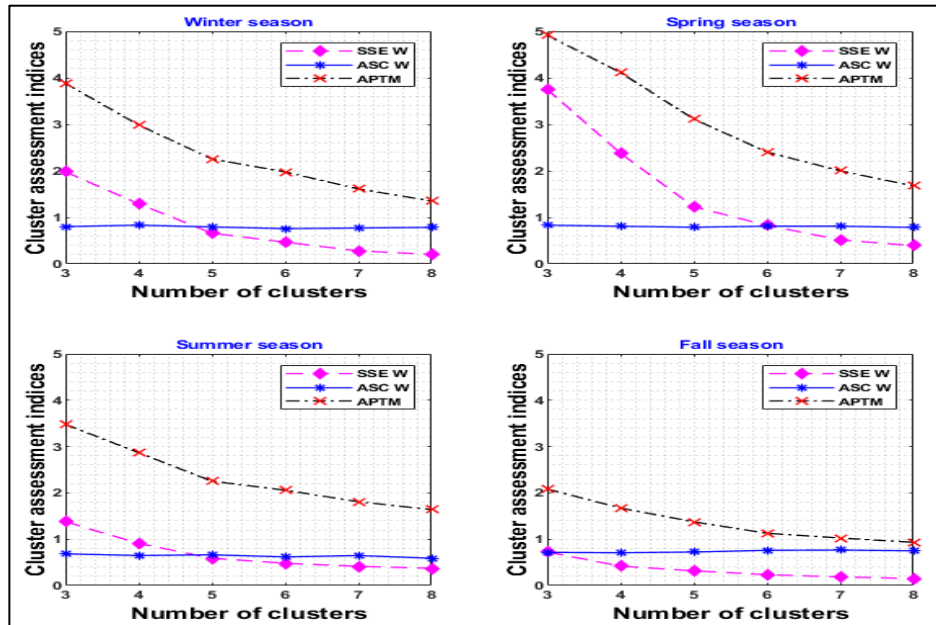


Figure 6.8 Cluster Assessment for Residential Load Profile in Climate Zone 4C

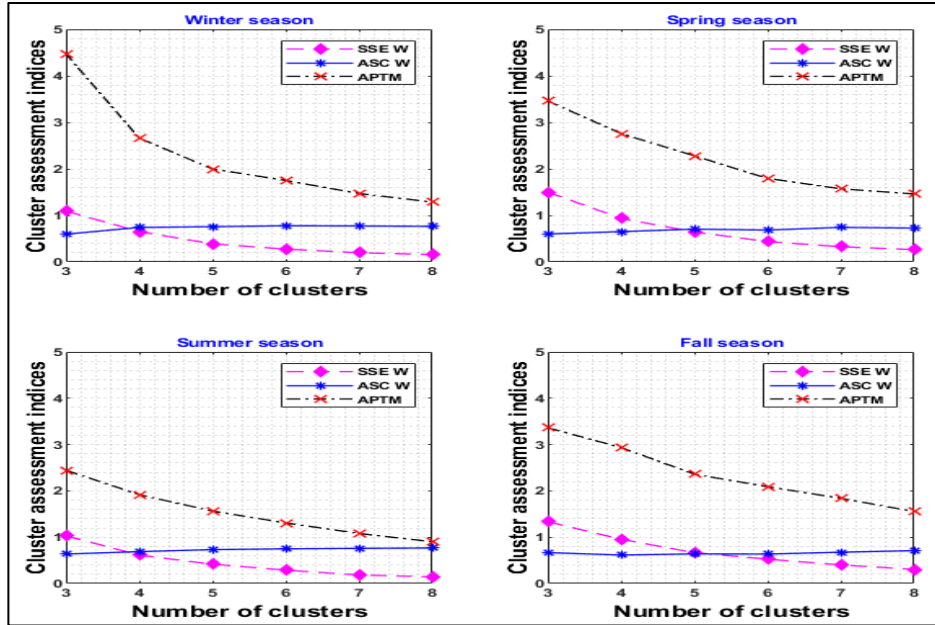


Figure 6.9 Cluster Assessment for Supermarket Load Profile in Climate Zone 4C

For instance, 20% of the winter season (90 days) for the residential load is represented by cluster 6, as shown in Figure 6.13. This means that 18 days ($20\% \times 90$) in the winter season are represented by the same day of which every hour is utilized to represent the centroid of cluster 6. In contrast, 18 days of the winter season are represented by cluster 1 for the commercial profile. Figure 6.13 can be used to generate the frequency of occurrence and the cumulative frequency distribution, accordingly. Figure 6.13 shows the frequency of occurrence as a percent of the total days in each season for commercial (supermarket) and residential load profiles located in climate zone 4C. The variation of the eight clusters are described using a measure of dispersion as illustrated in Figure 6.14 and Figure 6.15, for the residential and commercial (supermarket) loads, respectively. The upper dashed lines represent the maximum values of each hours of the 8 days in each season, whereas the lower dashed lines represent the minimum values. The cyan area indicates the interquartile range whereas the red line shown is the median values of each hour in the 8 clusters.

The variability is large in the residential load during the early hours of the day in the winter and spring seasons, as presented in Figure 6.10.

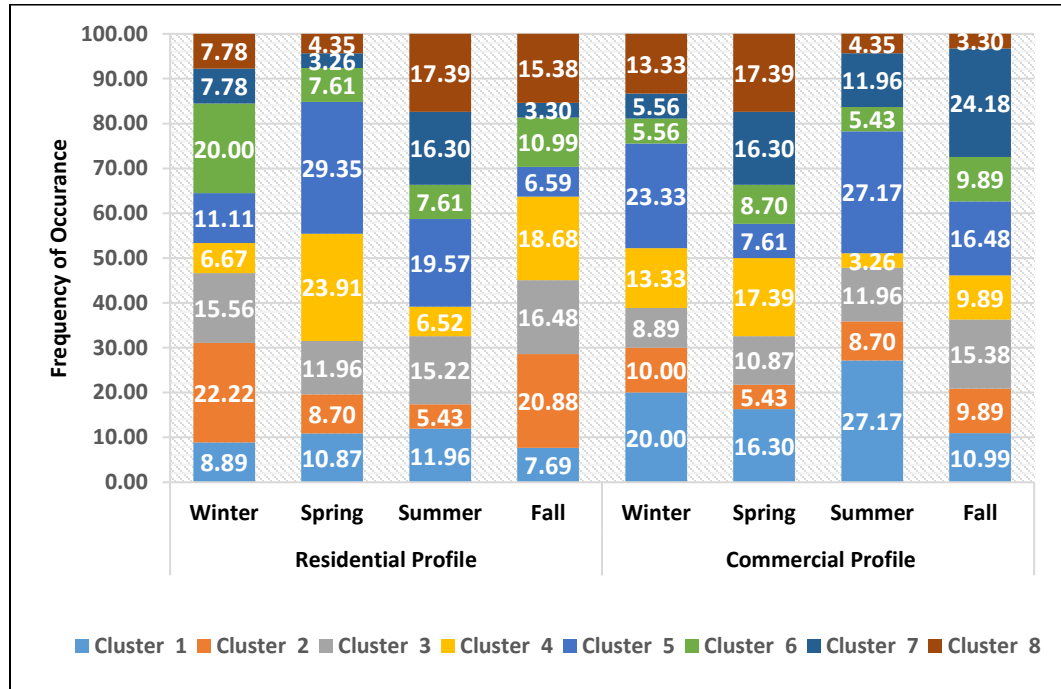


Figure 6.10 Frequency of Occurrence of Load Profile Located in Climate Zone 4C

Also, the figures show that each day is represented by 24 hours. Instead of that, the values of each cluster in each hour is utilized to generate profile for each minute in the day. Beta distribution is proposed to generate random variables over a bounded interval where one bound is represented by the minimum value of that hour in the clusters, and the other bound is chosen to obtain a mean value of the generated samples over that hour and should be equal to the value of the representative day of that hour. To prevent the sharp variations in consecutive samples, the similarity between them is assumed to be 98% or more. Therefore, each cluster consists of 24 hours whereas each hour is represented by 60 minutes. The average value of each hour (60 minutes) is equal to its corresponding hour of the 24 hours' profile.

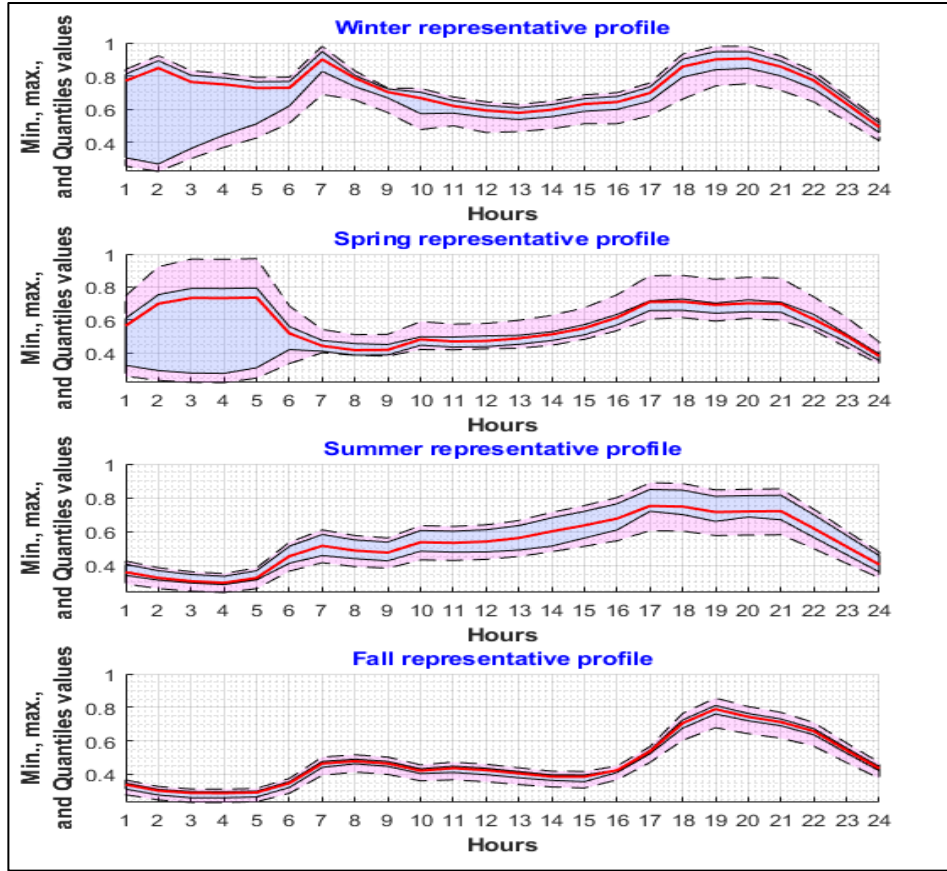


Figure 6.11 Max., Min., and Quantile Values of the Residential Clusters in Climate Zone 4C

In most seasons, cluster number 5 is utilized to represent their profile in both a commercial and residential load profile, as illustrated in Figure 6.13. Therefore, cluster number 5 is used to show the difference between its daily profile, which represents 24 samples (sample/hour), and its averaged profile, which consists of 2,880 samples (sample/30 second) generated using Beta distribution as explained above. The difference is depicted in Figures 6.16 and 6.17 and they clearly show that the generated profile based on the proposed method is similar to the daily profile at all times except in the early hours of the day in the winter and spring seasons for the residential load due to its large variability during that period, as shown in Figure 6.14.

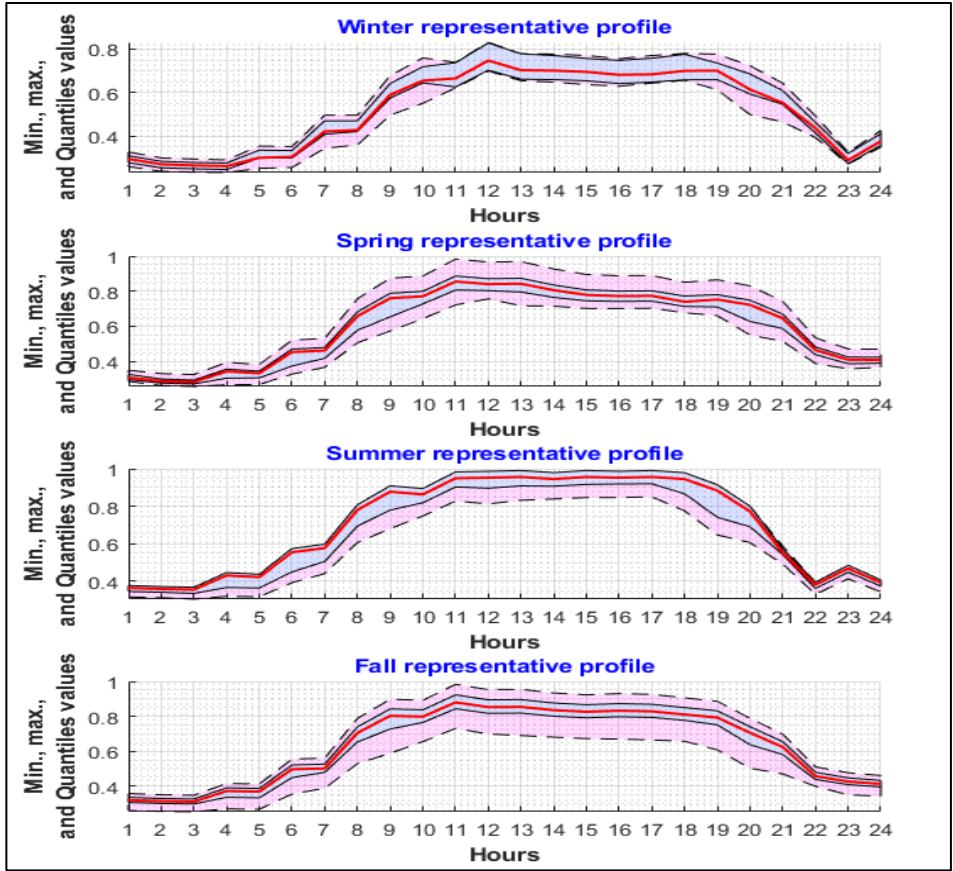


Figure 6.12 Max., Min., and Quantile Values of the Commercial (Supermarket) Clusters in Climate Zone 4C

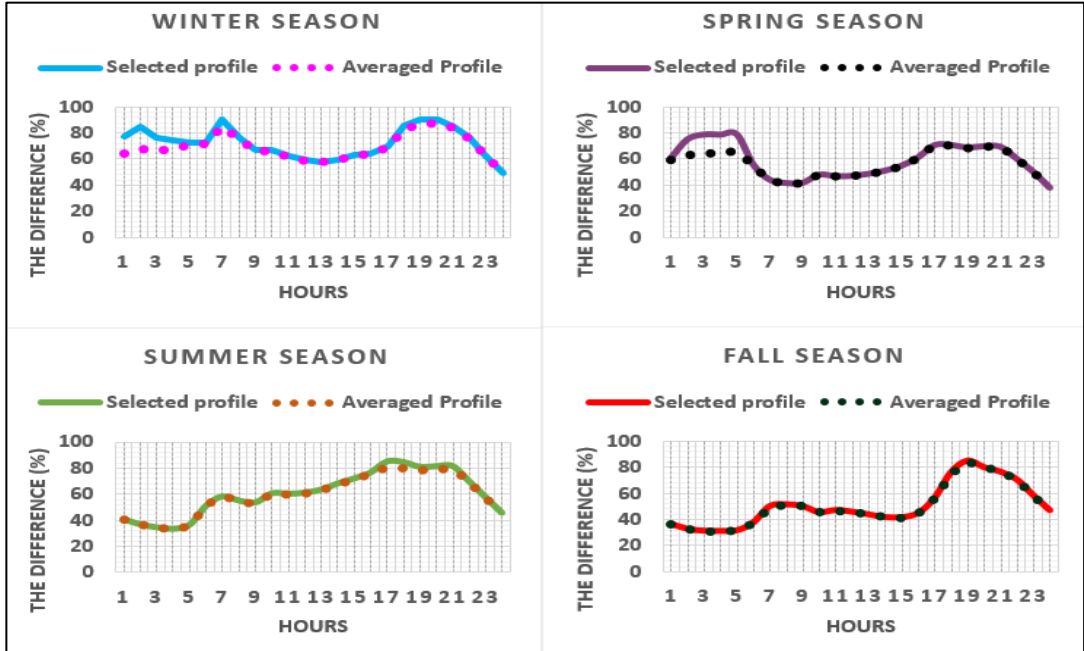


Figure 6.13 Max., Min., and Quantile Values for the Residential Load

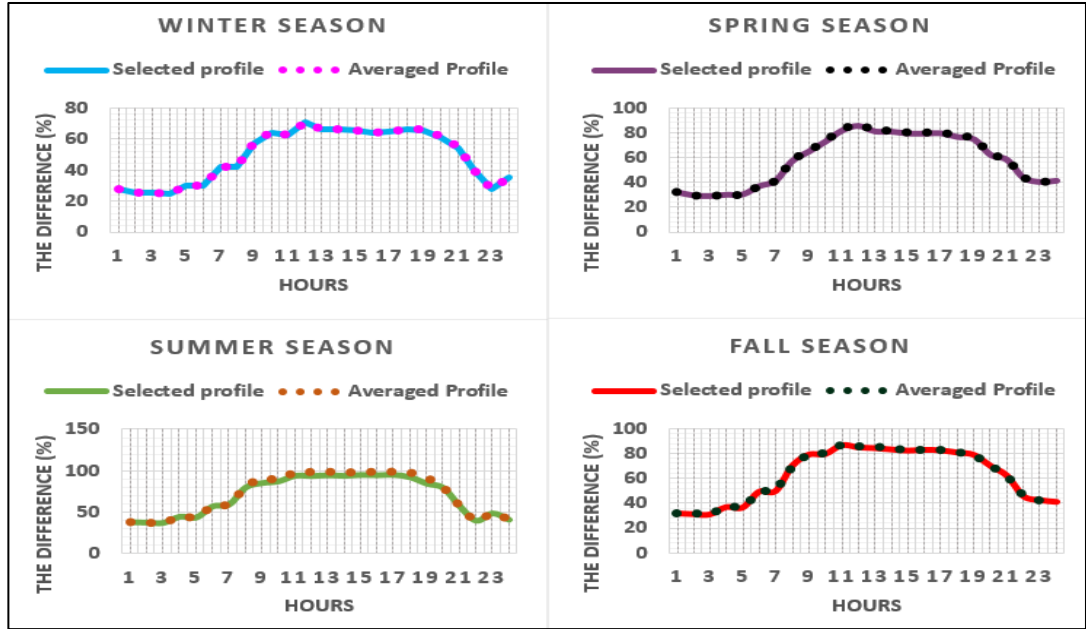


Figure 6.14 Max., Min., and Quantile Values for the Commercial Load

Chapter 7. Probabilistic Charging Demand Modeling

The main objective of this chapter is to model a probabilistic demand profile that represents the energy requirements of the FCS when it is utilized to charge EVs with different battery capacities, different State-of-Charge (SOC) levels, and at different periods of time.

7.1 Introduction

An FCS is characterized by two features: high power consumption from the electric network and charging that power over a period of time into the PEVs. The required power from the electric grid depends on the rated power of the FCS and it is affected by the length of the charging period which is, in turn, a function of the state-of-charge and the capacity of the vehicle's battery [24]. Therefore, the electric vehicle can be seen by the grid as a variable electric load due to its state of charge and battery capacity. Also, the charging times and charging intervals are dependent on customer needs or preferences, and these are additional uncertain factors affecting the electric grid. Also, the daily travel distances, which varied among customers, will increase the randomness in the search space. The aim of this chapter is to model a profile that represents the power demands of EVs considering the aforementioned parameters. It is unrealistic to consider all types of EVs and/or to observe their possible state of charge and their charging times. Instead, a subset of EVs, include different state of charge levels, charge at different times and can be used to generate the load profile and then make inferences about all types of EVs. Therefore, the inferential statistics are adopted in this chapter to develop probabilistic charging profiles for different

types of EVs. It is called a probabilistic profile due to the randomization in these parameters. Two models are utilized in this chapter to generate the load profile of EVs. The first model assumes that the distribution system feeds the FCS by a power equals to the rated power of the FCS and that power is always constant as proposed in [5]. The second model supplies the FCS by a power derived from a typical FCS dataset where both have the same rated power. The next section starts by determining the EVs market share and then their battery capacities are reported. After that, the distributions of daily distance travelled and the arrival time at FCS for some of the EVs are extracted. These parameters are common between the two models.

7.2 Type Selection of Electric Vehicles

There are three main types of EVs classified based on their degrees of energy use. These types are 1) Hybrid Electric Vehicles (HEVs), Plug-in Hybrid Electric Vehicles (PHEVs), and Plug-in Battery Electric Vehicles (PBEVs). The first two types are powered by both gas and electricity whereas the PBEVs are powered only by the electricity. In this study, only the PBEVs, or all-electric cars, are selected in both models to generate the charging profiles. Figure 7.1 shows the PBEVs sales and their shares in the Canadian market for the period of July 2011 to October 2018 [208]. The market shares of the Nissan Leaf, Tesla Model S, and Chevy Bolt are 25.8%, 18.7%, and 10.4% and thus these types are selected in this study to generate the charging profiles. These three different types are selected because of their high market share, which almost amounts to 55% in the Canadian market, as illustrated on the right side of Figure 7.1.

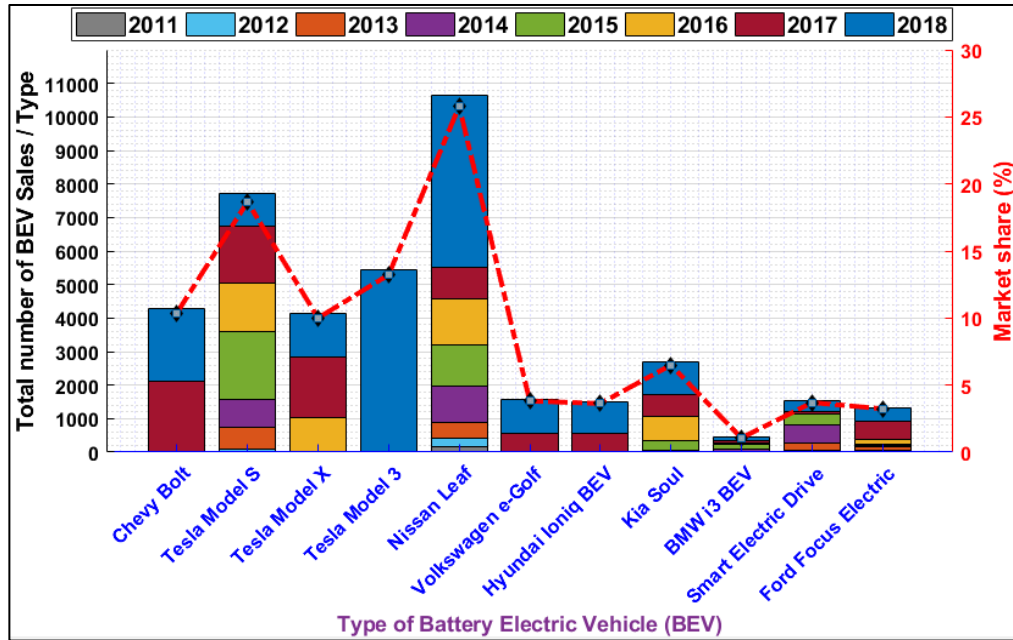


Figure 7.1 PBEVs Sales and their Share in the Canadian Market [208]

7.3 Battery Capacity and Driving Range

Although the PBEVs are powered by the same energy source, they are diversified in terms of their battery capacities and their driving ranges. These two factors are so important from the perspective of the electric grid. In general, when the battery capacity of the PBEV is large, a longer charging period is needed, which means more energy is consumed from the grid by that vehicle in each charging event. In contrast, a long driving range means that less charging events are required. From the perspective of the probabilistic model, specifying the battery capacity is important to quantify the required energy from the grid and the driving range is also important to determine the daily distance travelled by each PBEV. Figure 7.2 shows battery capacities and their total driving ranges for different types of PBEVs [209]. Vehicles depicted in Figure 7.2 characterized as Plug-in Battery Electric Vehicles. The reason of selecting them is that if these vehicles require a charging on the way, they do not

have another option to complete the trip such as in case of Plug-in Hybrid Electric Vehicles where they may use a gas station instead of a fast charging station. Therefore, Plug-in Battery Electric Vehicles are considered only in this study to illustrate the impact of the fast charging station.

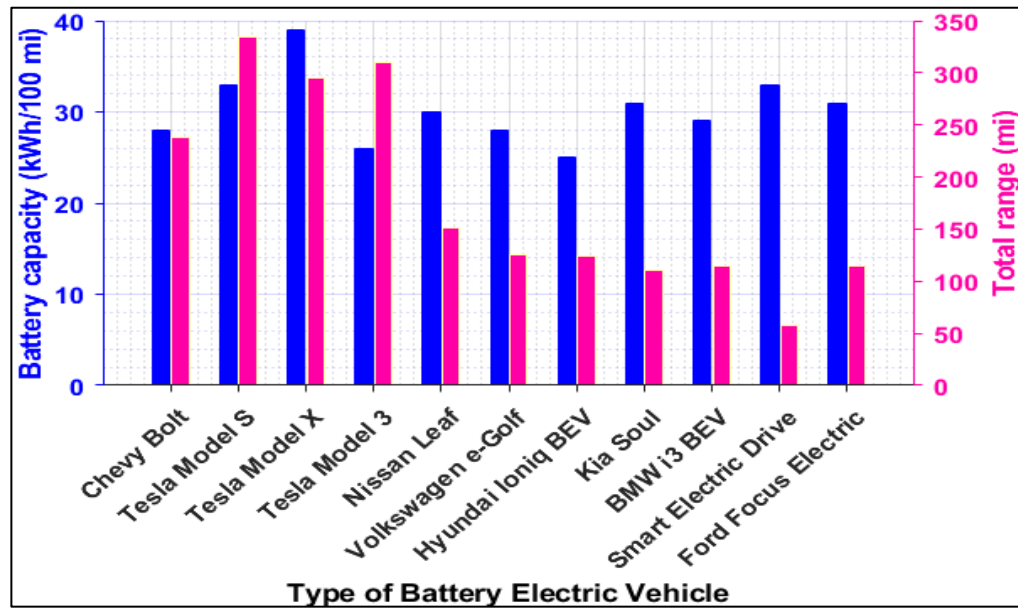


Figure 7.2 PBEVs Battery Capacities and their Driving Ranges [210]

Table 7-1 demonstrates the total ranges, battery capacity, and the market shares for the three types of PBEVs used in this study.

Table 7-1 PBEV Specification and Market Shares Used in This Study

Make	Model	Total Range (mi)	Battery capacity (kwh)	Market share (%)
Nissan	Leaf	151	45.3	47.02
Tesla	Model S	335	110.5	34.03
Chevrolet	Bolt	238	66.6	18.95

7.4 Distribution of Daily Mileage Travelled

The daily distance travelled is one of the most important parameters to generate the charging profile because of its impacts on the per-unit consumed energy and the

remaining battery SOC. Estimating the daily distance travelled is a key factor in determining the battery energy requirement from the electric grid by each PBEV. The daily distance travelled is estimated by a standard distribution function. The standard distribution function is selected based on the distribution fitting of three different daily distance travelled datasets. The Markov Chain Monte Carlo Based Approach (MCMC) is utilized in this study to generate the daily distance travelled by each PBEV listed in Table 7-1.

7.4.1 The Canadian Plug-In Electric Vehicle Survey (CPEVS-2015)

The CPEVS contains data from two different sources that are the 2013 New Vehicle Owners Survey (NVOS) and the 2015 Plug-in Electric Vehicle Owners Survey (PEVOS) [211]. The NVOS includes a sample of new conventional vehicle owners across most of the Canadian provinces whereas the PEVOS represents a sample of PEV owners in British Columbia. One of the main objectives of the CPEVS study is to describe how current and potential PEV owners drive and charge their vehicles. Our main interest will be on the PEVOS dataset for two reasons. The first reason is that the study comprises 568 driving days and thus representing the driving pattern of 157 PEV owners. The majority of those owners (81%) drive PEVs used in this study where their daily distance travelled are extracted and shown in Figure 7.3. The figure illustrates the cumulative percent of the daily diary (568 driving days) for three groups of PEV owners: Tesla owners (10 EV), Nissan owners (38 EV), and Chevrolet owners (74 EV), which represent more than 77% of the total sample. The second reason for using this data is that most of the three types PEV owners are living in

cities of Vancouver and Victoria in British Columbia, as indicated in this map [212]. These cities are characterized by a 4C climate zone [36], which is consistent with the commercial and residential load profiles modelled in the previous chapter. The extracted data are represented as a cumulative percentage of 568 driving days. Figure 7.3 includes two dimensions where the horizontal axis depicts the daily distance travelled by a cumulative number of PBEVs (as in the figure legend) illustrated in the vertical values. The data of daily distances travelled are utilized for distribution fitting corresponding to the three types of PBEVs mentioned above. It is not possible to select the best distribution that fits the extracted data set in their format. Instead of using the cumulative sum of driving days, the vertical axis will be represented using the percent of driving days. In order to achieve that, the extracted samples from Figure 7.3 will be paired and the difference between each pair of adjacent samples will be calculated starting from the first sample. The procedure will be repeated n times (e.g. 40 times) and in each time the data set will be found by taking the difference of every n^{th} element in the extracted data. This difference describes the increment between samples and can be used to estimate the percentage values of driving days in the vertical axis.

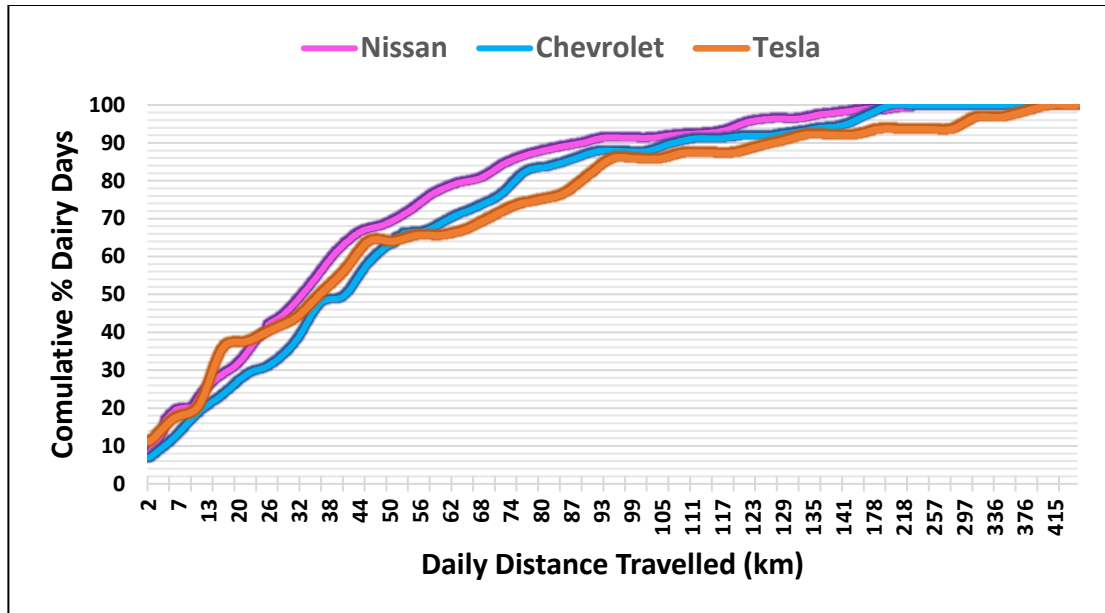


Figure 7.3 Daily Distance Travelled Distribution Based on 568 Driving Days

The empirical cumulative distribution will be calculated for each data set extracted, as stated above, and will then be compared to theoretical CDFs calculated from seven standard distribution functions; these are Exponential, Gamma, Normal, Poisson, Rayleigh, Weibull, and Birnbaum–Saunders distribution functions. The difference between each data sample of the empirical and the theoretical CDFs is assessed using the SSE as in (6.3). The minimum SSE value and its corresponding standard distribution function are recorded for each comparative case. The 40 winning standard distribution functions and their values (has minimum SEE) are obtained for each PBEV. The frequency of occurrence is calculated for each winning standard distribution function and its value is averaged, as demonstrated in Table 7.2. The idea is to select a standard distribution with more frequency of occurrence and less SSE. If that is not acquired, equation (7.1) is applied to select the best distribution that fits the data set extracted from Figure 7.3.

Table 7-2 Frequency of Occurrence and Mean SSE Values for the Winning Distributions

	Volt		Leaf		Tesla	
Winning Standard Distribution	Frequency of Occurrence	Mean of Minimum SSE	Frequency of Occurrence	Mean of Minimum SSE	Frequency of Occurrence	Mean of Minimum SSE
Exponential	0.35	0.0421	0.5	0.0489	0.075	0.0783
Gamma	0.325	0.0596	0.125	0.0335	0.075	0.0628
Weibull	0.3	0.122	0.05	0.3023	0.5	0.0561
Birnbaum–Saunders	0.025	0.1321	0.325	0.0613	0.35	0.1413

$$\phi^v = \min\{\psi_1^v, \dots, \dots, \psi_s^v\} \tag{7.1}$$

Where ψ_i^v represents a value calculated from Table 7.2 based on standard distribution i of PBEV v as in equation (7.2).

$$\psi_i^v = \frac{\varphi}{\tau} \tag{7.2}$$

Where φ symbolizes to the mean value obtained in Table 7.2 and τ indicates to the corresponding frequency of occurrence. This equation is used to overcome the case when we have a standard distribution of less φ and less τ or more φ and less τ in comparing to the rest of the distribution. Equation (7.2) resolves this issue by giving equal weight for both φ and τ .

In order to verify the proposed steps of estimation the best standard distribution using equation (7.1), Figure 7.4 is extracted from [211] and is utilized to validate the methodology. This figure is used because it includes both the cumulative percent of vehicles and the percent of vehicles, which were not included in Figure 7.3. The

distribution of cumulative percentage of vehicles, which is represented in the right side of the y-axis is utilized for the distribution fitting by taking the difference of each adjacent samples, as illustrated above. Then, the selected best distribution was compared with the selected best distribution coming from the bar plot in Figure 7.4. The results are identical, which indicates the validity of the proposed steps. Algorithm 7.1 depicts the steps of selecting the best distribution function.

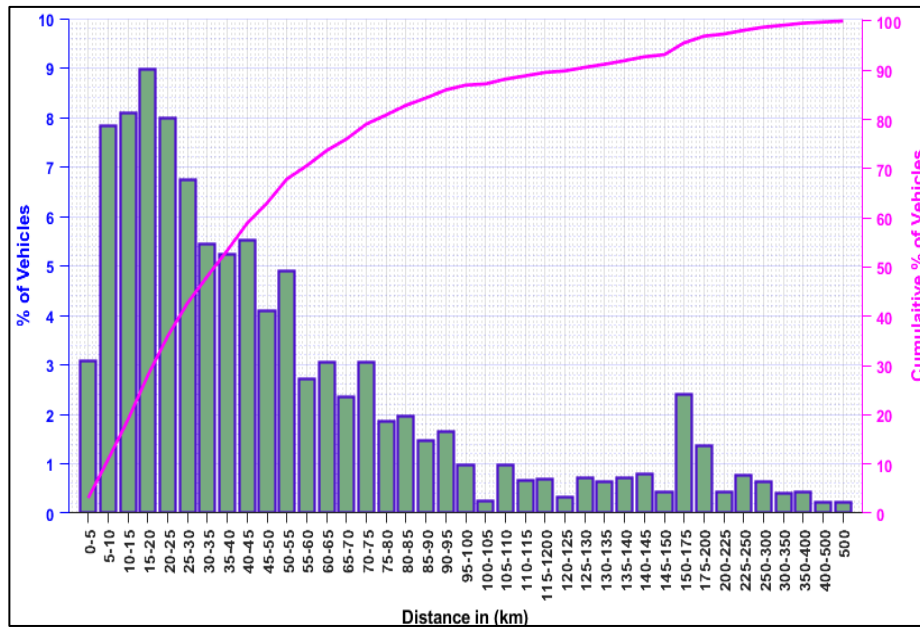


Figure 7.4 Daily Distance Travelled Utilized to Verify the Proposed Approach [210]

Algorithm 7.1 Estimation of Best Distribution that Fits the Daily Distance Travelled

- 1: **Start**
- 2: **Input:**
 - Three distributions of daily distance travelled extracted from Figure 7.3
 - Seven theoretical standard distribution functions as mentioned in section 7.4.1
- 3: **For** each distribution of daily distance travelled **do**
- 4: **For** C = 1:40 Case **do**
- 5: Dataset = extracted data from Figure 7.3 (1: C: end)

- 6: Compute the absolute difference between each pair as indicated above
- 7: Compute the empirical CDF for the dataset
- 8: **For** each SDF = 1:7 standard distribution function **do**
- 9: Find the maximum likelihood estimates for parameters of standard distribution calculated using the dataset
- 10: Compute the theoretical CDF for the specified SDF using the computed parameters evaluated at the values in step 7
- 11: Evaluate the empirical CDF and the theoretical CDF using SSE given in equation (6.3)
- 12: **End For**
- 13: Record the minimum SSE and its corresponding standard distribution
- 14: **End For**
- 15: Find the frequency of occurrence of the recorded distributions and their arithmetic mean
- 16: **End For**
- 17: **Output:**

The winning standard distribution function evaluated using equation (7.1)
- 18: **End**

The work in [58] utilizes the same type of EV proposed in this study to model its daily distance extracted from real mobility data [214]. The work represents the daily distance travelled using an exponential distribution which confirms the validity of the proposed distribution here for the same type of EV.

7.4.2 Fundamentals of Markov Chain Monte Carlo

The Markov Chain Monte Carlo (MCMC) in this study is used to generate a sample (random variable) representing the daily distance travelled and derived from a given standard distribution function selected, as illustrated in the section 7.4.1. A Monte Carlo is a general term used to generate outcomes from random sampling. A sequence of random samples is called a Markov chain. A Markov chain is a stochastic

process in which the state of the current sequence is influenced only by the latest state. Let $\{D_{(n)} ; n \geq 0\}$ represent a Markov chain, which includes a collection of random variables $D_{(0)}, D_{(1)}, \dots, D_{(n-1)}, D_{(n)}, \dots$ then the probability distribution of $D_{(n+1)}$, given the past states $D_{(0)}, D_{(1)}, \dots$, depends only on the present state $D_{(n)}$ [215]. The Metropolis-Hastings Algorithm is considered as one of the most common MCMC algorithms and is thus proposed in this study [216].

7.4.2.1 Metropolis-Hastings Algorithms

The Metropolis-Hastings methods are divided into the Metropolis-Hastings sampler, the Metropolis sampler, the independence sampler, and the random-walk. The last three methods are special cases of the first one [217]. Therefore, the Metropolis-Hastings sampler is utilized to generate samples from a Markov chain. A Markov chain is called irreducible if in a finite number of transitions, the sequence $\{D_{(n)} ; n \geq 0\}$ can reach any region (state) in the state-space regardless of the arbitrary starting point $D_{(0)}$. A Markov chain is called aperiodic if there is nonzero probability that the chain remains in the same state and will not be trapped in a cycle. Obtaining a new sample k_p from a candidate distribution $S(. | D_{(n)})$ is subjected to two previously mentioned regularity conditions: irreducibility and aperiodicity. To satisfy these conditions, a normal distribution can be used to generate a sample k_N around the current sample in the chain. The candidate sample $k_p = D_{(n)} + k_N$ is accepted as a new point at state $n + 1$ with a probability given as in equation (7.3). The chain will not move if the new sample k_p is rejected and then $D_{(n+1)} = D_{(n)}$.

Algorithm 7.2 outlines the steps of sampling the daily distance travelled using the Metropolis-Hastings method.

$$\rho(D_{(n)}, k_p) = \min \left\{ \frac{\sigma(k_p) \cdot S(D_{(n)} | k_p)}{\sigma(D_{(n)}) \cdot S(k_p | D_{(n)})}, 1 \right\} \quad 7.3$$

Algorithm 7.2 Steps of Metropolis-Hastings Algorithm

- 1: **Start**
- 2: **Input:**
 - The proposal distribution $S(\cdot | D_{(n)})$ found as in Algorithm 7.1
 - Number of chains ϑ
 - Specify the starting points of each chain $D_{(0)} := (D_{(0)}^1, D_{(0)}^2, \dots, D_{(0)}^\vartheta)$
 - $D_{(0)} \sim U([\text{round}(\zeta \times SOC_{min}), \text{round}(\zeta \times SOC_{max})], 1, \vartheta)$ and
 - set $n = 0$ and iterate for $n = 1, 2, \dots$
- 3: **For** each PBEV **do**
- 4: **For** iteration $n = 1$: until satisfy the convergence **do**
- 5: **For** each ϑ **do**
- 6: Generate a perturbation point k_N from a standard normal distribution
- 7: Generate a potential sample from the candidate distribution $k_p = D_{(n-1)} + k_N$
- 8: Draw Γ from a standard uniform distribution from an open interval (0,1)
- 9: Compute the acceptance probability $\rho(D_{(n-1)}^\vartheta, k_p)$ in equation (7.3)
- 10: If $\Gamma \leq \rho(D_{(n-1)}^\vartheta, k_p)$
- 11: then accept the new sample and set $D_{(n)}^\vartheta = k_p$
- 12: else
- 13: reject the sample and remain in the same state $D_{(n)}^\vartheta = D_{(n-1)}^\vartheta$
- 14: **End For**
- 15: **End For**
- 16: **Start**
- 17: **Input:**

18: Specify the quantity of interest (e.g. primary/secondary voltage)

19: Length of the chain n which is equal to number of iterations

20: Number of chains $\vartheta = 5$

21: **For** sample $y = 2$: n of the quantity of interest **do**

22: Compute the between-sequence variance as in equation (7.4)

23: Compute the within-sequence variance as in equation (7.5)

24: Compute the estimated variance of the quantity of interest as in equation (7.8)

25: Compute the estimated potential scale reduction $\sqrt{\hat{R}}$ as in equation (7.9)

26: If $1 \leq \sqrt{\hat{R}} < 1.1$

27: Then stop the chains due to the convergence

28: else

29: Iterate the chains more

30: **End For**

31: **End**

7.4.2.2 MCMC Convergence Monitoring and Assessment

In this study, MCMC is used to randomly draw a sequence of samples called a Markov chain and generated based on a given distribution. The chain is utilized to estimate outcomes obtained based on the inferences. If the chain is converged to the target distribution, then the inferences that we obtain from the chain are reliable, while are otherwise questionable [217]. The Gelman and Rubin method is utilized widely in the literature to monitor and evaluate the convergence of MCMC. This approach is adopted in this study because it is simple to be implement and it can be used in any MCMC algorithms [217], [218]. The method works by running ϑ multiple chains in parallel, starting from different initial points widely dispersed in the distribution. This is done to increase the chance of visiting most regions in the target distribution [219]. A quantity of interest (e.g. primary/secondary voltage) is

monitored and then evaluated using the stopping rule of the Gelman and Rubin method, which relies on the between-sequence variance and the within- sequence variance, as shown in equations (7.4) and (7.5) respectively. The convergence is diagnosed using equation (7.9) by calculating the “estimated potential scale reduction” $\sqrt{\hat{R}}$, which is typically less than 1.1 for all quantities of interest. If $\sqrt{\hat{R}}$ is higher than that, it is recommended to generate more sequences for each chain, namely more iterations [217].

$$B = \frac{n}{\vartheta - 1} \sum_{l=1}^{\vartheta} (\bar{\omega}_l - \bar{\omega}_{..})^2 \quad 7.4$$

$$W = \frac{1}{\vartheta} \sum_{l=1}^{\vartheta} \left[\frac{1}{n-1} \sum_{y=1}^n (\bar{\omega}_{ly} - \bar{\omega}_l)^2 \right] \quad 7.5$$

$$\bar{\omega}_l = \frac{1}{n} \sum_{y=1}^n \omega_{ly} \quad 7.6$$

$$\bar{\omega}_{..} = \frac{1}{\vartheta} \sum_{l=1}^{\vartheta} \bar{\omega}_l \quad 7.7$$

$$\widehat{var}(\omega) = \frac{n-1}{n} W + \frac{1}{n} B \quad 7.8$$

$$\sqrt{\hat{R}} = \sqrt{\frac{\widehat{var}(\omega)}{W}} \quad 7.9$$

Where, ω_{ij} indicates to the y^{th} sample in the l^{th} chain of the quantity of interest, $\bar{\omega}_l$ represents the average of each n elements starting from y^{th} sample in the l^{th} chain

whereas $\bar{\omega}_{..}$ denotes to the average of all chains' samples. Algorithm 7.4 illustrates the steps of monitoring the convergence using the Gelman and Rubin method.

Algorithm 7.2 Convergence Assessment Using Gelman and Rubin Approach

- 1: **Start**
 - 2: **Input:**
 - Specify the quantity of interest (e.g. primary/secondary voltage)
 - Length of the chain n which is equal to number of iterations
 - Number of chains $\vartheta = 5$
 - 3: **For** sample $y = 2:n$ of the quantity of interest **do**
 - 4: Compute the between-sequence variance as in equation (7.4)
 - 5: Compute the within-sequence variance as in equation (7.5)
 - 6: Compute the estimated variance of the quantity of interest as in equation (7.8)
 - 7: Compute the estimated potential scale reduction $\sqrt{\hat{R}}$ as in equation (7.9)
 - 8: If $1 \leq \sqrt{\hat{R}} < 1.1$
 - 9: Then stop the chains due to the convergence
 - 10: else
 - 11: Iterate the chains more
 - 12: **End For**
 - 13: **End**
-

7.5 Arrival Time Distribution and Rated Power of the FCSs

The arrival time at the FCS for charging the EV is another important parameter to generate the demand profile of the FCS, which is highly influenced by the charging events. A charging event means that an EV has arrived at the FCS and started charging its battery by one of the available ports of the station. Estimating the arrival time for the charge is a main factor in determining the starting time and the end time of each charging event. The arrival time is estimated based on a standard distribution

function. Typical data represents the arrival time (charge events) at the FCS and is utilized to select the best standard distribution function that fits the typical dataset. MCMC is utilized to estimate the arrival time at the FCS based on the selected distribution.

7.5.1 Typical Arrival Time and Rate at FCSs

Typical data, for a period of three years, from seven FCSs, are individually extracted and analyzed for distribution fittings. These FCSs are located in different locations such as workplaces, retail locations, and malls; but all of them are in Vancouver in British Columbia where its climate zone characterized as zone 4. These data are utilized to obtain arrival time distributions which, in turn, are utilized to select the best standard distribution function that fits them. The first step then, is to obtain the arrival time distribution of EVs at FCSs. To accomplish that, typical datasets are extracted for the years of 2015, 2016, 2017 and 2018 . The dataset for each year includes the number of charging times in each hour (24 hours), of each day (365 days). Each yearly dataset (365 days) is divided into 12 months and then all the datasets are grouped based on their monthly basis. Therefore, each hour is represented by accumulated number of charging times from the same hour from different months (12 months) from different years (3 years). Table 7-3 demonstrates more details about the FCSs utilized in this work. This table shows that the utilized FCSs have the same number of ports (one port) and the same maximum power (50 kW) and thus their charge events are not affected by these factors. For each distribution of the 14 arrival time distributions, the empirical CDF will be calculated

and then compared to theoretical CDFs calculated from seven standard distribution functions, whereas their dissimilarity is evaluated using SSE index as mentioned in section 7.4.1.

Table 7-3 Charge Events and Maximum Output Power of FCSs Utilized in This Work

FCS number	Period		Charge Events		Details	
	Start date	End date	Weekday	Weekend	Max power (kW)	Number of Ports
1	01-01-2015	31-05-2018	5653	2287	50	1
2	01-01-2015	31-05-2018	2560	1040	50	1
3	01-01-2015	31-05-2018	2227	883	50	1
4	01-01-2015	31-05-2018	2221	900	50	1
5	01-01-2015	31-05-2018	1932	742	50	1
6	01-01-2015	31-05-2018	1733	864	50	1
7	01-01-2015	31-05-2018	1384	503	50	1

For each arrival time distribution, seven SSE values will be obtained of the comparison, whereas one of the theoretical CDFs will be selected to represent that arrival time distribution based on its minimum SSE value. The 14 selected theoretical CDFs are utilized to represent the 14-typical arrival time distribution functions and their frequency of occurrences are tabulated. In all comparative cases, the Birnbaum–Saunders distribution function is the winning distribution and is therefore utilized in this work to represent the arrival time distribution at the FCS. MCMC is proposed to sample the arrival time distribution using the MHA and then monitoring the convergence, as illustrated in section 7.4.2. Algorithm 7.4 states the steps of sampling the arrival time distribution using MHA. The output of Algorithm 7.4 is the arrival time at the FCS, which represents the start of charging at the FCS. The period of charge is influenced by three parameters: the battery SOC, the battery capacity, and the rated power of the FCS. The effect of the first and second parameters are clarified in section 7.3 whereas the effect of the rated power of the FCS is elucidated below.

Algorithm 7.4 Steps of Sampling the Arrival Time Distribution using MHA

1: **Start**
2: **Input:**
 The proposal distribution $S(\cdot | A_{(n)})$ selected as in section 7.5.1
 Number of chains ϑ
 Specify the starting points of each chain $A_{(0)} := (A_{(0)}^1, A_{(0)}^2, \dots, A_{(0)}^\vartheta)$
 $A_{(0)} \sim [U([8 \ 21], 1, \vartheta) + N(0,3)]$ and
 set $n = 0$ and iterate for $n = 1, 2, \dots$
3: **For** iteration $n = 1$: until satisfy the convergence **do**
4: **For** each PBEV **do**
5: **For** each ϑ **do**
6: Generate a perturbation point k_N from a standard normal distribution
7: Generate a potential sample from the candidate distribution $k_p = A_{(n-1)} + k_N$
8: Draw Γ from a standard uniform distribution from an open interval (0,1)
9: Compute the acceptance probability $\rho(A_{(n-1)}^\vartheta, k_p)$ as per section 7.4.2.1
10: If $\Gamma \leq \rho(A_{(n-1)}^\vartheta, k_p)$
11: then accept the new sample and set $A_{(n)}^\vartheta = k_p$
12: else
13: reject the sample and remain in the same state $A_{(n)}^\vartheta = A_{(n-1)}^\vartheta$
14: **End For**
15: **End For**
16: Check the convergence by applying Algorithm 7.4
17: **End For**
18: **End**

7.6 Input Data Required for Vehicle Charging Model

7.6.1 Number of PBEVs

The number of electric vehicles in the system, \mathcal{N}^{BPEV} , is represented as a share of the total number of vehicles, which in turn is a function of the total number of houses in the system. The share of electric vehicles in the system is determined as follows [220]:

$$\mathcal{N}^{BPEV} = x^{pen} \cdot n^{house} \cdot n^{car} \quad 7.10$$

where,

\mathcal{N}^{BPEV}	Number of electric vehicles in the system
x^{pen}	Share of electric vehicles with respect to the total number of vehicles in the system, %
n^{house}	Number of residential houses in the system, house
n^{car}	Number of vehicles per house, vehicles/house

7.6.2 Type of PBEV and Charging Locations

The aim of the charging model is to compare the impacts of a typical FCS with an estimated one, on the voltage fluctuation and light flicker. A typical FCS profile is generated when a depleted battery of a Chevy Bolt was charged from a FCS with a rated power of 50 kW. The profile is available only for the Chevy Bolt and thus only one type of PBEV is selected in this case that is Chevy Bolt.

Therefore, there is \mathcal{V}^{CB} number of Chevy Bolts in the system with battery capacity of μ^{CB} .

$$\mathcal{V}^{CB} = \mathcal{N}^{BPEV} \quad 7.11$$

The battery capacity of each $v \in \mathcal{V}^{CB}$ is [210]:

$$\mu^{CB} = 66.6 \text{ kwh} \quad 7.12$$

The \mathcal{N}_{FCS}^{CB} number of Chevy Bolt charges at the FCS is:

$$\mathcal{V}_{FCS}^{CB} = \eta_{FCS}^{CB} \cdot \mathcal{V}^{CB} \quad 7.13$$

where,

\mathcal{N}^{BPEV}	Number of PBEV in the system
μ^{CB}	battery capacity of Chevy Bolt, kwh

\mathcal{V}_{FCS}^{CB} Number of Chevy Bolt charges from FCS

η_{FCS}^{CB} Share of Chevy Bolt charge requires a service from fast charger, %

7.6.3 Arriving Rate and Time at FCS

Figure 9.2 presents the distribution of vehicle arrival time and the rate at FCS prior to charge [221]. The given share of vehicles charging from FCSs, i.e., η_{FCS}^{CB} %, and the arrival rate is determined based on the data given in Figure 9.2. Probability distribution of arrival rate is based on an hourly time interval; thus, this distribution is used to randomly assign the corresponding number of PBEVs, i.e., \mathcal{V}_{FCS}^{CB} , to each hour.

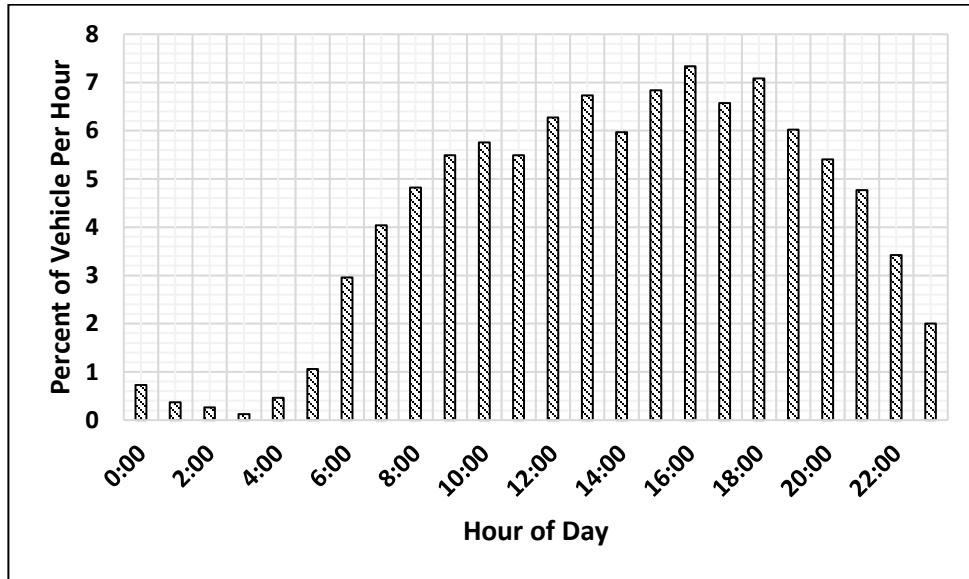


Figure 7.5 Distribution of Vehicle Arrival Time at FCS Prior to Charge [221]

7.6.4 Chevy Bolt Driving Pattern and Level of their Charged Batteries at the FCS

It is assumed that when any vehicle $v \in \mathcal{V}_{FCS}^{CB}$ start their trips, it starts from homes. Most of these vehicles start with almost a fully charged battery, according to the

distribution shown in Figure 7.6. Some of these vehicles are required to charge from the FCS according to their η_{FCS}^{CB} .

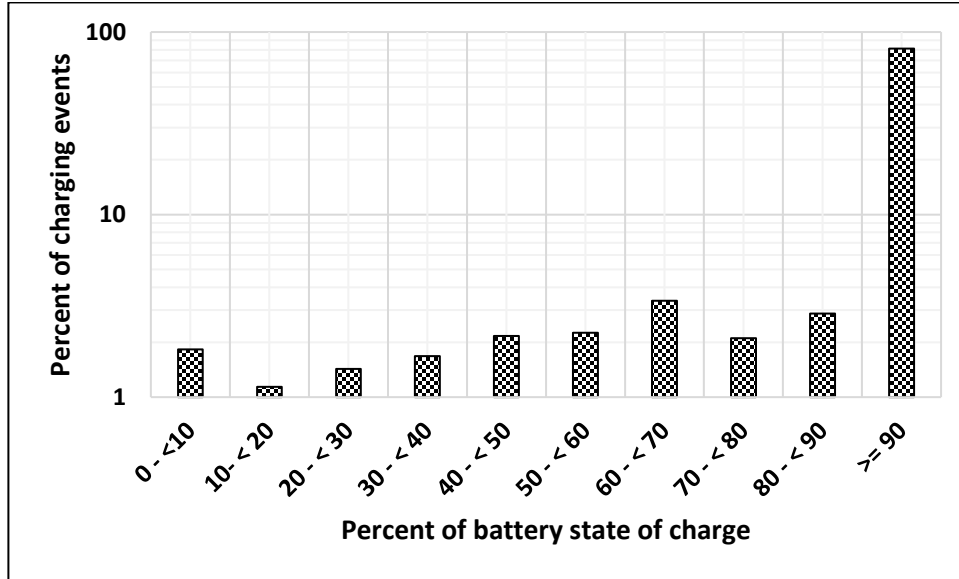


Figure 7.6 Battery State of Charge at End of Charging from Home Charger Prior to Driving [222]

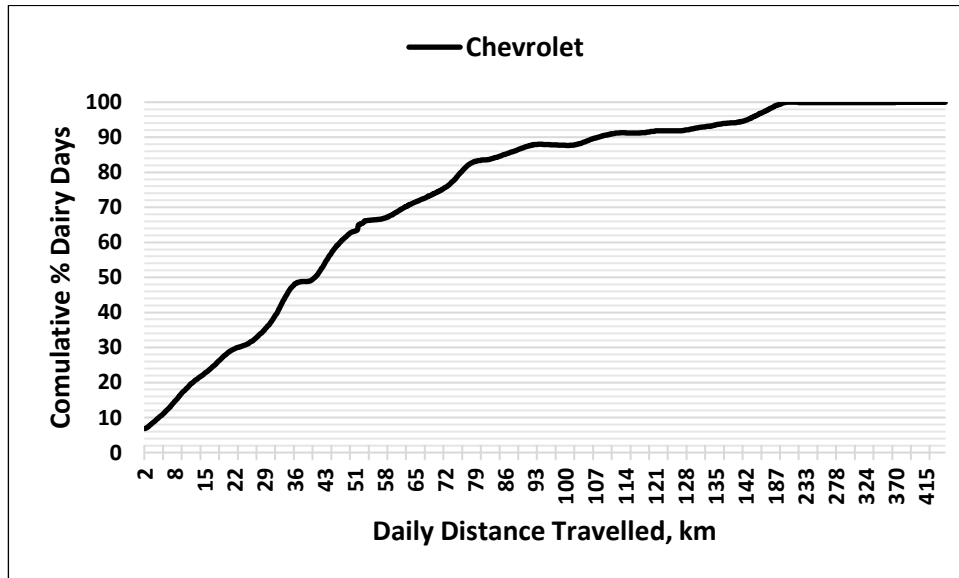


Figure 7.7 Daily Distance Travelled Distribution [211]

The daily distance travelled for each vehicle $v \in \mathcal{V}_{FCS}^{CB}$ is represented by an exponential distribution function [210]. Given these distribution functions, Markov

Chain Monte Carlo is carried out to sample these distributions and generate random daily trips and accordingly generate the remaining battery SOC [40]. It is assumed that when any vehicle $v \in \mathcal{V}_{FCS}^{CB}$ start their trips, it starts from homes. These vehicles start with a fully charged battery. According to their η_{FCS}^{CB} , some of these vehicles charge from FCS.

7.6.5 Charging Power

It was illustrated that the arrival time at the FCS shapes the start point of the charging event. Similarly, the rated power of the FCS is an essential factor contributing to shape the end point of the charging event (departure time). To clarify, the PBEV is assumed in this work to be a constant real and reactive power load that draws power depending on the rated power of the FCS. If, for example, a PBEV charges from an FCS with a rated power of 50 kW starting from a specific time, it means that the power consumed from the electric grid at that instant will jump by an amount equal to or less than the rated power of the FCS. The PBEV will be charged until it reaches γ_{FCS} . When the rated power of the FCS is high, the period of charge will be less especially in the case of low battery capacity or high SOC level. Two different scenarios are considered in this chapter: actual charging rates, and estimated charging rates of the FCS, as explained below.

7.6.5.1 Constant Charging Rate of FCSs

In this case, the FCS with β^{est} rated power, is utilized to charge one type of PBEV, the Chevy Bolt. The output power of the FCS is assumed to be stationary and will not be changed over time as the Chevy Bolt battery SOC changes. It is assumed that

the battery of the Chevy Bolt is charged linearly until it reaches to γ_{FCS} . For instance, the day is represented by 2,880 samples (1 sample / 30 second). If a Chevy Bolt arrives at FCS at 14:50 p.m. with 10 % SOC (6.66 kW), then it requires 51.8 kWh to reach 80% of its capacity. Given $\beta^{est} = 50kW$, then the required charging time is equal to $\frac{51.8 kWh}{\eta_{FCS} \times \beta^{est}} \cong 1.15h$, which means 138 samples based on our resolution. The end time of charging is at 16:05 p.m., which corresponds to the sample number 1,918 in our daily profile. It means that the FCS will draw a constant power from the electric grid equals to 50 kW from 14:50 p.m. to 16:05 p.m.

7.6.5.2 Variable Charging Rates of FCSs

A Chevy Bolt was charged from a FCS with a rated power of β^{act} . The FCS was connected to the secondary of a distribution pad-mounted transformer characterized as (4.16Y/0.6Y KV) with 50 kVA. The output power of the FCS will not be constant over time as the Chevy Bolt battery SOC increases. The active power per phase and its corresponding power factor is shown in Figure 7.5. It clearly shows the variation of the output power over time. This work presumes that the Chevy Bolt will be charged based on a linear rate. For example, the FCS takes 119 minutes or 238 samples, as the profile indicates, to charge 80 % of the battery capacity. Then the battery SOC will increase based on constant rate equal to $\frac{\gamma_{BEV}}{238}$ where in this case $\gamma_{BEV} = 53.28$ and the rate is equal to 0.223. This means that, based on the charging rate, the depleted Chevy Bolt requires 119 minutes or 238 charging samples to reach 80% of its battery capacity.

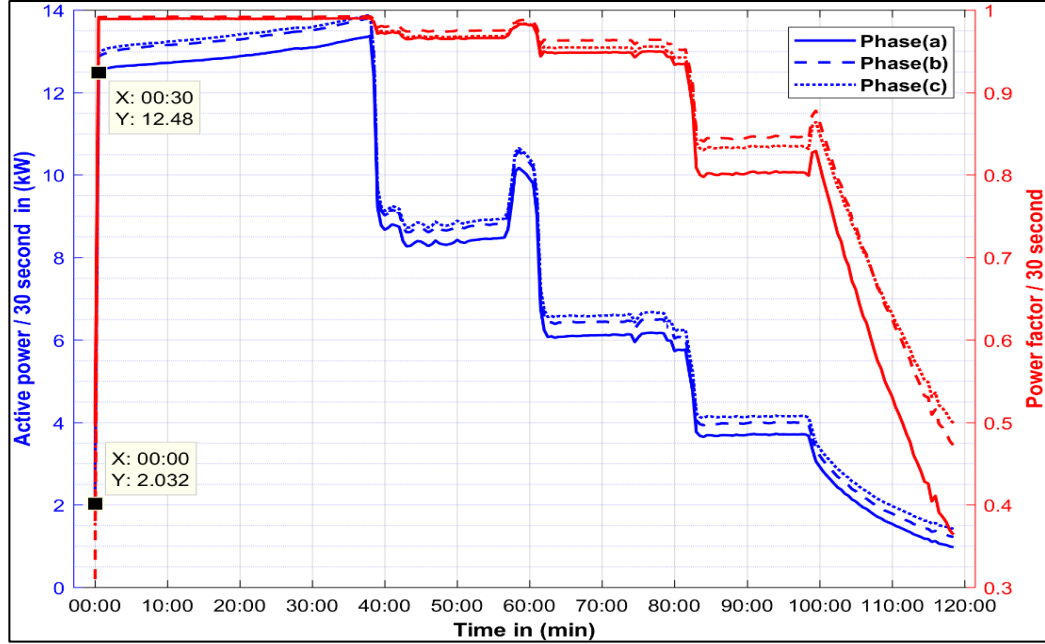


Figure 7.8 A Typical Output of FCS When It Charges a Depleted Chevy Bolt [223]

7.6.6 Length of Time with Chevy Bolt Drawing Power from FCS

In order to determine the energy required from the FCS for each charging event, the probability distribution in Figure 9.5 is utilized to estimate the length of time with a vehicle drawing power from the FCS. Given the length of the charging event L_{FCS}^{CB} , the rated power β of FCS, and the efficiency η^{FCS} of the charger, the energy required kwh^{FCS} from the FCS is estimated linearly as follows:

$$kwh^{FCS} = \left(\frac{L_{FCS}^{CB}}{\frac{\mu^{CB}}{\beta^{FCS} \cdot \eta^{FCS} \cdot \vartheta}} \right) \cdot \mu^{CB} \quad 7.14$$

$$\beta^{FCS} := \begin{cases} \beta^{est} & \text{if estimated charging power is utilized} \\ \beta^{act}, & \text{if actual charging charging is utilized} \end{cases} \quad 7.15$$

where,

kwh^{FCS} Energy required for vehicle v from FCS, kwh

L^{FCS}	Length of time with vehicle connected to the fast charger, minute
μ^{CB}	Battery capacity of vehicle v , kwh
η^{FCS}	Efficiency of the fast charger, %
ϑ	Factor to convert hour into minutes
β^{FCS}	Rated power of fast charging station, kw
β^{est}	Estimated charging power, kw
β^{act}	Estimated charging power, kw

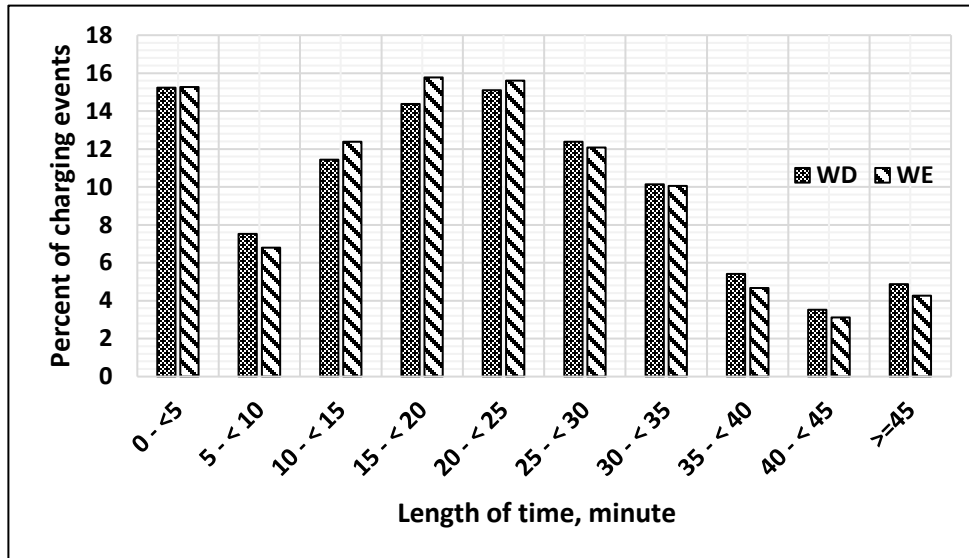


Figure 7.9 Distribution of Length of Time With a Vehicle Drawing Power From FCS per Charging Event [222]

The state-of-charge of each vehicle v charges from the FCS $v \in \mathcal{V}_{FCS}^{CB}$ is equal to soc_t^{CB} , and thus while the vehicle remains in the FCS i.e., $t_{CB}^{ar} < t \leq t_{CB}^{de}$, the state-of-charge is updated as follows:

$$soc_t^{CB} := \begin{cases} \left(\frac{\mu^{CB} \cdot soc_{t-1}^{CB} + \frac{\beta_{t-1}^{est}}{\vartheta}}{\mu^{CP}} \right) \cdot 100, \text{ using estimated charging power} \\ \left(\frac{\mu^v \cdot soc_{t-1}^v + \frac{\beta_{t-1}^{act}}{\vartheta}}{\mu^{CB}} \right) \cdot 100, \text{ using actual charging power} \end{cases} \quad 7.16$$

The required SOC soc_{des}^{CB} for vehicle v is determined by the customer upon the arrival at the FCS. The desired SOC is bounded by the maximum SOC soc_{max}^{CB} permitted from the FCS and the minimum increment in SOC soc^{req} for each charging event as in (9.40). The minimum SOC required for each charging event is specified by the FCS operator and defined as in (7.15).

$$soc^{req} < soc_{des}^{CB} \leq soc_{max}^{CB}, \forall v \in \mathcal{V}^{FCS} \quad 7.17$$

$$soc^{req} := \begin{cases} \left(\frac{\frac{L^{FCS}}{\mu^{CB}}}{\beta_t^{est} \cdot \eta^{FCS} \cdot \vartheta} \right) \cdot 100, \text{ for estimated charging power} \\ \left(\frac{\frac{L^{FCS}}{\mu^{CB}}}{\beta_t^{act} \cdot \eta^{FCS} \cdot \vartheta} \right) \cdot 100, \text{ for actual charging power} \end{cases} \quad 7.18$$

where,

soc_t^{CB}	State-of-charge of vehicle v at time t , %
soc_{t-1}^{CB}	State-of-charge of vehicle v at time $t - 1$, %
μ^{CB}	Battery capacity of vehicle v , kwh
t_{CB}^{ar}	The arrival time of vehicle v , hour and minute
t_{CB}^{de}	The departure time of vehicle v , hour and minute
soc^{req}	Minimum increment in battery state-of-charge, %
soc_{des}^{CB}	Desired state-of-charge at the end of charging event, %
soc_{max}^{CB}	Maximum increment in battery state-of-charge using FCS, %

As the required SOC is achieved, vehicle v departs from the FCS as follows:

$$t_v^{de} := \begin{cases} t + \mu^{CB} \cdot \left(\frac{SOC_{des}^{CB} - SOC_t^{CB}}{\beta_t^{est}} \right) \cdot \vartheta, \text{ using estimated charging power} \\ t + \mu^{CB} \cdot \left(\frac{SOC_{des}^{CB} - SOC_t^{CB}}{\beta_t^{act}} \right) \cdot \vartheta, \text{ using actual charging power} \end{cases} \quad 7.19$$

7.7 Demand Profile of the FCS

The probabilistic demand profile of the FCSs is generated in this section. The profile is considered the most important factor in quantifying the impact of the FCS on the electric power quality. All parameters that we need to generate the demand profile were previously defined in this chapter. The parameters include the distribution of the daily distance travelled, arrival time, battery capacity, PBEV type, and the FCS rate of power. Algorithm 7.5 outlines the steps to generate the FCS demand profile considering the aforementioned parameters.

Algorithm 7.5 Steps of Generating the FCS Demand Profile

- 1: **Start**
- 2: **Input:**
 - The probability density function $S(\cdot | D_{(n)})$ found as in Algorithm 7.1
 - The probability density function $S(\cdot | A_{(n)})$ selected as in section 7.5.1
 - Number of chains ϑ
 - Number of vehicles, n^{car}
 - Number of PBEVs, \mathcal{N}^{PBEV}
 - Number of PBEVs charges from FCS, \mathcal{V}_{FCS}^{CB}
 - The total range/PBEV
 - The battery capacity, μ^{CB}
 - FCS rated power, β^{est}, β^{act}
 - Specify the starting points $D_{(0)} := (D_{(0)}^1, D_{(0)}^2, \dots, D_{(0)}^\vartheta)$
 - $D_{(0)} \sim U([\text{round}(\zeta \times SOC_{min}) \text{ round}(\zeta \times SOC_{max})])$
 - Specify the starting points $A_{(0)} := (A_{(0)}^1, A_{(0)}^2, \dots, A_{(0)}^\vartheta)$
 - $A_{(0)} \sim [U([8 \ 21]) + N(0,3)]$
 - set $n = 0$ and iterate for $n = 1, 2, \dots$
- 3: **For** iteration $n = 1$: until satisfy the convergence **do**
- 4: **For** each PBEV **do**
- 5: **For** each ϑ **do**
- 6: Generate a sample representing the PBEV distance travelled $D_{(n)}^\vartheta$ as in Algorithm 7.2
- 7: Generate a sample representing its arrival time $A_{(n)}^\vartheta$ at the FCS as in Algorithm 7.2
- 8: Convert the arrival time to a sample equivalent to (1 sample / 30 second)
- 9: Calculate its required energy using Algorithm 7.4
- 10: Check the FCS port availability

```

11:   If the port is not available and ( $\mu^{CB} > 10\%$ )
12:   PBEV may or may not wait until the port becomes available, based on a random
      number uniformly distribution
13:   else
14:   PBEV will wait until the port becomes available
15:   End If
16:   If Actual Charging Rate is considered
17:     then PBEV belongs to the Chevy Bolt
18:     Extract the output of the FCS from Figure 7.4 (in samples) to increase the SOC
      level to  $soc_{des}^{CB} \%$ 
19:     Affix the extracted profile to the daily demand profile starting from the sample
      calculated as in step 8

20:   else
21:     Calculate the required period to increase the SOC level to  $soc_{des}^{CB} \%$ 
22:     Convert the required period to samples equivalent to (1 sample / 30 second) in
      which the output of the FCS is constant over this period and equal to  $\beta^{est}$ 
23:     Affix the output of the FCS as in step 17 to the daily demand profile starting from the
      sample calculated as in step 8
24:   End If
25:   End For
26: End For
27: Check the convergence by applying Algorithm 7.4
28: End For
29: End

```

Chapter 8. Results of Flicker Mitigation Using DSTATCOM

The aim of this chapter is to present the simulation results. A distribution test system is proposed and modified to include FCSs, commercial, and residential loads. Multiple scenarios are defined and applied on the proposed grid to assess and address the anticipated impacts of FCSs on three power quality phenomena representing the overall quality of the distribution systems.

8.1 Test System Description

In order to perform a load flow analysis and to examine the impact of FCSs, a test system is required. The IEEE 123-Node standard distribution test feeder, published in [224], is utilized in this research to conduct the study. The original 123-Node feeder is a real system consisting of two feeders leaving the substation; the published IEEE 123-Node feeder combines the two feeders into one and then adds several downstream voltage regulators, according to [225]. The map of the original system is displayed in [167], while the published system is depicted in Figure 8.1. The system is a radial distribution system and operates at a nominal voltage of 4.16 kV. The primary distribution system is served by one three-phase transformer bank with a rated capacity of 5,000 kVA located at the substation. The primary distribution system contains a main feeder and laterals tap-off of it. The main feeder consists of three-phase overhead lines and underground cables while the laterals are one- and two- phase overhead lines. The system's loading is unbalanced and includes single, two, and three- phase spot loads interconnected with the substation using the primary feeder. It is worth mentioning that a three-phase distribution transformer with a rated

capacity of 150 kVA, steps down the distribution nominal voltage to the utilization level feeding the spot load located at bus 610, as shown in Figure 8.1. The first version of the published IEEE 123-Node feeder [226], includes a spot load of a 150-horsepower induction motor located at bus 610 and connected to the secondary side of that distribution transformer. This spot load is not included in the second version of the published IEEE 123-Bus feeder, but the distribution transformer is included and is able to serve an equivalent loading amount. The IEEE 123-node system is modelled using the MATrix LABoratory (MATLAB) software [227], and simulated in the Open Distribution System Simulator (OpenDSS) [228], using the Component Object Model (COM) interface. Specifications of all the components of the proposed test system are presented in Appendix A.

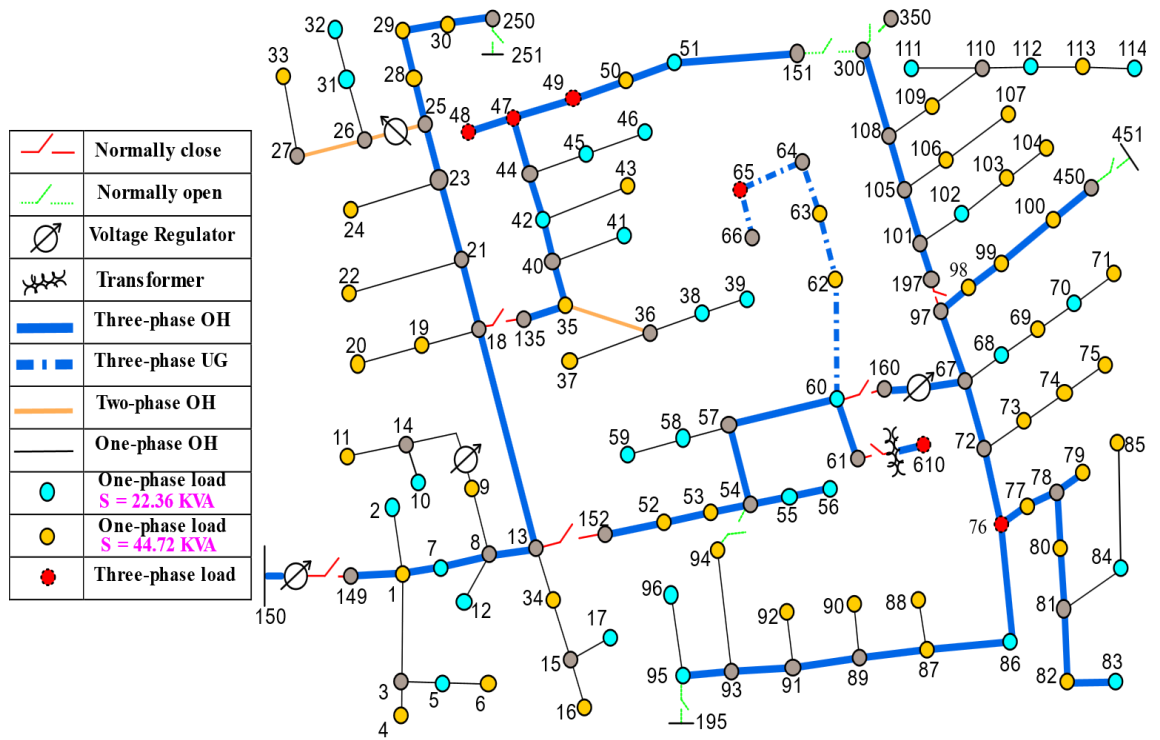


Figure 8.1 IEEE 123-Node Test Feeder [224]

8.2 Test System Modification

8.2.1 Primary Distribution System Expansion

As mentioned above, the spot loads in the test system are mainly supplied by the primary feeder, which operates at a nominal voltage of 4.16 kV. In order to study the impact of FCSs, they need to be included in the test system and supplied at their utilization voltage level. Therefore, the primary distribution system needs to be modified and expanded to include secondary distribution circuits; this includes distribution transformers to reduce the primary voltage to the utilization voltage level required by the FCSs and base loads. Two types of base loads are considered in this study: residential homes and commercial facilities. The proposed system shown in Figure 8.1 includes three-phase and single-phase spot loads. The three-phase loads are replaced with multiple three-phase distribution transformers utilized to supply the FCSs and commercial facilities. The rated power of these three-phase distribution transformers are 50 kVA, 30 kVA, and 15 kVA. The test system has six loads of this types, three of which are unbalanced spot loads. Also, the system contains 31 and 47 single-phase spot loads rated 22.36 kVA and 44.72 kVA. These spot loads are replaced with 31 center-tapped distribution transformers rated 25 kVA and 47 rated 50 kVA. These 78 center-tapped distribution transformers are utilized to feed the secondary distribution circuits which are used to flow electrical power to residential homes.

8.2.2 Secondary Distribution System Representation

Secondary distribution circuits are added in this study to connect customers (the base loads) to distribution transformers. Once the base loads are connected, their profiles can be generated and added to the system beside the demand profile of FCSs where the system's voltage quality is analyzed accordingly.

8.2.2.1 Residential Homes

Each center-tapped distribution transformer rated 50 kVA and 25 kVA is utilized to feed a group of 12 residential homes and a group of 6 residential houses, respectively. The number of homes served by each distribution transformer is equivalent to the corresponding single-phase spot load in the primary system. Therefore, a total of 750 residential homes is connected to 78 distribution transformers via service drops with random lengths between 80 to 100 feet; this is emanated from a routing single-phase triplex 120/240 V secondary main with length 125 feet. Specifications of secondary distribution system components (distribution transformer, secondary main, and service drop) utilized in this study, are illustrated in Appendix B. Figure 8.2 shows the layout of the secondary distribution circuits adopted in this study. This study presumes that all residential houses are in the same climate zone, namely a 4C, and thus their daily load profile are specified accordingly, as detailed in chapter 6 section 6. According to the analyzed residential yearly load profiles in chapter 6, all dwellings located in climate zone 4C equipped with gas heaters, but without electric water heaters. In [229], findings show that the median of the annual peak demand for

similar dwellings is 4.93 kVA. Thus, 4.93 kVA, at 0.9 lagging power factor, is assigned to represent the required peak load of each residential house in this study.

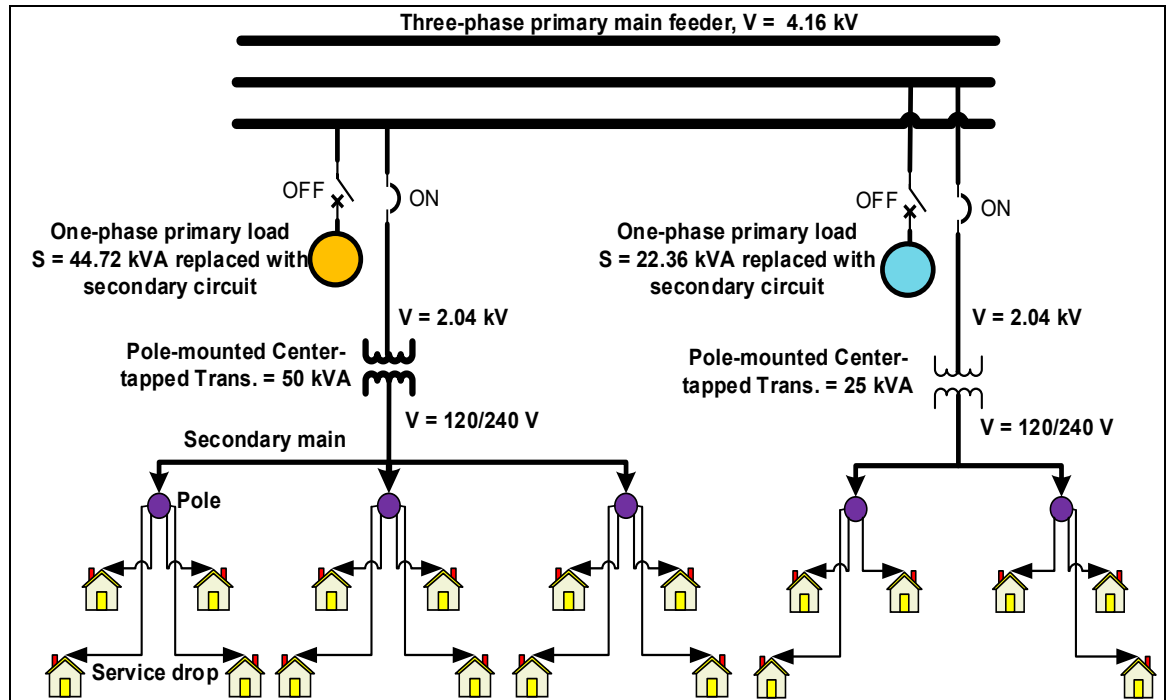


Figure 8.2 Layout of Secondary Distribution Circuits Used to Supply Residential Homes

8.2.2.2 Commercial Facilities

Four commercial facilities are utilized in this work; three of which are quick service restaurants connected to the test system at nodes 47, 49, 65, and one medium office connected at node 48. These commercial loads are connected to the primary distribution system using three-phase two-winding distribution transformers of which three are rated 30 kVA and one is rated 15 kVA. The peak load of each type of commercial building is assigned by analyzing the annual load profile (before they are normalized in chapter 6 section 6.4.3) determining the median of the maximum demand value. Their load profiles in 4C climate zone are used and obtained, as explained in chapter 7 section 7. The peak load for a quick service restaurant is a

28.56 kVA while it is a 13.33 kVA for a medium office, this is at 0.9 lagging power factor for both of them. Connection of the aforementioned facilities to the test system proposed in this work is depicted in Figure 8.3.

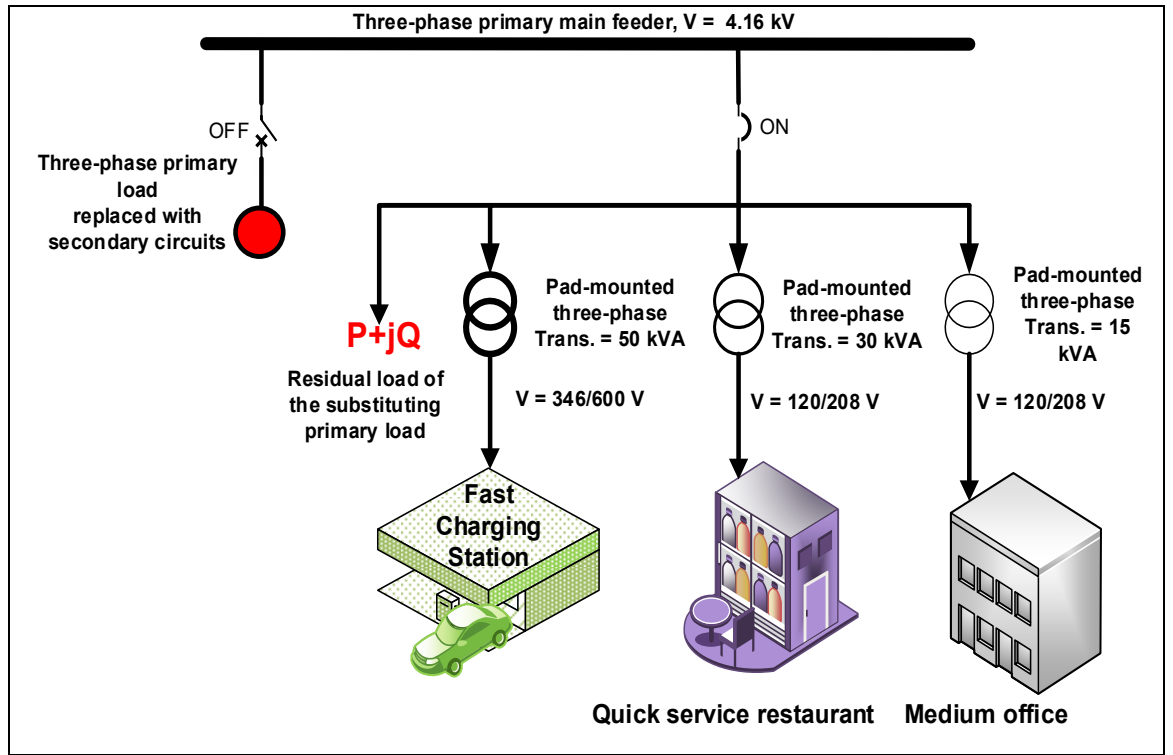


Figure 8.3 Sample of Three-Phase Secondary Loads Connected to the Primary Feeder

8.2.3 Fast Charging Stations' Inclusion

There are two approaches to represent the output power of FCSs: charging with a real profile and charging with an estimated profile. The distinctions of these two approaches are illustrated in detail in chapter 7 section 7.2. These two methods of charging are considered in this work and their impacts on the modified IEEE 123–Node are compared. Each FCS is connected to the primary main feeder using a three-phase distribution transformer rated 50 kVA as indicated in Figure 8.3. The number of FCSs utilized in this work and their locations are illustrated in Table 8.1. The load

profile for these FCSs are generated as previously described in detail in chapter 5 section 6. This study assumes that only 15% of the total number of residential homes have EVs and recharge them at the FCSs. The 15% represents the electric portion of new passenger car sales in British Columbia, according to [230].

Table 8-1 Locations and Numbers of FCSs

Location	Number of FCSs	Number of Ports
Node 47	2	2
Node 48	5	5
Node 49	2	2
Node 65	2	2
Node 76	5	5
Node 610	3	3

8.2.4 Battery Energy Storage Units' Integration

Battery Energy Storage Systems (BESUs) are proposed in this study to mitigate the impact of FCSs on voltage quality. BESUs are installed in the test system at the same locations where the FCSs are connected, as shown in Table 8.1. Each BESU is connected to the secondary side of the distribution transformer where its rated storage capacity is 250 kWh and its rated power is 50 kW [81]. BESUs are operated in three different states: idling state, discharging state, and charging/discharging state. In the idling operating mode, the BESUs do not absorb or supply any power to the FCS. In the discharge mode, the BESUs produce power to the FCSs and do not consume any power from the system. In the charge/discharge operating mode, the BESUs consume power from the grid when the FCSs are not occupied and inject that power to FCSs when they are being utilized by EVs.

8.2.5 Distribution Static Compensators' Placement

Distribution Static Compensator (D-STATCOM) is a shunt device operated in two different modes: a voltage control mode and a current control mode. In the voltage control mode, D-STATCOM is utilized to regulate the bus voltage to which the device is connected. In the current control mode, D-STATCOM is used to compensate the line current to become a balanced undistorted sinusoid. The aim of using D-STATCOMs in this study is to maintain the bus voltages to which D-STATCOMs are placed; this is either by producing or absorbing reactive power to alleviate the effect of FCSs on the primary distribution system. A three-phase D-STATCOM is connected to the primary side of the three-phase distribution transformers, as displayed in Figure 8.3. It is assumed that the reactive power of D-STATCOM that can be absorbed or injected into the system varies from -2000 kVAr to 2,000 kVAr.

8.3 Conducting the Load Flow Analysis

At this point, the test system was modeled, its nominal voltage was given, its configuration was described, and some of the primary nodes were modified to include secondary distribution circuits. The secondary circuits' components were specified and installed in the system. Parameters for residential houses, commercial facilities, FCSs, BESUs, and D-STATCOM were defined and their load profiles were generated accordingly. Therefore, a load flow analysis is required to determine the voltage magnitudes and phase angles at all nodes of the modified test system, which consists of 2,415 nodes. The load flow analysis is repeated until the termination

condition is satisfied. The termination condition is explained in chapter 7 section 7.4.2.2. The mean value of the voltage magnitudes and phase angles over all trials are utilized in this study. The result of this is a matrix in which the number of rows correspond to the number of nodes in the system and the number of columns represent the daily voltage profile. The values of this matrix represent the possible impact of FCSs on the electric distribution system. Therefore, these values are analyzed and compared with the limits of power quality variations explained in Chapter 6.

8.4 Scenarios and Results

In this section, multiple cases are considered to highlight the impact of the FCSs on the test system and to demonstrate the effectiveness of the proposed mitigation methods on voltage quality. Whenever the word "modified test system" is used, henceforth it indicates the IEEE 123-bus feeder modified to include residential houses and commercial facilities as previously explained. Four scenarios have been conducted on the modified test system in order to integrate: 1) FCS only, 2) FCSs equipped with BESUs in discharge mode only, 3) FCSs equipped with BESUs in charge and discharge modes, and 4) D-STATCOMs placed in the primary system. The first scenario is utilized as a base case to show the impacts of FCSs on the power quality variations, whereas the remaining cases are utilized to address these impacts in different degrees. The impacts and proposed mitigation methods are depicted and reported numerically for two types of FCSs: those with estimated charging rates and

those with real charging rates. In each scenario, three types of power quality indices are calculated and compared with the related standards.

8.4.1 Description of the Applied Scenarios

8.4.1.1 Connecting FCSs Only

In this case, only FCSs are connected to the modified test system. The system consists of 750 houses; 15% of these houses are assumed to have EVs and recharge them using FCSs. Two types of charging methods are considered: an estimated output power of the FCS equals to its rated power, and a real output power of the FCS obtained experimentally. The two charging profiles will be utilized to charge one type of EVs, that is a Chevy Bolt. Only one type of EV was considered because the real charging profile corresponds to the demand profile of a Chevy Bolt. Therefore, two independent simulations are conducted in this case in order to compare the impact of these FCSs on the power quality of the system.

8.4.1.2 Connecting FCSs Equipped with BESUs in Discharge Mode Only

In this scenario, each FCS integrated in the first case is equipped with a BESU with a rated storage capacity of 250 kWh and a rated power of 50 kW. The number of BESUs in the modified system are equal to number of FCSs and they are connected to the secondary side of the distribution transformers. BESUs are operated in this case in the discharging state to produce a specified active power in order to alleviate the demand of FCSs on the grid. The rate of discharge of each BESU is specified to be equivalent to the output power of the FCS in which that BESU is equipped with. The output of BESUs follows the output power of FCSs until either the BESU is

depleted or the EV's battery is full. Therefore, the BESUs are active and in the discharging state when the FCSs are busy; the BESUs are in the idling state when the FCSs are unoccupied. In the case of an estimated output power of the FCS, the BESU rate of discharge is a constant and equal to 50 kW, which is equivalent to the rated power of the FCS under consideration. In contrast, the BESU rate of discharge is a variable in the case of a variant output power of the FCS.

8.4.1.3 Connecting FCSs Equipped with BESUs in Charge and Discharge Modes

The main distinction between this and the previous case is that the BESUs operate in both the discharging and charging states. When the BESU operates in the discharging state, it injects a power to the system corresponding to its rate of discharge. When the BESU operates in the charging state, it absorbs power from the system depending on its rate of charge. As explained previously, the BESU operates in the discharging state when there is an EV consuming power from the FCS. The BESU operates in the charging state when the FCS is not utilized. Therefore, unlike the previous case, the BESU operates in the idling state only when it is full, and the FCS is not used. The BESU charging and discharging rates are equivalent and equal to the output power of the FCS in which that BESU is equipped with. In the previous scenario, BESUs were utilized to alleviate the impact of FCSs using a specified storage capacity of 250 kWh. As a number of discharging cycles are increased, the storage capacity is decreased by an equivalent amount of its discharging rate until either the battery is exhausted, or the discharging cycle is no longer required. Contrary to the previous case, the BESU is utilized in this case in its charging state in order to

investigate the situation when the storages were depleted in the previous case and more discharging cycles were required.

8.4.1.4 Connecting FCSs and Placing D-STATCOMs in primary Systems

In this case, instead of equipping the FCSs with BESUs, D-STATCOMs are connected at the point-of-common coupling to mitigate the possible impacts of FCSs. Therefore, D-STATCOMs are used in this study to inject or absorb reactive power varying from -2000 kVAr to 2,000 kVAr to maintain the secondary voltage of each three-phase transformer close to its nominal value which is 600 V. Also, there are commercial facilities connected to different distribution transformers, and these distribution transformers are supplied by the same primary buses that are utilized to feed other distribution transformers to which FCSs are connected. Thus, D-STATCOMs are used in the primary distribution system to regulate the bus voltages to which these commercial facilities are linked.

8.4.2 Voltage Quality Assessment Results and Discussion

The impact of FCSs on the modified system is analyzed and quantified using three different assessment methods: the voltage range, the voltage unbalance, and the voltage flicker. In the case of voltage range, the undervoltage and the overvoltage limits are utilized and compared respectively with the minimum voltage and the maximum voltage experienced by each node in the primary distribution system. In the case of voltage unbalance, the unbalance limit is compared with the maximum deviation from the average of each three-phase primary voltage divided by the average of the corresponding three-phase primary voltage. In the case of voltage

flicker, the ratio of the primary voltage deviation to the nominal primary voltage value is calculated and compared with the tolerance of irritation for a 15-minute period. Also, the percentile of short- and long-term flicker severity indices are calculated and compared with the compatibility levels explained in Table 3-11. The node 65 is utilized to compare between the two methods of charging and to compare between the effectiveness of the considered scenarios on the system. Node 65 is used to apply the comparisons because it is a primary node at which the voltage is 4.16 kV and represents a point of common coupling to which three different three-phase distribution transformers are connected to supply two FCSs operating at 600 V and one quick service restaurant operating at 208 V.

8.4.2.1 Assessment and Discussion of Under-Voltage and Over Voltage

Figure 8.4 to Figure 8.9 depict the assessment in this subsection. Figure 8.4 represents the evaluation of the first scenario when only FCSs are connected to the modified system. The figure shows the minimum and the maximum line-to-neutral voltages experienced during the day by each node in the primary of the system under study. Also, the minimum and maximum limits are illustrated in this figure. Exceeding the minimum limit means that there is under-voltage while exceeding the maximum limit indicates an over-voltage. Figure 8.4 clarifies that none of the primary nodes violate the limits of under-voltage or over-voltage. Also, the figure explains that the system under study is unbalanced of which the phases A and C have higher loads than phase B. FCS is a three-phase device connected to a three-phase distribution transformer as depicted in Figure 8.3; thus, there is no impact on the balance of the system by the FCSs. Regarding to the output power of the FCSs,

Figure 8.5 compares between two methods of charging: a charging with constant rate, and a charging with variant rate.

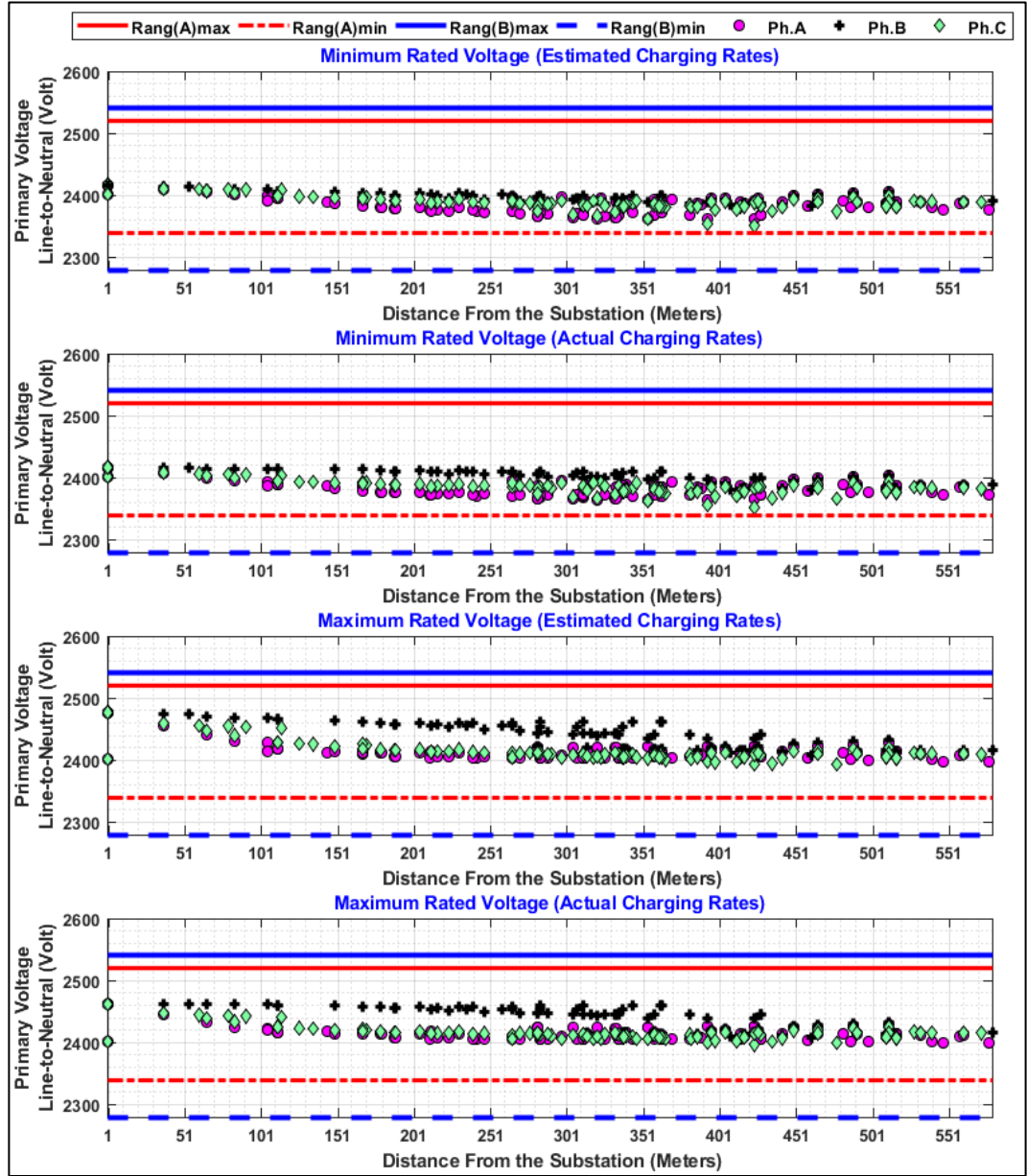


Figure 8.4 Minimum and Maximum Voltage Experienced by Each Primary Node When only FCSs are Connected (First Scenario)

Figure 8.5 consists of three graphs: the first graph represents the voltage measured at the primary side of the distribution transformers, the second graph explains the voltage profile measured at the secondary side of one of the two distribution

transformers connected to the FCSs, and the third graph shows the voltage profile measured at the secondary side of the distribution transformer used to supply the quick service restaurant.

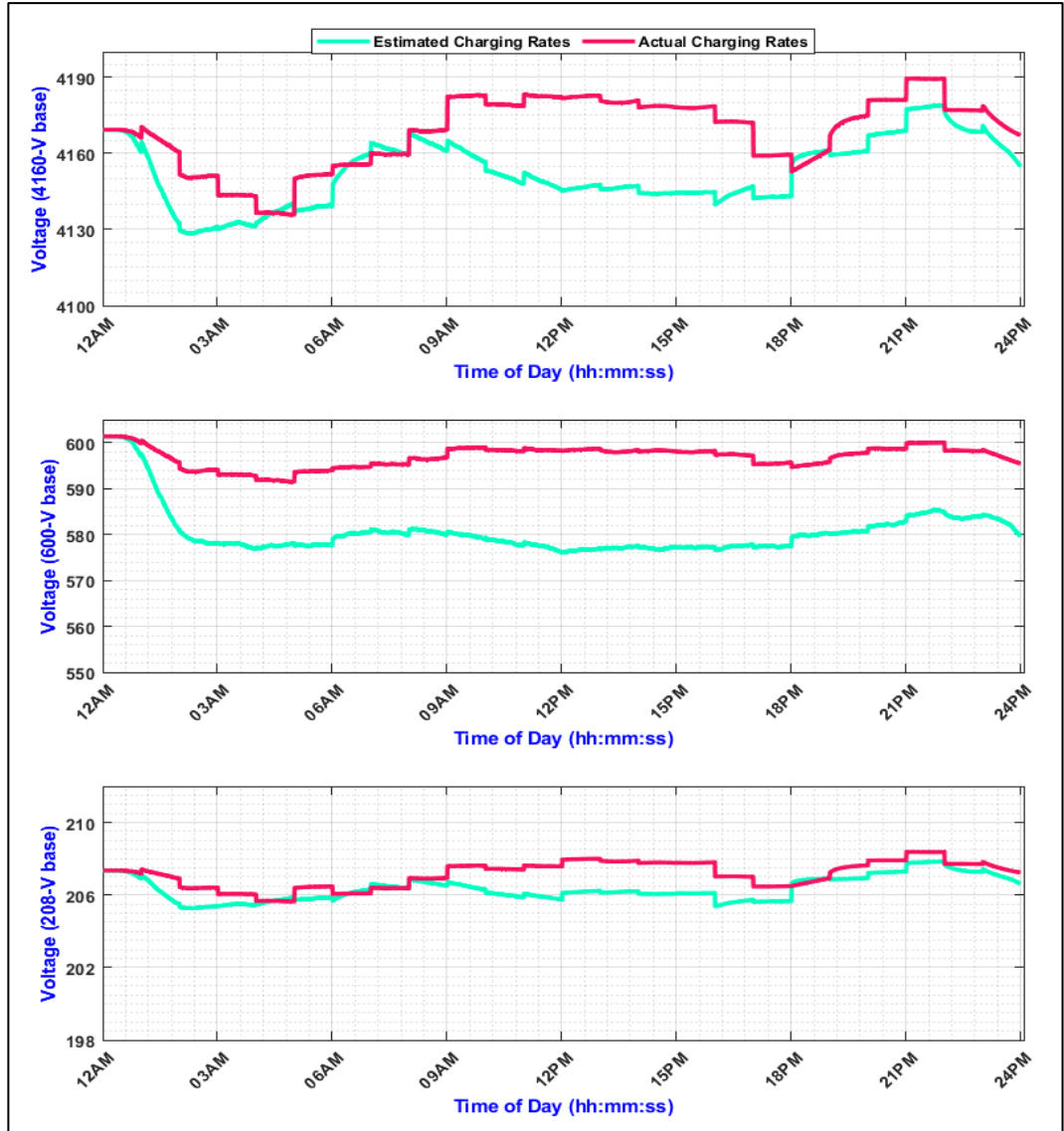


Figure 8.5 Voltage Waveform Measured at PCC at Node 65 When only FCSs are Connected (First Scenario)

The nominal voltage of each graph is shown in the y-axis whereas the x-axis represents the time of day. Although both charging methods operate within the service voltage limits, charging with constant rates has more effect as can be seen in

Figure 8.5. When refereeing to the voltage waveform for a 600-voltage base in Figure 8.5, the FCS is represented in the modified system as a constant real and reactive power load, and its voltage is required at each time. When the output power of the FCS is increased, the voltage at the FCS bus is decreased and vice versa. In the case of estimated charging rates, the output power always equals the rated power of the FCS, which is 50 kW. Therefore, the voltage in this case is mainly affected by the rated power of the FCS and not by the SOC of the EVs. In case of variant charging rates, the output power of the FCS is a function of the battery SOC. When the battery SOC is increased, the required power from the FCS is reduced, as shown in Figure 8.6. Accordingly, there is an obvious distinction in the voltage profiles corresponding to the two methods of charging. The primary voltage profiles in Figure 8.5 are influenced by the demand on their corresponding FCSs. There are some variations in the pattern between the primary voltage profiles and their corresponding secondary profiles. The variations in the pattern of the primary and secondary voltages in Figure 8.5 are produced due to the demand on their corresponding second FCS supplied from the same primary node, as mentioned above. Figure 8.6 below depicts the impact of the second scenario when the BESUs are included in the secondary buses to which the FCSs are connected. The output of the BESUs is equivalent to the output power of the FCSs and thus the BESUs rate of discharge is either a constant and equal 50 kW or is a variable determined by the EV's battery SOC.

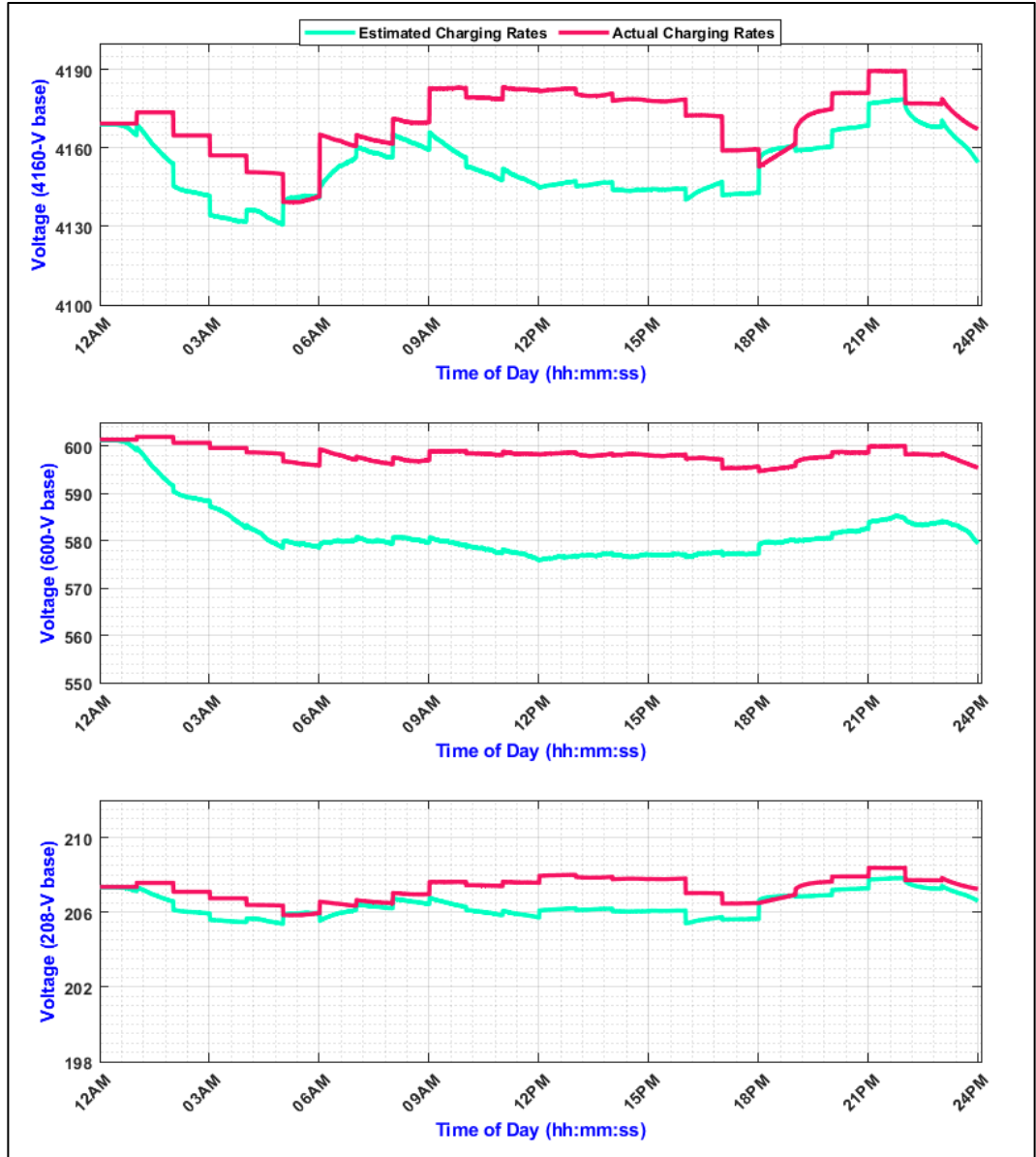


Figure 8.6 Voltage Waveform Measured at PCC at Node 65 When FCSs are Equipped BESUs in Discharging Mode only (Second Scenario)

Therefore, the BESU in this case is in the idling state when the power is not required. Otherwise, the BESU supplies the required power until it is exhausted or the EV's battery is full. When refereeing to the voltage waveforms for a 600-voltage base in Figure 8.6, during the period of 12 AM to 06 AM, the voltage profiles for both charging methods are gradually decreased comparing to their profiles during the

same times in the first scenario. At 06:00 am, the BESUs are depleted and the FCSs are fed by the distribution system and thus the voltage profiles after that are identical to the profiles in the first scenario, for the FCSs and for the quick service restaurant. The voltage profile of the commercial load is affected because the BESUs inject the required power of the FCSs, and this will relieve the voltage at the primary node, which is a common bus-bar between the two types of distribution transformers feeding the FCSs and commercial facilities. Figure 8.7 shows the impact of the third scenario when the BESUs operate in charging and discharging states. In this case, the system is loaded either by the FCSs demand or by the BESUs demand in the charging state. The system is alleviated in this case only when no charging events are required and the BESUs are in the idling state. Figure 8.7 clarifies that when the BESU operates in charging and discharging states, the voltage profile in the case of estimated charging rates is improved, as shown around 12:00 pm, comparing to the previous scenario when the BESUs were operated in idling or discharging states. In contrast, the voltage profiles in the case of variant charging rates are almost similar in both scenarios due to the injected power by the BESU, which lasts longer in serve when compared to its state in the first charging method which depletes quickly. Figure 8.8 illustrates the effect of the fourth scenario when the D-STATCOMs are connected to the primary side of the distribution transformers from which the FCSs are supplied. Instead of using BESUs to produce active power, D-STATCOMs are utilized to inject a reactive power to mitigate the impact of the FCSs. Figure 8.8 clearly shows that D-STATCOMs are able to maintain the voltage at the point of common coupling and hence mitigate the impact of FCSs.

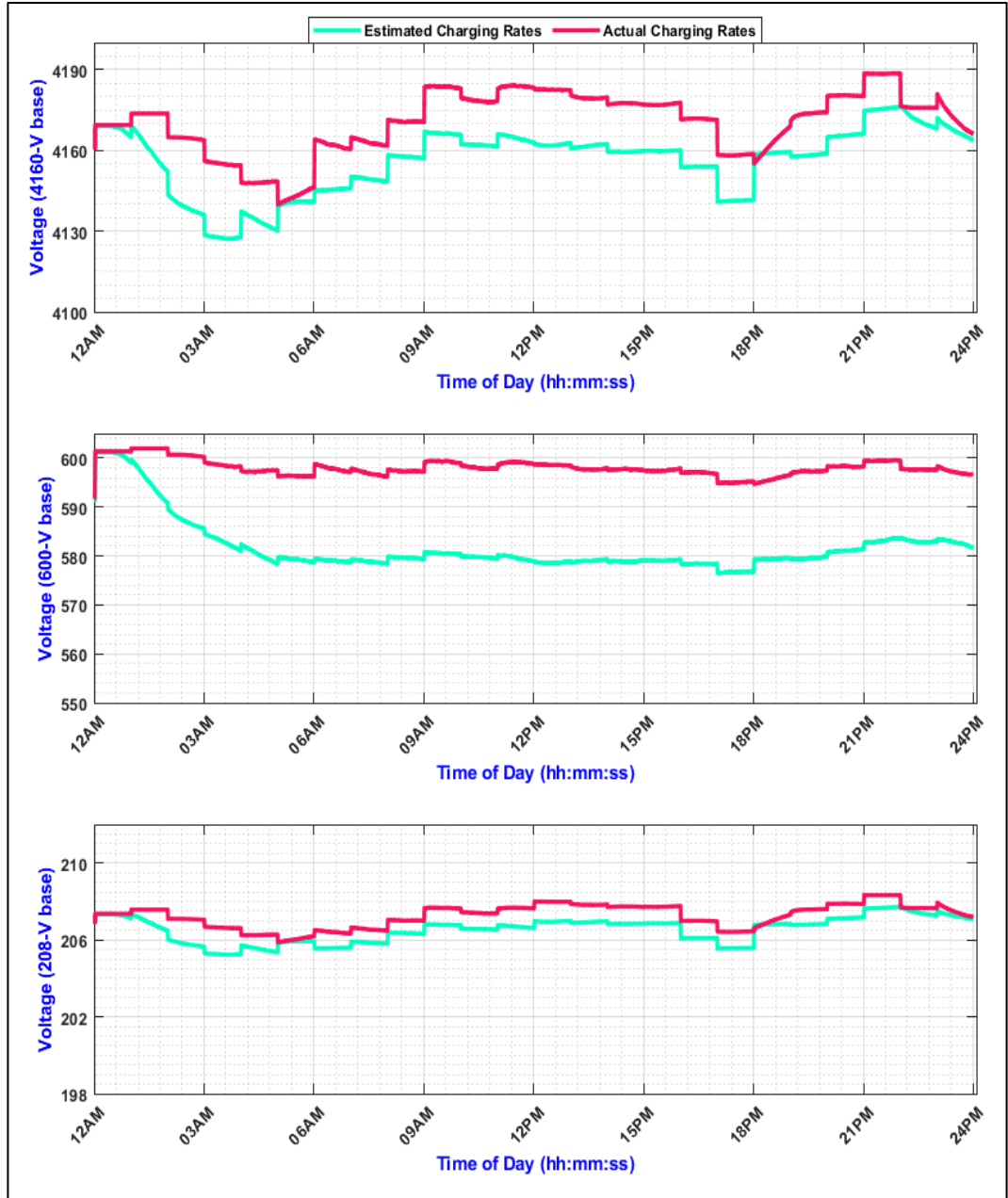


Figure 8.7 Voltage Waveform Measured at PCC at Node 65 When FCSs are Equipped with BESUs in Discharging and Charging Modes (Third Scenario)

Although both methods of charging in Figure 8.8 depict a similar voltage profile, the voltages at the primary side of distribution transformers are not maintained at their nominal values.

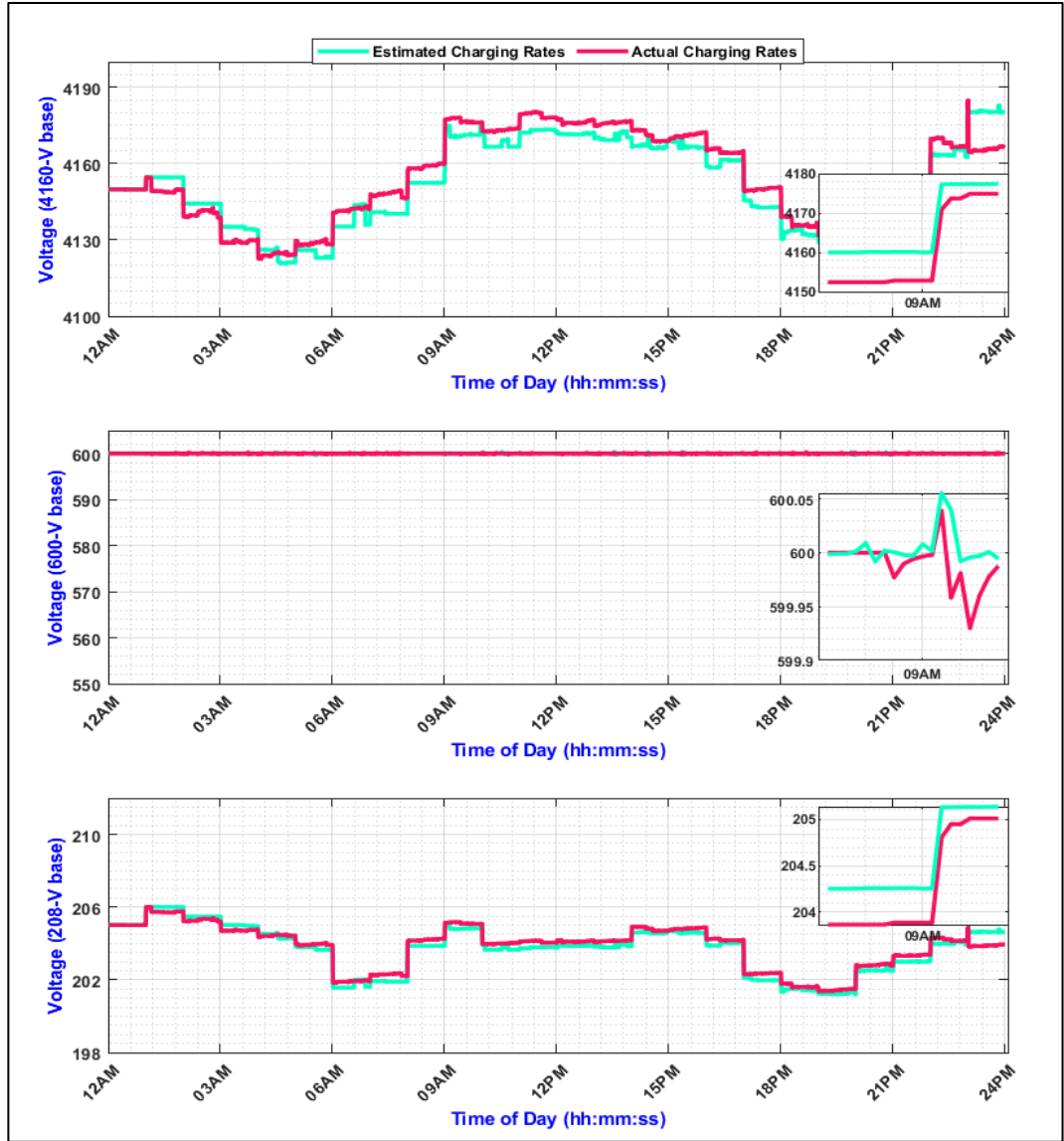


Figure 8.8 Voltage Waveform Measured at PCC at Node 65 When FCSs are Connected and D-STATCOMs are Placed in the Primary System (Fourth Scenario)

The minimum and the maximum line-to-neutral voltages encountered during the day, corresponding to the fourth scenario are shown in Figure 8.10. Every group of points in Figure 8.10 that is lined vertically represent the minimum or maximum voltage values experienced corresponding to a specific node (phases). It is deduced that from that figure the difference in the voltage magnitudes, corresponding to a three or two

-phase node, is reduced on the test system under study. Not only is the impact of the FCSs mitigated, but also the voltage of the nodes is enhanced.

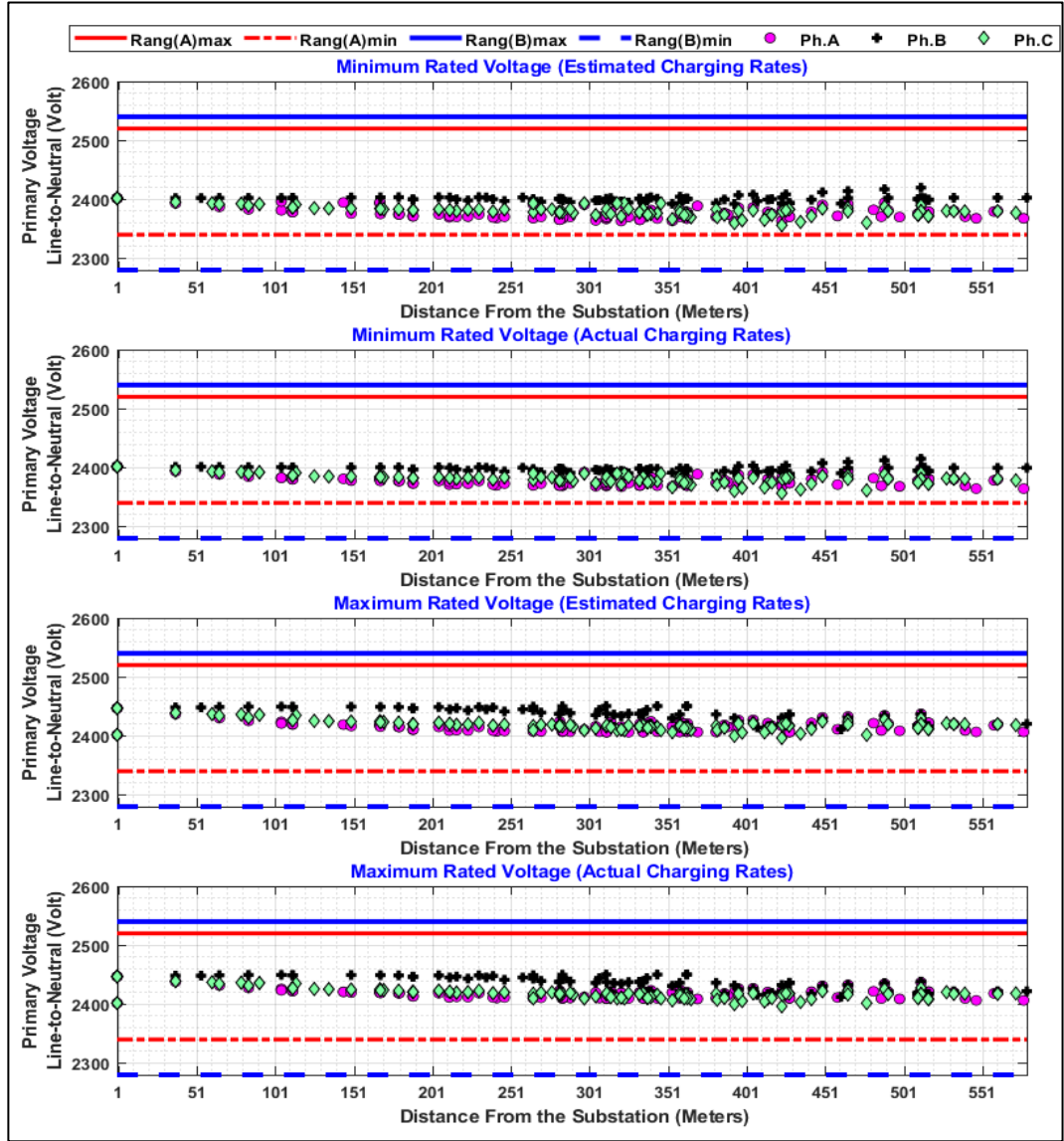


Figure 8.9 Minimum and Maximum Voltage Experienced by Each Primary Node When FCSs are Connected and D-STATCOMs are Placed in the Primary System (Fourth Scenario)

8.4.2.2 Assessment and Discussion of Voltage Unbalance

Table 8-2 shows the maximum voltage unbalance that occurred in each scenario and its corresponding time of the day. The voltage unbalance is calculated for each node as explained in chapter 6 section 6.3.2, and then the maximum value of each scenario

is recorded in Table 8-2. Inspecting the values of maximum voltage unbalance demonstrates that none of the conducted scenarios violate the limit of voltage unbalance. This is due to the connection of FCSs as balanced three-phase components, and thus they impact the unbalanced phases of the system under study by the same degree. Moreover, the outcome of the table implies that in the case of estimated charging rates, the effects on the voltage unbalance is more than the effects in the case of variants charging rates. Also, BESUs and D-STATCOMs are connected as balanced three-phase components, but their performance is different in regard to the voltage unbalance. When the D-STATCOMs are utilized, the system's voltage is improved and the deviation between its phases is reduced. Accordingly, this may lead to decrease the system's power losses.

Table 8-2 The Maximum Voltage Unbalance Encountered for Each Scenario

Scenarios	Charging Methods	Max. Voltage Unbalance (%)	Time (hh:mm:ss)
First	Estimated charging rates	2.072	19:03
	Actual charging rates	1.979	19:01
Second	Estimated charging rates	2.074	19:03
	Actual charging rates	1.979	19:01
Third	Estimated charging rates	2.091	19:10:30
	Actual charging rates	1.981	19:01:30
Fourth	Estimated charging rates	0.946	19:01
	Actual charging rates	0.929	19:01

8.4.2.3 Assessment and Discussion of Voltage Fluctuation and Light Flicker

The results of voltage fluctuations and light flickers are summarized in Table 8-3 and 8-4. Four types of descriptive statistics are presented in each table: the minimum, the average, the 95th percentile, the maximum values, and in addition to locations of the maximum values encountered. The results compare two methods of charging using

three indices: the borderline of irritation, the Percentile Long Term (P_{LT}) flicker severity index, and the Percentile Short Term (P_{ST}) flicker severity index. If the presented minimum value in the tables below is less than the limit corresponding to one of these indices, then there is no light flicker according to the indicator for that specified scenario. The results shown in Table 8-3 reveal that the light flicker is due to fluctuating the voltage in the first and second scenarios, which exceed the limits of all three indices in all phases. In the case of estimated charging rates, the violations are more than those caused by variant charging rates. Likewise, the results indicate that the flicker sensation indices were exceeded mostly in phase C, as illustrated in Table 8-3. The outcomes of the third scenario reported in Table 8-4, depict a similar pattern to the first and second scenarios regarding the flicker sensation. This is due to the changes in the operating modes of the BESUs, which depict a similar operating pattern as the FCSs. When the state of BESUs changes regularly between idling and discharging, as in the second scenario, or between idling, discharging, and charging states, as in the third scenario, voltage of the system changes in response to changing the states, which leads to the light flicker. The results of the fourth scenario are demonstrated in Table 8-4. The voltage is improved in this scenario as the borderline of irritation and P_{ST} were not violated by both methods of charging. However, the limit of P_{LT} was exceeded. Table 8-5 shows the results when D-STATCOMs are connected to the primary and secondary systems. The statistics of Table 8-5 clearly indicate that no light flicker was encountered by any phase at all when monitored by nodes in the system.

Table 8-3 Statistics for Voltage Fluctuation and Light Flicker Indices (First and Second Scenarios)

		First Scenario			Second Scenario				
		Statistics	Phase A	Phase B	Phase C	Phase A	Phase B	Phase C	
Estimated Charging Rates	Standard GE Flicker Curve	Minimum	2.104514	2.100132	2.100139	2.100335	2.100044	2.100111	
		Average	3.829982	2.72028	3.600796	3.827626	2.700978	3.578397	
		95%	4.843636	3.548384	4.750689	4.878515	3.588395	4.776827	
		Maximum	5.50102	4.151198	5.813875	5.533173	4.158636	5.84223	
		Location	Node 65	Node 76	Node 65	Node 65	Node 76	Node 65	
	IEEE 1453 Standard Flicker Meter	P _{LT}	Minimum	0.800015	0.800999	0.800142	0.800791	0.800638	0.800844
			Average	1.302334	1.040018	1.23584	1.27646	1.031208	1.222055
			95%	1.55094	1.291831	1.507641	1.555034	1.293797	1.510696
			Maximum	1.585818	1.380742	1.631712	1.590915	1.384817	1.635308
			Location	Node 151	Node 49	Node 51	Node 151	Node 49	Node 51
P _{ST}		Minimum	1.001107	1.000042	1.000137	1.000333	1.000345	1.000181	
		Average	1.381796	1.161789	1.335829	1.372318	1.148406	1.326598	
		95%	1.558298	1.347758	1.552578	1.565473	1.352752	1.551008	
		Maximum	1.609648	1.410413	1.659118	1.614746	1.41442	1.663479	
		Location	Node 151	Node 48	Node 51	Node 151	Node 49	Node 51	
Actual Charging Rates	Standard GE Flicker Curve	Minimum	2.101144	2.100092	2.100783	2.100007	2.100077	2.101413	
		Average	2.334734	2.310633	2.372522	2.346644	2.310767	2.370005	
		95%	2.474487	2.473983	2.585045	2.474487	2.473911	2.614384	
		Maximum	2.474489	2.476119	2.693905	2.474489	2.476047	2.695528	
		Location	Node 150	Node 2	Node 65	Node 150	Node 2	Node 65	
	IEEE 1453 Standard Flicker Meter	P _{LT}	Minimum	0.805646	0.801584	0.802932	0.805152	0.801465	0.800061
			Average	0.913962	0.934765	0.89153	0.913768	0.935327	0.891679
			95%	1.001467	1.09084	1.099189	1.073112	1.090922	1.075755
			Maximum	1.12708	1.127173	1.127123	1.127221	1.127314	1.127264
			Location	Node 150	Node 150	Node 150	Node 150	Node 150	Node 150
P _{ST}		Minimum	1.000036	1.000253	1.001256	1.001437	1.000326	1.000607	
		Average	1.05734	1.076277	1.08842	1.072284	1.076156	1.083192	
		95%	1.127094	1.127057	1.136327	1.127236	1.127182	1.137955	
		Maximum	1.127094	1.12718	1.153111	1.127236	1.127321	1.153178	
		Location	Node150	Node150	Node 51	Node150	Node150	Node 51	

Table 8-4 Statistics for Voltage Fluctuation and Light Flicker Indices (Third and Fourth Scenarios)

			Third Scenario			Fourth Scenario			
		Statistics	Phase A	Phase B	Phase C	Phase A	Phase B	Phase C	
Estimated Charging Rates	Standard GE Flicker Curve	Minimum	2.100121	2.100003	2.100069	6.63E-08	1.05E-05	1.06E-08	
		Average	3.731865	2.571804	3.499518	0.373022	0.545681	0.322703	
		95%	4.909215	3.394763	4.613607	0.052648	0.605559	0.109406	
		Maximum	5.392168	3.81736	5.695721	1.222637	1.22277	1.222742	
		Location	Node 65	Node 76	Node 65	Node150	Node150	Node 66	
	IEEE 1453 Standard Flicker Meter	P _{LT}	Minimum	0.80793	0.802097	0.800873	0.003456	0.003709	0.003013
			Average	1.28503	1.028678	1.226992	0.381892	0.456663	0.355725
			95%	1.549205	1.261633	1.506106	0.793667	0.94245	0.782379
			Maximum	1.609083	1.338798	1.634354	0.977421	0.977479	0.977468
			Location	Node 151	Node 48	Node 51	Node 1	Node 1	Node 1
		P _{ST}	Minimum	1.000509	1.000064	1.000472	0.003176	0.002178	0.000718
			Average	1.368176	1.129835	1.319034	0.371226	0.454293	0.344512
			95%	1.579031	1.31328	1.534912	0.783401	0.94275	0.795578
			Maximum	1.630537	1.354907	1.677372	0.97747	0.977506	0.989715
			Location	Node 151	Node 49	Node 51	Node 60	Node 60	Node 21
Actual Charging Rates	Standard GE Flicker Curve	Minimum	2.100261	2.10005	2.100089	8.38E-09	5.72E-07	8.66E-09	
		Average	2.398404	2.313614	2.37507	0.358414	0.49457	0.306707	
		95%	2.499484	2.49975	2.499661	0.091325	0.604404	0.119856	
		Maximum	2.499485	2.499862	2.689301	1.222529	1.222674	1.222644	
		Location	Node 150	Node 150	Node 65	Node 150	Node 150	Node 150	
	IEEE 1453 Standard Flicker Meter	P _{LT}	Minimum	0.800319	0.801508	0.800981	0.004821	0.003443	0.001632
			Average	0.919812	0.935763	0.894694	0.374076	0.427697	0.342615
			95%	1.094794	1.094419	1.094462	0.770103	0.943785	0.768267
			Maximum	1.128538	1.128631	1.128581	0.977391	0.977452	0.977439
			Location	Node 150	Node 150	Node 150	Node 1	Node 1	Node 1
		P _{ST}	Minimum	1.001689	1.000007	1.001393	0.000979	0.000869	0.000811
			Average	1.082293	1.075673	1.090387	0.36252	0.424386	0.329842
			95%	1.128553	1.127787	1.128592	0.782466	0.943693	0.804648
			Maximum	1.128553	1.128638	1.139586	0.97744	0.977479	0.977471
			Location	Node 150	Node 150	Node 51	Node 61	Node 61	Node 61

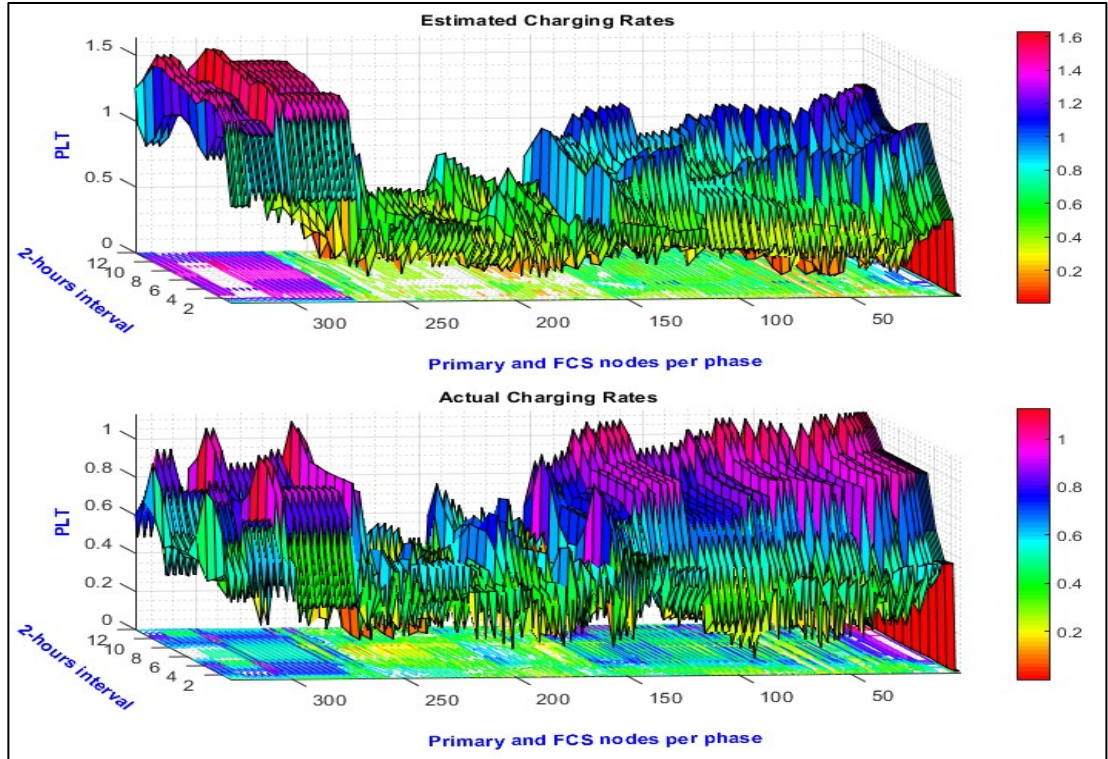


Figure 8.10 Percentile Long Term (PLT) Flicker Severity Index Corresponding to the First Scenario

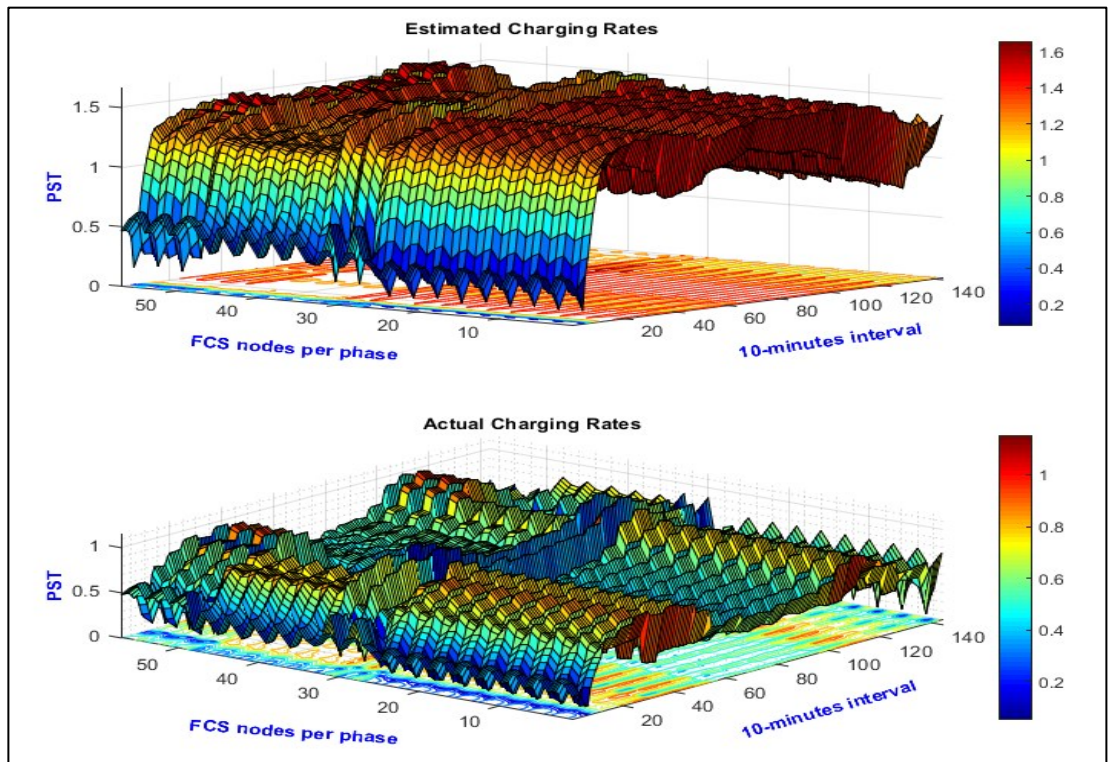


Figure 8.11 Percentile Short Term (PST) Flicker Severity Index Corresponding to the First Scenario

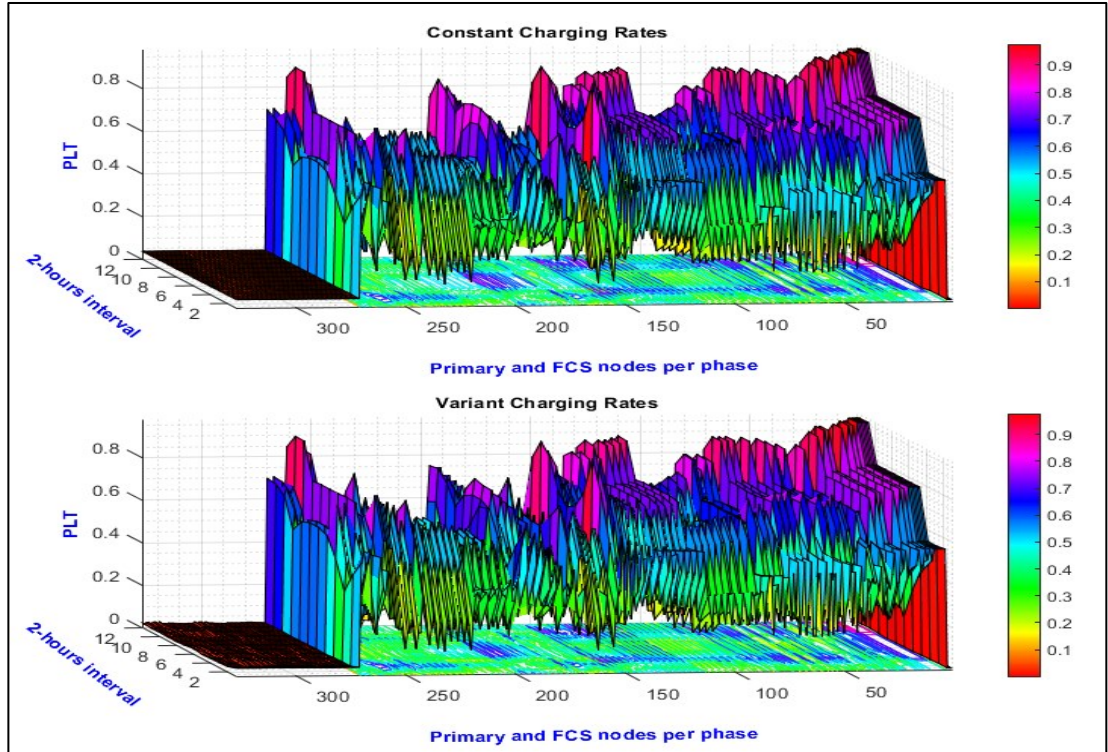


Figure 8.12 Percentile Long Term (PLT) Flicker Severity Index Corresponding to the Fourth Scenario

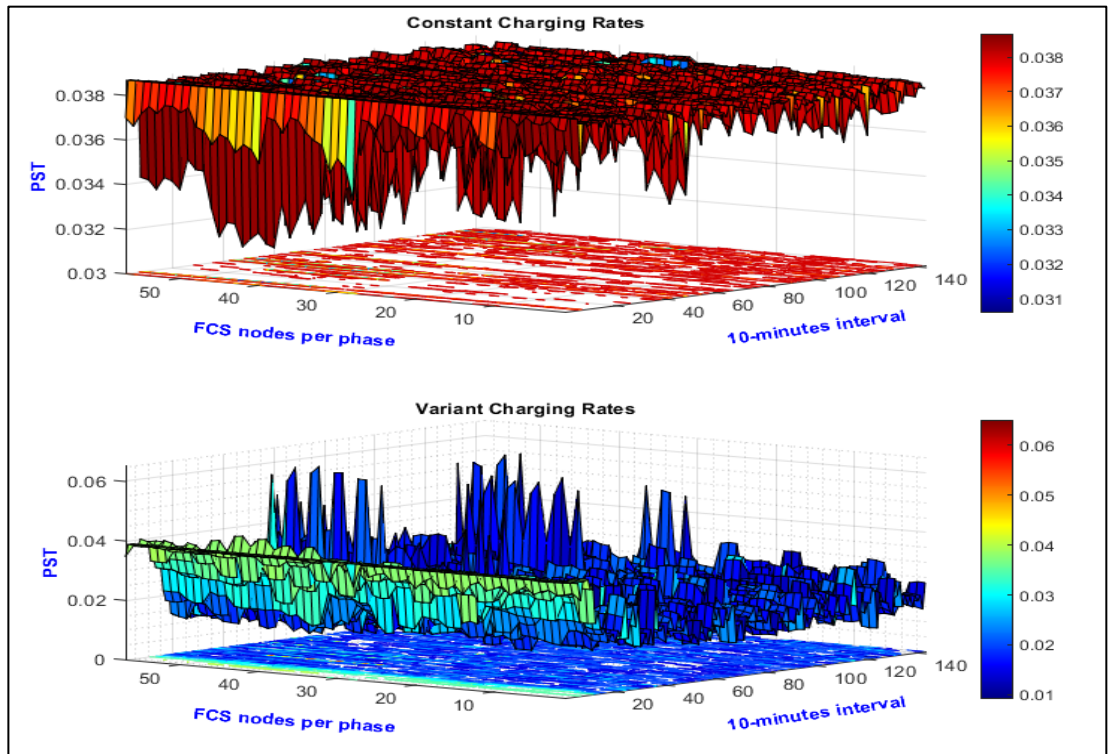


Figure 8.13 Percentile Short Term (PST) Flicker Severity Index Corresponding to the Fourth Scenario

The overall impacts of the first scenario, when only FCSs are connected on the system under study, are summarized in Figure 8.11 and 8.12. These figures depict the P_{LT} values for the primary and FCS nodes, and the P_{ST} values for the FCS nodes only, for two methods of charging. A visual inspection for these two figures shows that the values of P_{LT} and P_{ST} exceed their corresponding limits. The P_{LT} and P_{ST} values are increased at the substation and at the point of common coupling to which the FCSs are connected. In contrast, Figure 8.13 and 8.14 reveal an overview of the improvement caused by connecting the D-STATCOMs on the primary sides of the distribution transformers. The P_{LT} and P_{ST} values are extremely minimized at the point of common coupling as shown in Figure 8.13 and 8.14, respectively. The P_{ST} results in Figure 8.14 represent the values only for the nodes to which the FCSs are connected.

Chapter 9. A Novel Smart Charging Method Applied on Fast Charging Stations to Mitigate Voltage Fluctuation and Light Flicker

This chapter presents a novel smart charging approach utilized in fast charging stations to mitigate the impact of voltage fluctuation and light flicker. The results of the proposed smart charging are compared with results of the uncontrolled charging conducted in this chapter as well.

9.1 Input Data Required for Vehicle Charging Model

9.1.1 Number of PBEVs

The number of electric vehicles in the system, \mathcal{N}^{BPEV} , is determined as in (9.1). It is a function of number of houses in the system and number of vehicles in each house. As explained in section 8.2, a total of 750 residential homes are connected to 78 distribution transformers in the distribution system under study. It is assumed that there are two vehicles per house, as proposed in [93], resulting in a total of 1500 vehicles. A share of \mathcal{N}^{BPEV} requires charging their batteries using fast charging stations, as will be explained later.

$$\mathcal{N}^{BPEV} = x^{pen} \cdot n^{house} \cdot n^{car} \tag{9.1}$$

where,

\mathcal{N}^{BPEV}	Number of electric vehicles in the system
x^{pen}	Share of electric vehicles with respect to the total number of vehicles in the system, 10% - 50%
n^{house}	Number of residential houses in the system, 750 houses

n^{car} Number of vehicles per house, 2 vehicles/house

9.1.2 Types of PBEVs, their Shares and Charging Locations

Figure 9.1 shows shares and charging locations for three types of vehicles. PBEVs are classified based on their battery capacities μ into:

- PBEVs with small battery capacities, μ^s
- PBEVs with medium battery capacities, μ^m
- PBEVs with large battery capacities, μ^l .

Therefore, there is \mathcal{V}^s number of PBEVs in the system with small battery capacity μ^s . The battery capacity limit of each $v \in \mathcal{V}^s$ is:

$$\mu^s \leq 50 \text{ kwh} \quad 9.2$$

Also, there are \mathcal{V}^m and \mathcal{V}^l numbers of PBEVs with medium μ^m and μ^l large battery capacities in the system.

$$50 \text{ kwh} < \mu^m \leq 100 \text{ kwh} \quad 9.3$$

$$\mu^l > 100 \text{ kwh} \quad 9.4$$

Each vehicle v in the system can charge using home charger or FCS.

$$\mathcal{V}^s = \{\mathcal{V}_{FCS}^s \cup \mathcal{V}_{Home}^s\} \quad 9.5$$

$$\mathcal{V}^m = \{\mathcal{V}_{FCS}^m \cup \mathcal{V}_{Home}^m\} \quad 9.6$$

$$\mathcal{V}^l = \{\mathcal{V}_{FCS}^l \cup \mathcal{V}_{Home}^l\} \quad 9.7$$

$$\mathcal{V} = \{\mathcal{V}^s \cup \mathcal{V}^m \cup \mathcal{V}^l\} \quad 9.8$$

$$\mathcal{V}^{FCS} = \{\mathcal{V}_{FCS}^s, \mathcal{V}_{FCS}^m, \mathcal{V}_{FCS}^l\} \quad 9.9$$

Assumptions:

- Three different PBEVs are utilized in the system because of their high market shares representing more than 50% [210]. These vehicles are the Tesla Model S, Chevy Bolt, and Nissan Leaf.
- The Nissan Leaf is assumed to represent the group of PBEVs \mathcal{V}^s with large battery capacity, μ^s .
- The group of PBEVs \mathcal{V}^m with medium battery capacity μ^m is represented by the Chevy Bolt.
- The Tesla Model S is utilized to represent the group of PBEVs \mathcal{V}^l with large battery capacity, μ^l .

The aforementioned vehicles charge from home and public charging stations. It is assumed that all public charging stations in [211] are FCS. This seems to be a realistic assumption for the following reasons:

- As the battery price decreases, the battery capacity increases and thus it would not be sufficient (if there is a willingness and need) to charge the vehicle from slow charging stations.
- EVs market share is forecasted to be 50% by 2030 [231]. As the market share of PBEVs increases, public charging stations need to meet the share increased

by increasing the utilization rate; that is not achievable by assuming slow charging stations.

- Considering the value of charging time, especially for Ride-hailing EVs, commercial, and automated car-sharing EVs, FCSs are extremely important in reducing downtime due to charging.

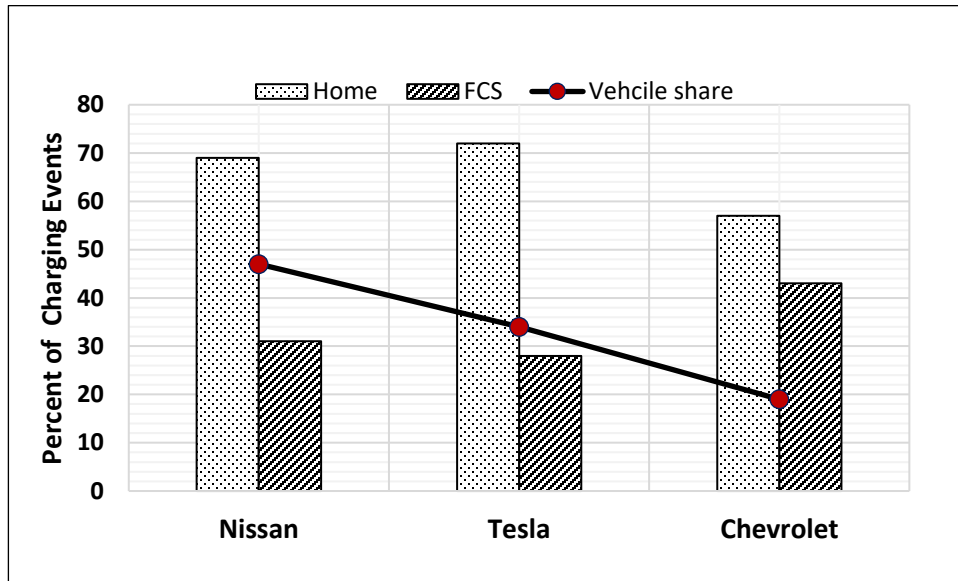


Figure 9.1 Charging Events by Locations [211]

9.1.3 PBEVs Arriving Rate at FCS

Figure 9.2 depicts a probability distribution of vehicle arrival rate and time at the FCS prior to charge [221]. The probability distribution in this figure is utilized to estimate the arrival rate according to their arrival time at the FCS by Markov Chain Monte Carlo simulation. The Birnbaum–Saunders distribution function is selected, as explained in section 7.5.1, to be the best distribution that fits the distribution shown in Figure 9.2. Markov Chain Monte Carlo is utilized to sample the selected distribution

as presented in Algorithm 7.4. The output of Algorithm 7.4 indicates to the hourly arrival rate at the FCS, which represents the start of charging at the FCS.

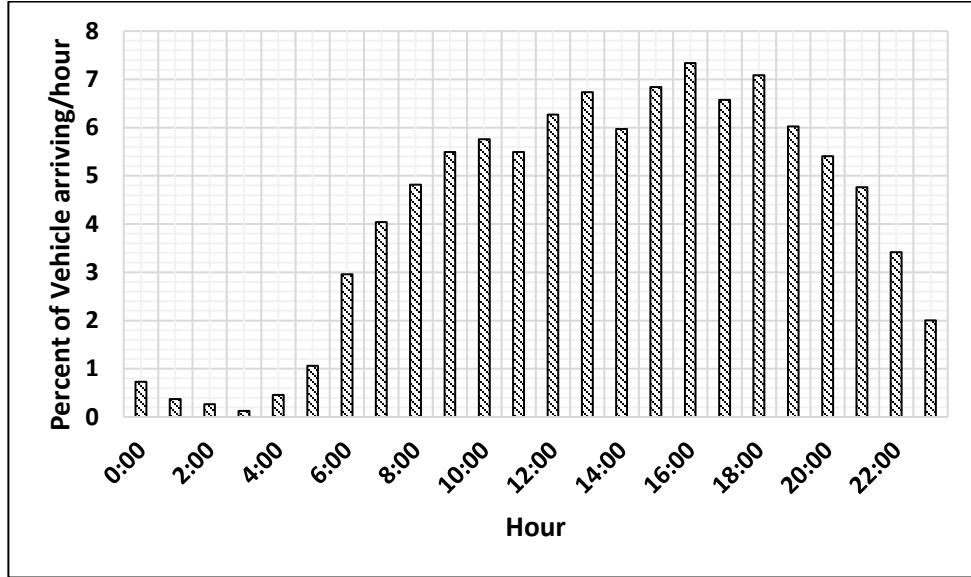


Figure 9.2 Percent of PBEVs arriving per hour at the fast charging station(Arrival rate) [221]

9.1.4 Level of Charged Batteries at the Starting of Charging from FCS

In Chapter 7, section 7.6.4, the daily distance traveled is utilized to estimate the level of charged batteries at the starting of charging from FCS. However, in this chapter, the level of charged batteries, when they arrive at the FCS, is determined based on probability distributions. Figure 9.3 and 9.4 shows the battery state of charge (soc) at the starting of charging events at two different locations: at home and away from home. Based on the assumptions stated in section 9.1.2, it is assumed charging events at away from home charging locations will occurred at FCS and thus their corresponding probability distributions represent the level of charged batteries at FCS.

The probability distributions from Figure 9.3 and 9.4 are averaged as in Figure 9.5 to depict the SOC level at the time of arrival at the FCS for the three types of vehicles mentioned in Section 9.1.2. It is not permitted for vehicles to charge from FCS more than 80% of their SOC [232], and thus Figure 9.5 shows the removed percent of charging events of 80% SOC and up.

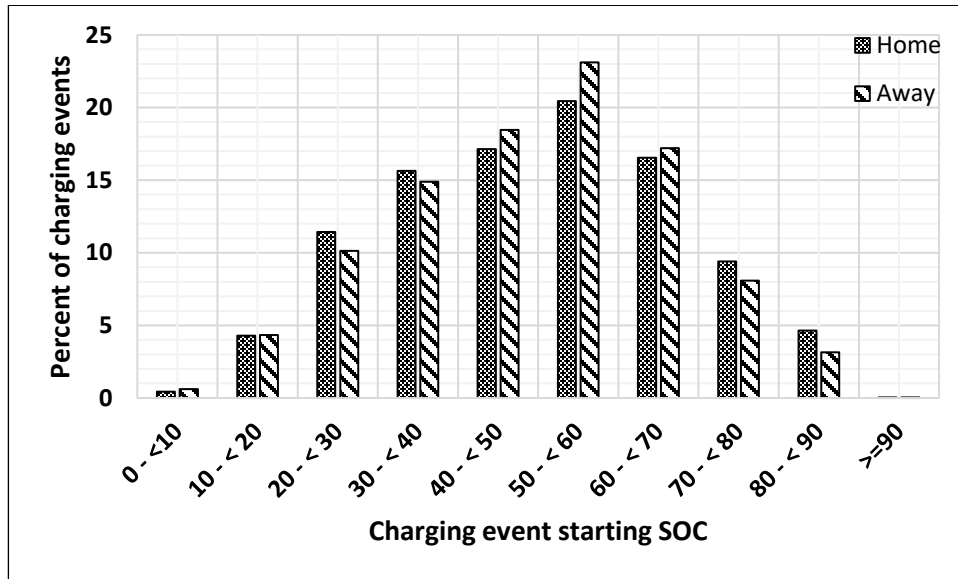


Figure 9.3 Nissan battery state of charge at the starting of charging events [233]

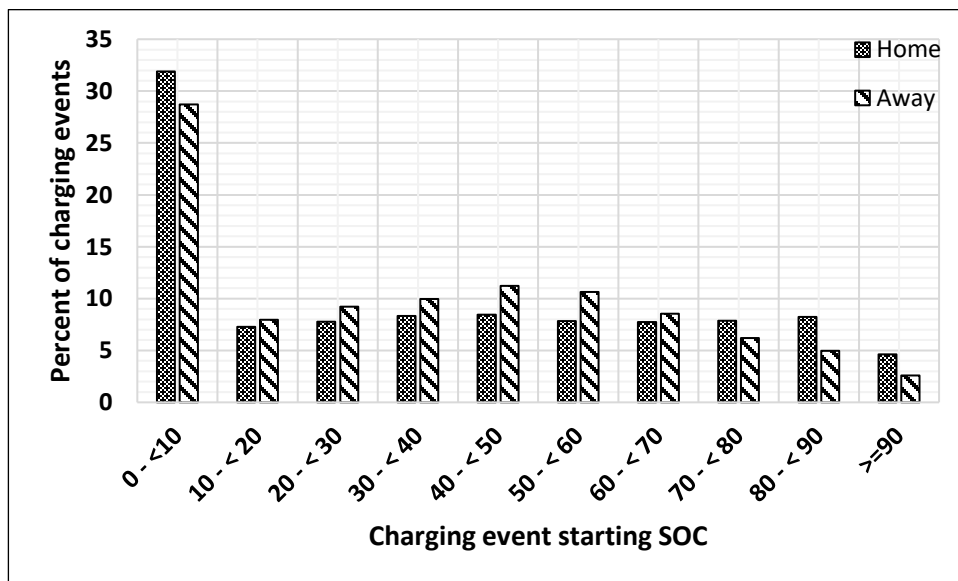


Figure 9.4 Chevrolet battery state of charge at the starting of charging events [233]

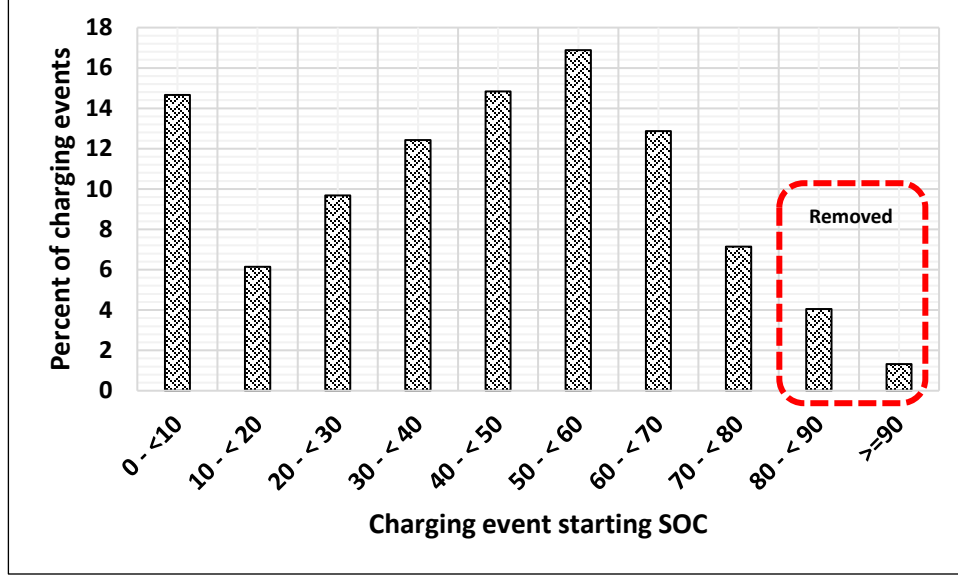


Figure 9.5 Average battery state of charge at the starting of charging events at FCS

9.2 Length of Time with PBEVs Drawing Power from FCS

At this point, types of vehicles are specified as well as their share and charging locations are determined (Figure 9.1), their arrival rate at the FCS (Figure 9.2), and their level of charged batteries when they arrive at the FCS are depicted (Figure 9.5). To determine the energy required from the FCS for each charging event, Figure 9.6 is utilized to estimate the length of time with a vehicle drawing power from the FCS. Given the length of the charging event, the rated power β of FCS, and the efficiency η^{FCS} of the charger, the energy required from the FCS is estimated linearly, as shown in Figure 9.7. Therefore, given length of time L^{FCS} in Figure 9.6, the kwh required kwh^{FCS} from the FCS in Figure 9.6 is generated as follows:

$$kwh^{FCS} = \left(\frac{L^{FCS}}{\frac{\mu^v}{\beta \cdot \eta^{FCS} \cdot \vartheta}} \right) \cdot \mu^v \quad 9.10$$

$$\mu^v := \begin{cases} \mu^s, & \text{if } v \in \mathcal{V}^s \\ \mu^m, & \text{if } v \in \mathcal{V}^m \\ \mu^l, & \text{if } v \in \mathcal{V}^l \end{cases} \quad 9.11$$

- kwh^{FCS} Energy required for vehicle v from FCS, kwh
- L^{FCS} Length of time with vehicle connected to the fast charger, minute
- μ^v Battery capacity of vehicle v , kwh
- η^{FCS} Efficiency of the fast charger, %
- ϑ Factor to convert hour into minutes

In Figure 9.7, the percentage increment of battery SOC is added to the initial battery SOC recorded at the time of arrival. The length of time is generated randomly by Monte Carlo Simulation to estimate the required energy from the grid. The minimum length of time with a vehicle drawing power from the FCS is assumed to be 5 minutes (Figure 9.6 for weekday (WD) and thus the minimum kwh required from the FCS per any charging event is 4 kwh (Figure 9.7).

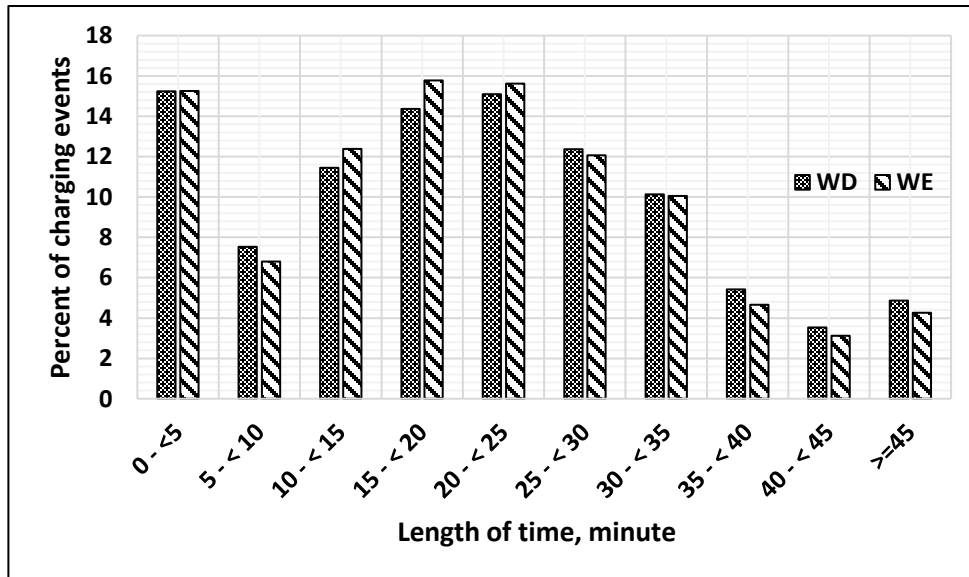


Figure 9.6 Distribution of Length of Time With a Vehicle Drawing Power From FCS per Charging Event [222]

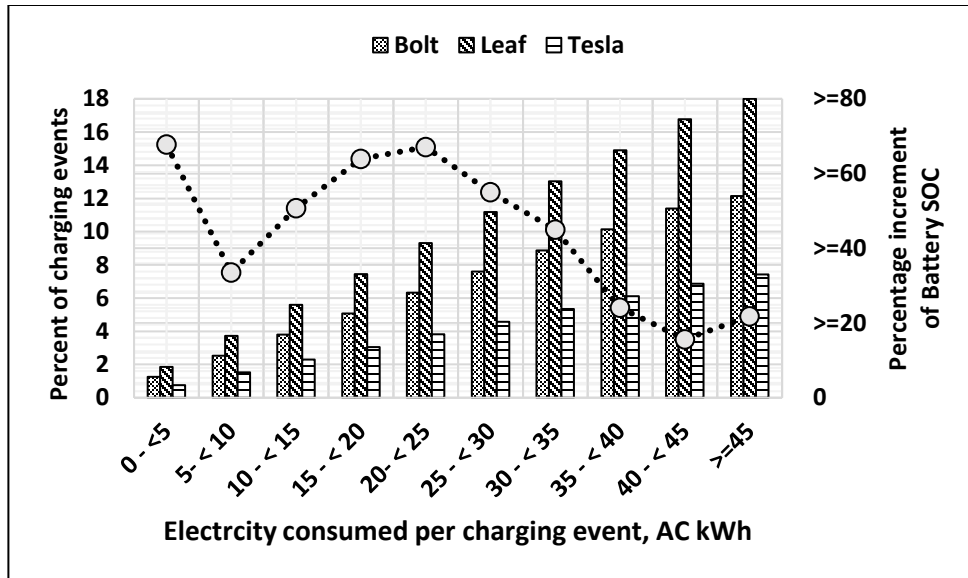


Figure 9.7 Battery State of Charge at End of Charging From FCS Prior to Driving

9.3 Length of Time with PBEVs Connected to FCS

At this point, the required energy from the FCS per charging event is determined (as in Figure 9.7) and thus the customer can be billed according to the consumed energy from the FCS. However, customers who use commercial charging station are billed based on the length of time the vehicle is connected to FCS, not the length of time the vehicle draws power from the FCS [234]. Therefore, Figure 9.8 is utilized to show if there is a variation in the length of time when a vehicle is connected to or drawing power from a fast charging station. Distribution of the length of time a vehicle is connected to FCS per charging event (Figure 9.8) is nearly identical to the distribution of the length of time a vehicle is drawing power from FCS, per charging event (Figure 9.6). It is assumed that the customer departs from the FCS when the vehicle is charged with the required energy. Therefore, the customer is billed in this work only based on the electricity consumed per charging event.

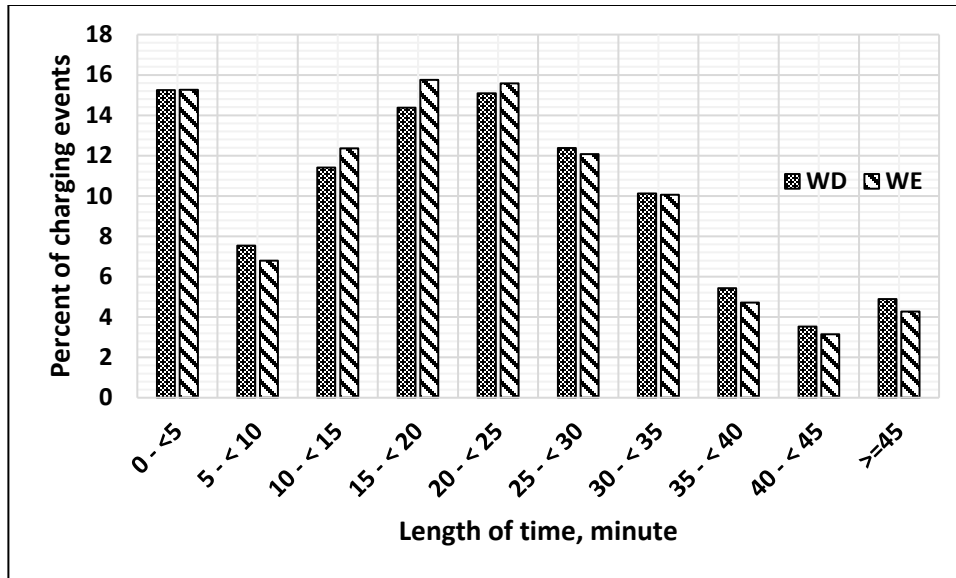


Figure 9.8 Distribution of length of time with a vehicle connected to FCS per charging event [222]

9.4 Charging Power

9.4.1 Uncontrolled Charging

The uncontrolled charging power β^u is equal to the maximum output power of the charger. In this case, when a vehicle arrives at the FCS, it charges using the maximum output power of the FCS and thus the charging duration is estimated accordingly.

$$\beta^u = \beta \quad 9.12$$

9.4.2 Smart (Controlled) Charging

In this case, FCS encompasses three charging powers:

1. Premium,
2. Regular, and
3. Economic.

Each port can provide any of these services (charging power).

Premium charging power: can provide an EV with an output power (β^p) ranging from \bar{p} % to \underline{p} % of the maximum output power β .

Regular charging power: can provide an EV with an output power (β^r) ranging from \bar{r} % to \underline{r} % of the maximum output power β .

Economic charging power: can provide an EV with an output power (β^e) ranging from \bar{e} % to \underline{e} % of the maximum output power β .

When a customer arrives at the FCS, a vehicle can be charged using any of the three available charging powers, which is determined randomly by the customer, based on a uniform random number. Once the charging power is determined, the vehicle will be charged using the selected power until the battery capacity reaches the required SOC. The costs of these charging powers are varied as well as their output powers, as will be explained in Chapter 10.

9.5 Case Study and Assumptions

We have three types of PBEVs, classified based on their battery capacities μ into:

1. Small battery capacity, i.e. Nissan Leaf ($\mu^s = 45.3 \text{ kwh}$),
2. Medium battery capacity, i.e. Chevrolet Bolt ($\mu^m = 66.6 \text{ kwh}$), and
3. Large battery capacity, i.e. Tesla Model S ($\mu^l = 110.5 \text{ kwh}$).

These EVs charged from the Fast Charging Station (FCS) where this FCS consists of \mathcal{L}^{ports} number of ports. Each port has similar maximum output power β . The

output of this FCS is $\mathcal{L}^{ports} \times \beta^{FCS}$. Therefore, the total output of the FCS at any instance of time can change from zero up to $\mathcal{L}^{ports} \times \beta^{FCS}$.

$$\beta^{FCS} := \begin{cases} \beta^u, & \text{if uncontrolled charging} \\ \beta^p, \beta^r, \beta^e, & \text{if smart charging} \end{cases} \quad 9.13$$

The objective is to maximize the output power of this FCS as follows:

$$OF = \sum_t^T (\beta_t^p \cdot \mathcal{N}_t^p + \beta_t^r \cdot \mathcal{N}_t^r + \beta_t^e \cdot \mathcal{N}_t^e) \quad 9.14$$

$$\begin{cases} \beta = \beta^p = \beta^r = \beta^e, & \text{if uncontrolled charging} \\ \beta \geq \beta^p > \beta^r > \beta^e, & \text{if smart charging} \end{cases} \quad 9.15$$

where,

β_t^p	Premium charging power, kw
β_t^r	Regular charging power, kw
β_t^e	Economic charging power, kw
\mathcal{N}_t^p	Number of PEV that charging using premium charging power at time t
\mathcal{N}_t^r	Number of PEV that charging using regular charging power at time t
\mathcal{N}_t^e	Number of PEV that charging using economic charging power at time t

9.6 Smart Charging Constraints

Charging power constraints are to specify limits of each charging power. Premium, regular, and economic charging powers are bounded as follows:

$$\underline{p} \cdot \beta \leq \beta_t^p \leq \bar{p} \cdot \beta \quad 9.16$$

$$\underline{r} \cdot \beta \leq \beta_t^r \leq \bar{r} \cdot \beta \quad 9.17$$

$$\underline{e} \cdot \beta \leq \beta_t^e \leq \bar{e} \cdot \beta \quad 9.18$$

Constrain (9.19) ensures that the drawing power from the FCS at any instance in time is not zero during the charging event, whereas (9.20) is to ensure that the maximum output power of the charger is not exceeded. Also, constrain (9.20) determines that the output of premium charging power is more than the output of regular charging power, which in turn is more than the output of the economic charging power.

$$\bar{p}, \underline{p}, \bar{r}, \underline{r}, \bar{e}, \underline{e} > 0 \quad 9.19$$

$$\bar{e} < \bar{r} < \bar{p} \leq 1 \quad 9.20$$

$$\underline{p} \leq \bar{p} \quad 9.21$$

$$\underline{r} \leq \bar{r} \quad 9.22$$

$$\underline{e} \leq \bar{e} \quad 9.23$$

Constraint (9.24) ensures that the output power of the FCS is limited to its capacity.

$$\mathcal{K} \leq \mathcal{L}^{ports} \times \beta \quad 9.24$$

where,

β	Maximum charging power per port, kw
\bar{p}	Factor to set the upper limits of premium charging power, %
\underline{p}	Factor to set the lower limits of premium charging power, %
\bar{r}	Factor to set the upper limits of regular charging power, %
\underline{r}	Factor to set the lower limits of regular charging power, %
\bar{e}	Factor to set the upper limits of economic charging power, %

\underline{e} Factor to set the lower limits of economic charging power, %

Constraints (9.25) to (9.27) determine the number of PBEVs and the required charging power according to vehicles' share. These constraints ensure that the share of vehicle charges from the FCS is not exceeded at any instance in time.

$$\mathcal{N}_t^p = \left(\eta^s \cdot \alpha_{t,s,p}^{t^{de}} + \eta^m \cdot \alpha_{t,m,p}^{t^{de}} + \eta^l \cdot \alpha_{t,l,p}^{t^{de}} \right) \cdot \mathcal{V}^{FCS}, \quad \text{if } t^{de} > t \quad 9.25$$

$$\mathcal{N}_t^r = \left(\eta^s \cdot \alpha_{t,s,r}^{t^{de}} + \eta^m \cdot \alpha_{t,m,r}^{t^{de}} + \eta^l \cdot \alpha_{t,l,r}^{t^{de}} \right) \cdot \mathcal{V}^{FCS}, \quad \text{if } t^{de} > t \quad 9.26$$

$$\mathcal{N}_t^e = \left(\eta^s \cdot \alpha_{t,s,e}^{t^{de}} + \eta^m \cdot \alpha_{t,m,e}^{t^{de}} + \eta^l \cdot \alpha_{t,l,e}^{t^{de}} \right) \cdot \mathcal{V}^{FCS}, \quad \text{if } t^{de} > t \quad 9.27$$

$$\mathcal{V}^{FCS} = \Lambda^{FCS} \cdot \mathcal{N}^{BPEV} \quad 9.28$$

where,

\mathcal{N}^{BPEV} Number of PBEV in the system

Λ^{FCS} Share of PBEV that uses FCS, *p. u.*

\mathcal{V}^{FCS} Number of vehicles charge from FCS

η^s Share of PBEV with small battery capacity *s* charges at the FCS at time *t*, *p. u.*

η^m Share of PBEV with medium battery capacity *m* charges at the FCS at time *t*, *p. u.*

η^l Share of PBEV with large battery capacity *l* charges at the FCS at time *t*, *p. u.*

$\alpha_{t,bc,p}^{de}$ Share of PBEV that have battery capacity *bc* charged using premium charging power at FCS at time *t* and required departure time of *de*, *p. u.*

$\alpha_{t,bc,r}^{de}$ Share of PBEV that have battery capacity *bc* charged using regular charging power at time *t* and required departure time of *de*, *p. u.*

$\alpha_{t,bc,e}^{de}$

Share of PBEV that have battery capacity bc charged using economic charging power at time t and required departure time of de , $p. u.$

Constraints (9.29) to (9.31) ensure that vehicles, i.e. with small, medium, or large battery capacities charge from the FCS according to their shares (η). Therefore, at any instance in time the total number of vehicles, with the same battery capacities (\mathcal{V}_{FCS}^s , \mathcal{V}_{FCS}^m , or \mathcal{V}_{FCS}^l), is not exceeded. Constraint (9.32) is to accommodate vehicles according to the fast charging station's capacity.

$$(\alpha_{t,s,p} + \alpha_{t,s,r} + \alpha_{t,s,e}) \cdot \eta^s \cdot \mathcal{V}^{FCS} \leq \mathcal{V}_{FCS}^s \quad 9.29$$

$$(\alpha_{t,m,p} + \alpha_{t,m,r} + \alpha_{t,m,e}) \cdot \eta^m \cdot \mathcal{V}^{FCS} \leq \mathcal{V}_{FCS}^m \quad 9.30$$

$$(\alpha_{t,l,p} + \alpha_{t,l,r} + \alpha_{t,l,e}) \cdot \eta^l \cdot \mathcal{V}^{FCS} \leq \mathcal{V}_{FCS}^l \quad 9.31$$

$$\mathcal{N}_t^p + \mathcal{N}_t^r + \mathcal{N}_t^e \leq \mathcal{L}^{ports} \quad 9.32$$

$$\mathcal{V}_{FCS,p}^v := \begin{cases} \alpha_{t,s,p} \cdot \eta^s \cdot \mathcal{V}^{FCS}, & \text{if } v \in \mathcal{V}_{FCS}^s \\ \alpha_{t,m,p} \cdot \eta^m \cdot \mathcal{V}^{FCS}, & \text{if } v \in \mathcal{V}_{FCS}^m \\ \alpha_{t,l,p} \cdot \eta^l \cdot \mathcal{V}^{FCS}, & \text{if } v \in \mathcal{V}_{FCS}^l \end{cases} \quad 9.33$$

$$\mathcal{V}_{FCS,r}^v := \begin{cases} \alpha_{t,s,r} \cdot \eta^s \cdot \mathcal{V}^{FCS}, & \text{if } v \in \mathcal{V}_{FCS}^s \\ \alpha_{t,m,r} \cdot \eta^m \cdot \mathcal{V}^{FCS}, & \text{if } v \in \mathcal{V}_{FCS}^m \\ \alpha_{t,l,r} \cdot \eta^l \cdot \mathcal{V}^{FCS}, & \text{if } v \in \mathcal{V}_{FCS}^l \end{cases} \quad 9.34$$

$$\mathcal{V}_{FCS,e}^v := \begin{cases} \alpha_{t,s,e} \cdot \eta^s \cdot \mathcal{V}^{FCS}, & \text{if } v \in \mathcal{V}_{FCS}^s \\ \alpha_{t,m,e} \cdot \eta^m \cdot \mathcal{V}^{FCS}, & \text{if } v \in \mathcal{V}_{FCS}^m \\ \alpha_{t,l,e} \cdot \eta^l \cdot \mathcal{V}^{FCS}, & \text{if } v \in \mathcal{V}_{FCS}^l \end{cases} \quad 9.35$$

where,

\mathcal{V}_{FCS}^s Number of PEV with small battery capacity uses the FCS

\mathcal{V}_{FCS}^m Number of PEV with medium battery capacity uses the FCS

\mathcal{V}_{FCS}^l	Number of PEV with large battery capacity uses the FCS
\mathcal{L}^{ports}	Number of ports in the fast charging station
$\mathcal{V}_{FCS,p}^v$	The set of PEV charging by premium power
$\mathcal{V}_{FCS,r}^v$	The set of PEV charging by regular power
$\mathcal{V}_{FCS,e}^v$	The set of PEV charging by economic power

At the time of arriving and plugging-in to the FCS, the SOC of each vehicle v charges from the FCS $v \in \Lambda^{FCS}$ is equal to soc_t^v , and thus while the vehicle remains in the FCS i.e., $t_v^{ar} < t \leq t_v^{de}$, the SOC is updated as follows:

$$soc_t^v := \begin{cases} \left(\frac{\mu^v \cdot soc_{t-1}^v + \frac{\beta_{t-1}^p}{\vartheta}}{\mu^v} \right) \cdot 100, & \text{if } v \in \mathcal{V}_{FCS,p}^v \\ \left(\frac{\mu^v \cdot soc_{t-1}^v + \frac{\beta_{t-1}^r}{\vartheta}}{\mu^v} \right) \cdot 100, & \text{if } v \in \mathcal{V}_{FCS,r}^v \\ \left(\frac{\mu^v \cdot soc_{t-1}^v + \frac{\beta_{t-1}^e}{\vartheta}}{\mu^v} \right) \cdot 100, & \text{if } v \in \mathcal{V}_{FCS,e}^v \end{cases} \quad 9.36$$

where,

soc_t^v	State-of-charge of vehicle v at time t , %
soc_{t-1}^v	State-of-charge of vehicle v at time $t - 1$, %
μ^v	Battery capacity of vehicle v , kwh
ϑ	Factor to convert hour into minutes

$$\mathcal{V}_{FCS,p}^v = \{ \mathcal{V}_{FCS,p}^s \cup \mathcal{V}_{FCS,p}^m \cup \mathcal{V}_{FCS,p}^l \} \quad 9.37$$

$$\mathcal{V}_{FCS,r}^v = \{ \mathcal{V}_{FCS,r}^s \cup \mathcal{V}_{FCS,r}^m \cup \mathcal{V}_{FCS,r}^l \} \quad 9.38$$

$$\mathcal{V}_{FCS,e}^v = \{\mathcal{V}_{FCS,e}^s \cup \mathcal{V}_{FCS,e}^m \cup \mathcal{V}_{FCS,e}^l\} \quad 9.39$$

where,

μ^s Capacity of small battery, *kwh*

μ^m Capacity of medium battery, *kwh*

μ^l Capacity of large battery, *kwh*

At the time of arriving at the FCS, the customer specifies the desired SOC soc_{des}^v

The desired SOC is bounded as in (9.40). The soc^{req} is determined as in (9.41) which represents here the minimum energy required from the FCS, according to the minimum length of time, $L^{FCS} = 5$ minutes (Figure 9.6), with a vehicle v drawing power from the FCS.

$$soc^{req} < soc_{des}^v \leq soc_{max}^v, \forall v \in \mathcal{V}^{FCS} \quad 9.40$$

$$soc^{req} := \begin{cases} \left(\frac{L^{FCS}}{\frac{\mu^v}{\beta_t^p \cdot \eta^{FCS}} \cdot \vartheta} \right) \cdot 100, \text{ if } v \in \mathcal{V}_{FCS,p}^v \\ \left(\frac{L^{FCS}}{\frac{\mu^v}{\beta_t^r \cdot \eta^{FCS}} \cdot \vartheta} \right) \cdot 100, \text{ if } v \in \mathcal{V}_{FCS,r}^v \\ \left(\frac{L^{FCS}}{\frac{\mu^v}{\beta_t^e \cdot \eta^{FCS}} \cdot \vartheta} \right) \cdot 100, \text{ if } v \in \mathcal{V}_{FCS,e}^v \end{cases} \quad 9.41$$

As the vehicle SOC is updated as in (9.36), the desired SOC is achieved. Upon achieving soc_{des}^v , vehicle v departs from the FCS. The departure time is determined as in (9.42).

$$t_v^{de} := \begin{cases} t + \mu^v \cdot \left(\frac{SOC_{des,p}^v - SOC_{t,p}^v}{\beta_t^p} \right) \cdot \vartheta, & \text{if } v \in \mathcal{V}_{FCS,p}^v \\ t + \mu^v \cdot \left(\frac{SOC_{des,r}^v - SOC_{t,r}^v}{\beta_t^r} \right) \cdot \vartheta, & \text{if } v \in \mathcal{V}_{FCS,pr}^v \\ t + \mu^v \cdot \left(\frac{SOC_{des,e}^v - SOC_{t,e}^v}{\beta_t^e} \right) \cdot \vartheta, & \text{if } v \in \mathcal{V}_{FCS,e}^v \end{cases} \quad 9.42$$

where,

$SOC_{des,p}^v$	Desired state-of-charge at the departure time t_v^{de} of vehicle v charging by premium power, %
$SOC_{des,r}^v$	Desired state-of-charge at the departure time t_v^{de} of vehicle v charging by regular power, %
$SOC_{des,e}^v$	Desired state-of-charge at the departure time t_v^{de} of vehicle v charging by economic power, %
$SOC_{t,p}^v$	State-of-charge of vehicle v charging by premium power at time t , %
$SOC_{t,r}^v$	State-of-charge of vehicle v charging by regular power at time t , %
$SOC_{t,e}^v$	State-of-charge of vehicle v charging by economic power at time t , %
t_v^{de}	The departure time of vehicle v

It is noted that the departure time (t_v^{de}) is inversely proportional to the FCS charging power, i.e., β_t^p , β_t^r , and β_t^e . When the charging output power increases, the required service time (charging duration) decreases and vice versa. Therefore, when we maximize the output power of the FCS (the objective function), it leads to a reduction in wait time for other customers in the queue to charge their vehicles. However, the aim of using the proposed smart charging in this study is to reduce the voltage fluctuation to the point that it does not make any light flicker. Although, controlling the charging power leads to a reduction in voltage fluctuation, the proposed smart

charging does not sacrifice the main characteristic of the charging station, which is the FCS's speed of charge.

9.7 Flicker Assessment and Relation to Output Power of Fast Charging Station

The flicker assessment approach proposed in this section is based on the assessment provided in [235], [236]. The approach relies on the following three steps [130]:

1. Determining the maximum relative voltage change, Γ , caused by the offending load [FCS],
2. Computing the corresponding flicker severity raised by that change,
3. Adding flicker severity from all fluctuating loads.

9.7.1 Relative Voltage Change Assessment

In this step, the percent ratio of the voltage change caused by the fluctuation load (FCS) to the point-of-common-coupling (PCC) nominal voltage is calculated as follows [235].

$$\Gamma = \frac{\Delta \mathcal{U}}{\mathcal{U}_{pcc}} \cdot 100\% \quad 9.43$$

where,

- Γ Relative voltage changes caused by FCS at point-of-common, %
- $\Delta \mathcal{U}$ Voltage variation at point-of-common coupling, kV
- \mathcal{U}_{pcc} Nominal voltage at point-of-common, kV

The voltage fluctuation $\Delta \mathcal{U}$ at the PCC of the FCS is approximated as follows [237]:

$$\Delta \mathcal{U} = \Delta I (r_{pcc} \cdot \cos(\theta) + \chi_{pcc} \cdot \sin(\theta)) \quad 9.44$$

The fluctuation in the FCS current is calculated as follows:

$$\Delta I = \frac{\Delta S}{\mathcal{U}_{pcc}} \quad 9.45$$

Therefore, the voltage fluctuation at the PCC is expressed as in (9.45).

$$\Delta \mathcal{U} = \frac{\Delta S (r_{pcc} \cdot \cos(\theta) + \chi_{pcc} \cdot \sin(\theta))}{\mathcal{U}_{pcc}} \quad 9.46$$

Given the power factor of the fluctuation load, active and reactive power variations ($\Delta \mathfrak{P}$ and $\Delta \mathfrak{Q}$) caused by the fluctuation load are calculated as follows:

$$\Delta \mathfrak{P} = \Delta S \cdot \cos(\theta) \quad 9.47$$

$$\Delta \mathfrak{Q} = \Delta S \cdot \sin(\theta) = \Delta \mathfrak{P} \cdot \tan(\theta) \quad 9.48$$

where,

ΔS	Apparent power variation at point-of-common coupling, <i>kVA</i>
$\Delta \mathfrak{P}$	Active power load change at point-of-common coupling, <i>kw</i>
$\Delta \mathfrak{Q}$	Reactive power load change at point-of-common coupling, <i>kVAr</i>
ΔI	Current load change at point-of-common coupling, <i>Amp</i>
θ	Network impedance angle, degree
χ_{pcc}	Network reactance at point-of-common, ohms
r_{pcc}	Network resistance at point-of-common, ohms

Therefore, $\Delta \mathfrak{P}$ represents the active power variations of the FCS; it varies from zero (all FCS ports are not utilized) to the maximum load \mathcal{K} (all ports are occupied).

Given that, the relative voltage change Γ is expressed in terms of the active power variations as follows:

$$\Gamma = \frac{\Delta U}{U_{pcc}} = \frac{\Delta \mathfrak{P} \cdot r_{pcc} + \Delta \mathfrak{P} \cdot \chi_{pcc} \cdot \tan(\theta)}{U_{pcc}^2} \cdot 100 \quad 9.49$$

9.7.2 Flicker Severity Caused by the FCS

Once the relative voltage fluctuation caused by the FCS is determined, the flicker severity at the PCC can be calculated based on the method provided in IEC 61000-3-3 [236]. This method relies on the flicker time \mathcal{F} and the flicker curve provided in IEC 610003-7 [235]. The flicker time \mathcal{F} is expressed as follows:

$$\mathcal{F} = \ell \cdot (\Gamma \cdot \varphi)^\gamma \quad 9.50$$

where,

\mathcal{F}	Flicker time represents the flicker impression of a single voltage change, second
φ	Factor represents the waveform shape of voltage fluctuation, rectangular change
ℓ	Factor to comply with the flicker curve (Figure 9.9)
γ	Coefficient to describe the source of disturbance

The short-term flicker severity p_{pcc}^{st} is obtained by adding all flicker times, \mathcal{F} , over 10-minute interval, ζ . The proposed assessment of the flicker severity caused by the FCS at the PCC is expressed as follows [130]:

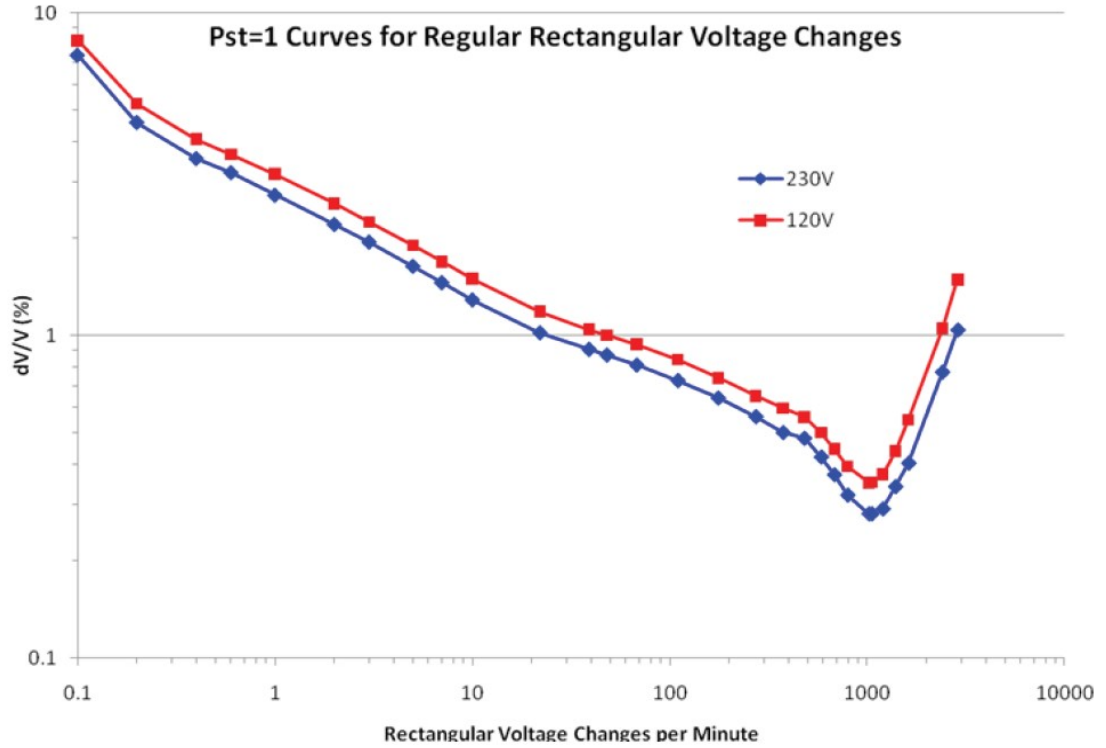


Figure 9.9 Flicker Curves for Incandescent Light [130]

$$p_{pcc}^{st} = \left(\frac{\sum_t^{t+\xi} \mathcal{F}}{\zeta} \right)^{\frac{1}{\gamma}} \quad 9.51$$

Given the number of voltage changes Ω caused by the FCS per minute, the short-term flicker severity is determined as follows:

$$p_{pcc}^{st} = \left(\frac{\xi \cdot \Omega \cdot \ell \cdot (\Gamma \cdot \varphi)^\gamma}{\zeta} \right)^{\frac{1}{\gamma}} \quad 9.52$$

where,

- ξ Summation of all flicker times, minute
- Ω Number of voltage dips per minute
- ζ Total time interval of all flicker times, second

Substituting the expression of Γ (equation (9.48)) into (9.51) relates the active power variations $\Delta \mathfrak{P}$, at PCC, with the flicker severity p_{pcc}^{st} . The limit of p_{pcc}^{st} , in the low voltage power system, is specified as a unity [116]. If that limit is not exceeded, the light flicker will not be observed. Therefore, the known limit of p_{pcc}^{st} , variations of the active power $\Delta \mathfrak{P}$ at PCC can be controlled to ensure it is not violating the limit of the flicker.

$$p_{pcc}^{st} = \left(\frac{\xi \cdot \Omega \cdot \ell \cdot \left(\frac{\Delta \mathfrak{P} \cdot (r_{pcc} + \chi_{pcc} \cdot \tan(\theta))}{U_{pcc}^2} \cdot 100 \cdot \varphi \right)^\gamma}{\zeta} \right)^{\frac{1}{\gamma}} \quad 9.53$$

From equation (9.23), variations of the active power at PCC is equal to FCS capacity.

$$\Delta \mathfrak{P} = \mathcal{K} \quad 9.54$$

Therefore, equation (9.52) can be rewritten in term of \mathcal{K} as follows:

$$\mathcal{K} = \left(\frac{\zeta \cdot p_{pcc}^{st}}{\xi \cdot \Omega \cdot \ell \cdot \left(\frac{(r_{pcc} + \chi_{pcc} \cdot \tan(\theta))}{U_{pcc}^2} \cdot 100 \cdot \varphi \right)^\gamma} \right)^{\frac{1}{\gamma}} \quad 9.55$$

Given the limit of short-term flicker severity, $p_{pcc}^{st} < 1$, equation (9.55) means that variation of the active power of the FCS at PCC will not lead to a noticeable light

flicker. Therefore, constraint (9.56) is imposed to maximize the output power of the FCS (objective function) while complying with the flicker severity limit.

$$\beta_t^p \cdot \mathcal{N}_t^p + \beta_t^r \cdot \mathcal{N}_t^r + \beta_t^e \cdot \mathcal{N}_t^e \leq \mathcal{K} \quad 9.56$$

9.8 Test System

The distribution system under study consists of 123 buses and operates at nominal voltage of 4.16 kV [224]. The main feeder is emanated from the substation radially and is fed by a three-phase transformer bank of 5 MVA at the substation. Two different charging methods, namely uncontrolled charging and smart charging are performed to evaluate their impacts on voltage fluctuation and light flicker. In each charging method, five case studies are considered whereas in each case a subset of all PBEVs in the system needs to charge from the FCS. In each case, the subset penetration is increased from 10% to 50%, by 10%.

9.9 Case Study

Case-1: Uncontrolled charging

In this case, when vehicles arrive at the FCS, they charge using the maximum rated power of the charger. Therefore, there is no control on the output power of the charger. A daily charging profile is generated accordingly. This profile represents the demand of the FCS on the distribution system under study. Given that, the flicker severity is assessed as in equation (9.54).

Case -2: Smart charging

In this case, a control is applied on the output power of the FCS. Therefore, three smart (controlled) charging powers are available at the FCS, namely premium, regular, and economic power. Constraint (9.55) is imposed in this case to generate the daily charging profile, which was generated, as explained in section 9.4. The generated profile, as per the proposed smart charging method, represents the demand of the FCS on the system under study. As explained before, this profile is affixed to the PCC to which the FCS is connected, and thus utilized to estimate the flicker severity, as in equation (9.54).

The following are assumptions related to flicker assessment, whether in case of smart charging or uncontrolled charging:

β is the maximum output power of the charger, 50 kw.

\mathcal{L}^{ports} is assumed to be 4,

p_{pcc}^{st} is assumed to be 1,

φ is assumed to be 1,

ℓ is a factor considered to be 2.3,

γ is an exponent assumed to be 3.2,

ξ is considered to be 10 minutes, and

ζ is considered to be 600 seconds.

The flicker severity in equation (9.52) is affected by number of voltage dips per minutes (Ω). The dips per minute is a function of the status of the chargers. When a

fast charger is activated (ON), it charges the vehicle with an output power of β^{FCS} kw. When the charger is deactivated (OFF), the output power goes to zero kw. In the ON/OFF status of the charger, the voltage at the PCC dips and deviates (ΔU). The dips per minute is affected by the penetration of PBEVs charging from the FCS. When the penetration is increased, the dips per minute is increased, and vice versa. Therefore, different FCS penetrations (10%, 20%, 30%, 40, and 50%) have been considered. In each penetration, the dips per minute is determined and the flicker severity in (9.54) is calculated accordingly. The penetration of vehicles charging from the FCS, Λ^{FCS} , is a function of the total PBEVs in the system, \mathcal{N}^{PBEV} , which in turn is a function of the number of houses, i.e. 750 houses, two vehicle per house [93]. Vehicles, that charge from the FCS, arrive there according to the distribution shown in Figure 9.2. The highest rate of arrival at the FCS, as presented in Figure 9.2, occurs at 4:00 p.m., $> 7\%$. This means that more than 7% of all vehicles charge from the FCS at 4:00 p.m. Given the arrival rate at the FCS at 4:00 p.m., the penetration of vehicles charges from the FCS, and the number of PBEVs in the system, the dips per minute are determined accordingly, as shown in Table 9-1.

If using the FCS contributes to light flicker, the light flicker mostly occurs at the hour that has highest arrival rate (at 4:00 p.m.), and thus at this hour the flicker severity index is at its highest value. If the smart charging is able to mitigate the flicker severity at that hour (4:00 p.m.), it implies that the flicker severity during the rest of the day is reduced by the proposed smart charging (according to the arrival rates and times in Figure 9.2). Therefore, the FCS flicker severity at 4:00 p.m. is evaluated by

both the proposed smart charging and the uncontrolled charging methods. Results of the evaluation are presented below.

Table 9-1 Number of PBEVs Charging Via Fast Charging Station

Penetration Level (Increase of Λ^{FCS})	Number of PBEVs in the System (\mathcal{N}^{PBEV})	Number of PBEVs Use FCS (Λ^{FCS})		Dips per minute (Ω)
		in 24 Hours	at 4:00 p.m.	
10%	150	51	4	0.14
20%	300	102	8	0.28
30%	450	153	12	0.42
40%	600	204	16	0.56
50%	750	255	20	0.7

9.9.1 Results and Discussions

In this section, the voltage fluctuation is assessed, and the resultant flicker severity is presented when vehicles are charged from the FCS using the uncontrolled and proposed smart charging methods. Figure 9.10 shows the daily charging demand on the FCS. Figure 9.10 encompasses three groups of vehicles, according to the used charging power. These groups charge from the FCS using the premium, regular, and economic charging power (as shown in the y-axis titles). Each horizontal bar in Figure 9.10 represents the charging duration of a vehicle using that charging power mentioned in y-axis. The total number of horizontal bars show the total number of vehicles charge from the FCS in that day. In the case of uncontrolled charging power, all vehicles in Figure 9.10 charge using the same charging power (β^u) and thus the charging durations are changed accordingly (not shown in Figure 9.10). When the penetration of vehicles charge from the FCS is increased, the number of horizontal bars, in Figure 9.10, is increased which, in turn, increases the daily voltage dips because of the on/off status of the chargers. Figure 9.11 depicts the comparison of

flicker severity for both methods of charging. The x-axis shows different penetration levels which represent the increased demand of vehicles on the FCS at the same hour of the day, i.e. at 4:00 p.m. The flicker severity values are depicted in the y-axis in Figure 9.11. A light flicker is observed if the flicker severity exceeds 1. It is noted from Figure 9.11 that as the penetration level is increased, the flicker index is increased. When the FCS charges vehicles by the uncontrolled charging method, the FCS violates the flicker tolerance especially when the demand on its service is increased by 20% and beyond. In contrast, the flicker limit was not violated when vehicles charge from the FCS, as per the proposed smart charging approach, even though when the penetration on the FCS is increased by 50%. Therefore, the proposed smart charging approach clearly shows that it is effective not only in mitigating the voltage fluctuations and light flicker, but also in reducing the flicker severity even when the FCS voltage dip per minute is increased five times.

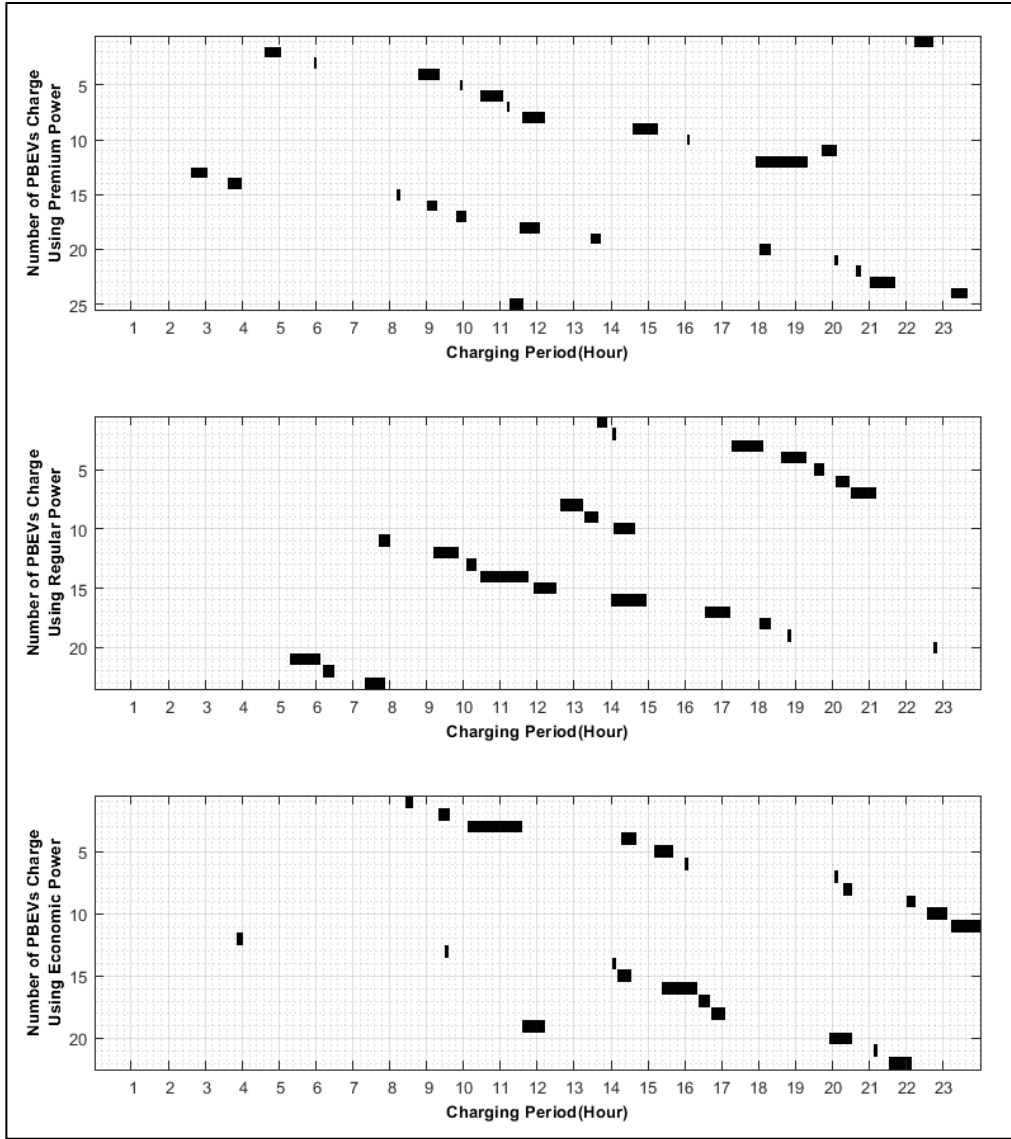


Figure 9.10 Daily Demand per each Charging Power in FCS

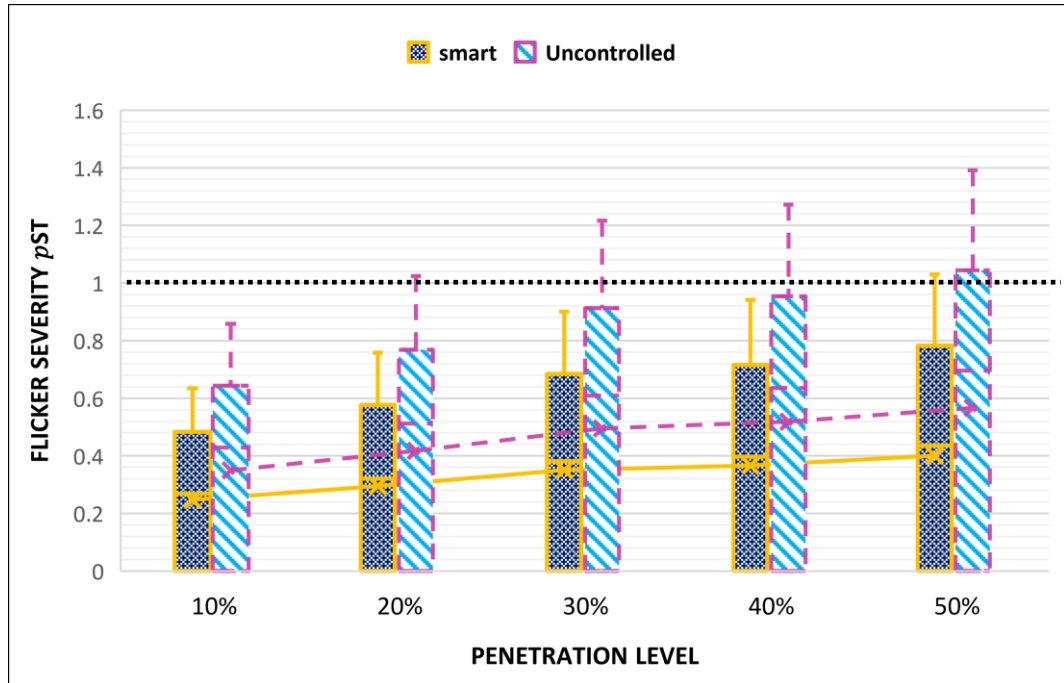


Figure 9.11 Comparison of Flicker Level for the Uncontrolled and Proposed Smart Charging

9.9.2 Effect of Full Charging of the Batteries on Flicker Severity

In the previous section, the reported results assume that vehicles start their first trip from home with different states-of-charge, as shown in Figure 7.6. Most of these vehicles start the trip with almost fully charged batteries (i.e. > 90%). The reported results assume that vehicles are charged at night and then in the morning vehicles start the trip with different states-of-charge, as shown in Figure 7.6. Before they arrive home, a share of these vehicles requires a charge from the FCS, according to Figure 9.1, and arrived at the FCS with different states-of-charges distributed as in Figure 9.5, at different arrival rate as in Figure 9.2.

There is no direct effect of fully charging the battery on the flicker severity index. Equation 9.52 shows factors that affect the flicker severity. The flicker severity is affected mainly by dips per unit time. The dip is a function of the on/off states of the

fast charger. When penetration of PBEVs that use the FCS is increased, the dips per unit time is increased as well. The question is what would motivate a customer to pay for charging via the fast charger while he/she has a home charger; the battery capacity is large; the daily round trip to/from home is within the battery driving range.

The willingness to pay for charging is driven by the value of charging time or the opportune cost of charging; that is in turn varied according to segment of the market and consumers [238]. For personal use and privately-owned electric vehicles, most charging events are performed by home or work chargers where the vehicle is parked for a long time. During that period of time, the value of charging time is low and thus home or work chargers characterized as slow chargers are convenient. However, for shared privately-owned ride hailing or commercial automated ride-hailing electric vehicles, the value of charge time is high, especially on-shift charging [238]. Electric vehicles in this sector drive 29% more daily miles, require two times more charging power, and utilize fast chargers three times more, than personal-use vehicles, as reported in [239]. As free-floating car-sharing is adopted, the dependency on the FCS is increased to reduce downtime due to charging and, thus, the dips per unit time is expected to increase because of increasing FCS daily usage.

9.9.3 Effect of Envelope of Flickers

In this section, the flicker severity is investigated when the daily usage of the FCS is increased considering the proposed smart charging method. Results of flicker severity are depicted in Figure 9.12.

Although the penetration of vehicles charge from FCS in Figure 9.12 is like their penetration in Figure 9.11, they are different in that shares of vehicles (25%, 50%, and 75%) per penetration level in Figure 9.12 charges from the FCS three times a day, to imitate the charging pattern of shared electric vehicles. Therefore, according to the arrival rate presented in Figure 9.2, the highest rate of vehicles arriving at the FCS is at 4:00 p.m. The dips per hour in Figure 9.12 is three times more than that in Figure 9.11. The idea is to show the ability of the proposed smart charging method to reduce the flicker level if daily usage of the FCS per vehicle is increased.

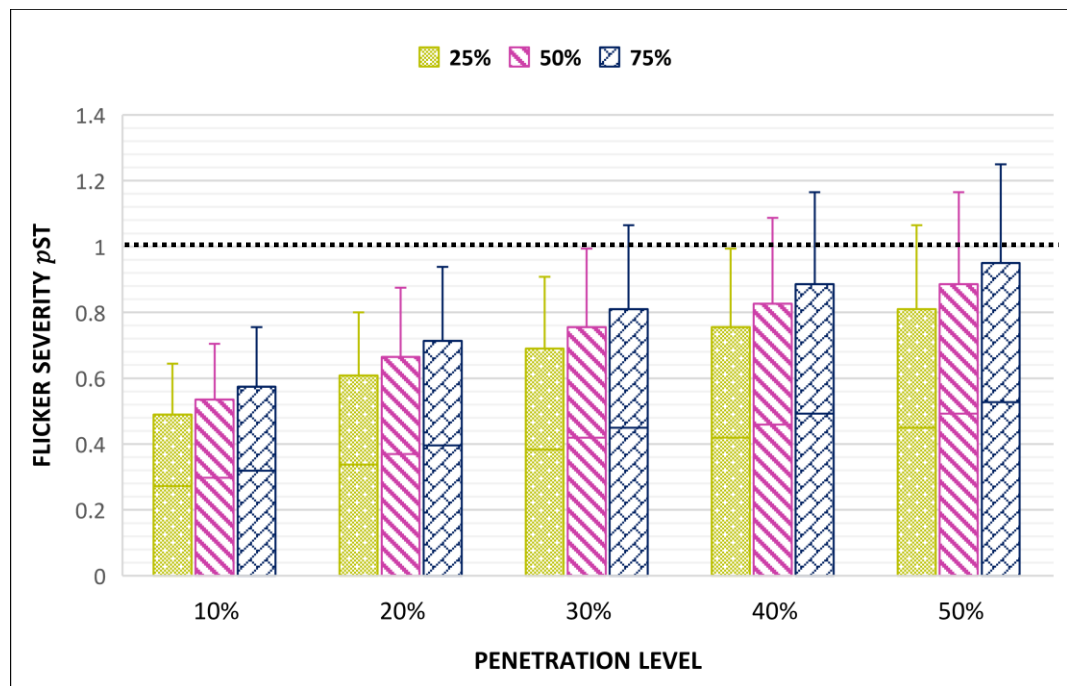


Figure 9.12 Flicker Level when the Penetration on the Proposed Smart Charging increases

Results in Figure 9.12 show that the proposed smart charging can mitigate the flicker level, even if the penetration of vehicles charge from the FCS is increased up to 20% and 75% and these vehicles charge from FCS three times a day. When the share of vehicles that charge from FCS three times a day, is reduced to 25%, the proposed

smart charging is able to reduce the flicker, even if the penetration of vehicles charging from FSC is increased to 40%. Beyond this penetration and daily utilization rates, the flicker limit is exceeded.

9.9.4 Effect of Smart Charging on Charging Duration

Figure 9.13 presents the required charging time to charge vehicles with different battery capacities (explained in section 9.4) via a 50kw fast charger. The charging duration for each vehicle is calculated when its battery SOC is changed from 20% to 80% using the uncontrolled and the proposed smart charging methods.

As the output power of the charger is increased, the time it takes to charge the vehicle's battery is decreased. The uncontrolled charging provides the highest output power and thus it requires less time to charge the battery SOC from 20% to 80% in comparison to the economic and regular charging methods, as depicted in Figure 9.13. However, when the station encompasses multiple fast chargers and their operations are uncontrolled, a voltage fluctuation may occur, which, in turn, may cause exceeding the limit of light flicker.

In contrast, the limit of the light flicker will not be violated when the proposed smart charging is utilized, as shown in section 9.9. However, the time it takes vehicles to charge their batteries the same amount of energy using the smart charging (economic or regular) is more than what it takes to charge by the uncontrolled charging.

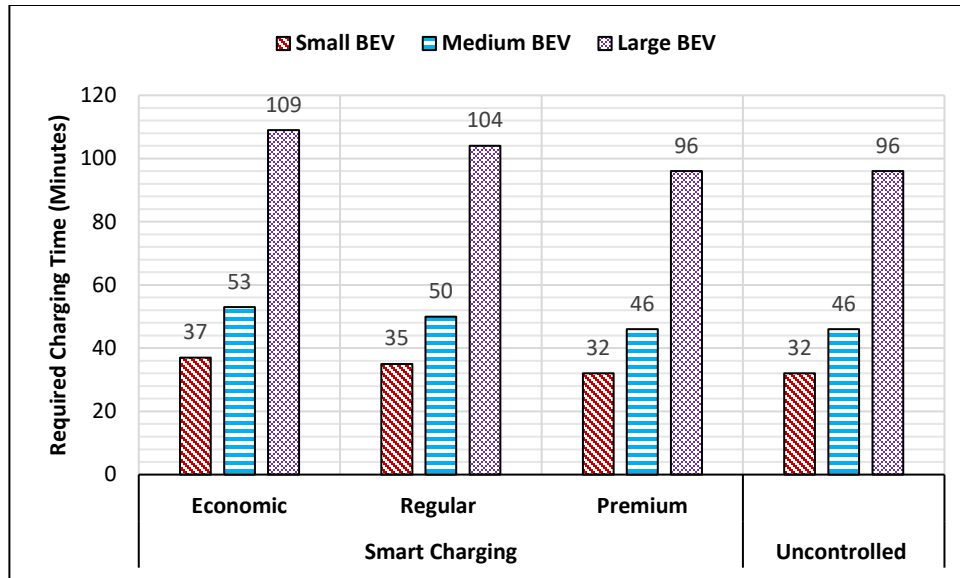


Figure 9.13 Charging Duration to Increase Battery SOC from 20% to 80% using the Smart and Uncontrolled Charging

Therefore, in order to make customers adopt smart charging method, the FCS operator/investor must offer a compromised solution that meets the regulation of the service provider and the needs of customers. The proposed compromise solution in this study is explained in Chapter 10.

9.10 A comparative study

In this section, a comparison study is conducted among the proposed method and other studies existing in the literature. The comparison is conducted according to three aspects: the charging power, the smart charging approach, and the reported flicker value. The previous work can be classified broadly into four groups: the first group considers uncontrolled and/or smart charging via a slow charging station (i.e., home charger). The second group applies the uncontrolled and/or smart charging but via a fast charger (i.e., fast charging station). Neither of these two groups study the impact of the charging station on the voltage fluctuation and light flicker. The third

group analyzes the impact of the voltage fluctuation on the light flicker whereas the fourth group of studies addresses and mitigates the light flicker. The source of the flicker in the last two groups is not the charging stations, it is caused by conventional loads such as arc furnace and rolling mill. The proposed method in this study addresses the impact of the fast charging station on voltage fluctuation and light flicker, and mitigates that impact using a novel smart charging approach that has not been utilized previously, to the best of the author’s knowledge. Table 9-2 presents a comparison of the proposed method in this thesis and other studies existing in literature. Table 9-3 illustrates impacts of charging electric vehicles according to the method and type on electricity systems, as per the previous work as well as the proposed smart charging method.

Table 9-2 Comparison of the Previous Work and Proposed Method According to their charging Type and Effect on Light Flicker

Reference	Charging power		Charging type		Flicker	
	Slow	Fast	Uncontrolled	Smart	Analysis	Mitigation
[90], [91], [93], [240]	✓	✗	✗	✓	✗	✗
[220]	✓	✗	✓	✓	✗	✗
[241]	✗	✓	✓	✗	✗	✗
[92]	✓	✓	✗	✓	✗	✗
[242]	✗	✓	✓	✓	✗	✗
[243], [244], [245]	✗	✗	✗	✗	✓	✓
[237],[246], [247], [248], [249]	✗	✗	✗	✗	✓	✗
[250]	✓	✗	✗	✓	✗	✗
Proposed Smart Charging	✗	✓	✓	✓	✓	✓

✓ : Considered, ✗ : Not considered

Table 9-3 Impact of Charging Method and Type [251]

	Slow charging		Fast charging		
	uncontrolled	Smart charging	uncontrolled	with battery	smart charging
Electricity demand	+	+	+	+	+
Peak demand	++	+	++	+	+
Distribution grids	++	+	++	+	+
Light flicker	✗	✗	✓	✓	✗

✗ : Not exceed the limit, ✓ : Exceed the limit, + : affected, ++ : affected more

The concept of smart charging currently in the literature is listed in Figure 9.14. It encompasses different levels of control over the charging process, aiming to support the power system by achieving different objectives, as shown in Figure 9.14. The proposed smart charging in this study targets the future smart grid. It assumes that the same port (nozzle) of the fast charger is able to provide three different charging powers, namely economic, regular, and premium. The rate of charging in each charging power is defined by the FCS operator/investor and can be changed within the day according to different variables such as on-/off- peak hours and the local level of the produced renewable energy. Unlike smart charging in the previous work, customers can select the charging power in the proposed smart charging according to their priority. At the time of arrival at the FCS, if time is most important for a customer, the premium charging power can be selected. In contrast, if a customer prioritizes cost, regular or economic charging power can be utilized. Therefore, the proposed smart charging method provides less control than those currently in the literature. Also, the proposed charging method opens the door for market competition among different fast charging providers to offer competitive rate of charging as well as competitive price for each charging power.

Table 9.4 presents a comparison of flicker values as reported in the previous work as well as the current study. Unlike the uncontrolled charging, the proposed smart charging is able to reduce the light flicker and makes the FCS increase its rate of utilization without exceeding the standard limit of flicker. It is to be noted that the flicker values shown in Table 9.4 represent the short-term flicker severity index.

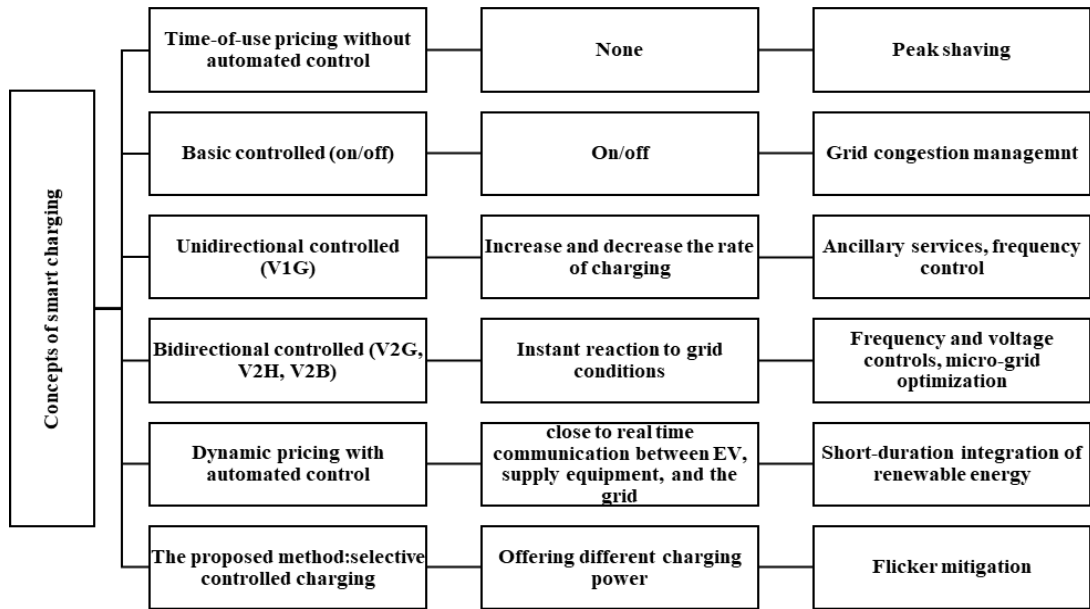


Figure 9.14 Comparison of Smart Charging and services provided to the Grid [252]

Table 9-4 Comparison of the Previous Work and Proposed Method According to Flicker Level

	Reference	Reported flicker value
Previous work	[248]	2
	[247]	1.7
	[253]	1.05
	[254]	1.4
	[255]	1.26
	[249]	2.78
	[99]	2.6
Current study	Uncontrolled FCS, at 10% up to 40% of FCS utilization rate	0.9-1.3
	FCS with energy storage system	1.3
	FCS with DSTATCOM	0.79
	FCS with Smart charging, at 10% up to 40% of FCS utilization rate	0.6-0.9

Chapter 10.A Novel Cost Model for Adopting the Smart Charging at the Fast Charging Station

The proposed smart charging was explained in detail in Chapter 9. It was shown that the proposed smart charging is effective in regulating the voltage fluctuation and minimizing the light flicker. However, the cost of the flicker minimization was not clear. In this chapter, a novel cost model is developed assuming that the smart charging is operating with fairness policy that is (from the viewpoint of FCS operator) the value of cost for any customer at the FCS is equivalent to his/her value of time. Therefore, the cost of the proposed smart charging is determined and utilized to be compared with the cost of other flicker mitigation devices explained in Chapter 4.

10.1 Cost of Premium, Regular, and Economic Charging power

10.1.1 Determining the Per Unit Time of the Smart Charging

In Ontario, when a vehicle charges via a fast charger, the service is offered based on a fixed amount per hour, but the customer is billed by the minute, according to [256]. In order to determine the cost of any charging power proposed in this study, i.e. premium, regular, or economic, it is required to determine first the time the charging power takes to charge 1kwh in the battery. Then, that cost (\$/1kwh) is multiplying by the total energy transferred (kwh).

When the customer arrives at the FCS, two parameters are shared with the FCS: the initial and the required battery SOC. Therefore, given the required battery SOC and the relation of 1kwh per minute, the total kwh required from the FCS can be

calculated, and then the required time is determined. The required time to charge 1kwh is inversely proportional to rate of the charging power. As the rated power increases, the time required to charge 1kwh decreases, and vice versa. The times it takes to charge 1kwh by premium, regular, and economic power are given as follows:

$$\mathcal{T}^p = \frac{1 \cdot \vartheta}{\beta^p} \quad 10.1$$

$$\mathcal{T}^r = \frac{1 \cdot \vartheta}{\beta^r} \quad 10.2$$

$$\mathcal{T}^e = \frac{1 \cdot \vartheta}{\beta^e} \quad 10.3$$

Where,

\mathcal{T}^p The time it takes to charge 1kwh by premium power, (*min./kwh*)

\mathcal{T}^r The time it takes to charge 1kwh by regular power, (*min./kwh*)

\mathcal{T}^e The time it takes to charge 1kwh by economic power, (*min./kwh*)

β^p Premium charging power, kw

β^r Regular charging power, kw

β^e Economic charging power, kw

ϑ Factor to convert hour into minutes

10.1.2 Determining the Per Unit Cost of the Smart Charging

After the required time to charge 1kwh per minute is found, the per unit cost can be modeled as follows:

$$\Gamma^p = \mathcal{C} \cdot \mathcal{T}^p \quad 10.4$$

$$\Gamma^r = \Gamma^p \cdot \frac{\mathcal{T}^p}{\mathcal{T}^r} \quad 10.5$$

$$\Gamma^e = \Gamma^p \cdot \frac{\mathcal{T}^p}{\mathcal{T}^e} \quad 10.6$$

$$\mathcal{C} = \frac{\mathfrak{h}}{\vartheta} \quad 10.7$$

Where,

Γ^p	The per unit cost of the premium charging, (\$/kwh)
Γ^r	The per unit cost of the regular charging, (\$/kwh)
Γ^e	The per unit cost of the economic charging, (\$/kwh)
ϑ	Factor to convert hour into minutes
\mathfrak{h}	The per hour PBEV Fast charging cost, (\$/h)
\mathcal{C}	The per minutes PBEV Fast charging cost, (\$/min.)

10.1.3 The Per Unit Cost of The Premium Charging Power

In equation (10.4), the per unit cost for the premium charging power (Γ^p) is a function of two factors: the premium charging power (β^p), where ($\Gamma^p = \mathcal{C} \cdot \mathcal{T}^p = \frac{\mathcal{C} \cdot \vartheta}{\beta^p}$), and the per hour charging cost (\mathcal{C}). β^p does not change and represents the maximum rated power available in the charger. Charging the battery using the maximum rated power will minimize the duration of the charge, which, in turn, saves the customer time. The other factor is the per hour charging cost which may change during the day (on- and off- peaks). When the per hour charging cost increases, the per unit cost of the premium charging power increases as well, and vice versa. The main advantage of using premium charging power is to get the maximum charging

rate and reduce the charging duration but at the highest cost, as explained in equation (10.1).

10.1.4 The Per Unit Cost of The Regular Charging Power

The per unit cost of the regular charging power (Γ^r) is modeled as in equation (10.5). Γ^r will not utilize the maximum charging rate which adversely increases the charging duration. The per unit regular charging cost is a function of two factors: the per unit cost of premium charging power (Γ^p) and a scaling factor ($\frac{\mathcal{T}^p}{\mathcal{T}^r}$). The scaling factor represents a rebate offered to the customer to adopt the regular charging power. The rebate is designed to compensate the increase in the charging duration by reducing the per unit regular charging cost. The per unit time of the premium power (\mathcal{T}^p) is less than the per unit time of the regular power (\mathcal{T}^r). Thus, the scaling factor ($\frac{\mathcal{T}^p}{\mathcal{T}^r}$) will scale down the per unit cost of the premium power (Γ^p) in equation (10.5) which in turn will reduce the per unit cost of the regular charging power (Γ^r). When the premium charging power is utilized, the customer will save time but not money. In contrast, when the regular charging power is utilized, the customer will save money but not time. The rebate factor is designed to save the per unit cost of the regular charging power by the same percent that the premium charging power saves the per unit charging time.

10.1.5 The Per Unit Cost of The Economic Charging Power

The economic charging power has the lowest cost but the highest charging duration according to its per unit cost and per unit charging time, respectively. The per unit

cost of the economic charging power (Γ^e) is modeled as in equation (10.6). It is a function of two factors: the per unit cost of premium charging power (Γ^p) and a scaling factor ($\frac{\mathcal{J}^p}{\mathcal{J}^e}$). \mathcal{J}^e is more than \mathcal{J}^r which makes the scaling factor in Γ^e is less than that in Γ^r and thus the economic charging power offers more rebate. In this charging power the rebate is modeled to reduce the per unit charging cost, by the same percent that would reduce the per unit charging time if the premium charging power is utilized.

10.2 Determining the Maximum Charging Cost

The maximum cost of charge (\mathbb{C}^{max}) is estimated for any vehicle $\nu \in \mathcal{V}^{FCS}$ as in equation (10.8). The difference between the maximum and minimum state-of-charge (SoC^{max}) and (SoC^{min}) is multiplied by the battery capacity μ^ν as in (10.8), to find the required energy in kwh. The cost of the required energy is calculated according to the per unit cost of the utilized charging power (\mathcal{J}^{FCS}).

$$\mathbb{C}^{max} = \Gamma^{FCS} \cdot \mu^\nu \cdot (SoC^{max} - SoC^{min}) \quad 10.8$$

$$SoC^{max} = \bar{\ell} \cdot \mu^\nu \quad 10.9$$

$$SoC^{min} = \underline{\ell} \cdot \mu^\nu \quad 10.10$$

$$\mu^\nu := \begin{cases} \mu^s, & \text{if } \nu \in \mathcal{V}_s^{FCS} \\ \mu^m, & \text{if } \nu \in \mathcal{V}_m^{FCS} \\ \mu^l, & \text{if } \nu \in \mathcal{V}_l^{FCS} \end{cases} \quad 10.11$$

$$\mathcal{J}^{FCS} := \begin{cases} \Gamma^p, & \text{if } \nu \in \mathcal{V}_{FCS,p}^\nu \\ \Gamma^r, & \text{if } \nu \in \mathcal{V}_{FCS,r}^\nu \\ \Gamma^e, & \text{if } \nu \in \mathcal{V}_{FCS,e}^\nu \end{cases} \quad 10.12$$

Where,

$$\mathcal{V}_{FCS,p}^v = \{\mathcal{V}_s^{FCS,p} \cup \mathcal{V}_m^{FCS,p} \cup \mathcal{V}_l^{FCS,p}\} \quad 10.13$$

$$\mathcal{V}_{FCS,r}^v = \{\mathcal{V}_s^{FCS,r} \cup \mathcal{V}_m^{FCS,r} \cup \mathcal{V}_l^{FCS,r}\} \quad 10.14$$

$$\mathcal{V}_{FCS,e}^v = \{\mathcal{V}_s^{FCS,e} \cup \mathcal{V}_m^{FCS,e} \cup \mathcal{V}_l^{FCS,e}\} \quad 10.15$$

Where,

\mathbb{C}^{max} The maximum cost of charging a PBEV from FCS, \$

Γ^{FCS} The per unit cost of fast charging, \$/kwh

SoC^{max} The maximum allowable SOC for any PBEV, *p. u.*

SoC^{min} The minimum allowable SOC for any PBEV, *p. u.*

$\bar{\ell}$ A percent to determine the maximum SOC, *p. u.*

$\underline{\ell}$ A percent to determine the minimum SOC, *p. u.*

$\mathcal{V}_{FCS,p}^v$ A set of PBEVs charging by premium power

$\mathcal{V}_{FCS,r}^v$ A set of PBEVs charging by regular power

$\mathcal{V}_{FCS,e}^v$ A set of PBEVs charging by economic power

μ^v Capacity of a PBEV battery, *kwh*

μ^s Capacity of a small battery, *kwh*

μ^m Capacity of a medium battery, *kwh*

μ^l Capacity of a large battery, *kwh*

\mathcal{V}_s^{FCS} A set of PEVs with small battery capacity uses the FCS

\mathcal{V}_m^{FCS} A set of PEVs with medium battery capacity uses the FCS

\mathcal{V}_l^{FCS} A set of PEVs with large battery capacity uses the FCS

10.3 Determining the Maximum Charging Duration

When a vehicle $v \in \mathcal{V}^{FCS}$ arrives at the FCS with a minimum battery SOC (SoC^{min}) and requires to charge the battery from the FCS to the maximum allowable limit (SoC^{max}), this duration of the charge represents the maximum charging time if v utilizes the maximum per unit charging power \mathcal{J}^{FCS} . The maximum duration of the charge is calculated in (10.16); it is a function of a battery capacity μ^v as in (10.11), and a type of the charging power \mathcal{J}^{FCS} .

$$\mathbb{T}^{max} = \mathcal{J}^{FCS} \cdot \mu^v \cdot (SoC^{max} - SoC^{min}) \quad 10.16$$

Where,

$$\mathcal{J}^{FCS} := \begin{cases} \mathcal{J}^p, & \text{if } v \in \mathcal{V}^p \\ \mathcal{J}^r, & \text{if } v \in \mathcal{V}^r \\ \mathcal{J}^e, & \text{if } v \in \mathcal{V}^e \end{cases} \quad 10.17$$

Where,

\mathbb{T}^{max} The maximum time it takes a PBEV to be charged, from its minimum to its maximum state-of-charge, using FCS, (*min.*)

\mathcal{J}^{FCS} The per unit time it takes to charge a PBEV, from its minimum to its maximum state-of-charge, using FCS, (*min./kwh*)

10.4 FCS Data

The number of vehicles that charge from an FCS may be influenced to a large extent by the location of that FCS. Therefore, the number of charging events may vary from location to location, leading to a variation in their demands/impacts on the grid. In order to estimate the demand of the FCS, multiple FCSs in different locations are

considered to generate an averaged energy profile representing the demand of the FCS on the grid. In this section, real data from nine FCSs are extracted and utilized to estimate the cost of smart charging. The reason of considering the average of these nine FCSs is to reduce the distinct variations of their annual profiles due to their locations. These FCSs are in Canada and sharing the same characteristics such as their rated power and the number of ports, but are located in different facilities such as workplaces, retail locations, and malls [221]. The typical data depicts vehicles' energy consumption from the FCSs. Each energy demand profile consists of a number of charging events per each FCS distributed over a period of one year, and the required energy demand in kwh from the FCS for each charging event.

10.5 Modelling of Per Event Energy Demand from the FCS

To construct the average of the FCS demand profile, five values from each FCS typical data are utilized. These values are the maximum value ul_i^{max} , the minimum value ul_i^{min} , and the three sample quartiles ($\underline{q}_i, q_i, \bar{q}_i$), which represent the 25th, 50th, and 75th percentiles for FCS i . Given a cumulative distribution function F_i for the i^{th} FCS, percentiles can be calculated using the inverse of the cumulative distribution function as follows:

$$\underline{q}_i = q_{25} = F_i^{-1}(25) \quad 10.18$$

$$q_i = q_{50} = F_i^{-1}(50) \quad 10.19$$

$$\bar{q}_i = q_{75} = F_i^{-1}(75) \quad 10.20$$

$$ul_i^{max} = q_{100} = F_i^{-1}(100) \quad 10.21$$

$$ul_i^{min} = q_1 = F_i^{-1}(1) \quad 10.22$$

where,

- \underline{q}_i The 25th percentile of charging energy per charging event of FCS i in a year, (kwh)
- q_i The 50th percentile of charging energy per charging event of FCS i in a year, (kwh)
- \bar{q}_i The 75th percentile of charging energy per charging event of FCS i in a year, (kwh)
- ul_i^{max} The maximum of charging energy per charging event of FCS i in a year, (kwh)
- ll_i^{min} The minimum of charging energy per charging event of FCS i in a year, (kwh)
- i Index for FCS, $i = 1, 2, \dots, f$
- f Total number of considered FCSs

The maximum values in the constructed FCS profile UL^{max} , is calculated by finding the average of all maximum values extracted from each FCS profile as shown in equation (10.23). Similarly, the minimum value of each FCS profile is collected and then averaged to construct the minimum value UL^{max} in the constructed FCS profile as in equation (10.24). The three sample quartiles ($\underline{Q}, Q, \bar{Q}$), in the constructed FCS profile are determined by collecting the first, second, and third quartiles of each FCS and then independently finding their average as in equations (10.25)-(10.27).

$$UL^{max} = \frac{\sum_{i=1}^f ul_i^{max}}{f} \quad 10.23$$

$$LL^{min} = \frac{\sum_{i=1}^f ll_i^{min}}{f} \quad 10.24$$

$$\underline{Q} = \frac{\sum_{i=1}^f q_i}{f} \quad 10.25$$

$$Q = \frac{\sum_{i=1}^f q_i}{f} \quad 10.26$$

$$\bar{Q} = \frac{\sum_{i=1}^f \bar{q}_i}{f} \quad 10.27$$

where,

- \underline{Q} The average value of the first quartile of charging energy per charging event in a year, for f number of FCSs, ($kwh/event$)
- Q The average value of the second quartile of charging energy per charging event in a year, for f number of FCSs, ($kwh/event$)
- \bar{Q} The average value of the third quartile of charging energy per charging event in a year, for f number of FCSs, ($kwh/event$)
- UL^{max} The average value of the maximum of charging energy per charging event in a year, for f number of FCSs, ($kwh/event$)
- LL^{min} The average value of the minimum of charging energy per charging event in a year, for f number of FCSs, ($kwh/event$)

10.6 Modelling of Annual Energy Demand from the FCS

In this section, annual energy consumption from the FCS profile is determined and utilized to estimate the cost of smart charging. The annual energy demand from the FCS is calculated using two factors: the kwh per charging event and the average annual total number of charging events (\bar{E}). The kwh per charging events is calculated in the previous section and it consists of five values: \underline{Q} , Q , \bar{Q} , UL^{max} , and UL^{min} . The annual number of charging events at an FCS is

influenced by the FCS's location. Therefore, the annual number of charging events is represented by taking the average of all the annual charging events at all nine FCSs.

The average annual total number of charging events is calculated as follows.

$$\bar{\varepsilon} = \frac{\sum_{i=1}^f \varepsilon_i}{f} \quad 10.28$$

Where,

$\bar{\varepsilon}$ The average number of annual charging events in f number of FCSs,
(*event/year*)

ε_i The number of annual charging events in FCS i

After the annual number of charging events and the energy demand for each charging event are determined, the annual energy demand from the FCS is estimated as follows:

$$\underline{U} = \underline{Q} \cdot \bar{\varepsilon} \quad 10.29$$

$$\bar{U} = \bar{Q} \cdot \bar{\varepsilon} \quad 10.30$$

$$\bar{U} = \bar{Q} \cdot \bar{\varepsilon} \quad 10.31$$

$$U_{max} = UL^{max} \cdot \bar{\varepsilon} \quad 10.32$$

$$U_{min} = LL^{min} \cdot \bar{\varepsilon} \quad 10.33$$

Where,

\underline{U} The estimated 25th percentile value of annual charging energy for a
FCS, (*kwh/year*)

U The estimated 50th percentile value of annual charging energy for a FCS, (*kwh/year*)

\bar{U} The estimated 75th percentile value of annual charging energy for a FCS, (*kwh/year*)

U_{max} The estimated maximum value of annual charging energy for a FCS, (*kwh/year*)

U_{min} The estimated minimum value of annual charging energy for a FCS, (*kwh/year*)

U^{max} : represents the maximum annual energy demand by vehicles from the FCS in kwh per year.

U^{min} : represents the minimum annual energy demand by vehicles from the FCS in kwh per year.

\underline{U} : represents the 25th percentile annual energy demand by vehicles from the FCS in kwh per year.

\bar{U} : represents the median annual energy demand by vehicles from the FCS in kwh per year.

\bar{U} : represents the 75th percentile annual energy demand by vehicles from the FCS in kwh per year.

The meaning of \mathcal{U}^{max} , for instance, is illustrated as follows: given the annual total number of charging events \mathcal{E} (*event*), if $UL^{max} \left(\frac{kwh}{event} \right)$ is the maximum kwh required from a FCS per any charging event, then the total maximum kwh required from that FCS in that year is \mathcal{U}^{max} and equals to $UL^{max} \cdot \mathcal{E}$. The value of \mathcal{U}_{max} represents the total annual demand from the FCS if all vehicles, require UL^{max} for each charging event occurs in that year.

10.7 Computing the Cost of Smart Charging

The annual cost of the proposed smart charging in this thesis can be divided into the rebate paid to customers for using regular and economic charging powers, and the revenue for energy sold to customers when using the FCS.

10.7.1 Computing the Rebates

In this section, the rebate of using the smart charging is computed. The proposed rebate is assumed to be instant and it is a function of the duration of the charge. When a customer uses the FCS, the customer can choose one of three charging powers: premium, regular, or economic charging power. When the premium charging power is chosen, the customer would not get a rebate. The rebate is paid instantly upon using regular or economic charging power. The annual rebate is computed as follows:

$$\underline{C}^{Reb} = \underline{U} \cdot [(\mathcal{r} \cdot (\Gamma^p - \Gamma^r)) + ((1 - \mathcal{r}) \cdot (\Gamma^p - \Gamma^e))] \cdot \frac{\eta^{sm}}{100} \quad 10.34$$

$$C^{Reb} = \mathcal{U} \cdot [(\mathcal{r} \cdot (\Gamma^p - \Gamma^r)) + ((1 - \mathcal{r}) \cdot (\Gamma^p - \Gamma^e))] \cdot \frac{\eta^{sm}}{100} \quad 10.35$$

$$\bar{C}^{Reb} = \bar{U} \cdot [(r \cdot (\Gamma^p - \Gamma^r)) + ((1 - r) \cdot (\Gamma^p - \Gamma^e))] \cdot \frac{\eta^{sm}}{100} \quad 10.36$$

$$C_{max}^{Reb} = U_{max} \cdot [(r \cdot (\Gamma^p - \Gamma^r)) + ((1 - r) \cdot (\Gamma^p - \Gamma^e))] \cdot \frac{\eta^{sm}}{100} \quad 10.37$$

$$C_{min}^{Reb} = U_{min} \cdot [(r \cdot (\Gamma^p - \Gamma^r)) + ((1 - r) \cdot (\Gamma^p - \Gamma^e))] \cdot \frac{\eta^{sm}}{100} \quad 10.38$$

Where,

\underline{C}^{Reb} The 25th percentile annual rebate paid to customers for using smart charging power, (\$/year)

C^{Reb} The median annual rebate paid to customers for using smart charging power, (\$/year)

\bar{C}^{Reb} The 75th percentile annual rebate paid to customers for using smart charging power, (\$/year)

C_{max}^{Reb} The maximum annual rebate paid to customers for using smart charging power, (\$/year)

C_{min}^{Reb} The minimum annual rebate paid to customers for using smart charging power, (\$/year)

r A uniform random number

η^{sm} Share of PBEV that utilize smart charging power at FCS, *p. u.*

If $\Gamma^r = \Gamma^e = \Gamma^p$ in equations (10.34) to (10.38), then $\eta^{sm} = 0$. It means that all customers utilize the premium charging power because the share of customers using regular and economic charging powers (η^{sm}) is zero. Therefore, the (maximum, minimum, 25th percentile, 50th percentile, 75th percentile) annual rebates in equations (10.34) to (10.38) are zero. In that case, the FCS operator would not pay any rebate

to customers and the annual cost is represented only by revenue from selling the energy to customers who use the premium charging power.

If, in equations (10.34) to (10.38), $\Gamma^r \neq \Gamma^e$ and/or $\Gamma^e \neq \Gamma^p$, then $\eta^{sm} \neq 0$. It means that regular and/or charging power have/has been utilized in that year. The share of customers utilizing these two charging powers (regular and economic) is determined by the factor η^{sm} . Multiple penetrations of the smart charging (η^{sm}) are considered in this regard. The penetration is varied from 0% up to 100% by 10%. The factor r , in equations (10.34) to (10.38), is utilized to determine the percent of customers who used regular charging power and the percent of customer who used economic charging power. The factor r is randomly generated using a uniform random number and repeated multiple times. In equation (10.34) for instance, when $r = 1$, it means that share of vehicle uses the regular charging power is η^{sm} , and thus the economic charging power has not been utilized. In contrast, when $r = 0$, it means that shares of vehicle use the economic charging power is η^{sm} and thus the regular charging power has not been utilized. When $r = 0.5$, it means that 50% of η^{sm} uses the regular charging power while the economic charging power is utilized by the other 50% of η^{sm} . Therefore, r is a shaping factor utilized to assign, based on the penetration of η^{sm} , percent of vehicles that uses the regular charging power, and the percent of vehicles that uses the economic charging power. Equations (10.34) to (10.38) can be written in a long form as follows:

$$\underline{C}^{Reb} = \left[\frac{1}{f} \cdot \sum_{i=1}^f q_i \cdot \varepsilon_i \right] \left[\frac{C \cdot \vartheta}{\beta^p} \left[\left(r \cdot \left(1 - \frac{\beta^r}{\beta^p} \right) \right) + \left((1 - r) \cdot \left(1 - \frac{\beta^e}{\beta^p} \right) \right) \right] \left[\left(\frac{\eta^{sm}}{100} \right) \right] \right] \quad 10.39$$

$$C^{Reb} = \left[\frac{1}{f} \cdot \sum_{i=1}^f q_i \cdot \varepsilon_i \right] \left[\frac{C \cdot \vartheta}{\beta^p} \left[\left(r \cdot \left(1 - \frac{\beta^r}{\beta^p} \right) \right) + \left((1 - r) \cdot \left(1 - \frac{\beta^e}{\beta^p} \right) \right) \right] \left[\left(\frac{\eta^{sm}}{100} \right) \right] \right] \quad 10.40$$

$$\bar{C}^{Reb} = \left[\frac{1}{f} \cdot \sum_{i=1}^f \bar{q}_i \cdot \varepsilon_i \right] \left[\frac{C \cdot \vartheta}{\beta^p} \left[\left(r \cdot \left(1 - \frac{\beta^r}{\beta^p} \right) \right) + \left((1 - r) \cdot \left(1 - \frac{\beta^e}{\beta^p} \right) \right) \right] \left[\left(\frac{\eta^{sm}}{100} \right) \right] \right] \quad 10.41$$

$$C_{max}^{Reb} = \left[\frac{1}{f} \cdot \sum_{i=1}^f ul_i^{max} \cdot \varepsilon_i \right] \left[\frac{C \cdot \vartheta}{\beta^p} \left[\left(r \cdot \left(1 - \frac{\beta^r}{\beta^p} \right) \right) + \left((1 - r) \cdot \left(1 - \frac{\beta^e}{\beta^p} \right) \right) \right] \left[\left(\frac{\eta^{sm}}{100} \right) \right] \right] \quad 10.42$$

$$C_{min}^{Reb} = \left[\frac{1}{f} \cdot \sum_{i=1}^f ul_i^{min} \cdot \varepsilon_i \right] \left[\frac{C \cdot \vartheta}{\beta^p} \left[\left(r \cdot \left(1 - \frac{\beta^r}{\beta^p} \right) \right) + \left((1 - r) \cdot \left(1 - \frac{\beta^e}{\beta^p} \right) \right) \right] \left[\left(\frac{\eta^{sm}}{100} \right) \right] \right] \quad 10.43$$

10.7.2 Computing the Revenue

The revenue of selling energy to vehicles from the FCS is determined in this section.

The FCS makes revenue when customers utilize it to charge their vehicles, regardless of which charging power was utilized. There are three charging power available in the FCS: premium, regular, and economic charging power. The revenue is a function of the charging duration. Therefore, annual charging energy is utilized to estimate annual revenues. The annual revenue is computed as follows:

$$\underline{\mathcal{R}}^{Rev} = \underline{U} \cdot \left[\left(\frac{((100 - \eta^{sm}) \cdot \Gamma^p)}{100} \right) + \left(((r \cdot \Gamma^r) + ((1 - r) \cdot \Gamma^e)) \cdot \frac{\eta^{sm}}{100} \right) \right] \quad 10.44$$

$$\mathcal{R}^{Rev} = U \cdot \left[\left(\frac{((100 - \eta^{sm}) \cdot \Gamma^p)}{100} \right) + \left(((r \cdot \Gamma^r) + ((1 - r) \cdot \Gamma^e)) \cdot \frac{\eta^{sm}}{100} \right) \right] \quad 10.45$$

$$\bar{\mathcal{R}}^{Rev} = \bar{U} \cdot \left[\left(\frac{((100 - \eta^{sm}) \cdot \Gamma^p)}{100} \right) + \left(((r \cdot \Gamma^r) + ((1 - r) \cdot \Gamma^e)) \cdot \frac{\eta^{sm}}{100} \right) \right] \quad 10.46$$

$$\mathcal{R}_{max}^{Rev} = \mathcal{U}_{max} \cdot \left[\left(\frac{((100 - \eta^{sm}) \cdot \Gamma^p)}{100} \right) + \left(((r \cdot \Gamma^r) + ((1 - r) \cdot \Gamma^e)) \cdot \frac{\eta^{sm}}{100} \right) \right] \quad 10.47$$

$$\mathcal{R}_{min}^{Rev} = \mathcal{U}_{min} \cdot \left[\left(\frac{((100 - \eta^{sm}) \cdot \Gamma^p)}{100} \right) + \left(((r \cdot \Gamma^r) + ((1 - r) \cdot \Gamma^e)) \cdot \frac{\eta^{sm}}{100} \right) \right] \quad 10.48$$

Where,

$\underline{\mathcal{R}}^{Rev}$ The 25th percentile annual revenue from customers for using smart charging power, (\$/year)

\mathcal{R}^{Rev} The median annual revenue from customers for using smart charging power, (\$/year)

$\overline{\mathcal{R}}^{Rev}$ The 75th percentile annual revenue from customers for using smart charging power, (\$/year)

\mathcal{R}_{max}^{Rev} The maximum annual revenue from customers for using smart charging power, (\$/year)

\mathcal{R}_{min}^{Rev} The minimum annual revenue from customers for using smart charging power, (\$/year)

In equation (10.44) for example, η^{sm} represents the share of vehicles that utilize smart charging (regular and economic charging powers). If $\eta^{sm} = 0$, it means that only premium charging power was utilized, and the annual revenue is calculated accordingly. It also means that the annual revenue of using regular or economic charging powers is zero. In contrast, when $\eta^{sm} = 100$, revenue of using premium charging power is zero because the premium charging power was not utilized by any vehicles. Different penetration levels of η^{sm} are considered to compute annual

revenue of the FCS. In equation (10.44) for instance, the factor r is used to define the share of customers that use regular charging power from those who use economic charging power. The factor r is generated using uniform random number and it is effective only when $\eta^{sm} > 0$. The function of r in equation (10.44) is as illustrated in the previous section. For instance, when $\eta^{sm} = 10\%$ and $r = 0.3$, according to equation (10.44), it means that:

- The percent of vehicles that uses premium charging power is $100 - \eta^{sm} = 90\%$,
- The percent of vehicles that uses regular charging power is $r \cdot \eta^{sm} = 0.3 * 10\% = 3\%$,
- The percent of vehicles that uses premium charging power is $(1 - r) \cdot \eta^{sm} = 0.7 * 10\% = 7\%$.

Therefore, the (maximum, minimum, 25th percentile, 50th percentile, 75th percentile) annual revenue in equations (10.44) to (10.48) is determined according to deterministic and stochastic factors:

- The deterministic factor is penetration level η^{sm} , which is varied from 0% up to 100% by 10%.
- The stochastic factor is r , which is generated using a uniform distribution.
- The annual charging energy ($\underline{U}, \bar{U}, \overline{U}, U_{max}, U_{min}$) is another stochastic factor which represents the vehicle demand from the FCS per year.

Equations (10.44) to (10.48) can be written in a long form as follows:

$$\underline{\mathcal{R}}^{Rev} = \left[\frac{1}{f} \sum_{i=1}^f (q_i \cdot \varepsilon_i) \right] \left[\frac{\mathcal{C} \cdot \vartheta}{\beta^p} \cdot \left[\left(\frac{(100 - \eta^{sm})}{100} \right) + \left(\left(r \cdot \frac{\beta^r}{\beta^p} \right) + \left((1 - r) \cdot \frac{\beta^e}{\beta^p} \right) \right) \cdot \frac{\eta^{sm}}{100} \right] \right] \quad 10.49$$

$$\mathcal{R}^{Rev} = \left[\frac{1}{f} \sum_{i=1}^f (q_i \cdot \varepsilon_i) \right] \left[\frac{\mathcal{C} \cdot \vartheta}{\beta^p} \cdot \left[\left(\frac{(100 - \eta^{sm})}{100} \right) + \left(\left(r \cdot \frac{\beta^r}{\beta^p} \right) + \left((1 - r) \cdot \frac{\beta^e}{\beta^p} \right) \right) \cdot \frac{\eta^{sm}}{100} \right] \right] \quad 10.50$$

$$\overline{\mathcal{R}}^{Rev} = \left[\frac{1}{f} \sum_{i=1}^f (\bar{q}_i \cdot \varepsilon_i) \right] \left[\frac{\mathcal{C} \cdot \vartheta}{\beta^p} \cdot \left[\left(\frac{(100 - \eta^{sm})}{100} \right) + \left(\left(r \cdot \frac{\beta^r}{\beta^p} \right) + \left((1 - r) \cdot \frac{\beta^e}{\beta^p} \right) \right) \cdot \frac{\eta^{sm}}{100} \right] \right] \quad 10.51$$

$$\begin{aligned} \mathcal{R}_{max}^{Rev} = & \left[\frac{1}{f} \sum_{i=1}^f (ul_i^{max} \cdot \varepsilon_i) \right] \left[\frac{\mathcal{C} \cdot \vartheta}{\beta^p} \cdot \left[\left(\frac{(100 - \eta^{sm})}{100} \right) \right. \right. \\ & \left. \left. + \left(\left(r \cdot \frac{\beta^r}{\beta^p} \right) + \left((1 - r) \cdot \frac{\beta^e}{\beta^p} \right) \right) \cdot \frac{\eta^{sm}}{100} \right] \right] \end{aligned} \quad 10.52$$

$$\begin{aligned} \mathcal{R}_{min}^{Rev} = & \left[\frac{1}{f} \sum_{i=1}^f (ul_i^{min} \cdot \varepsilon_i) \right] \left[\frac{\mathcal{C} \cdot \vartheta}{\beta^p} \cdot \left[\left(\frac{(100 - \eta^{sm})}{100} \right) \right. \right. \\ & \left. \left. + \left(\left(r \cdot \frac{\beta^r}{\beta^p} \right) + \left((1 - r) \cdot \frac{\beta^e}{\beta^p} \right) \right) \cdot \frac{\eta^{sm}}{100} \right] \right] \end{aligned} \quad 10.53$$

10.8 Comparison of Rebate and Revenue

In this section, the ratio of revenue to rebate per maximum charging duration using regular/economic charging power is explained. When a customer charges his/her vehicle from the FCS, this makes revenue for the FCS. A rebate is given for the charging event if that customer uses regular or economic charging power. Therefore,

the per event charging cost can be utilized to estimate the revenue and rebate given to customers if they charge their vehicles via regular or economic charging power.

The maximum cost of charge was determined previously as follows:

$$\mathcal{R}^{Rev,p} = \Gamma^p \cdot \mu^v \cdot (SoC^{max} - SoC^{mic}) \quad 10.54$$

$$\mathcal{R}^{Rev,r} = \Gamma^r \cdot \mu^v \cdot (SoC^{max} - SoC^{min}) \quad 10.55$$

$$\mathcal{C}^{\mathcal{R}^{Rev,e}} = \Gamma^e \cdot \mu^v \cdot (SoC^{max} - SoC^{min}) \quad 10.56$$

The maximum rebate per charge is estimated similarly as follow:

$$\mathcal{C}^{Reb,p} = (\Gamma^p - \Gamma^p) \cdot \mu^v \cdot (SoC^{max} - SoC^{min}) \quad 10.57$$

$$\mathcal{C}^{Reb,r} = (\Gamma^p - \Gamma^r) \cdot \mu^v \cdot (SoC^{max} - SoC^{min}) \quad 10.58$$

$$\mathcal{C}^{Reb,e} = (\Gamma^p - \Gamma^e) \cdot \mu^v \cdot (SoC^{max} - SoC^{min}) \quad 10.59$$

The ratio of the revenue to the rebate of the regular charging power, for example, per the maximum charging duration is estimated using equations (10.55) and (10.58) as follows:

$$\frac{\mathcal{R}^{Rev,r}}{\mathcal{C}^{Reb,r}} = \frac{\Gamma^r \cdot \mu^v \cdot (SoC^{max} - SoC^{min})}{(\Gamma^p - \Gamma^r) \cdot \mu^v \cdot (SoC^{max} - SoC^{min})} = \frac{\Gamma^r}{(\Gamma^p - \Gamma^r)} \quad 10.60$$

Where,

$\mathcal{R}^{Rev,r}$ Revenue from a customer when the regular charging power is utilized, \$

$\mathcal{C}^{Reb,r}$ Rebate paid to a customer when the regular charging power is utilized, \$

From equation (10.5), the per unit cost of the regular charging power Γ^r , is

$$\Gamma^r = \Gamma^p \cdot \frac{\mathcal{J}^p}{\mathcal{J}^r} \quad 10.61$$

Substituting (10.61) into (10.60), we get

$$\begin{aligned} \frac{\mathcal{R}^{Rev,r}}{\mathcal{C}^{Reb,r}} &= \frac{\Gamma^r}{(\Gamma^p - \Gamma^r)} = \frac{\Gamma^p \cdot \frac{\mathcal{J}^p}{\mathcal{J}^r}}{(\mathcal{C} \cdot \mathcal{J}^p - \Gamma^p \cdot \frac{\mathcal{J}^p}{\mathcal{J}^r})} = \frac{\Gamma^p \cdot \mathcal{J}^p}{(\mathcal{C} \cdot \mathcal{J}^p \cdot \mathcal{J}^r - \Gamma^p \cdot \frac{\mathcal{J}^p \cdot \mathcal{J}^r}{\mathcal{J}^r})} \\ &= \frac{\Gamma^p \cdot \mathcal{J}^p}{(\mathcal{C} \cdot \mathcal{J}^p \cdot \mathcal{J}^r - \Gamma^p \cdot \mathcal{J}^p)} \end{aligned} \quad 10.62$$

Taking \mathcal{J}^p as common factor in (10.62), we get

$$\frac{\mathcal{R}^{Rev,r}}{\mathcal{C}^{Reb,r}} = \frac{\Gamma^p \cdot \mathcal{J}^p}{\mathcal{J}^p \cdot (\mathcal{C} \cdot \mathcal{J}^r - \Gamma^p)} = \frac{\Gamma^p}{(\mathcal{C} \cdot \mathcal{J}^r - \Gamma^p)} \quad 10.63$$

Substituting equation (10.4), the per unit cost of the premium charging power Γ^p , into (10.63), we get:

$$\frac{\mathcal{R}^{Rev,r}}{\mathcal{C}^{Reb,r}} = \frac{\mathcal{C} \cdot \mathcal{J}^p}{(\mathcal{C} \cdot \mathcal{J}^r - \mathcal{C} \cdot \mathcal{J}^p)} \quad 10.64$$

Taking \mathcal{C} as common factor in (10.64), we get

$$\frac{\mathcal{R}^{Rev,r}}{\mathcal{C}^{Reb,r}} = \frac{\mathcal{C} \cdot \mathcal{J}^p}{\mathcal{C} \cdot (\mathcal{J}^r - \mathcal{J}^p)} = \frac{\mathcal{J}^p}{\mathcal{J}^r - \mathcal{J}^p} \quad 10.65$$

From equation (10.1) and (10.2), the per unit time of the premium and regular charging powers \mathcal{J}^p and \mathcal{J}^r , are:

$$\mathcal{J}^p = \frac{\vartheta}{\beta^p} \quad 10.66$$

$$\mathcal{T}^r = \frac{\vartheta}{\beta^r} \quad 10.67$$

Substituting equation (10.66) and (10.67) into (10.65), we get:

$$\frac{\mathcal{R}^{Rev,r}}{\mathcal{C}^{Reb,r}} = \frac{\frac{\vartheta}{\beta^p}}{\left(\frac{\vartheta}{\beta^r} - \frac{\vartheta}{\beta^p}\right)} \quad 10.68$$

$$\frac{\mathcal{R}^{Rev,r}}{\mathcal{C}^{Reb,r}} \Gamma^r = \frac{1}{\left(\frac{\beta^p}{\beta^r} - \frac{\beta^p}{\beta^p}\right)} = \frac{1}{\left(\frac{\beta^p}{\beta^r} - 1\right)} \quad 10.69$$

From equation (9.15) and (9.16), the premium and regular charging powers β^p and β^r , are functions of the maximum rated power of the charger β , and are bounded as follows:

$$\underline{p} \cdot \beta \leq \beta^p \leq \bar{p} \cdot \beta \quad 10.70$$

$$\underline{r} \cdot \beta \leq \beta^r \leq \bar{r} \cdot \beta \quad 10.71$$

Also, from equations (9.19) and (9.20), we have

$$\bar{p} \leq 1 \quad 10.72$$

$$\underline{p}, \bar{p} > \bar{r} \quad 10.73$$

Therefore,

$$\beta^p > \beta^r \quad 10.74$$

If,

$$p^{op} \cdot \beta \in [\underline{p} \cdot \beta, \bar{p} \cdot \beta] \quad 10.75$$

$$r^{op} \cdot \beta \in [\underline{r} \cdot \beta, \bar{r} \cdot \beta] \quad 10.76$$

Then,

$$p^{op} > r^{op} \quad 10.77$$

$$p^{op}, r^{op} \in (0,1] \quad 10.78$$

Where,

p^{op} Optimal factor to set the limit of premium charging power, $p \cdot u$.

r^{op} Optimal factor to set the limit of regular charging power, $p \cdot u$.

Substituting equations (10.75) and (10.76) in equation (10.69), we get

$$\frac{\mathcal{R}^{Rev,r}}{C^{Reb,r}} = \frac{1}{\left(\frac{\beta^p}{\beta^r} - 1\right)} = \frac{1}{\left(\frac{p^{op} \cdot \beta}{r^{op} \cdot \beta} - 1\right)} = \frac{1}{\left(\frac{p^{op}}{r^{op}} - 1\right)} \quad 10.79$$

Equation (10.79) means that, as the charging duration from the FCS increases, the rebate increases as well; however, the revenue increases much more by the factor of $\frac{\mathcal{R}^{Rev,r}}{C^{Reb,r}}$. This factor $\frac{\mathcal{R}^{Rev,r}}{C^{Reb,r}}$ is shaped by the ratio of $\frac{p^{op}}{r^{op}}$. The rebate is increased when the rated power of regular charging is decreased. The rated power of the regular charging is controlled by r^{op} , as equations in (9.16) and (10.76). Therefore, decreasing r^{op} results in an increase in the ratio of $\frac{p^{op}}{r^{op}}$, ($p^{op} \gg r^{op}$) making the $\frac{\mathcal{R}^{Rev,r}}{C^{Reb,r}}$ to decrease. In contrast, when the r^{op} is increased it results in a reduction in the ratio of $\frac{p^{op}}{r^{op}}$, ($p^{op} \approx r^{op}$) which in turns makes the $\frac{\mathcal{R}^{Rev,r}}{C^{Reb,r}}$ in (10.79) to increase.

Similarly, given the optimal factor to set the limit of economic charging power, e^{op} , as follows:

$$e^{op} \cdot \beta \in [\underline{e} \cdot \beta, \bar{e} \cdot \beta] \quad 10.80$$

$$p^{op} > e^{op} \quad 10.81$$

Then, the ratio of the revenue to the rebate of the economic charging power per the maximum charging duration is estimated as follows:

$$\frac{\mathcal{R}^{Rev,e}}{\mathcal{C}^{Reb,e}} = \frac{1}{\left(\frac{p^{op}}{e^{op}} - 1\right)} \quad 10.82$$

Where,

$\mathcal{R}^{Rev,e}$ Revenue from a customer when the economic charging power is utilized, \$

$\mathcal{C}^{Reb,e}$ Rebate paid to a customer when the economic charging power is utilized, \$

10.9 Results and Discussions

10.9.1 Per Unit Time and Per Unit Cost of the Smart Charging

Figures 10.1 and 10.2 depict the required time and cost, as explained in section 10.1, to charge vehicles with 1kwh and 25kwh using premium, regular, and economic charging powers. It is noted that premium charging power achieves the shortest time to charge a vehicle with 1kwh, but it has highest per unit charging cost. Also, it is noted that regular charging power requires lower time to charge 1kwh but more cost than economic power. The proposed smart charging preserves a balance between the

required time and cost to charge 1kwh by the proposed charging power. For example, referring to Figure 10.1, the required time to charge 1kwh by premium power is 1.333 minute whereas it is 1.447 minutes by regular power. The proposed cost to charge 1kwh by premium power is 0.3777 \$ whereas it is a 0.347 \$ to charge by regular power. The ratio of time required by premium power to the time required by regular power is $\frac{1.333}{1.447} = 0.92$, whereas the ratio of the cost incurred by using premium power to regular power is $\frac{0.377}{0.347} = 1.08$. This means that when premium power is utilized, the required time to charge 1kwh is decreased by 8% than the required time to charge the same energy by regular power. However, the incurred cost when premium power is utilized is increased by 8% than the incurred cost when the regular charging power is utilized. Similarly, the ratio of premium power to regular is found to be $\pm 13\%$. It is obvious that the proposed smart charging preserves a balance between the time and cost to charge 1kwh, by different charging powers.

10.9.2 Effect of Charging Power on Charging Duration and Charging Cost

The maximum charging duration and the corresponding charging costs are determined based on the following assumptions:

- The minimum state-of-charge of vehicles is $SoC^{min} = 0.2 p.u$ [257], [258].
- Given the battery safety considerations, the maximum state-of-charge using FCS is $SoC^{max} = 0.8 p.u.$, as in [232].
- Given SoC^{max} and SoC^{min} , the maximum charging duration is determined as in equation (10.16).

- The charging efficiency is 90%, as in [259], [260].
- The Nissan Leaf is utilized to represent a vehicle with a small battery capacity, $\mu^s = 45 \text{ kwh}$.
- The Chevy Bolt is utilized to represent a vehicle with a small battery capacity, $\mu^m = 66 \text{ kwh}$.
- The Tesla Model S is utilized to represent a vehicle with a small battery capacity, $\mu^l = 110 \text{ kwh}$.

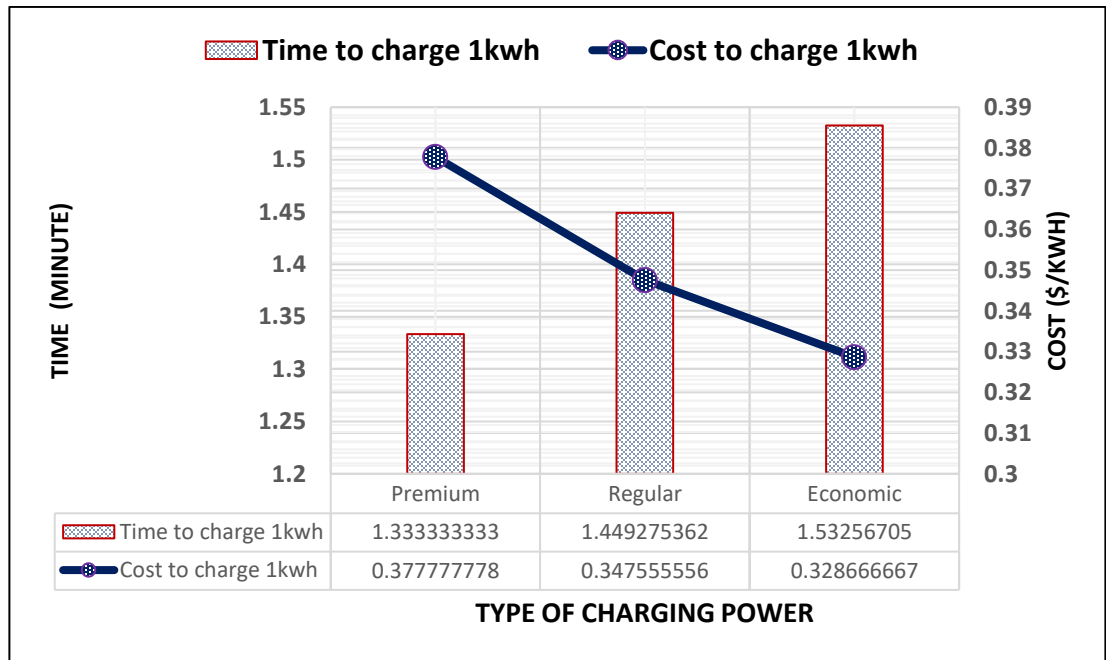


Figure 10.1 Required Time and Cost to Charge 1kwh by the Smart Charging

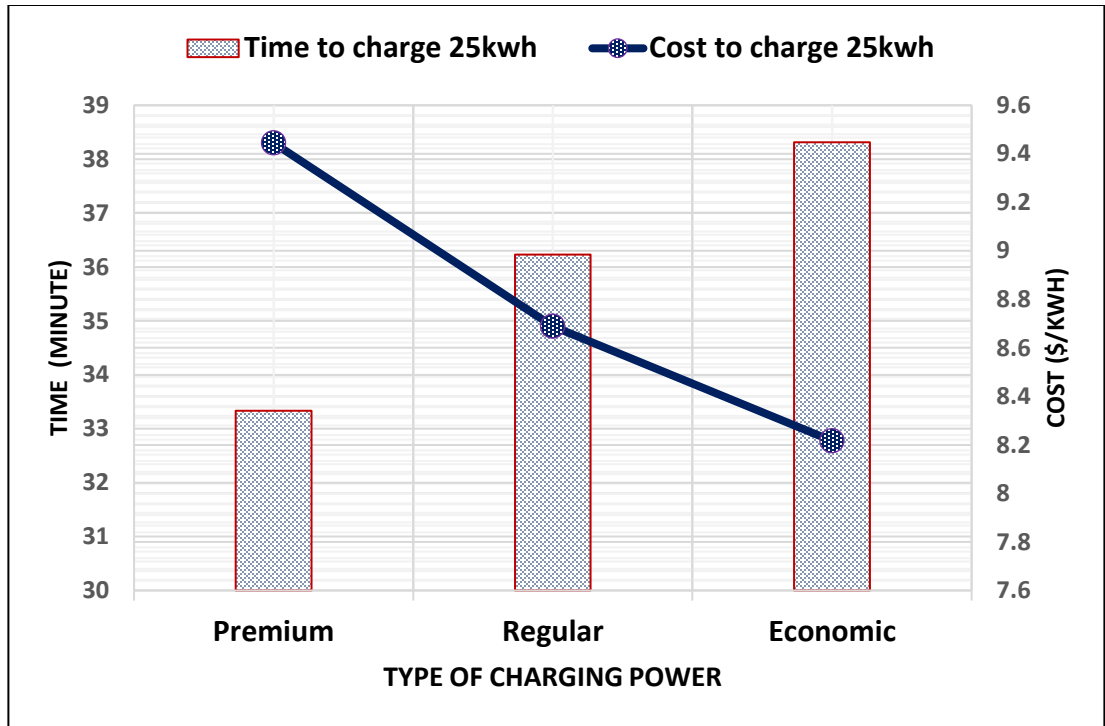


Figure 10.2 Required Time and Cost to Charge 25kwh by the Smart Charging

The maximum per unit charging duration is determined by taking the difference between SoC^{max} and SoC^{min} . Given the battery capacity μ^s, μ^m , or, μ^l , and the charging type Γ^p, Γ^r , or Γ^e , maximum charging durations and costs are obtained as in (10.8) and (10.16). Figures 10.3 to 10.5 visualize the effect of the proposed smart charging on vehicles with different battery capacities. It is noted that the charging duration and charging costs increase when the battery capacity increases.

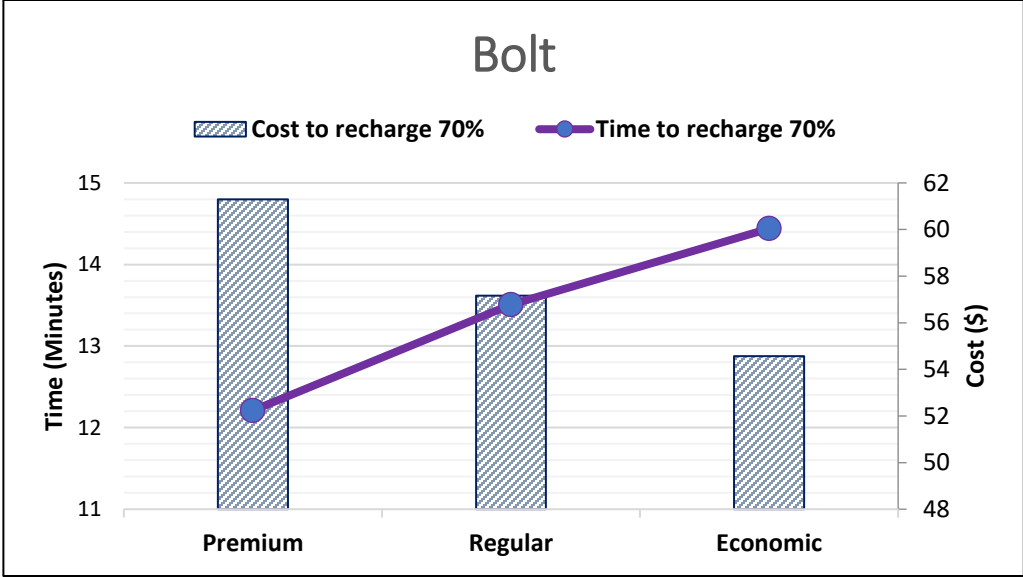


Figure 10.3 Required Time and Cost to add 70% SOC into Bolt EV Battery

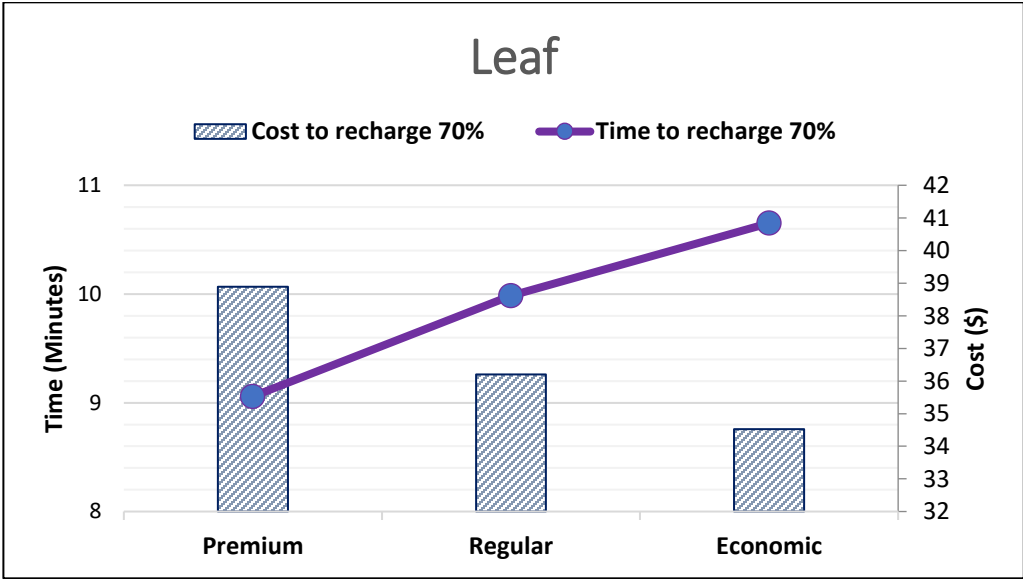


Figure 10.4 Required Time and Cost to add 70% SOC into Leaf EV Battery

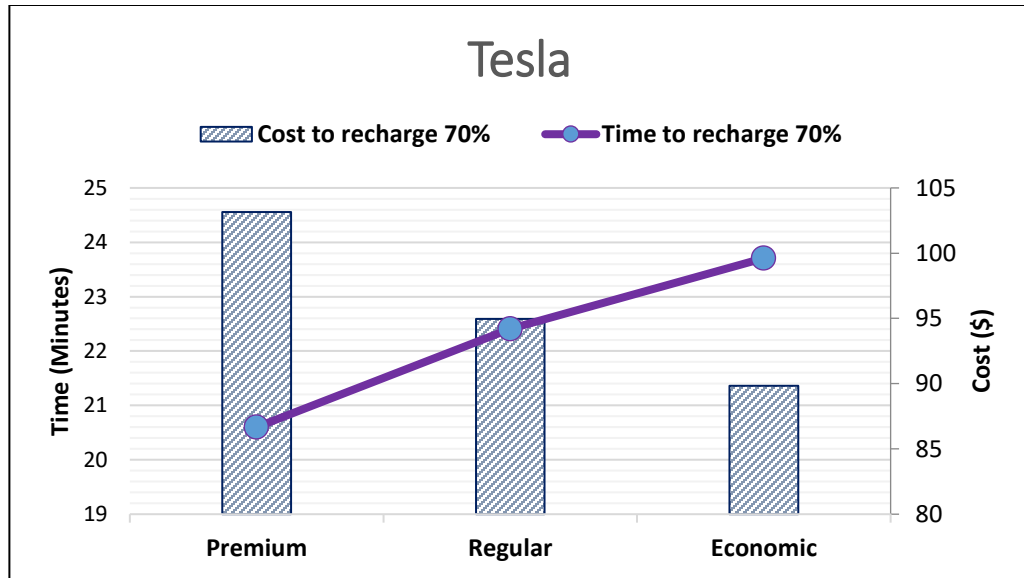


Figure 10.5 Required Time and Cost to add 70% SOC into Tesla Model S Battery

10.9.3 Descriptive Statistics of Annual Data for Multiple FCSs

The per event annual energy profile for FCSs are obtained as in [221], and described by maximum value, minimum value, and 25th, 50th, and 75th percentiles, as presented in Figure 10.6. The annual number of charging events occurs in FCSs, as presented in Figure 10.7. A clear variation among these annual profiles is depicted in Figure 10.6 and 10.7.

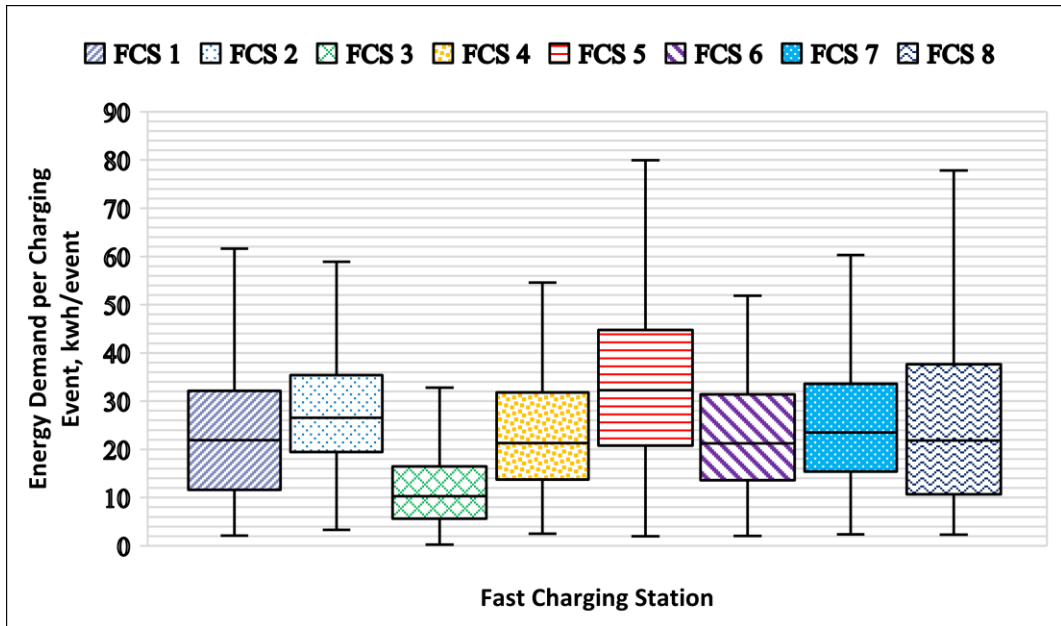


Figure 10.6 A boxplot of the Energy Demand on FCS per Charging Event in a Year

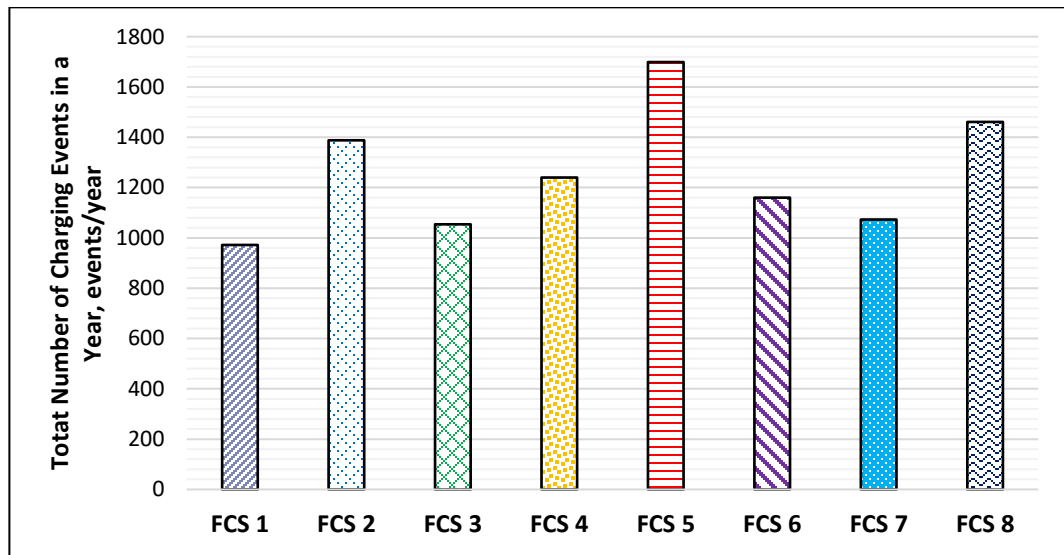


Figure 10.7 Number of Annual Charging Events for Different FCSs

10.9.4 Average Annual Energy Required from FCS

Given the per event energy profiles and the annual charging events for FCSs, the average energy profile and the average number of charging events for FCSs are obtained, as in (10.23) -(10.27) and (10.28). Figure 10.8 depicts the per event energy profiles using the following values: the maximum and the minimum values as well

as the three quartiles ($Q_1 = 25^{th}$, $Q_2 = \text{median}$, and $Q_3 = 75^{th}$) percentiles. As explained previously, the average number of charging events (\bar{E}) represents the annual number of charging events that may occur at the FCS. Given \bar{E} , the energy required by vehicles for each charging event from the FCS is not determined.

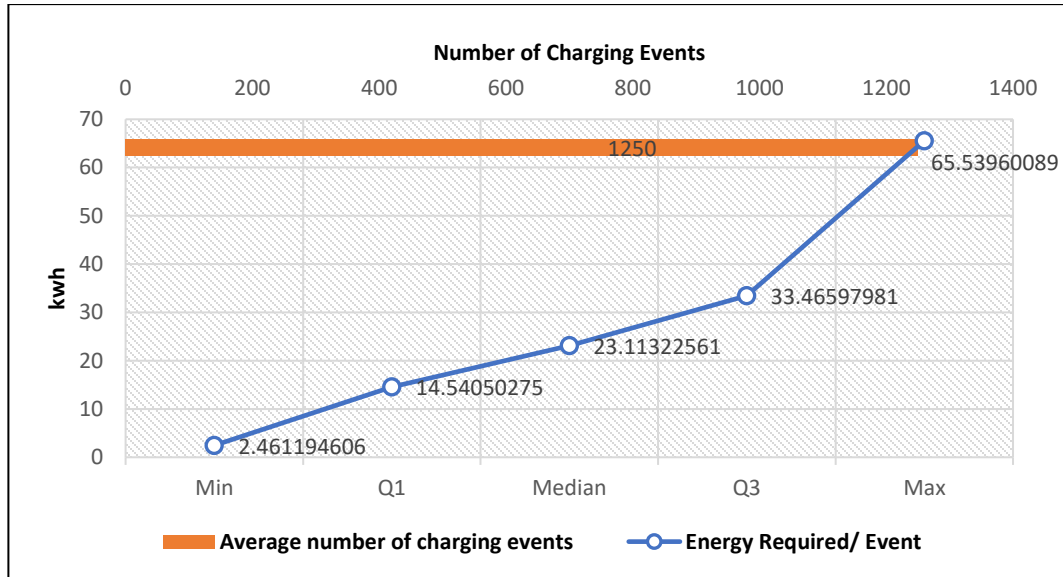


Figure 10.8 The Energy Required Per Changing Event and the Average Numbers of Events

In order to determine the annual energy required from the FCS in both extreme directions, the maximum (UL^{max}) and minimum (UL^{min}) values are utilized. The percentiles are utilized to quantitatively describe the annual energy required from the FCS. The average annual energy required from the FCS is obtained, as shown in equation (10.29) – (10.33). The reason of generating the average energy required from the FCS, is to compute the annual costs of rebate and revenue. The annual cost of the rebate is a function of penetration of the smart charging. Given the annual energy required from the FCS, different penetration levels of \bar{E} are considered, as presented in Table 10-1.

Table 10-1 Max., Min., and Quantile Annual Energy Required by Different Penetration Levels of the Proposed Smart Charging

		Penetration of Smart Charging										
		0%	10%	20%	30%	40%	50%	60%	70%	80%	90%	100%
Annual Energy Required in kwh	UL^{min}	0	312.5	625	937.5	1250	1562.5	1875	2187.5	2500	2812.5	3125
	\bar{U}	0	1812.5	3625	5437.5	7250	9062.5	10875	12687	14500	16312	18125
	\bar{U}	0	2887.5	5775	8662.5	11550	14437	17325	20212	23100	25987	28875
	\bar{U}	0	4187.5	8375	12562	16750	20937	25125	29312	33500	37687	41875
	UL^{max}	0	8187.5	16375	24562	32750	40937	49125	57312	65500	73687	81875

10.9.5 Fast Charging Station Annual Revenue and Rebate

Figure 10.9 to 10.13 present the annual rebate and revenue considering different energy required from the FCS:

- the minimum annual charging energy (Figure 10.9) obtained as in (10.33),
- the 25th percentile annual charging energy (Figure 10.10) obtained as in (10.29),
- the 50th percentile annual charging energy (Figure 10.11) obtained as in (10.30),
- the 75th percentile annual charging energy (Figure 10.12) obtained as in (10.31),
- and the maximum charging energy (Figure 10.13) obtained as in (10.32).

In each figure, the rebate represents the annual cost paid to the customer for using smart charging with regular and/or economic charging power. The annual rebate is

shown in the right y-axis of each figure. The revenue is shown in the left y-axis of each figure and represents the costs obtained from selling the energy to customers when customers charge via premium β^p , regular β^r , and/or economic β^e charging power. Each bar represents a result for a specific penetration of smart charging.

For example, result of the first bar in Figure 10.9 is obtained as follows:

given:

- the minimum annual charging energy as shown in Figure 10.8, $\underline{Q} = 2.461 \text{ kwh/event}$.
- the average annual charging energy as presented in Figure 10.8 is $\bar{E} = 1250 \text{ event}$.
- penetration of the smart charging $\eta^{sm} = 0$.
- the costs of premium, regular, and economic charging powers as shown in Figure 10.1 are $\Gamma^p = 0.378 \text{ \$/kwh}$, $\Gamma^r = 0.348 \text{ \$/kwh}$, and $\Gamma^e = 0.329 \text{ \$/kwh}$.
- the uniform random number r is to determine the share of regular and economic power for each penetration.
- the optimal factors for the premium p^{op} , regular r^{op} , and economic e^{op} power are 1, 0.925, and 0.875.

then,

- the average minimum annual charging energy required from the FCS is

$$\underline{Q}. \underline{E} = 3076.25 \text{ kwh}$$

- the annual rebate and revenue are calculated as in Equations (10.83) and (10.84) (rewritten below) as follows:

$$\underline{\mathcal{R}}^{Rev} = \underline{U}. \left[\left(\frac{((100 - \eta^{sm}). \Gamma^p)}{100} \right) + \left(((r. \Gamma^r) + ((1 - r). \Gamma^e)) \cdot \frac{\eta^{sm}}{100} \right) \right] \quad 10.83$$

$$\underline{\mathcal{C}}^{Reb} = \underline{U}. \left[(r. (\Gamma^p - \Gamma^r)) + ((1 - r). (\Gamma^p - \Gamma^e)) \right] \cdot \frac{\eta^{sm}}{100} \quad 10.84$$

- the revenue of the smart charging is zero because $\eta^{sm} = 0$, as well as the rebate $\underline{\mathcal{C}}^{Reb} = 0$.
- thus, the revenue $\underline{\mathcal{R}}^{Rev}$ is calculated from selling the energy from using the premium power only, $\underline{\mathcal{R}}^{Rev} = 3076.25 * 0.378 = 1162.82 \text{ \$/year}$.
- the ratio of the revenue to the rebate of using the smart charging is 9 and obtained by averaging optimal factors, r^{op} and e^{op} , and substituting the average into equations (10.79) or (10.82).

By increasing η^{sm} , the rest of the bars in Figure 10.9 can be obtained. When $\eta^{sm} \neq 0$, the revenue and rebate of using regular and economic charging power are determined by randomly assigned r . The revenue and rebate of using the smart charging are assigned by taking their average, individually, after multiple iteration (350 iterations) as recommended in [258].

From Figure 10.9 to 10.13, it is noted that:

- the annual revenue changes slightly as the penetration of the smart charging increases. This means that as the revenue of using the premium power decreases, it is compensated by using the regular and economic charging powers. Therefore, the proposed smart charging preserves the annual revenue.
- the annual revenue is increased as the energy required from the FCS is increased (i.e. increased from \underline{U} to \bar{U} as presented in Figures 10.9 and 10.13).
- the rebate is increased as the penetration of the smart charging is increased (i.e., η^{sm} increased considering the same Figure 10.9).
- also, the amount of the annual rebate is increased as the annual energy required from the FCS is increased (i.e. increased from U_{min} to U_{max} as shown in Figures 10.9 and 10.13).

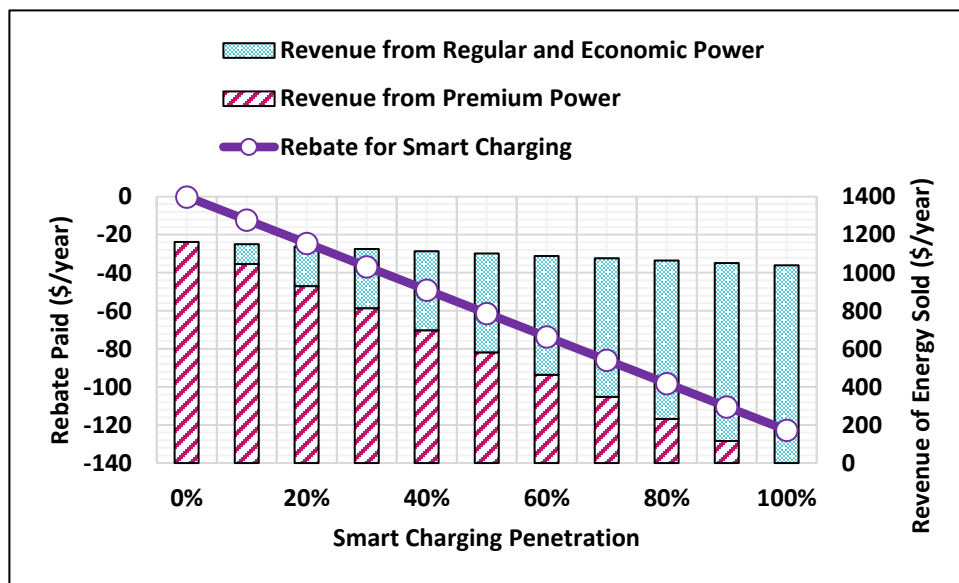


Figure 10.9 Revenue and Rebate of the Minimum Annual Charging Energy

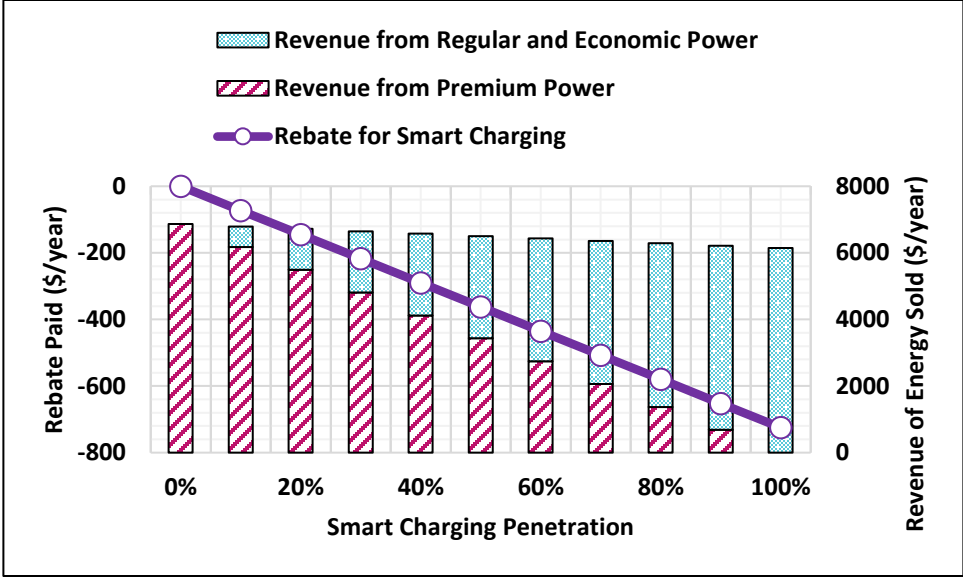


Figure 10.10 Revenue and Rebate of the 25th percentile Annual Charging Energy

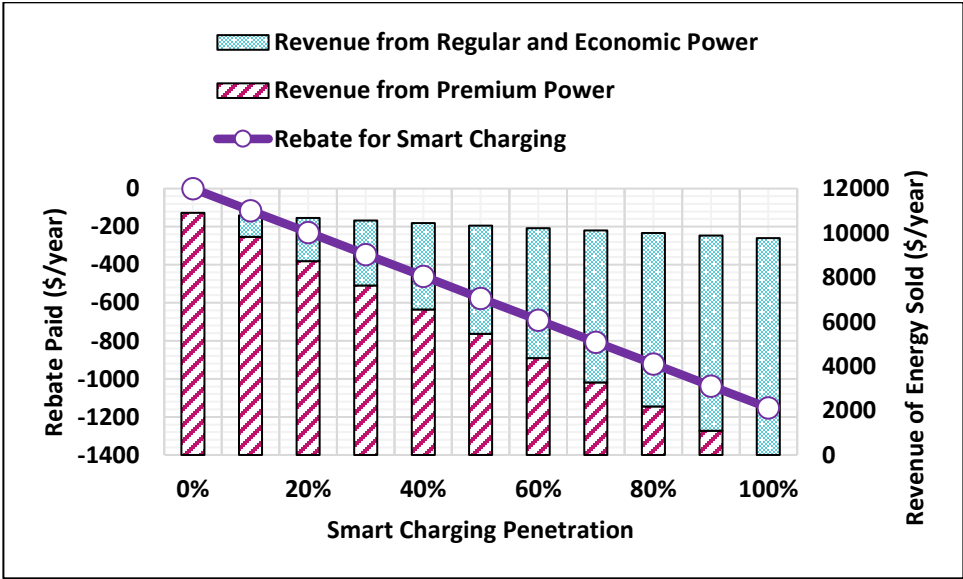


Figure 10.11 Revenue and Rebate of the Median Annual Charging Energy

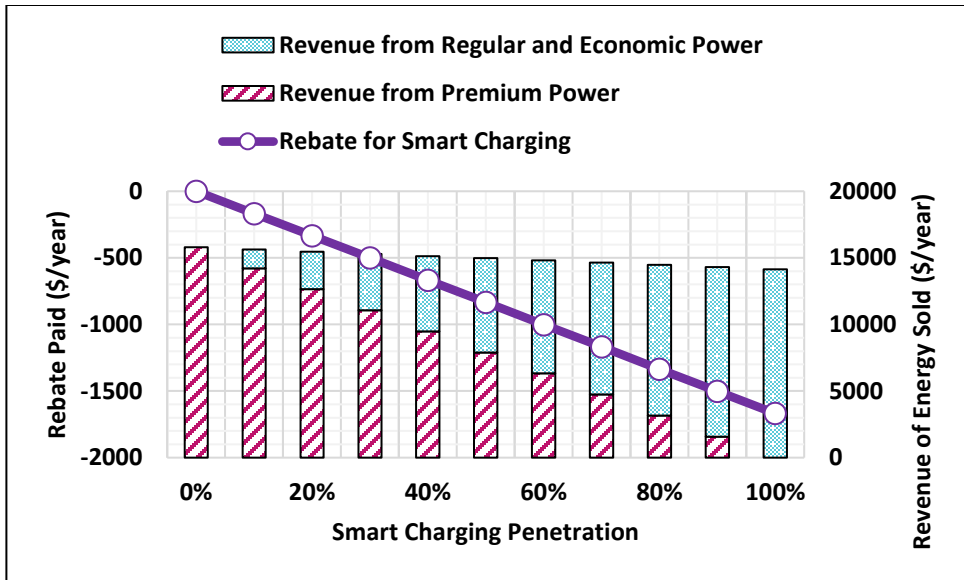


Figure 10.12 Revenue and Rebate of the 75th percentile Annual Charging Energy

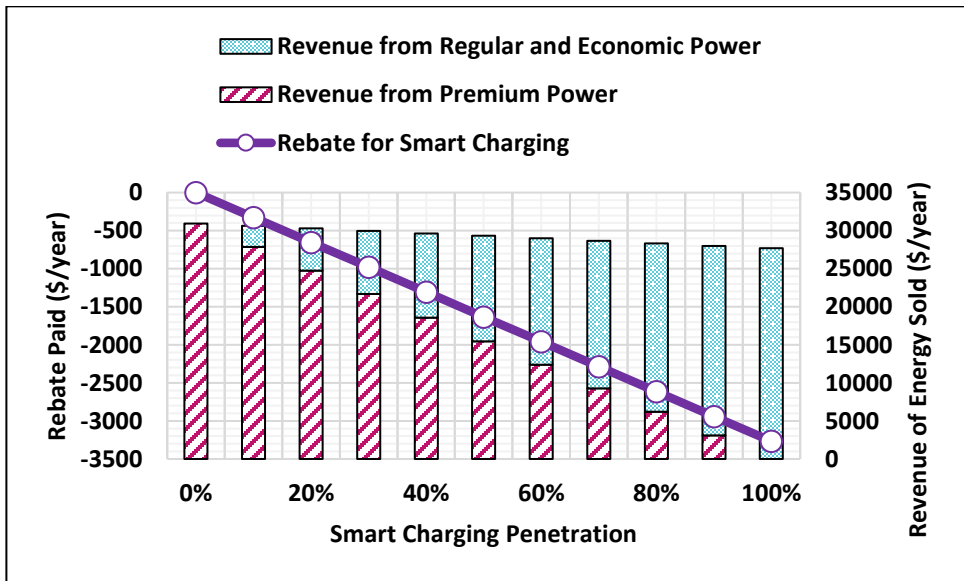


Figure 10.13 Revenue and Rebate of the Maximum Annual Charging Energy

10.9.6 Cost Comparison of the Proposed Smart Charging and DSTATCOM

As per the utility general standard practice, if flicker complaints result from the operation of the customer's equipment, the customer's equipment shall be disconnected. From the viewpoint of the investor, the main benefit of mitigation of

the flicker is to avoid the service disconnection on the facility. The utility point of view is to protect their equipment as well as nearby customers.

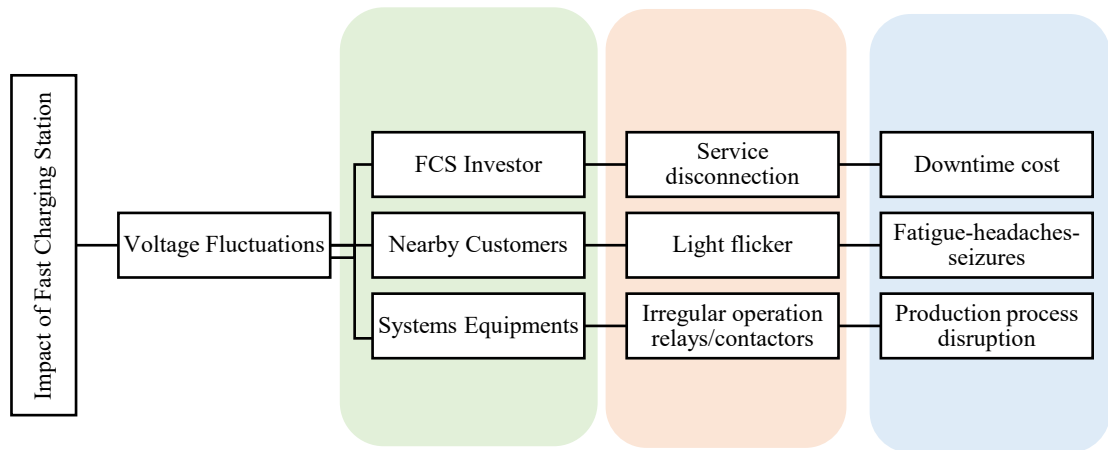


Figure 10.14 Effect of Voltage Fluctuations on Different Stakeholders

When the operation of fast charging stations causes a voltage fluctuation and light flicker, the FCSs may get disconnected resulting in financial losses. The financial losses are represented by the FCS downtime. The downtime is the total amount of time that the FCS is not accessible. The FCS downtime and its losses can be interpreted as the cost of voltage flicker incurred by the FCS’s owner.

In order to avoid FCS downtime, voltage fluctuation and light flicker should be mitigated. In chapter 4, several flicker mitigation devices are analyzed and compared, based on different criteria. It was found that the cheapest mitigation device is the

DSTATCOM, according to the cost per kVAr basis and the total annual equivalent cost. The total annual equivalent cost of DSTATCOM is 14,568 \$/year.

The proposed smart charging in this study can also be utilized to mitigate the voltage fluctuation and light flicker. To make customers adopt the proposed smart charging, an instant rebate is paid to the customer for each charging event from the FCS, as explained in 10.7. The annual rebate can be interpreted as the annual cost incurred by the FCS to mitigate the light flicker thereby avoiding financial losses due to the FCS downtime. The annual rebate is a function of the annual penetration of smart charging, as illustrated in section 10.9.5. Figure 10.15 shows the annual rebates of different penetrations of the proposed smart charging.

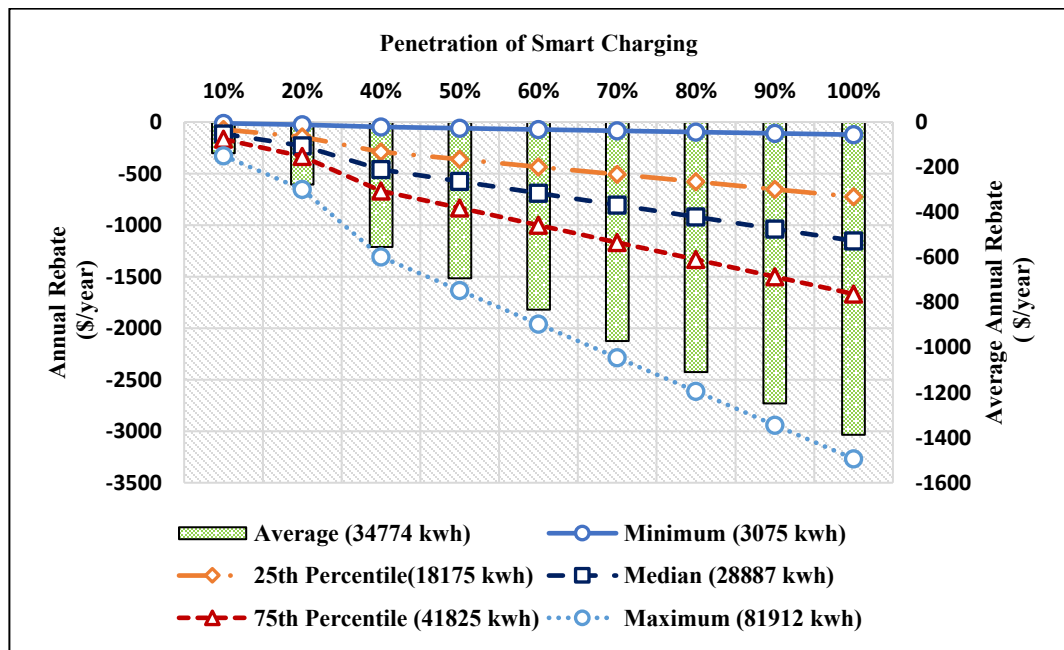


Figure 10.15 Annual Cost of the Proposed Smart Charging

As presented in Figure 10.15, the rebate is not only a function of the penetration of the smart charging, but is also a function of the minimum, maximum, 25th, 50th, and 75th percentiles of annual energy required from the FCS. To compare the annual cost

of the smart charging with the annual cost of the DSTATCOM, the annual average rebate of using the smart charging is calculated. The annual average rebate is estimated by averaging the values of equations (10.39) – (10.43). From Figure 10.15, it is noted that the average rebate increases from nearly \$140 to \$1400 as the smart charging penetration increases from 10% to 100%. This means that the minimum annual cost incurred by the FCS when the proposed smart charging is applied is \$140, whereas the maximum annual incurred cost by the FCS is \$1400.

Figure 10.16 represents the cost percentage decrease when the proposed smart charging is utilized, in comparison to the cost of DSTATCOM. The annual cost of the proposed smart charging is reduced by a minimum of 90% to a maximum of 99% of the cost of the DSTATCOM, in comparison to the annual cost of the DSTATCOM. Figure 10.16 clearly shows that the proposed smart charging achieves a tremendous reduction in the cost of mitigating voltage fluctuation and light flicker.

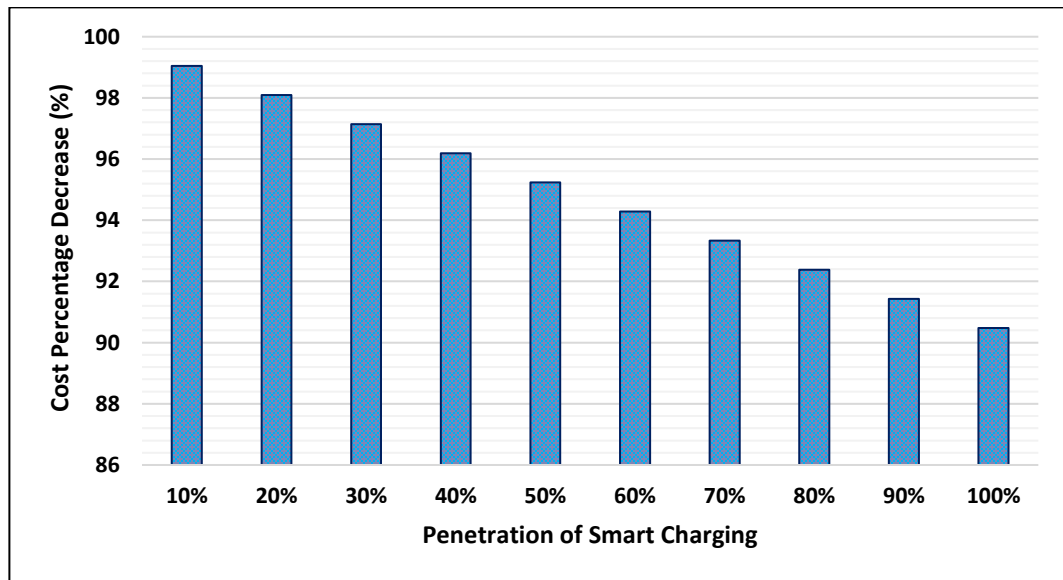


Figure 10.16 Comparison of Costs of the Proposed Smart Charging and DSTATCOM

Chapter 11. Conclusion and Future Work

11.1 Summary and Conclusions

The goal of the research in this thesis was to quantify the impact of integrating the fast charging station on the voltage fluctuation and light flicker, and to mitigate that impact. The motivation for the study was explained in Chapter 1 as well as the objectives.

In Chapter 2, the previous work related to the impacts and mitigation techniques of FCSs are reviewed. The chapter can be classified into two parts: the first part aimed to review the impacts of FCSs reported by the previous studies; the second part attempted to investigate the proposed mitigation methods for the anticipated impacts of FCSs found according to the first part. In this chapter, the impacts of FCS were surveyed from two perspectives: the first was on the power quality of distribution systems while the second was on generating the demand profile of the FCS.

In Chapter 3, the response of lighting technology to voltage fluctuation has been discussed. Characteristics of different types of lamps such as lifetime, efficacy, cost, and market share were presented. The adverse impacts of voltage fluctuation on the lighting technology and the power system were indicated. Several flicker metrics were explained in this chapter as well as the flicker response of different types of lamps.

In Chapter 4, mitigation of voltage fluctuation and light flicker has been discussed. The standard utility practice when a customer's equipment violates the flicker limit as well as the responsibility to mitigate that violation are presented. Multiples voltage

fluctuation mitigation technologies were reviewed and compared based on different criteria such as their control range, harmonic content, losses, overload capability, and response time. Besides, this chapter attempted to quantify and compare the costs of several flicker mitigation devices, considering the initial purchase price and the maintenance costs. Also, the advantages and the disadvantages of these flicker mitigation devices were discussed in this chapter. The best flicker mitigation device was selected according as per these comparisons.

In Chapter 5, an overview of electric distribution networks was introduced. Overhead and underground main components, whether in the primary or secondary systems, were explained and their functions were illustrated as well.

In Chapter 6, benchmark models for residential and multiple commercial loads, located in different cities, are utilized to develop corresponding probabilistic profiles. The cities are classified based on their climate zones the corresponding residential and commercial profiles are grouped accordingly. Each profile of each group is divided based on the seasons into four subgroups and then each subgroup is further divided into weekdays and weekends. The principle component analysis is applied to reduce and prepare the aggregated data in each subgroup for the clustering using the k-means method. The cluster is evaluated using supervised and unsupervised validity indices. The obtained load profiles are utilized to represent the loads in the electric distribution system under study.

In Chapter 7, a probabilistic charging profile was proposed to represent the fast charging stations energy requirements when they are utilized by PBEVs. Several

parameters were considered to generate the probabilistic profiles such as number of electric vehicles, size of battery capacities, arriving rate and time, battery state-of-charge at the time of arrival, and length of time with a battery drawn power from the charger. The Markov Chain Monte Carlo, relying on Metropolis-Hastings sampler, was utilized to estimate these parameters based on selected distributions. Also, two charging methods were explained in this chapter: the first method assumes that the output power of the charging station is estimated, and the second method presumes that the output power is actual.

In Chapter 8, the test system is developed and modified to include fast charging stations, commercial loads, and residential houses. Different scenarios were applied on the test system, to quantify the impact of the FCSs on the voltage quality, and to mitigate that impact by different mitigation devices such as DSTATCOMDs and battery energy storage unit. The voltage quality of each scenario in this chapter was analyzed based on three different assessment methods: the voltage range, the voltage unbalance, and the voltage fluctuation and light flicker.

In Chapter 9, a novel smart charging approach is proposed to mitigate the impact of voltage fluctuation and light flicker. The proposed charging method assumes that the same port of the fast charger can provide three different charging powers, namely economic, regular, and premium. Selection of the charging power is determined by the customer, but their charging rates are defined by the FCS operator/investor and can be changed within the day according to different variables such as system peak, FCS demand, and the local level of the produced renewable energy. Objective and

constraints of the smart charging are included in this chapter. Effect of the proposed charging on the charging duration as well as the effect of full charging of batteries are analyzed. Two case studies were conducted in this chapter to evaluate impacts of the proposed charging method as well as uncontrolled charging, on voltage fluctuation and light flicker. A comparative study is presented in this chapter to compare results of the proposed method with the relevant work.

In Chapter 10, the per unit cost and time of the proposed smart charging are determined. The per unit regular/economic charging cost is modeled to be a function of the per unit cost of premium charging power and a scaling factor. A scaling factor is proposed to represent a rebate offered to the customer to adopt the regular and economic charging powers. The rebate is designed to compensate the increase in the charging duration by reducing the per unit cost of regular and economic charging power. The cost is modeled to preserve a balance in the required cost to charge 1kwh by the regular or economic power to the required time to charge 1kwh by the premium power, and vice versa. The annual cost of the proposed smart charging is estimated in this chapter and compared with the cost of best flicker mitigation device as selected in Chapter 4.

The main findings of this thesis are as follows:

- Results reveal that integrating the fast charging station has adverse impacts on the voltage fluctuations which lead to light flicker. The impact is a function of different parameters such as the rated power of the charger, the

number of chargers in the station, and share of vehicles charges from the fast charging station.

- The study shows that flicker response of different types of lamps is varied. Some of modern lamps are immune to flicker. Nevertheless, the voltage fluctuation still has adverse impact on power system equipment and may lead them to irregular operation.
- Results indicate that voltage fluctuation and light flicker caused by integrating the fast charging station can be mitigated. Among several mitigation devices, the distribution static compensator is selected according to the defined criteria in this study. The study shows that not only the voltage fluctuation is mitigated by the distribution static compensator, but also the voltage unbalance in the system is reduced. Nevertheless, the cost of the distribution static compensators is very high (14,568 \$/year), and it is not reasonable to be incurred by the fast charging station operator/investor.
- When the uncontrolled charging method is applied, the flicker limit is exceeded when the demand on the fast charging station is increased by 20%. In contrast, the proposed smart charging can mitigate the voltage fluctuation and light flicker even though when the penetration on the FCS is increased by 50%.
- Three different charging powers are proposed in the smart charging: the premium, regular, and economic charging power. A rebate is given to customer to adopt the smart charging. Results reveal that as the smart

charging penetration increases from 10% to 100% the average annual rebate increases from \$140 to \$1400. The annual cost of the proposed smart charging is less than the annual cost of the DSTATCOM by a minimum of 90% to a maximum of 99%.

- Results show that the required time to charge 1kwh by premium, regular and economic powers are 1.333, 1.449, and 1.532 minute/kwh, respectively. The proposed cost to charge 1kwh by the aforementioned powers are 0.377, 0.347, and 0.328 \$/kwh. The ratio of time required by premium power to the time required by regular and economic power are 0.92 and 0.87 whereas the ratio of the cost incurred by using premium power to regular and economic powers are 1.08 and 1.14. This means that when premium power is used, the required time to charge 1kwh are decreased by 8% and 14% than the required time to charge the same energy by regular and economic power, but the incurred cost of using the premium power are increased by 8% and 14% than the incurred cost when the regular and economic charging power are utilized, and vice versa.

11.2 Research Contributions of the Thesis

The main contributions of this research are as follows:

- Proposing a novel smart charging approach that quantifies and mitigates the impact of FCS on the voltage fluctuation and light flicker.
- The development of a novel set of smart charging constraints which offers more flexibility to customers than those currently in the literature, in which

customer can select the charging power according to customer's priority whether to time or the cost.

- The development of a novel cost model of the proposed smart charging that preserves the balance of customer's value of time and value cost.
- Developing probabilistic demand profiles for FCS based on two approaches: when the output power of FCSs are estimated, and when the output power of FCSs are actual.
- Estimating the cost of several voltage fluctuation mitigation devices and compared them based on different criteria such as their response time, losses, harmonic content, and control range.
- Proposing probabilistic models at different climate zones for different commercial and residential loads.

11.3 Future Work

Different topics related to this work can be investigated in the future. Some of these topics are as follow:

- Equipping the fast charging station with photovoltaics may contribute positively to reduce the difference between the premium to the regular and economic charging powers; however, the photovoltaics may contribute negatively on the flicker level. A future work can be conducted to determine the effect.

- The proposed smart charging in this thesis mainly aims to reduce the voltage fluctuation and flicker level and to balance the customer's value of time to the value of cost. The first aim is for benefit of the FCS investor while the second is for benefit of the customer. Reducing the system peak was not considered and it is a benefit for the system operator. The smart charging can be formulated to consider the system peak and the time-of-use price in its constraints, which is open the door for a future work.
- Studying the impacts of the climate zones on EV driving patterns, which impacts the charging patterns and affecting several power components in the distribution grids.

Bibliography

- [1]H. Lee and G. Lovellette, “Will Electric Cars Transform the U.S. Market?,” *SSRN Electron. J.*, 2011, doi: 10.2139/ssrn.1927351.
- [2]S. C. Davis and R. G. Boundy, “Transportation Energy Data Book Edition 37,” Oak Ridge National Laboratory, Retrieved from <http://cta.ornl.gov/data>, 2019.
- [3]Colin McKerracher, “Electric Vehicle Outlook 2018.” Bloomberg New Energy Finance, Accessed: Apr. 04, 2019. [Online]. Available: <https://about.bnef.com/electric-vehicle-outlook/>.
- [4]S. Howell, H. Lee, and A. Heal, “Leapfrogging or Stalling Out? Electric Vehicles in China,” *SSRN Electron. J.*, 2014, doi: 10.2139/ssrn.2493131.
- [5]S. M. Alshareef and W. G. Morsi, “Impact of fast charging stations on the voltage flicker in the electric power distribution systems,” in *2017 IEEE Electrical Power and Energy Conference (EPEC)*, Saskatoon, SK, Oct. 2017, pp. 1–6, doi: 10.1109/EPEC.2017.8286226.
- [6]L. Xu, M. Marshall, and L. Dow, “A framework for assessing the impact of plug-in electric vehicle to distribution systems,” in *2011 IEEE/PES Power Systems Conference and Exposition*, Phoenix, AZ, USA, Mar. 2011, pp. 1–6, doi: 10.1109/PSCE.2011.5772531.
- [7]A. Zahedmanesh, D. Sutanto, and K. M. Muttaqi, “Analyzing the impacts of charging plug-in electric vehicles in low voltage distribution networks: A case study of utilization of droop charging control system based on the SAE J1772 Standard,” in *2017 Australasian Universities Power Engineering Conference (AUPEC)*, Melbourne, VIC, Nov. 2017, pp. 1–6, doi: 10.1109/AUPEC.2017.8282409.
- [8]H. Ramadan, A. Ali, and C. Farkas, “Assessment of plug-in electric vehicles charging impacts on residential low voltage distribution grid in Hungary,” in *2018 6th International Istanbul Smart Grids and Cities Congress and Fair (ICSG)*, Istanbul, Apr. 2018, pp. 105–109, doi: 10.1109/SGCF.2018.8408952.
- [9]L. Pieltain Fernandez, T. Gomez San Roman, R. Cossent, C. Mateo Domingo, and P. Frias, “Assessment of the Impact of Plug-in Electric Vehicles on Distribution Networks,” *IEEE Trans. Power Syst.*, vol. 26, no. 1, pp. 206–213, Feb. 2011, doi: 10.1109/TPWRS.2010.2049133.
- [10] M. J. M. Al Essa and L. M. Cipcigan, “Effects of randomly charging electric vehicles on voltage unbalance in micro grids,” in *2015 50th International Universities Power Engineering Conference (UPEC)*, Stoke On Trent, United Kingdom, Sep. 2015, pp. 1–6, doi: 10.1109/UPEC.2015.7339906.

- [11] K. Zafred, J. Nieto-Martin, and E. Butans, “Electric Vehicles - effects on domestic low voltage networks,” in *2016 IEEE International Energy Conference (ENERGYCON)*, Leuven, Belgium, Apr. 2016, pp. 1–6, doi: 10.1109/ENERGYCON.2016.7514060.
- [12] M. S. Islam, N. Mithulananthan, and K. Bhumkittipich, “Feasibility of PV and battery energy storage based EV charging in different charging stations,” in *2016 13th International Conference on Electrical Engineering/Electronics, Computer, Telecommunications and Information Technology (ECTI-CON)*, Chiang Mai, Thailand, Jun. 2016, pp. 1–6, doi: 10.1109/ECTICon.2016.7561448.
- [13] B. Rotthier, T. Van Maerhem, P. Blockx, P. Van den Bossche, and J. Cappelle, “Home charging of electric vehicles in Belgium,” in *2013 World Electric Vehicle Symposium and Exhibition (EVS27)*, Barcelona, Spain, Nov. 2013, pp. 1–6, doi: 10.1109/EVS.2013.6914759.
- [14] P. Richardson, D. Flynn, and A. Keane, “Impact assessment of varying penetrations of electric vehicles on low voltage distribution systems,” in *IEEE PES General Meeting*, Minneapolis, MN, Jul. 2010, pp. 1–6, doi: 10.1109/PES.2010.5589940.
- [15] B. Marah, Y. R. Bhavanam, G. A. Taylor, and A. O. Ekwue, “Impact of electric vehicle charging systems on low voltage distribution networks,” in *2016 51st International Universities Power Engineering Conference (UPEC)*, Coimbra, Sep. 2016, pp. 1–6, doi: 10.1109/UPEC.2016.8114052.
- [16] L. Pinter and C. Farkas, “Impacts of electric vehicle chargers on the power grid,” in *2015 5th International Youth Conference on Energy (IYCE)*, Pisa, Italy, May 2015, pp. 1–6, doi: 10.1109/IYCE.2015.7180811.
- [17] P. Lico, M. Marinelli, K. Knezovic, and S. Grillo, “Phase balancing by means of electric vehicles single-phase connection shifting in a low voltage Danish grid,” in *2015 50th International Universities Power Engineering Conference (UPEC)*, Stoke On Trent, United Kingdom, Sep. 2015, pp. 1–5, doi: 10.1109/UPEC.2015.7339967.
- [18] D. Wu, Chengrui Cai, and D. C. Aliprantis, “Potential impacts of aggregator-controlled plug-in electric vehicles on distribution systems,” in *2011 4th IEEE International Workshop on Computational Advances in Multi-Sensor Adaptive Processing (CAMSAP)*, San Juan, PR, USA, Dec. 2011, pp. 105–108, doi: 10.1109/CAMSAP.2011.6135898.
- [19] L. Pinter, “Statistical analysis of the electric vehicle chargers’ impacts on the low-voltage distribution system,” in *2016 18th Mediterranean Electrotechnical Conference (MELECON)*, Lemesos, Cyprus, Apr. 2016, pp. 1–6, doi: 10.1109/MELCON.2016.7495304.
- [20] S. Pazouki, A. Mohsenzadeh, and M.-R. Haghifam, “The effect of aggregated plug-in electric vehicles penetrations in charging stations on electric distribution networks

reliability,” in *2014 Smart Grid Conference (SGC)*, Tehran, Dec. 2014, pp. 1–5, doi: 10.1109/SGC.2014.7090883.

[21] A. Dubey, S. Santoso, and M. P. Cloud, “Understanding the effects of electric vehicle charging on the distribution voltages,” in *2013 IEEE Power & Energy Society General Meeting*, Vancouver, BC, 2013, pp. 1–5, doi: 10.1109/PESMG.2013.6672557.

[22] H. Committee, “SAE electric vehicle and plug in hybrid electric vehicle conductive charge coupler,” *SAE Int. Detroit Mich. Stand. J.*, vol. 1772, 2016.

[23] O. Veneri, C. Capasso, L. Ferraro, and A. Del Pizzo, “Performance analysis on a power architecture for EV ultra-fast charging stations,” in *2013 International Conference on Clean Electrical Power (ICCEP)*, Alghero, Italy, Jun. 2013, pp. 183–188, doi: 10.1109/ICCEP.2013.6586987.

[24] K. Yunus, H. Z. De La Parra, and M. Reza, “Distribution grid impact of plug-in electric vehicles charging at fast charging stations using stochastic charging model,” in *Power Electronics and Applications (EPE 2011), Proceedings of the 2011-14th European Conference on*, 2011, pp. 1–11.

[25] C. Sourkounis and N. Becker, “Efficient operation of high power charging stations in weak grids,” in *MedPower 2014*, Athens, Greece, 2014, p. 14 (5 .)-14 (5 .), doi: 10.1049/cp.2014.1647.

[26] R. Pawelek, P. Kelm, and I. Wasiak, “Experimental analysis of DC electric vehicles charging station operation and its impact on the supplying grid,” in *2014 IEEE International Electric Vehicle Conference (IEVC)*, Florence, Italy, Dec. 2014, pp. 1–4, doi: 10.1109/IEVC.2014.7056152.

[27] C. Roe, A. P. Meliopoulos, J. Meisel, and T. Overbye, “Power System Level Impacts of Plug-In Hybrid Electric Vehicles Using Simulation Data,” in *2008 IEEE Energy 2030 Conference*, Atlanta, GA, USA, Nov. 2008, pp. 1–6, doi: 10.1109/ENERGY.2008.4781048.

[28] M. Kintner-Meyer, K. Schneider, and R. Pratt, “Impacts assessment of plug-in hybrid vehicles on electric utilities and regional US power grids, Part 1: Technical analysis,” *Pac. Northwest Natl. Lab.*, vol. 1, pp. 1–20, 2007.

[29] Energy Efficiency and Renewable Energy-U.S. Department of Energy, “Summary Report - Discussion Meeting on Plug-In Hybrid Electric Vehicles,” Accessed: Mar. 01, 2018. [Online]. Available: https://www1.eere.energy.gov/vehiclesandfuels/pdfs/program/plug-in_summary_rpt.pdf.

[30] L. Dow, M. Marshall, Le Xu, J. Romero Aguero, and H. L. Willis, “A novel approach for evaluating the impact of electric vehicles on the power distribution system,” in *IEEE PES General Meeting*, Minneapolis, MN, Jul. 2010, pp. 1–6, doi: 10.1109/PES.2010.5589507.

- [31] G. Mauri and A. Valsecchi, “Fast charging stations for electric vehicle: The impact on the mv distribution grids of the milan metropolitan area,” in *2012 IEEE International Energy Conference and Exhibition (ENERGYCON)*, Florence, Italy, Sep. 2012, pp. 1055–1059, doi: 10.1109/EnergyCon.2012.6347725.
- [32] B. Pea-da and S. Dechanupaprittha, “Impact of fast charging station to voltage profile in distribution system,” in *2014 International Electrical Engineering Congress (iEECON)*, Chonburi, Thailand, Mar. 2014, pp. 1–4, doi: 10.1109/iEECON.2014.6925934.
- [33] A. Bosovic, M. Music, and S. Sadovic, “Analysis of the impacts of plug-in electric vehicle charging on the part of a real low voltage distribution network,” in *2015 IEEE Eindhoven PowerTech*, Eindhoven, Netherlands, Jun. 2015, pp. 1–5, doi: 10.1109/PTC.2015.7232401.
- [34] M. Gjelaj, C. Traeholt, S. Hashemi, and P. B. Andersen, “Optimal design of DC fast-charging stations for EVs in low voltage grids,” in *2017 IEEE Transportation Electrification Conference and Expo (ITEC)*, Chicago, IL, USA, Jun. 2017, pp. 684–689, doi: 10.1109/ITEC.2017.7993352.
- [35] Y. H. Febriwijaya, A. Purwadi, A. Rizqiawan, and N. Heryana, “A study on the impacts of DC Fast Charging Stations on power distribution system,” in *2014 International Conference on Electrical Engineering and Computer Science (ICEECS)*, Kuta, Bali, Indonesia, Nov. 2014, pp. 136–140, doi: 10.1109/ICEECS.2014.7045233.
- [36] M. Gjelaj, C. Traholt, S. Hashemi, and P. B. Andersen, “Cost-benefit analysis of a novel DC fast-charging station with a local battery storage for EVs,” in *2017 52nd International Universities Power Engineering Conference (UPEC)*, Heraklion, Aug. 2017, pp. 1–6, doi: 10.1109/UPEC.2017.8231973.
- [37] K. Joshi and A. Lakum, “Assessing the impact of Plug-in Hybrid Electric Vehicles on distribution network operations using Time-Series Distribution Power Flow analysis,” in *2014 IEEE International Conference on Power Electronics, Drives and Energy Systems (PEDES)*, Mumbai, India, Dec. 2014, pp. 1–6, doi: 10.1109/PEDES.2014.7042120.
- [38] B. Pea-da and S. Dechanupaprittha, “Impact analysis of fast charging to voltage profile in PEA distribution system by Monte Carlo simulation,” in *2015 7th International Conference on Information Technology and Electrical Engineering (ICITEE)*, Chiang Mai, Thailand, Oct. 2015, pp. 204–208, doi: 10.1109/ICITEED.2015.7408942.
- [39] V. Salapic, M. Grzanic, and T. Capuder, “Optimal sizing of battery storage units integrated into fast charging EV stations,” in *2018 IEEE International Energy Conference (ENERGYCON)*, Limassol, Jun. 2018, pp. 1–6, doi: 10.1109/ENERGYCON.2018.8398789.

- [40] S. M. Alshareef and W. G. Morsi, "Impact of fast charging stations on the voltage flicker in the electric power distribution systems," in *2017 IEEE Electrical Power and Energy Conference (EPEC)*, Saskatoon, SK, Oct. 2017, pp. 1–6, doi: 10.1109/EPEC.2017.8286226.
- [41] H. Zhang, S. J. Moura, Z. Hu, and Y. Song, "PEV Fast-Charging Station Siting and Sizing on Coupled Transportation and Power Networks," *IEEE Trans. Smart Grid*, vol. 9, no. 4, pp. 2595–2605, Jul. 2018, doi: 10.1109/TSG.2016.2614939.
- [42] Md. M. Islam, H. Shareef, and A. Mohamed, "Optimal location and sizing of fast charging stations for electric vehicles by incorporating traffic and power networks," *IET Intell. Transp. Syst.*, vol. 12, no. 8, pp. 947–957, Oct. 2018, doi: 10.1049/iet-its.2018.5136.
- [43] H. Zhang, S. J. Moura, Z. Hu, W. Qi, and Y. Song, "A Second-Order Cone Programming Model for Planning PEV Fast-Charging Stations," *IEEE Trans. Power Syst.*, vol. 33, no. 3, pp. 2763–2777, May 2018, doi: 10.1109/TPWRS.2017.2754940.
- [44] H. Zhang, Z. Hu, Z. Xu, and Y. Song, "An Integrated Planning Framework for Different Types of PEV Charging Facilities in Urban Area," *IEEE Trans. Smart Grid*, vol. 7, no. 5, pp. 2273–2284, Sep. 2016, doi: 10.1109/TSG.2015.2436069.
- [45] G. Joos, M. de Freige, and M. Dubois, "Design and simulation of a fast charging station for PHEV/EV batteries," in *2010 IEEE Electrical Power & Energy Conference*, Halifax, NS, Canada, Aug. 2010, pp. 1–5, doi: 10.1109/EPEC.2010.5697250.
- [46] T. Pothinun and S. Premrudeepreechacharn, "Power Quality Impact of Charging Station on MV Distribution Networks: A Case Study in PEA Electrical Power System," in *2018 53rd International Universities Power Engineering Conference (UPEC)*, Glasgow, United Kingdom, Sep. 2018, pp. 1–6, doi: 10.1109/UPEC.2018.8541921.
- [47] Chun-Lien Su, Hai-Ming Chin, Rong-Ceng Leou, and Chien-Hung Lin, "Power quality measurements of distribution systems with LRT ultra-fast charging infrastructures," in *2017 IEEE 3rd International Future Energy Electronics Conference and ECCE Asia (IFEEEC 2017 - ECCE Asia)*, Kaohsiung, Taiwan, Jun. 2017, pp. 823–827, doi: 10.1109/IFEEEC.2017.7992146.
- [48] Q. Li, S. Tao, X. Xiao, and J. Wen, "Monitoring and analysis of power quality in electric vehicle charging stations," in *2013 1st International Future Energy Electronics Conference (IFEEEC)*, Tainan, Taiwan, Nov. 2013, pp. 277–282, doi: 10.1109/IFEEEC.2013.6687516.
- [49] R. J. C. Pinto, J. Pombo, M. R. A. Calado, and S. J. P. S. Mariano, "An electric vehicle charging station: Monitoring and analysis of power quality," in *2015 9th International Conference on Compatibility and Power Electronics (CPE)*, Costa da Caparica, Portugal, Jun. 2015, pp. 37–42, doi: 10.1109/CPE.2015.7231046.

- [50] D. Meyer and J. Wang, “Integrating ultra-fast charging stations within the power grids of smart cities: a review,” *IET Smart Grid*, vol. 1, no. 1, pp. 3–10, Apr. 2018, doi: 10.1049/iet-stg.2018.0006.
- [51] B. EN, “50160: 2010 Voltage characteristics of electricity supplied by public electricity networks,” *Br. Stand. Inst.*, 2011.
- [52] A. Bosovic, M. Music, and S. Sadovic, “Analysis of the impacts of plug-in electric vehicle charging on the part of a real medium voltage distribution network,” in *IEEE PES Innovative Smart Grid Technologies, Europe*, Istanbul, Turkey, Oct. 2014, pp. 1–7, doi: 10.1109/ISGTEurope.2014.7028830.
- [53] “IEEE Recommended Practice and Requirements for Harmonic Control in Electric Power Systems,” *IEEE Std 519-2014 Revis. IEEE Std 519-1992*, pp. 1–29, Jun. 2014, doi: 10.1109/IEEESTD.2014.6826459.
- [54] “American National Standard for Electric Power Systems and Equipment—Voltage Ratings (60 Hz).” <https://www.nema.org/Standards/Pages/American-National-Standard-for-Electric-Power-Systems-and-Equipment-Voltage-Ratings.aspx> (accessed Dec. 29, 2018).
- [55] C. A. Roe, “Power system impacts of plug-in hybrid electric vehicles.” Georgia Institute of Technology, 2009, [Online]. Available: https://smartech.gatech.edu/bitstream/handle/1853/29636/roe_curtis_a_200908_mast.pdf.pdf.
- [56] F. H. Malik and M. Lehtonen, “Analysis of power network loading due to fast charging of Electric Vehicles on highways,” in *2016 Electric Power Quality and Supply Reliability (PQ)*, Tallinn, Estonia, Aug. 2016, pp. 101–106, doi: 10.1109/PQ.2016.7724097.
- [57] C.-M. Chan, H.-R. Liou, and C.-N. Lu, “Operation of distribution feeders with electric vehicle charging loads,” in *2012 IEEE 15th International Conference on Harmonics and Quality of Power*, Hong Kong, China, Jun. 2012, pp. 695–700, doi: 10.1109/ICHQP.2012.6381197.
- [58] S. Negarestani, M. Fotuhi-Firuzabad, M. Rastegar, and A. Rajabi-Ghahnavieh, “Optimal Sizing of Storage System in a Fast Charging Station for Plug-in Hybrid Electric Vehicles,” *IEEE Trans. Transp. Electrification*, vol. 2, no. 4, pp. 443–453, Dec. 2016, doi: 10.1109/TTE.2016.2559165.
- [59] U.S. Department of Transportation, Federal Highway Administration., “National Household Travel Survey (2015),” Accessed: Dec. 30, 2018. [Online]. Available: <https://nhts.ornl.gov/>.

- [60] F. A. V. Pinto, L. H. M. K. Costa, D. S. Menasche, and M. D. de Amorim, "Space-Aware Modeling of Two-Phase Electric Charging Stations," *IEEE Trans. Intell. Transp. Syst.*, vol. 18, no. 2, pp. 450–459, Feb. 2017, doi: 10.1109/TITS.2016.2580127.
- [61] M. Gjelij, S. Hashemi, C. Traeholt, and P. B. Andersen, "Grid integration of DC fast-charging stations for EVs by using modular li-ion batteries," *IET Gener. Transm. Distrib.*, vol. 12, no. 20, pp. 4368–4376, Nov. 2018, doi: 10.1049/iet-gtd.2017.1917.
- [62] D. Tang, P. Wang, and Q. Wu, "Probabilistic modeling of nodal electric vehicle load due to fast charging stations," in *2016 International Conference on Probabilistic Methods Applied to Power Systems (PMAPS)*, Beijing, Oct. 2016, pp. 1–7, doi: 10.1109/PMAPS.2016.7764219.
- [63] W. A. V. Clark, Y. Huang, and S. Withers, "Does commuting distance matter? Commuting tolerance and residential change," *Reg. Sci. Urban Econ.*, p. 23, 2003.
- [64] S. Cheng and P.-F. Gao, "Optimal allocation of charging stations for electric vehicles in the distribution system," in *2018 3rd International Conference on Intelligent Green Building and Smart Grid (IGBSG)*, Yi-Lan, Apr. 2018, pp. 1–5, doi: 10.1109/IGBSG.2018.8393550.
- [65] Z. Gao, D. Meyer, and J. Wang, "Visualizing the Impact of PEV Charging on the Power Grid," in *2018 IEEE Transportation Electrification Conference and Expo (ITEC)*, Long Beach, CA, USA, Jun. 2018, pp. 737–743, doi: 10.1109/ITEC.2018.8450103.
- [66] P. Schroeder, L. Kostyniuk, and M. Mack, "2011 national survey of speeding attitudes and behaviors.," United States. National Highway Traffic Safety Administration, 2013. [Online]. Available: <http://74.121.199.247/sites/default/files/pdf/evse/ABBDCFCFactSheetJune2016.pdf>.
- [67] J. Y. Yong, V. K. Ramachandaramurthy, K. M. Tan, A. Arulampalam, and J. Selvaraj, "Modeling of electric vehicle fast charging station and impact on network voltage," in *2013 IEEE Conference on Clean Energy and Technology (CEAT)*, Lankgkawi, Malaysia, Nov. 2013, pp. 399–404, doi: 10.1109/CEAT.2013.6775664.
- [68] G. Celli, G. G. Soma, F. Pilo, F. Lacu, S. Mocci, and N. Natale, "Aggregated electric vehicles load profiles with fast charging stations," in *2014 Power Systems Computation Conference*, Wroclaw, Poland, Aug. 2014, pp. 1–7, doi: 10.1109/PSCC.2014.7038402.
- [69] N. Clinton, and I. Boise, "New York State Electric Vehicle Charging Station Quarterly Report," 2016. [Online]. Available: <https://www.nyserda.ny.gov/-/media/Files/Publications/EV-Charging-Station-Data/2016-EVSE-Q3.pdf>.
- [70] "ABBDCFCFactSheetJune2016.pdf." Accessed: Dec. 29, 2018. [Online]. Available: <https://avt.inl.gov/sites/default/files/pdf/evse/ABBDCFCFactSheetJune2016.pdf>.

- [71] V. M. Iyer, S. Guler, G. Gohil, and S. Bhattacharya, "Extreme fast charging station architecture for electric vehicles with partial power processing," in *2018 IEEE Applied Power Electronics Conference and Exposition (APEC)*, San Antonio, TX, USA, Mar. 2018, pp. 659–665, doi: 10.1109/APEC.2018.8341082.
- [72] I. Pavic, T. Capuder, and I. Kuzle, "A Comprehensive Approach for Maximizing Flexibility Benefits of Electric Vehicles," *IEEE Syst. J.*, vol. 12, no. 3, pp. 2882–2893, Sep. 2018, doi: 10.1109/JSYST.2017.2730234.
- [73] Z. Zhou, M. Benbouzid, J. Frédéric Charpentier, F. Scuiller, and T. Tang, "A review of energy storage technologies for marine current energy systems," *Renew. Sustain. Energy Rev.*, vol. 18, pp. 390–400, Feb. 2013, doi: 10.1016/j.rser.2012.10.006.
- [74] B. Sun, T. Dragicevic, F. D. Freijedo, J. C. Vasquez, and J. M. Guerrero, "A Control Algorithm for Electric Vehicle Fast Charging Stations Equipped With Flywheel Energy Storage Systems," *IEEE Trans. Power Electron.*, vol. 31, no. 9, pp. 6674–6685, Sep. 2016, doi: 10.1109/TPEL.2015.2500962.
- [75] T. Dragicevic, S. Sucic, J. C. Vasquez, and J. M. Guerrero, "Flywheel-Based Distributed Bus Signalling Strategy for the Public Fast Charging Station," *IEEE Trans. Smart Grid*, vol. 5, no. 6, pp. 2825–2835, Nov. 2014, doi: 10.1109/TSG.2014.2325963.
- [76] A. Quadrelli *et al.*, "Power quality conditioning system based on Lithium-Ion Ultracapacitors for Electric Vehicles Quick Charging Stations," in *Electrical Systems for Aircraft, Railway, Ship Propulsion and Road Vehicles (ESARS), 2015 International Conference on*, 2015, pp. 1–6.
- [77] I. S. Bayram, G. Michailidis, M. Devetsikiotis, and F. Granelli, "Electric power allocation in a network of fast charging stations," *IEEE J. Sel. Areas Commun.*, vol. 31, no. 7, pp. 1235–1246, 2013.
- [78] M. Etezadi-Amoli, K. Choma, and J. Stefani, "Rapid-Charge Electric-Vehicle Stations," *IEEE Trans. Power Deliv.*, vol. 25, no. 3, pp. 1883–1887, Jul. 2010, doi: 10.1109/TPWRD.2010.2047874.
- [79] C. Capasso and O. Veneri, "Experimental study of a DC charging station for full electric and plug in hybrid vehicles," *Appl. Energy*, vol. 152, pp. 131–142, 2015.
- [80] T. Zhao, Y. Li, X. Pan, P. Wang, and J. Zhang, "Real-Time Optimal Energy and Reserve Management of Electric Vehicle Fast Charging Station: Hierarchical Game Approach," *IEEE Trans. Smart Grid*, vol. 9, no. 5, pp. 5357–5370, Sep. 2018, doi: 10.1109/TSG.2017.2687522.
- [81] L. Richard and M. Petit, "Fast charging station with battery storage system for ev: Optimal integration into the grid," in *2018 IEEE Power & Energy Society General Meeting (PESGM)*, 2018, pp. 1–5.

- [82] L. Richard and M. Petit, “Fast charging station with battery storage system for EV: Grid services and battery degradation,” in *2018 IEEE International Energy Conference (ENERGYCON)*, Limassol, Jun. 2018, pp. 1–6, doi: 10.1109/ENERGYCON.2018.8398744.
- [83] P. Mastny, J. Moravek, and M. Vrana, “Concept of fast charging stations with integrated accumulators — Assessment of the impact for operation,” in *2016 17th International Scientific Conference on Electric Power Engineering (EPE)*, Prague, Czech Republic, May 2016, pp. 1–6, doi: 10.1109/EPE.2016.7521788.
- [84] M. Molina and P. Mercado, “Control Design and Simulation of DSTATCOM with Energy Storage for Power Quality Improvements,” in *2006 IEEE/PES Transmission & Distribution Conference and Exposition: Latin America*, Caracas, Venezuela, 2006, pp. 1–7, doi: 10.1109/TDCLA.2006.311436.
- [85] M. G. Molina and P. E. Mercado, “Dynamic modeling and control design of DSTATCOM with ultra-capacitor energy storage for power quality improvements,” in *2008 IEEE/PES Transmission and Distribution Conference and Exposition: Latin America*, Bogota, Colombia, Aug. 2008, pp. 1–8, doi: 10.1109/TDC-LA.2008.4641872.
- [86] H. Molavi and M. M. Ardehali, “Application of Distribution Static Compensator (D-STATCOM) to Voltage Sag Mitigation,” *Univers. J. Electr. Electron. Eng.*, vol. 1, no. 2, pp. 11–15, Aug. 2013, doi: 10.13189/ujeee.2013.010201.
- [87] M. Bagheri, V. Nurmanova, O. Abedinia, and M. Salay Naderi, “Enhancing Power Quality in Microgrids With a New Online Control Strategy for DSTATCOM Using Reinforcement Learning Algorithm,” *IEEE Access*, vol. 6, pp. 38986–38996, 2018, doi: 10.1109/ACCESS.2018.2852941.
- [88] M. G. Molina and P. E. Mercado, “Power flow control of microgrid with wind generation using a DSTATCOM-UCES,” in *2010 IEEE International Conference on Industrial Technology*, Vi a del Mar, Chile, 2010, pp. 955–960, doi: 10.1109/ICIT.2010.5472545.
- [89] A. R. Gupta and A. Kumar, “Impact of DG and D-STATCOM Placement on Improving the Reactive Loading Capability of Mesh Distribution System,” *Procedia Technol.*, vol. 25, pp. 676–683, 2016, doi: 10.1016/j.protcy.2016.08.160.
- [90] M. van der Kam and W. van Sark, “Smart charging of electric vehicles with photovoltaic power and vehicle-to-grid technology in a microgrid; a case study,” *Appl. Energy*, vol. 152, pp. 20–30, Aug. 2015, doi: 10.1016/j.apenergy.2015.04.092.
- [91] Z. Moghaddam and D. Habibi, “Smart Charging Strategy for Electric Vehicle Charging Stations,” *IEEE Trans. Transp. ELECTRIFICATION*, vol. 4, no. 1, p. 13, 2018.

- [92] C. Diaz, F. Ruiz, and D. Patino, “Smart charge of an electric vehicles station: A model predictive control approach,” in *2018 IEEE Conference on Control Technology and Applications (CCTA)*, 2018, pp. 54–59.
- [93] A. S. B. Humayd and K. Bhattacharya, “Design of optimal incentives for smart charging considering utility-customer interactions and distribution systems impact,” *IEEE Trans. Smart Grid*, vol. 10, no. 2, pp. 1521–1531, 2017.
- [94] A. Sumper and A. Baggini, Eds., *Electrical Energy Efficiency: Technologies and Applications*. Chichester, UK: John Wiley & Sons, Ltd, 2012.
- [95] Lighting Research and Development, “Solid-State Lighting Research and Development: Multi-Year Program Plan,” Accessed: Feb. 02, 2020. [Online]. Available: https://www1.eere.energy.gov/buildings/publications/pdfs/ssl/ssl_mypp2012_web.pdf.
- [96] R. Cai, J. Cobben, J. Myrzik, and W. Kling, “Flicker curves of different types of lamps,” *China Int. Conf. Electr. Distrib. 2006 Beijing China*, 2006.
- [97] R. Marquardt, “Compact Fluorescent Lamp Recycling Project Phase I Draft Report: Background Research and Program Options,” Accessed: Apr. 02, 2020. [Online]. Available: <https://www.yumpu.com/en/document/read/33598137/compact-fluorescent-lamp-recycling-project-phase-i-draft-report>.
- [98] National Research Council, *Assessment of Advanced Solid State Lighting*. Washington, D.C.: National Academies Press, 2013.
- [99] C. international des grands réseaux électriques C. d’études C4, D. Arlt, and I. Papič, *Review of Flicker Objectives for LV, MV, and HV Systems: Cigre/Cired*. CIGRÉ, 2011.
- [100] M. M. Aman, G. B. Jasmon, H. Mokhlis, and A. H. A. Bakar, “Analysis of the performance of domestic lighting lamps,” *Energy Policy*, vol. 52, pp. 482–500, Jan. 2013, doi: 10.1016/j.enpol.2012.09.068.
- [101] L. Guo, *Intelligent road lighting control systems-experiences, measurements, and lighting control strategies*. Teknillinen korkeakoulu, 2008.
- [102] T. PO and W. QU, “Impact of Power Quality on Lighting Technology (2016),” Accessed: Mar. 02, 2020. [Online]. Available: <http://www.elec.uow.edu.au/apqrc/content/technotes/APQRC%20TN015-1604%20Impact%20of%20PQ%20on%20Lighting.pdf>.
- [103] Office of Energy Efficiency and Renewable Energy, Department of Energy, “Energy Conservation Standards for Fluorescent Lamp Ballasts: Public Meeting and Availability of the Preliminary Technical Support Document,” Accessed: Apr. 02, 2020. [Online]. Available: <https://www.govinfo.gov/content/pkg/FR-2011-04-11/pdf/2011-7592.pdf>.

- [104] D. DiLaura and Illuminating Engineering Society of North America, Eds., *The lighting handbook: reference and application*, 10. ed. New York, NY: Illuminating Engineering Society of North America, 2011.
- [105] DoE, “Lifetime of White LEDs Solid-State Lighting Program: U.S. Department of Energy.” 2011, Accessed: Mar. 24, 2020. [Online]. Available: https://betterbuildingssolutioncenter.energy.gov/sites/default/files/attachments/lifetime_white_leds.pdf.
- [106] U.S. Department of Energy, “Energy Savings Forecast of Solid-State Lighting in General Illumination Applications (2019),” Accessed: Mar. 03, 2020. [Online]. Available: https://www.energy.gov/sites/prod/files/2020/02/f72/2019_ssl-energy-savings-forecast.pdf.
- [107] D. Robinson, S. Perera, V. Gosbell, and V. Smith, “Voltage Fluctuations in the Electric Supply System (2003),” *Technical Note*, Accessed: Mar. 03, 2020. [Online]. Available: <http://www.elec.uow.edu.au/apqrc/content/technotes/technote7.pdf>.
- [108] U.S. Department of Energy, “SSL Technology Fact Sheet: Flicker.” A U.S. Department of Energy, Accessed: Mar. 20, 2020. [Online]. Available: https://www1.eere.energy.gov/buildings/publications/pdfs/ssl/flicker_fact-sheet.pdf.
- [109] International Commission on Illumination, “Visual Aspects of Time-Modulated Lighting Systems—Definitions and Measurement Models,” Accessed: Feb. 15, 2020. [Online]. Available: http://files.cie.co.at/883_CIE_TN_006-2016.pdf.
- [110] M. Perz, “Modelling visibility of temporal light artefacts (2019),” Accessed: Mar. 15, 2020. [Online]. Available: <https://research.tue.nl/en/publications/modelling-visibility-of-temporal-light-artefacts-stroboscopic-vis>.
- [111] Jim Gaines, “Temporal Light Artifacts (Flicker + Stroboscopic Effect),” 2016, Accessed: Mar. 24, 2020. [Online]. Available: <https://www.designlights.org/news-events/events/2016-dlc-stakeholder-meeting/presentation-downloads/temporal-light-artifacts-flicker-and-stroboscopic-effect/>.
- [112] Unios, “Driving the Flicker Free Effect White-Paper.” https://unios.com/wp-content/uploads/2016/06/UN_Driving-the-Flicker-Free-Effect_White-Paper-190205.pdf (accessed Mar. 24, 2020).
- [113] C. Andrus, “Application of the GE Flicker Curve,” 2012, Accessed: May 10, 2017. [Online]. Available: <https://library.powermonitors.com/application-of-the-ge-flicker-curve>.
- [114] J. M. Wikston, “The flicker meter - IEEE Std 1453/spl trade/-2004,” in *2006 IEEE Power Engineering Society General Meeting*, Montreal, Que., Canada, 2006, p. 2 pp., doi: 10.1109/PES.2006.1709225.

- [115] Cowles Andrus, “White PAPER: IEEE STD. 141 FLICKER CURVE VS. IEEE 1453 FLICKER METER,” 2016, Accessed: May 10, 2017. [Online]. Available: <https://library.powermonitors.com/ieee-std-141-flicker-curve-vs-ieee-1453-flicker-meter>.
- [116] “IEEE Recommended Practice--Adoption of IEC 61000-4-15:2010, Electromagnetic compatibility (EMC)--Testing and measurement techniques--Flickermeter--Functional and design specifications,” IEEE, Jan. 2019. doi: 10.1109/IEEESTD.2011.6053977.
- [117] S. Lodetti *et al.*, “Flicker of Modern Lighting Technologies Due to Rapid Voltage Changes,” *Energies*, vol. 12, no. 5, p. 865, Mar. 2019, doi: 10.3390/en12050865.
- [118] “IEEE Recommended Practices for Modulating Current in High-Brightness LEDs for Mitigating Health Risks to Viewers,” *IEEE Std 1789-2015*, pp. 1–80, Jun. 2015, doi: 10.1109/IEEESTD.2015.7118618.
- [119] M. S. Rea and Illuminating Engineering Society of North America, Eds., *The IESNA lighting handbook: reference & application*, 9. ed. New York, NY: IESNA, Publ. Dep, 2000.
- [120] T. Perrin, C. Brown, M. Poplawski, and N. Miller, “Characterizing Photometric Flicker,” *Pac. Northwest Natl. Lab.*, p. 24.
- [121] N. J. Miller, “GATEWAY Demonstrations: OLED Lighting in the Offices of Aurora Lighting Design, Inc.,” Pacific Northwest National Lab.(PNNL), Richland, WA (United States), 2016.
- [122] M. P. Royer, M. E. Poplawski, and N. J. Miller, “DOE CALiPER Program, Report 20.1 Application Summary Report 20: LED PAR38 Lamps,” Pacific Northwest National Lab.(PNNL), Richland, WA (United States), 2012.
- [123] U.S. Department of Energy, Solid-State Lighting Program, “OLED Lighting in the Offices of DeJoy, Knauf & Blood, LLP,” Accessed: Apr. 13, 2020. [Online]. Available: https://www.energy.gov/sites/prod/files/2017/08/f35/2017_gateway_dkb-oled.pdf.
- [124] N. None, “CALiPER Report 20.2: Dimming, Flicker, and Power Quality Characteristics of LED PAR38 Lamps,” Pacific Northwest National Lab.(PNNL), Richland, WA (United States), 2014.
- [125] Dominion Energy, “2017 Blue Book.” Dominion Energy Virginia and Dominion Energy North Carolina, 2019, [Online]. Available: <https://www.dominionenergy.com/>.
- [126] Duke Energy Midwest, “Duke Energy Midwest transmission systems Facility Connection Requirements.” Accessed: Apr. 14, 2020. [Online]. Available: <http://www.ferc.duke-energy.com/DEW/MidwestConnection.pdf>.
- [127] Engineering Recommendation P28, “Voltage fluctuations and the connection of disturbing equipment to transmission systems and distribution networks in the United

Kingdom.” Energy Networks Association, 2019, [Online]. Available: www.energynetworks.org.

[128] American Electric Power, “Guide for Electric Service and Meter Installations (2019).” American Electric Power Company Meter and Service Guide, Accessed: Jan. 09, 2020. [Online]. Available: <https://www.aeptexas.com/global/utilities/lib/docs/builders/meter/MeterandServiceGuide1-2-2019.pdf>.

[129] Copper Development Association, “Power quality application guide, voltage disturbances-flicker.” Accessed: Aug. 08, 2020. [Online]. Available: <http://copperalliance.org.uk/uploads/2018/03/514-flicker.pdf>.

[130] A. Baghini, *Handbook of power quality*. John Wiley & Sons, 2008.

[131] Electric Power Research Institute (EPRI), “Grid Shunt Reactive Power Compensation.” Palo Alto, CA 2008.

[132] T. A. Short, *Distribution reliability and power quality*. Crc Press, 2018.

[133] A. Ghosh and G. Ledwich, *Power quality enhancement using custom power devices*. Springer Science & Business Media, 2012.

[134] S. Kong, Z. Yin, R. Shan, and W. Shang, “A Survey on the Principle and Control of Dynamic Voltage Restorer,” in *2009 International Conference on Energy and Environment Technology*, Guilin, China, 2009, pp. 57–60, doi: 10.1109/ICEET.2009.250.

[135] S. Bageshwar and D. D. P. Kothari, “A Review on Power Quality Improvement by UPQC.” Accessed: Mar. 07, 2020. [Online]. Available: <https://pdfs.semanticscholar.org/9787/96a92169e1b8c633314456be16a27a4a8ae8.pdf>.

[136] W. Moncrief, J. Dougherty, L. Richardson, and K. Craven, “Power quality applications guide for architects and engineers,” *EPRICSG Palo Alto CA USA Tech Rep*, vol. 113874, 1999.

[137] X. ENERGY, “SAFETY, INTERFERENCE AND INTERCONNECTION GUIDELINES FOR COGENERATORS, SMALL POWER PRODUCERS AND CUSTOMER-OWNED GENERATION.” PUBLIC SERVICE COMPANY OF COLORADO, 2017.

[138] T. Gonen, *Electric Power Distribution Engineering*. CRC Press, 2015.

[139] P. G. Cardinal, D. Burns, and D. Sauer, “Lower Cost Solution for Medium Voltage Heater Control: An Affordable Evolution Using Variable Voltage Transformers,” *IEEE Ind. Appl. Mag.*, vol. 24, no. 2, pp. 57–66, Mar. 2018, doi: 10.1109/MIAS.2017.2740444.

- [140] W. K. Wong, D. L. Osborn, and J. L. McAvoy, "Application of compact static VAR compensators to distribution systems," *IEEE Trans. Power Deliv.*, vol. 5, no. 2, pp. 1113–1120, Apr. 1990, doi: 10.1109/61.53129.
- [141] S. M. Halpin, J. W. Smith, and C. A. Litton, "Designing industrial systems with a weak utility supply," *IEEE Ind. Appl. Mag.*, vol. 7, no. 2, pp. 63–70, Mar. 2001, doi: 10.1109/2943.911191.
- [142] Electric Power Research Institute (EPRI), "Guidebook on Custom Power Devices," 2000. Accessed: Jan. 04, 2020. [Online]. Available: <https://www.epri.com/research/products/000000000001000340>.
- [143] M. Eremia, C.-C. Liu, and A.-A. Edris, *Advanced solutions in power systems: HVDC, FACTS, and Artificial Intelligence*. John Wiley & Sons, 2016.
- [144] A. Eberhard, *POWER QUALITY*. India: InTech, 2011.
- [145] K. R. Padiyar, *FACTS controllers in power transmission and distribution*. New Age International, 2007.
- [146] K. Gholami, S. Karimi, and E. Dehnavi, "Optimal unified power quality conditioner placement and sizing in distribution systems considering network reconfiguration," *Int. J. Numer. Model. Electron. Netw. Devices Fields*, vol. 32, no. 1, p. e2467, Jan. 2019, doi: 10.1002/jnm.2467.
- [147] Energy Sector Management Assistance Program, "Compensation Devices to Support Grid Integration of Variable Renewable Energy," World Bank, Washington, DC., 2019. Accessed: Apr. 17, 2020. [Online]. Available: <http://hdl.handle.net/10986/32074>.
- [148] R. M. Mathur and R. K. Varma, *Thyristor-Based FACTS Controllers for Electrical Transmission Systems*. Wiley-IEEE Press, 2002.
- [149] T. Gönen, *Electric power distribution system engineering*, vol. 2. CRC press Boca Raton, 2008.
- [150] M. Salama, "Lecture 10 Application of Capacitors for Distribution Systems [pdf file]," p. 45, 2008.
- [151] Roger C. Dugan, H. Wayne Beaty, M. F. McGranaghan, and S. Santoso, *Electrical Power Systems Quality, Third Edition*, 3rd ed. New York: McGraw-Hill Education, 2012.
- [152] R. S. Vedam and M. S. Sarma, *Power quality: Var compensation in power systems*. CRC press, 2017.
- [153] A. Kusko and M. T. Thompson, *Power quality in electrical systems*. New York: McGraw-Hill, 2007.

- [154] K. Habur and D. O’Leary, “FACTS-flexible alternating current transmission systems: for cost effective and reliable transmission of electrical energy.” Siemens-World Bank Doc. Draft Rep. Erlangen, 2004, Accessed: Jan. 06, 2020. [Online]. Available: [http://www.rds.oeb.ca/HPECMWebDrawer/Record/176620/File/document#:~:text=Flexible%20alternating%20current%20transmission%20systems%20\(FACTS\)%20devices%20are%20used%20for,of%20high%20voltage%20AC%20lines.&text=Typically%20the%20construction%20period%20for,from%20contract%20signing%20through%20commissioning](http://www.rds.oeb.ca/HPECMWebDrawer/Record/176620/File/document#:~:text=Flexible%20alternating%20current%20transmission%20systems%20(FACTS)%20devices%20are%20used%20for,of%20high%20voltage%20AC%20lines.&text=Typically%20the%20construction%20period%20for,from%20contract%20signing%20through%20commissioning).
- [155] S. A. Taher and S. A. Afsari, “Optimal Location and Sizing of UPQC in Distribution Networks Using Differential Evolution Algorithm,” *Math. Probl. Eng.*, vol. 2012, pp. 1–20, 2012, doi: 10.1155/2012/838629.
- [156] S. Rezaeian Marjani, V. Talavat, and S. Galvani, “Optimal allocation of D-STATCOM and reconfiguration in radial distribution network using MOPSO algorithm in TOPSIS framework,” *Int. Trans. Electr. Energy Syst.*, vol. 29, no. 2, p. e2723, Feb. 2019, doi: 10.1002/etep.2723.
- [157] M. Saravanan, S. M. R. Slochanal, P. Venkatesh, and J. P. S. Abraham, “Application of particle swarm optimization technique for optimal location of FACTS devices considering cost of installation and system loadability,” *Electr. Power Syst. Res.*, vol. 77, no. 3–4, pp. 276–283, Mar. 2007, doi: 10.1016/j.epsr.2006.03.006.
- [158] A. Moghadasi, A. Sarwat, and J. M. Guerrero, “A comprehensive review of low-voltage-ride-through methods for fixed-speed wind power generators,” *Renew. Sustain. Energy Rev.*, vol. 55, pp. 823–839, Mar. 2016, doi: 10.1016/j.rser.2015.11.020.
- [159] M. Hosseinpour, A. Yazdian, M. Hohamadian, and J. Kazempour, “Desing and simulation of UPQC to improve power quality and transfer wind energy to grid,” *Jour Appl. Sci.*, vol. 8, no. 21, pp. 3770–3782, 2008.
- [160] K. Somsai and T. Kulworawanichpong, “Cost estimation for reactive power compensation in distribution power system by using D-STATCOM.” Accessed: Jan. 07, 2020. [Online]. Available: http://www.i-asem.org/publication_conf/anbre13/M3D.4.ER655_1199F.pdf.
- [161] J. V. Milanovic and Yan Zhang, “Global Minimization of Financial Losses Due to Voltage Sags With FACTS Based Devices,” *IEEE Trans. Power Deliv.*, vol. 25, no. 1, pp. 298–306, Jan. 2010, doi: 10.1109/TPWRD.2009.2035419.
- [162] M. McGranaghan and B. Roettger, “Economic Evaluation of Power Quality,” *IEEE Power Eng. Rev.*, vol. 22, no. 2, pp. 8–12, Feb. 2002, doi: 10.1109/MPER.2002.981339.
- [163] J. Arrillaga, Y. H. Liu, and N. R. Watson, *Flexible Power Transmission*. Chichester, UK: John Wiley & Sons, Ltd, 2007.

- [164] J. G. Nielsen and F. Blaabjerg, “A Detailed Comparison of System Topologies for Dynamic Voltage Restorers,” *IEEE Trans. Ind. Appl.*, vol. 41, no. 5, pp. 1272–1280, Sep. 2005, doi: 10.1109/TIA.2005.855045.
- [165] S. A. Taher and S. A. Afsari, “Optimal location and sizing of DSTATCOM in distribution systems by immune algorithm,” *Int. J. Electr. Power Energy Syst.*, vol. 60, pp. 34–44, Sep. 2014, doi: 10.1016/j.ijepes.2014.02.020.
- [166] A. J. Pansini, *Electrical distribution engineering*, 3rd ed. Lilburn, GA : Boca Raton, FL: Fairmont Press ; CRC Press, 2007.
- [167] W. H. Kersting, *Distribution system modeling and analysis*, Fourth edition. Boca Raton: CRC Press, Taylor & Francis Group, CRC Press is an imprint of the Taylor & Francis Group, an informa business, 2018.
- [168] R. E. Brown, *Electric power distribution reliability*. CRC press, 2008.
- [169] W. M. Strang *et al.*, “Distribution line protection practices industry survey results,” *IEEE Trans. Power Deliv.*, vol. 10, no. 1, pp. 176–186, Jan. 1995, doi: 10.1109/61.368400.
- [170] L. L. Grigsby, *The electric power engineering handbook*. CRC Press, 2000.
- [171] ANSI O5.1-2017, “AMERICAN NATIONAL STANDARD FOR WOOD UTILITY PRODUCTS: Wood Poles - Specifications and Dimensions.” Accessed: Jan. 29, 2019. [Online]. Available: https://webstore.ansi.org/preview-pages/ANSI/preview_ANSI+O5.1-2017.pdf.
- [172] T. A. Short, *Electric Power Distribution Equipment and Systems*. CRC Press, 2005.
- [173] J. J. Burke, *Power distribution engineering: fundamentals and applications*. CRC Press, 1994.
- [174] J. D. Glover, M. S. Sarma, and T. Overbye, *Power System Analysis & Design*, 6 E. Boston, MA : Cengage Learning, 2017.
- [175] Kevin Schneider, “Module 7: Energy storage and electric vehicles.” https://class.ece.uw.edu/smartgrid/g6/index_files/Page619.htm (accessed Mar. 28, 2019).
- [176] T. Anegawa, “Safety Design of CHAdeMO Quick Charging System,” *World Electr. Veh. J.*, vol. 4, no. 4, pp. 855–859, Dec. 2010, doi: 10.3390/wevj4040855.
- [177] Centre National du Transport Avancé, “ARRA EV Project Chevrolet Volt Data Summary Reports,” 2015. [Online]. Available: <https://www.energy.gov/eere/vehicles/downloads/avta-arra-ev-project-chevrolet-volt-data-summary-reports>.

- [178] M. Piao, H. S. Shon, J. Y. Lee, and K. H. Ryu, "Subspace Projection Method Based Clustering Analysis in Load Profiling," *IEEE Trans. Power Syst.*, vol. 29, no. 6, pp. 2628–2635, 2014, doi: 10.1109/TPWRS.2014.2309697.
- [179] J. Nazarko and Z. A. Styczynski, "Application of statistical and neural approaches to the daily load profiles modelling in power distribution systems," Apr. 1999, vol. 1, pp. 320–325 vol.1, doi: 10.1109/TDC.1999.755372.
- [180] A. Mutanen, M. Ruska, S. Repo, and P. Jarventausta, "Customer Classification and Load Profiling Method for Distribution Systems," *IEEE Trans. Power Deliv.*, vol. 26, no. 3, pp. 1755–1763, 2011, doi: 10.1109/TPWRD.2011.2142198.
- [181] B. Stephen and S. J. Galloway, "Domestic Load Characterization Through Smart Meter Advance Stratification," *IEEE Trans. Smart Grid*, vol. 3, no. 3, pp. 1571–1572, 2012, doi: 10.1109/TSG.2012.2198314.
- [182] B. Stephen, A. J. Mutanen, S. Galloway, G. Burt, and P. Järventausta, "Enhanced Load Profiling for Residential Network Customers," *IEEE Trans. Power Deliv.*, vol. 29, no. 1, pp. 88–96, 2014, doi: 10.1109/TPWRD.2013.2287032.
- [183] S. Zhong and K. S. Tam, "Hierarchical Classification of Load Profiles Based on Their Characteristic Attributes in Frequency Domain," *IEEE Trans. Power Syst.*, vol. 30, no. 5, pp. 2434–2441, 2015, doi: 10.1109/TPWRS.2014.2362492.
- [184] R. Li, F. Li, and N. D. Smith, "Multi-Resolution Load Profile Clustering for Smart Metering Data," *IEEE Trans. Power Syst.*, vol. 31, no. 6, pp. 4473–4482, 2016, doi: 10.1109/TPWRS.2016.2536781.
- [185] Y. Wang, Q. Chen, C. Kang, and Q. Xia, "Clustering of Electricity Consumption Behavior Dynamics Toward Big Data Applications," *IEEE Trans. Smart Grid*, vol. 7, no. 5, pp. 2437–2447, 2016, doi: 10.1109/TSG.2016.2548565.
- [186] V. Kamaraju, *Electrical Power Distribution Systems*. Tata McGraw-Hill Education (India) Pvt Limited, 2009.
- [187] A. Seack, J. Kays, and C. Rehtanz, "Time series based distribution grid planning approach with decentralised voltage regulation," Aug. 2014, pp. 1–7, doi: 10.1109/PSCC.2014.7038345.
- [188] S. A. Yin and C. N. Lu, "Distribution Feeder Scheduling Considering Variable Load Profile and Outage Costs," *IEEE Trans. Power Syst.*, vol. 24, no. 2, pp. 652–660, 2009, doi: 10.1109/TPWRS.2009.2016300.
- [189] S. Fezai and J. Belhadj, "Load profile impact on a Stand-Alone Photovoltaic system," Mar. 2016, pp. 1–6, doi: 10.1109/IREC.2016.7478897.

- [190] H. R. Atia, A. Shakya, P. Tandukar, U. Tamrakar, T. M. Hansen, and R. Tonkoski, "Efficiency analysis of AC coupled and DC coupled microgrids considering load profile variations," May 2016, pp. 0695–0699, doi: 10.1109/EIT.2016.7535324.
- [191] P. Wiest, K. Rudion, and A. Probst, "Weather data-based load profile modeling for grid expansion planning," Jun. 2015, pp. 1–6, doi: 10.1109/PTC.2015.7232315.
- [192] F. L. Quilumba, W. J. Lee, H. Huang, D. Y. Wang, and R. L. Szabados, "Using Smart Meter Data to Improve the Accuracy of Intraday Load Forecasting Considering Customer Behavior Similarities," *IEEE Trans. Smart Grid*, vol. 6, no. 2, pp. 911–918, 2015, doi: 10.1109/TSG.2014.2364233.
- [193] M. Espinoza, C. Joye, R. Belmans, and B. D. Moor, "Short-Term Load Forecasting, Profile Identification, and Customer Segmentation: A Methodology Based on Periodic Time Series," *IEEE Trans. Power Syst.*, vol. 20, no. 3, pp. 1622–1630, 2005, doi: 10.1109/TPWRS.2005.852123.
- [194] T. Hong, J. Wilson, and J. Xie, "Long Term Probabilistic Load Forecasting and Normalization With Hourly Information," *IEEE Trans. Smart Grid*, vol. 5, no. 1, pp. 456–462, 2014, doi: 10.1109/TSG.2013.2274373.
- [195] G. Graditi, M. L. D. Silvestre, R. Gallea, and E. R. Sanseverino, "Heuristic-Based Shiftable Loads Optimal Management in Smart Micro-Grids," *IEEE Trans. Ind. Inform.*, vol. 11, no. 1, pp. 271–280, 2015, doi: 10.1109/TII.2014.2331000.
- [196] B. Qela and H. T. Mouftah, "Peak Load Curtailment in a Smart Grid Via Fuzzy System Approach," *IEEE Trans. Smart Grid*, vol. 5, no. 2, pp. 761–768, 2014, doi: 10.1109/TSG.2013.2289922.
- [197] D. T. Nguyen, "Modeling Load Uncertainty in Distribution Network Monitoring," *IEEE Trans. Power Syst.*, vol. 30, no. 5, pp. 2321–2328, 2015, doi: 10.1109/TPWRS.2014.2364819.
- [198] M. S. ElNozahy, M. M. A. Salama, and R. Seethapathy, "A probabilistic load modelling approach using clustering algorithms," Jul. 2013, pp. 1–5, doi: 10.1109/PESMG.2013.6672073.
- [199] W. R. New, "The Utility Looks at Load Profiles of All-Electric Buildings," *IEEE Trans. Ind. Appl.*, vol. IA-10, no. 6, pp. 751–760, 1974, doi: 10.1109/TIA.1974.349226.
- [200] J. A. Jardini, C. M. V. Tahan, M. R. Gouvea, S. U. Ahn, and F. M. Figueiredo, "Daily load profiles for residential, commercial and industrial low voltage consumers," *IEEE Trans. Power Deliv.*, vol. 15, no. 1, pp. 375–380, 2000, doi: 10.1109/61.847276.
- [201] S. Zhong and K. S. Tam, "A Frequency Domain Approach to Characterize and Analyze Load Profiles," *IEEE Trans. Power Syst.*, vol. 27, no. 2, pp. 857–865, 2012, doi: 10.1109/TPWRS.2011.2170592.

- [202] M. Deru *et al.*, “US Department of Energy commercial reference building models of the national building stock.” 2011, Accessed: Jun. 06, 2020. [Online]. Available: <https://www.nrel.gov/docs/fy11osti/46861.pdf>.
- [203] S. M. Alshareef and W. G. Morsi, “Probabilistic commercial load profiles at different climate zones,” pp. 1–7, Oct. 2017, doi: 10.1109/epec.2017.8286233.
- [204] S. Wilcox and W. Marion, “Users Manual for TMY3 Data Sets.” 2008, Accessed: Aug. 03, 2017. [Online]. Available: <https://www.nrel.gov/docs/fy08osti/43156.pdf>.
- [205] “Appendix B | Postal Explorer.” <https://pe.usps.com/text/pub28/28apb.htm> (accessed Oct. 31, 2018).
- [206] M. K. Gray and W. G. Morsi, “Power Quality Assessment in Distribution Systems Embedded With Plug-In Hybrid and Battery Electric Vehicles,” *IEEE Trans. Power Syst.*, vol. 30, no. 2, pp. 663–671, 2015, doi: 10.1109/TPWRS.2014.2332058.
- [207] S. Zhong and K. S. Tam, “A Frequency Domain Approach to Characterize and Analyze Load Profiles,” *IEEE Trans. Power Syst.*, vol. 27, no. 2, pp. 857–865, 2012, doi: 10.1109/TPWRS.2011.2170592.
- [208] M. Klippenstein, “Plug-in Electric Car Sales in Canada, May 2018: Rewriting records,” *Green Car Reports*. https://www.greencarreports.com/news/1117062_plug-in-electric-car-sales-in-canada-may-2018-rewriting-records (accessed Dec. 20, 2018).
- [209] Fuel Economy, “Compare Cars Side-by-Side.” <https://www.fueleconomy.gov/feg/Find.do?action=sbsSelect> (accessed Dec. 19, 2018).
- [210] S. M. Alshareef and W. G. Morsi, “Probabilistic Modeling of Plug-in Electric Vehicles Charging from Fast Charging Stations,” in *2019 IEEE Electrical Power and Energy Conference (EPEC)*, Montréal, QU, Oct. 2019, vol. To be published, pp. 1–6.
- [211] J. Axsen *et al.*, “Electrifying vehicles: insights from the Canadian plug-in electric vehicle study,” *Simon Fraser Univ. Vanc. Can.*, 2015.
- [212] “PEV Map - Google Fusion Tables.” https://fusiontables.googleusercontent.com/embedviz?q=select+col2+from+1S9KxCRaKxbWjHA1TkmzAEYadManV9GvIxhgAZ_c&viz=MAP&h=false&lat=49.08664473390496&lng=-102.64343268749997&t=1&z=5&l=col2&y=2&tmplt=2&hml=TWO_COL_LAT_LNG (accessed Dec. 20, 2018).
- [213] “Energy Efficiency Requirements for Houses in British Columbia (Lower Mainland and Southern Vancouver Island).” <https://www.bchousing.org/research-centre/library/residential-design-construction/ig-energy-efficiency-houses-climate-zone-4-lowermainland&sortType=sortByDate> (accessed Dec. 20, 2018).

- [214] C.-S. N. Shiau, N. Kaushal, C. T. Hendrickson, S. B. Peterson, J. F. Whitacre, and J. J. Michalek, "Optimal plug-in hybrid electric vehicle design and allocation for minimum life cycle cost, petroleum consumption, and greenhouse gas emissions," *J. Mech. Des.*, vol. 132, no. 9, p. 091013, 2010.
- [215] S. Brooks, A. Gelman, G. Jones, and X.-L. Meng, *Handbook of markov chain monte carlo*. CRC press, 2011.
- [216] S. Chib and E. Greenberg, "Understanding the metropolis-hastings algorithm," *Am. Stat.*, vol. 49, no. 4, pp. 327–335, 1995.
- [217] W. R. Gilks, S. Richardson, and D. Spiegelhalter, *Markov chain Monte Carlo in practice*. Chapman and Hall/CRC, 1995.
- [218] S. P. Brooks and A. Gelman, "General methods for monitoring convergence of iterative simulations," *J. Comput. Graph. Stat.*, vol. 7, no. 4, pp. 434–455, 1998.
- [219] C. Robert and G. Casella, *Introducing Monte Carlo Methods with R*. New York, NY: Springer New York, 2010.
- [220] A. Almutairi and M. M. A. Salama, "Assessment and Enhancement Frameworks for System Reliability Performance Using Different PEV Charging Models," *IEEE Trans. Sustain. Energy*, vol. 9, no. 4, pp. 1969–1984, Oct. 2018, doi: 10.1109/TSTE.2018.2820696.
- [221] "evCloud | FleetCarma." <https://www.fleetcarma.com/evCloud> (accessed Dec. 19, 2018).
- [222] J. Francfort and R. Brion Bennett, "Plug-in electric vehicle and infrastructure analysis." Citeseer, 2015, Accessed: Mar. 03, 2017. [Online]. Available: <https://inldigitallibrary.inl.gov/sites/sti/sti/6799570.pdf>.
- [223] Unpublished confidential data, "50 kw Fast charging station profile," Canada, Ontario, 2017.
- [224] IEEE PES AMPS DSAS Test Feeder Working Group, "Resources | PES Test Feeder." <http://sites.ieee.org/pes-testfeeders/resources/> (accessed Mar. 11, 2019).
- [225] Kersting, William H., "Inquiry about IEEE 123 Node Test Feeder," Sep. 28, 2017.
- [226] W. H. Kersting, "Radial distribution test feeders," *IEEE Trans. Power Syst.*, vol. 6, no. 3, pp. 975–985, Aug. 1991, doi: 10.1109/59.119237.
- [227] MathWorks, "Download MATLAB, Simulink, Stateflow, and Other MathWorks Products." <https://www.mathworks.com/downloads/> (accessed Mar. 15, 2019).
- [228] "EPRI | Smart Grid Resource Center > Simulation Tool – OpenDSS." <http://smartgrid.epri.com/SimulationTool.aspx> (accessed Mar. 15, 2019).

- [229] J. Bishops, “Profiles on Residential Power Consumption : Phase I final report /.” Fire Protection Research Foundation, Quincy, MA :2010., [Online]. Available: <https://library.nfpa.org/GeniePLUS/GeniePLUS/Portal/Public.aspx?lang=en-US>.
- [230] “Electric vehicles sales update Q3 2018, Canada,” *FleetCarma*, Nov. 06, 2018. <https://www.fleetcarma.com/electric-vehicles-sales-update-q3-2018-canada/> (accessed May 03, 2019).
- [231] M. Duvall, E. Knipping, M. Alexander, L. Tonachel, and C. Clark, “Environmental assessment of plug-in hybrid electric vehicles, Volume 1: Nationwide greenhouse gas emissions,” *Electr. Power Res. Inst. Palo Alto CA*, vol. 1015325, 2007.
- [232] M. Gjelaj, C. Træholt, S. Hashemi, and P. B. Andersen, “DC Fast-charging stations for EVs controlled by a local battery storage in low voltage grids,” in *PowerTech, 2017 IEEE Manchester*, 2017, pp. 1–6.
- [233] VEHICLE TECHNOLOGIES OFFICE, “AVTA: ARRA EV Project Chevrolet Volt Data Summary Reports,” *ENERGY EFFICIENCY & RENEWABLE ENERGY*, 2013. <https://www.energy.gov/eere/vehicles/downloads/avta-arra-ev-project-chevrolet-volt-data-summary-reports>.
- [234] “Petro-Canada reveals \$0.33 per minute EV charging cost in Ontario.” <https://mobilesyrup.com/2020/01/22/petro-canada-33-cents-per-minute-ev-cost/> (accessed Sep. 11, 2020).
- [235] E. Compatibility, “Part 3: Limits—Section 7: Assessment of Emission Limits for Fluctuating Loads in MV and HV Power Systems,” *IEC Std*, vol. 61, pp. 000–003, 1996.
- [236] E. Compatibility, “Part 3-3, Limits–Limitation of voltage changes, voltage fluctuations and flicker in public low-voltage supply systems, for equipment with rated current ≤ 16 A per phase and not subject to conditional connection,” *IEC Stand.*, pp. 61000–3, 2013.
- [237] D. Perera, L. Meegahapola, S. Perera, and P. Ciufu, “Characterisation of flicker emission and propagation in distribution networks with bi-directional power flows,” *Renew. Energy*, vol. 63, pp. 172–180, Mar. 2014, doi: 10.1016/j.renene.2013.09.007.
- [238] J. Smart, “Charging Infrastructure for Shared and Autonomous EVs.” Idaho National Laboratory, 2019, [Online]. Available: https://sites.nationalacademies.org/cs/groups/depssite/documents/webpage/deps_193660.pdf.
- [239] E. Wood, C. Rames, E. Kontou, Y. Motoaki, J. Smart, and Z. Zhou, “Analysis of Fast Charging Station Network for Electrified Ride-Hailing Services,” Apr. 2018, pp. 2018-01–0667, doi: 10.4271/2018-01-0667.

- [240] A. S. B. Humayd, B. Lami, and K. Bhattacharya, "The effect of PEV uncontrolled and smart charging on distribution system planning," in *2016 IEEE Electrical Power and Energy Conference (EPEC)*, 2016, pp. 1–6.
- [241] Y. Zhang, "Modeling of fast charging station equipped with energy storage," *Glob. Energy Interconnect.*, vol. 1, no. 2, p. 8, 2018.
- [242] O. Hafez and K. Bhattacharya, "Integrating EV charging stations as smart loads for demand response provisions in distribution systems," *IEEE Trans. Smart Grid*, vol. 9, no. 2, pp. 1096–1106, 2016.
- [243] M. I. Marei, E. F. El-Saadany, and M. M. Salama, "Envelope tracking techniques for Flicker Mitigation and Voltage regulation," *IEEE Trans. Power Deliv.*, vol. 19, no. 4, pp. 1854–1861, 2004.
- [244] M. I. Marei and M. M. A. Salama, "Advanced Techniques for Voltage Flicker Mitigation," in *2006 IEEE International Power Electronics Congress*, 2006, pp. 1–5.
- [245] A. Elnady and M. M. Salama, "Unified approach for mitigating voltage sag and voltage flicker using the DSTATCOM," *IEEE Trans. Power Deliv.*, vol. 20, no. 2, pp. 992–1000, 2005.
- [246] N. Eghtedarpour, E. Farjah, and A. Khayatian, "Effective Voltage Flicker Calculation Based on Multiresolution S-Transform," *IEEE Trans. Power Deliv.*, vol. 27, no. 2, pp. 521–530, Apr. 2012, doi: 10.1109/TPWRD.2011.2182064.
- [247] A. Robert and M. Couvreur, "Recent experience of connection of big arc furnaces with reference to flicker level," in *INTERNATIONAL CONFERENCE ON LARGE HIGH VOLTAGE ELECTRIC SYSTEMS*, 1994, vol. 2, pp. 36–305.
- [248] D. Arlt, M. Stark, and C. Eberlein, "Examples of international flicker requirements in high voltage networks and real world measurements," in *2007 9th International Conference on Electrical Power Quality and Utilisation*, Barcelona, Spain, Oct. 2007, pp. 1–4, doi: 10.1109/EPQU.2007.4424222.
- [249] S. Perera *et al.*, "Synchronized flicker measurement for flicker transfer evaluation in power systems," *IEEE Trans. Power Deliv.*, vol. 21, no. 3, pp. 1477–1482, 2006.
- [250] I. Sharma, C. Canizares, and K. Bhattacharya, "Smart charging of PEVs penetrating into residential distribution systems," *IEEE Trans. Smart Grid*, vol. 5, no. 3, pp. 1196–1209, 2014.
- [251] IRENA, "INNOVATION OUTLOOK SMART CHARGING FOR ELECTRIC VEHICLES." 2019, Accessed: Jun. 07, 2020. [Online]. Available: https://irena.org/-/media/Files/IRENA/Agency/Publication/2019/May/IRENA_Innovation_Outlook_EV_smart_charging_2019.pdf.

- [252] IRENA, “Innovation landscape brief: Electric-vehicle smart charging.” 2019, Accessed: Jun. 07, 2020. [Online]. Available: https://www.irena.org/-/media/Files/IRENA/Agency/Publication/2019/Sep/IRENA_EV_Smart_Charging_2019.pdf?la=en&hash=E77FAB7422226D29931E8469698C709EFC13EDB2.
- [253] T. D. Brosnan and M. A. Murray, “Voltage fluctuation monitoring in an ESB Transmission station.” Irish colloquium on DSP & Control, Dublin, 1993.
- [254] T. D. Brosnan and M. A. Murray, “Flicker Severity Measurements on an Electric Arc Furnace during Switched Changes in an Transmission Network.” First International Conference on Power Quality, Paris, 1991.
- [255] D. Arlt and C. Eberlein, “Network Disturbances caused by Ultra High Power Electric Arc Furnaces and possible reduction Methods.” 4th International Conference of Electrical Power Quality and Utilisation, Cracow, 1997.
- [256] C. électrique inc, “50 kW fast-charge station,” *The Electric Circuit*. <https://lecircuitelectrique.com/en/stations/fast-charge-station/> (accessed Sep. 11, 2020).
- [257] A. Hajimiragha, C. A. Canizares, M. W. Fowler, and A. Elkamel, “Optimal transition to plug-in hybrid electric vehicles in Ontario, Canada, considering the electricity-grid limitations,” *IEEE Trans. Ind. Electron.*, vol. 57, no. 2, pp. 690–701, 2009.
- [258] A. Bin Humayd, “Distribution System Planning in Smart Grids to Accommodate Distributed Energy Resources and Electric Vehicles,” University of Waterloo, 2017.
- [259] Antonino Genovese, Fernando Ortenzi, and Carlo Villante, “On the energy efficiency of quick DC vehicle battery charging,” *World Electr. Veh. J.*, vol. 7, no. 4, pp. 570–576, Dec. 2015, doi: 10.3390/wevj7040570.
- [260] E. Saberbari and H. Saboori, “Evaluating PHEV impacts on domestic distribution grid in terms of power losses and voltage drop,” in *2014 19th Conference on Electrical Power Distribution Networks (EPDC)*, Tehran, Iran, May 2014, pp. 52–58, doi: 10.1109/EPDC.2014.6867498.

Appendices

Appendix A.

A1. IEEE 123-Bus Standard Test Distribution System Data

Table A-1 Three-Phase Switch Positions

Configuration	Phasing	Phasing Conductor ACSR	Normal Conductor ACSR	Spacing ID
1	ABCN	336,400 26/7	4/0 6/1	500
2	CABN	336,400 26/7	4/0 6/1	500
3	BCAN	336,400 26/7	4/0 6/1	500
4	CBAN	336,400 26/7	4/0 6/1	500
5	BACN	336,400 26/7	4/0 6/1	500
6	ACBN	336,400 26/7	4/0 6/1	500
7	CAN	336,400 26/7	4/0 6/1	505
8	ABN	336,400 26/7	4/0 6/1	505
9	AN	1/0	1/0	510
10	BN	1/0	1/0	510
11	CN	1/0	1/0	510

Table A-2 Overhead Line Configuration Data

Node A	Node B	Normal
13	152	closed
18	135	closed
60	160	closed
61	610	closed
97	197	closed
150	149	closed
250	251	open
450	451	open
54	94	open
151	300	open
300	350	open

Table A-3 Underground Line Configuration Data

Configuration	Phasing	Cable	Spacing ID
12	ABC	1/0 AA, CN	515

Table A-4 Primary Transformer Data

Transformer	kVA	kVA- High	kVA- Low	R%	X%
Substation	5000	115 - D	4.16 Gr - W	1	8
XFM-1	150	4.16 - D	0.480 - D	1.27	2.72

Table A-5 Shunt Capacitors Data

Node	Phase-A kVAr	Phase-B kVAr	Phase-C kVAr
83	200	200	200
88	50	0.0	0.0
90	0.0	50	0.0
92	0.0	0.0	250

Table A-6 Regulator Data

ID	Line Segment	Location	Monitoring Phase	Bandwidth	PT Ratio	Primary CT Rating	R	X	Voltage Level
1-A	150-149	150	A	2.0 Volt	20	700	3	7.5	120
2-A	9-14	9	A	2.0 Volt	20	50	0.4	0.4	120
3-A	25-26	25	A	1.0 Volt	20	50	0.4	0.4	120
3-C	25-26	25	C	1.0 Volt	20	50	0.4	0.4	120
4-A	160-67	160	A	2.0 Volt	20	300	0.6	1.3	124
4-B	160-67	160	B	2.0 Volt	20	300	1.4	2.6	124
4-C	160-67	160	C	2.0 Volt	20	300	0.2	1.4	124

Table A-7 Sport Load Data

Node	Load Model	Ph-1 kW	Ph-1 kVAr	Ph-2 kW	Ph-2 kVAr	Ph-3 kW	Ph-3 kVAr
1	Y-PQ	40	20	0	0	0	0
2	Y-PQ	0	0	20	10	0	0
4	Y-PQ	0	0	0	0	40	20
5	Y-I	0	0	0	0	20	10
6	Y-Z	0	0	0	0	40	20
7	Y-PQ	20	10	0	0	0	0
9	Y-PQ	40	20	0	0	0	0
10	Y-I	20	10	0	0	0	0
11	Y-Z	40	20	0	0	0	0
12	Y-PQ	0	0	20	10	0	0
16	Y-PQ	0	0	0	0	40	20
17	Y-PQ	0	0	0	0	20	10
19	Y-PQ	40	20	0	0	0	0
20	Y-I	40	20	0	0	0	0
22	Y-Z	0	0	40	20	0	0
24	Y-PQ	0	0	0	0	40	20
28	Y-I	40	20	0	0	0	0

Table A-8 Sport Load Data

Node	Load Model	Ph-1 kW	Ph-1 kVAr	Ph-2 kW	Ph-2 kVAr	Ph-3 kW	Ph-3 kVAr
29	Y-Z	40	20	0	0	0	0
30	Y-PQ	0	0	0	0	40	20
31	Y-PQ	0	0	0	0	20	10
32	Y-PQ	0	0	0	0	20	10
33	Y-I	40	20	0	0	0	0
34	Y-Z	0	0	0	0	40	20
35	D-PQ	40	20	0	0	0	0
37	Y-Z	40	20	0	0	0	0
38	Y-I	0	0	20	10	0	0
39	Y-PQ	0	0	20	10	0	0
41	Y-PQ	0	0	0	0	20	10
42	Y-PQ	40	20	0	0	0	0
43	Y-PQ	0	0	20	10	0	0
45	Y-PQ	0	0	0	0	40	20
46	Y-I	0	0	0	0	20	10
47	Y-Z	0	0	0	0	40	20
48	Y-PQ	20	10	0	0	0	0
49	Y-PQ	40	20	0	0	0	0
50	Y-I	20	10	0	0	0	0
51	Y-Z	40	20	0	0	0	0
38	Y-PQ	0	0	20	10	0	0
39	Y-PQ	0	0	0	0	40	20
41	Y-PQ	0	0	0	0	20	10
42	Y-PQ	20	10	0	0	0	0
43	Y-Z	0	0	40	20	0	0
45	Y-I	20	10	0	0	0	0
46	Y-PQ	20	10	0	0	0	0
47	Y-I	35	25	35	25	35	25
48	Y-Z	70	50	70	50	70	50
49	Y-PQ	35	25	70	50	35	25
50	Y-PQ	0	0	0	0	40	20
51	Y-PQ	20	10	0	0	0	0
52	Y-PQ	40	20	0	0	0	0
53	Y-PQ	40	20	0	0	0	0
55	Y-Z	20	10	0	0	0	0
56	Y-PQ	0	0	20	10	0	0
58	Y-I	0	0	20	10	0	0
59	Y-PQ	0	0	20	10	0	0
60	Y-PQ	20	10	0	0	0	0
62	Y-Z	0	0	0	0	40	20

Table A-9 Sport Load Data

Node	Load Model	Ph-1 kW	Ph-1 kVAr	Ph-2 kW	Ph-2 kVAr	Ph-3 kW	Ph-3 kVAr
63	Y-PQ	40	20	0	0	0	0
64	Y-I	0	0	75	35	0	0
65	D-Z	35	25	35	25	70	50
66	Y-PQ	0	0	0	0	75	35
68	Y-PQ	20	10	0	0	0	0
69	Y-PQ	40	20	0	0	0	0
70	Y-PQ	20	10	0	0	0	0
71	Y-PQ	40	20	0	0	0	0
73	Y-PQ	0	0	0	0	40	20
74	Y-Z	0	0	0	0	40	20
75	Y-PQ	0	0	0	0	40	20
76	D-I	105	80	70	50	70	50
77	Y-PQ	0	0	40	20	0	0
79	Y-Z	40	20	0	0	0	0
80	Y-PQ	0	0	40	20	0	0
82	Y-PQ	40	20	0	0	0	0
83	Y-PQ	0	0	0	0	20	10
84	Y-PQ	0	0	0	0	20	10
85	Y-PQ	0	0	0	0	40	20
86	Y-PQ	0	0	20	10	0	0
87	Y-PQ	0	0	40	20	0	0
88	Y-PQ	40	20	0	0	0	0
90	Y-I	0	0	40	20	0	0
92	Y-PQ	0	0	0	0	40	20
94	Y-PQ	40	20	0	0	0	0
95	Y-PQ	0	0	20	10	0	0
96	Y-PQ	0	0	20	10	0	0
98	Y-PQ	40	20	0	0	0	0
99	Y-PQ	0	0	40	20	0	0
100	Y-Z	0	0	0	0	40	20
102	Y-PQ	0	0	0	0	20	10
103	Y-PQ	0	0	0	0	40	20
104	Y-PQ	0	0	0	0	40	20
106	Y-PQ	0	0	40	20	0	0
107	Y-PQ	0	0	40	20	0	0
109	Y-PQ	40	20	0	0	0	0
111	Y-PQ	20	10	0	0	0	0
112	Y-I	20	10	0	0	0	0
113	Y-Z	40	20	0	0	0	0
114	Y-PQ	20	10	0	0	0	0

Table A-10 Line Segment Data

Node A	Node B	Length (feet)	Configuration
1	2	175	10
1	3	250	11
1	7	300	1
3	4	200	11
3	5	325	11
5	6	250	11
7	8	200	1
8	12	225	10
8	9	225	9
8	13	300	1
9	14	425	9
13	34	150	11
13	18	825	2
14	11	250	9
14	10	250	9
15	16	375	11
15	17	350	11
18	19	250	9
18	21	300	2
19	20	325	9
21	22	525	10
21	23	250	2
23	24	550	11
23	25	275	2
25	26	350	7
25	28	200	2
26	27	275	7
26	31	225	11
27	33	500	9
28	29	300	2
29	30	350	2
30	250	200	2
31	32	300	11
34	15	100	11
35	36	650	8
35	40	250	1
36	37	300	9
36	38	250	10
38	39	325	10
40	41	325	11

Table A-11 Line Segment Data

Node A	Node B	Length (feet)	Configuration
40	42	250	1
42	43	500	10
42	44	200	1
44	45	200	9
44	47	250	1
45	46	300	9
47	48	150	4
47	49	250	4
49	50	250	4
50	51	250	4
52	53	200	1
53	54	125	1
54	55	275	1
54	57	350	3
55	56	275	1
57	58	250	10
57	60	750	3
58	59	250	10
60	61	550	5
60	62	250	12
62	63	175	12
63	64	350	12
64	65	425	12
65	66	325	12
67	68	200	9
67	72	275	3
67	97	250	3
68	69	275	9
69	70	325	9
70	71	275	9
72	73	275	11
72	76	200	3
73	74	350	11
74	75	400	11
76	77	400	6
76	86	700	3
77	78	100	6
78	79	225	6
78	80	475	6

Ggg

Table A-12 Line Segment Data

Node A	Node B	Length (feet)	Configuration
80	81	475	6
40	41	325	11
40	42	250	1
81	82	250	6
81	84	675	11
82	83	250	6
84	85	475	11
86	87	450	6
87	88	175	9
87	89	275	6
89	90	225	10
89	91	225	6
91	92	300	11
91	93	225	6
93	94	275	9
93	95	300	6
95	96	200	10
97	98	275	3
98	99	550	3
99	100	300	3
100	450	800	3
101	102	225	11
101	105	275	3
102	103	325	11
103	104	700	11
105	106	225	10
105	108	325	3
106	107	575	10
108	109	450	9
108	300	1000	3
109	110	300	9
110	111	575	9
110	112	125	9
112	113	525	9
113	114	325	9
135	35	375	4
149	1	400	1
152	52	400	1
160	67	350	6
197	101	250	3

Line Configuration 1:

$$\begin{bmatrix} 0.4576 + j1.0780 & 0.1560 + j0.5017 & 0.1535 + j0.3849 \\ 0.1560 + j0.5017 & 0.4666 + j1.0482 & 0.1580 + j0.4236 \\ 0.1535 + j0.3849 & 0.1580 + j0.4236 & 0.4615 + j1.0651 \end{bmatrix} \frac{\Omega}{\text{mile}}$$
$$\begin{bmatrix} 5.6765 & -1.8319 & -0.6982 \\ -1.8319 & 5.9809 & -1.1645 \\ -0.6982 & -1.1645 & 5.3971 \end{bmatrix} \frac{\mu\text{S}}{\text{mile}}$$

Line Configuration 2:

$$\begin{bmatrix} 0.4666 + j1.0482 & 0.1580 + j0.4236 & 0.1560 + j0.5017 \\ 0.1580 + j0.4236 & 0.4615 + j1.0651 & 0.1535 + j0.3849 \\ 0.1560 + j0.5017 & 0.1535 + j0.3849 & 0.4576 + j1.0780 \end{bmatrix} \frac{\Omega}{\text{mile}}$$
$$\begin{bmatrix} 5.9809 & -1.1645 & -1.8319 \\ -1.1645 & 5.3971 & -0.6982 \\ -1.8319 & -0.6982 & 5.6765 \end{bmatrix} \frac{\mu\text{S}}{\text{mile}}$$

Line Configuration 3:

$$\begin{bmatrix} 0.4615 + j1.0651 & 0.1535 + j0.3849 & 0.1580 + j0.4236 \\ 0.1535 + j0.3849 & 0.4576 + j1.0780 & 0.1560 + j0.5017 \\ 0.1580 + j0.4236 & 0.1560 + j0.5017 & 0.4666 + j1.0482 \end{bmatrix} \frac{\Omega}{\text{mile}}$$
$$\begin{bmatrix} 5.3971 & -0.6982 & -1.1645 \\ -0.6982 & 5.6765 & -1.8319 \\ -1.1645 & -1.8319 & 5.9809 \end{bmatrix} \frac{\mu\text{S}}{\text{mile}}$$

Line Configuration 4:

$$\begin{bmatrix} 0.4615 + j1.0651 & 0.1580 + j0.4236 & 0.1535 + j0.3849 \\ 0.1580 + j0.4236 & 0.4666 + j1.0482 & 0.1560 + j0.5017 \\ 0.1535 + j0.3849 & 0.1560 + j0.5017 & 0.4576 + j1.0780 \end{bmatrix} \frac{\Omega}{\text{mile}}$$
$$\begin{bmatrix} 5.3971 & -1.1645 & -0.6982 \\ -1.1645 & 5.9809 & -1.8319 \\ -0.6982 & -1.8319 & 5.6765 \end{bmatrix} \frac{\mu\text{S}}{\text{mile}}$$

Line Configuration 5:

$$\begin{bmatrix} 0.4666 + j1.0482 & 0.1560 + j0.5017 & 0.1580 + j0.4236 \\ 0.1560 + j0.5017 & 0.4576 + j1.0780 & 0.1535 + j0.3849 \\ 0.1580 + j0.4236 & 0.1535 + j0.3849 & 0.4615 + j1.0651 \end{bmatrix} \frac{\Omega}{\text{mile}}$$

$$\begin{bmatrix} 5.9809 & -1.8319 & -1.1645 \\ -1.8319 & 5.6765 & -0.6982 \\ -1.1645 & -0.6982 & 5.3971 \end{bmatrix} \frac{\mu\text{S}}{\text{mile}}$$

Line Configuration 6:

$$\begin{bmatrix} 0.4576 + j1.0780 & 0.1535 + j0.3849 & 0.1560 + j0.5017 \\ 0.1535 + j0.3849 & 0.4615 + j1.0651 & 0.1580 + j0.4236 \\ 0.1560 + j0.5017 & 0.1580 + j0.4236 & 0.4666 + j1.0482 \end{bmatrix} \frac{\Omega}{\text{mile}}$$

$$\begin{bmatrix} 5.6765 & -0.6982 & -1.8319 \\ -0.6982 & 5.3971 & -1.1645 \\ -1.8319 & -1.1645 & 5.9809 \end{bmatrix} \frac{\mu\text{S}}{\text{mile}}$$

Line Configuration 7:

$$\begin{bmatrix} 0.4576 + j1.0780 & 0.0000 + j0.0000 & 0.1535 + j0.3849 \\ 0.0000 + j0.0000 & 0.0000 + j0.0000 & 0.0000 + j0.0000 \\ 0.1535 + j0.3849 & 0.0000 + j0.0000 & 0.4615 + j1.0651 \end{bmatrix} \frac{\Omega}{\text{mile}}$$

$$\begin{bmatrix} 5.1154 & 0.0000 & -1.0549 \\ 0.0000 & 0.0000 & 0.0000 \\ -1.0549 & 0.0000 & 5.1704 \end{bmatrix} \frac{\mu\text{S}}{\text{mile}}$$

Line Configuration 8:

$$\begin{bmatrix} 0.4576 + j1.0780 & 0.1535 + j0.3849 & 0.0000 + j0.0000 \\ 0.1535 + j0.3849 & 0.4615 + j1.0651 & 0.0000 + j0.0000 \\ 0.0000 + j0.0000 & 0.0000 + j0.0000 & 0.0000 + j0.0000 \end{bmatrix} \frac{\Omega}{\text{mile}}$$

$$\begin{bmatrix} 5.1154 & -1.0549 & 0.0000 \\ -1.0549 & 5.1704 & 0.0000 \\ 0.0000 & 0.0000 & 0.0000 \end{bmatrix} \frac{\mu\text{S}}{\text{mile}}$$

Line Configuration 9:

$$\begin{bmatrix} 1.3292 + j1.3475 & 0.0000 + j0.0000 & 0.0000 + j0.0000 \\ 0.0000 + j0.0000 & 0.0000 + j0.0000 & 0.0000 + j0.0000 \\ 0.0000 + j0.0000 & 0.0000 + j0.0000 & 0.0000 + j0.0000 \end{bmatrix} \frac{\Omega}{\text{mile}}$$

$$\begin{bmatrix} 4.5193 & 0.0000 & 0.0000 \\ 0.0000 & 0.0000 & 0.0000 \\ 0.0000 & 0.0000 & 0.0000 \end{bmatrix} \frac{\mu\text{S}}{\text{mile}}$$

Line Configuration 10:

$$\begin{bmatrix} 0.0000 + j0.0000 & 0.0000 + j0.0000 & 0.0000 + j0.0000 \\ 0.0000 + j0.0000 & 1.3292 + j1.3475 & 0.0000 + j0.0000 \\ 0.0000 + j0.0000 & 0.0000 + j0.0000 & 0.0000 + j0.0000 \end{bmatrix} \frac{\Omega}{\text{mile}}$$

$$\begin{bmatrix} 0.0000 & 0.0000 & 0.0000 \\ 0.0000 & 4.5193 & 0.0000 \\ 0.0000 & 0.0000 & 0.0000 \end{bmatrix} \frac{\mu\text{S}}{\text{mile}}$$

Line Configuration 11:

$$\begin{bmatrix} 0.0000 & 0.0000 & 0.0000 & 0.0000 & 0.0000 & 0.0000 \\ 0.0000 & 0.0000 & 0.0000 & 0.0000 & 0.0000 & 0.0000 \\ 0.0000 & 0.0000 & 0.0000 & 0.0000 & 1.3292 & 1.3475 \end{bmatrix} \frac{\Omega}{\text{mile}}$$

$$\begin{bmatrix} 0.0000 & 0.0000 & 0.0000 \\ 0.0000 & 0.0000 & 0.0000 \\ 0.0000 & 0.0000 & 4.5193 \end{bmatrix} \frac{\mu\text{S}}{\text{mile}}$$

Line Configuration 12:

$$\begin{bmatrix} 1.5209 + j0.7521 & 0.5198 + j0.2775 & 0.4924 + j0.2157 \\ 0.5198 + j0.2775 & 1.5329 + j0.7162 & 0.5198 + j0.2775 \\ 0.4924 + j0.2157 & 0.5198 + j0.2775 & 1.5209 + j0.7521 \end{bmatrix} \frac{\Omega}{\text{mile}}$$

$$\begin{bmatrix} 67.2242 & 0.0000 & 0.0000 \\ 0.0000 & 67.2242 & 0.0000 \\ 0.0000 & 0.0000 & 67.2242 \end{bmatrix} \frac{\mu\text{S}}{\text{mile}}$$

Appendix B.

B1. Secondary Distribution System Data

Table B-1 Secondary Distribution Transformer Data

Transformer Location	kVA	kVA- High	kVA- Low	R%	X%
Residential	25 kVA	2.402 Gr-W	0.240 Gr -W	0.5367	1.0733
Residential	50 kVA	2.402 Gr-W	0.240 Gr -W	1.0140	1.7238
Commercial	15 kVA	4.16 Gr-W	0.208 Gr -W	1.6	2.53
Commercial	30 kVA	4.16 Gr-W	0.208 Gr -W	1.96	2.4
FCS	50 kVA	4.16 Gr-W	0.600 Gr -W	1.61	3.98
FCS	150 kVA	4.16 Gr-W	0.600 Gr -W	1.53	5.8
FCS	300 kVA	4.16 Gr-W	0.600 Gr -W	1.81	7.17

Table B-2 Secondary Type and Conductor Data

Secondary Line Type	Conductor	GMR (feet)	Diameter (Inch)	Resistance ($\Omega/mi.$)	Insulation Thick. (mil)	Length (feet)
Main Line	4/0 AA	0.0158	0.522	0.484	80	125
Service Drop	1/0 AA	0.0111	0.368	0.97	80	[80,100]

Secondary Main Line

$$\begin{bmatrix} 0.1587 + j0.0711 & 0.0670 + j0.0417 \\ 0.0670 + j0.0417 & 0.1587 + j0.0711 \end{bmatrix} \frac{\Omega}{kfeet}$$

Secondary Service Drop

$$\begin{bmatrix} 0.2891 + j0.1159 & 0.1054 + j0.0842 \\ 0.1054 + j0.0842 & 0.2891 + j0.1159 \end{bmatrix} \frac{\Omega}{mile}$$